



NTNU – Trondheim
Norwegian University of
Science and Technology

Modeling of Amine Degradation in a CO₂ Absorption Column at Test Centre Mongstad

Fridtjof Finsnes Henriksen

Chemical Engineering and Biotechnology

Submission date: June 2012

Supervisor: Hallvard Fjøsne Svendsen, IKP

Co-supervisor: Hanna Knuutila, IKP

Toine Cents, TCM

Olav Falk-Pedersen, TCM

Norwegian University of Science and Technology

Department of Chemical Engineering

Abstract

Two different previously conducted oxidative degradation experiments, were used as a basis of modeling monoethanolamine-degradation reactions. Literature and previous experience was used to construct reaction equations for the formation of five main degradation products; ammonia, N-(2-hydroxyethyl)formamide (HEF), N-(2-hydroxy ethyl)imidazole (HEI), N,N-Bis(2-hydroxy ethyl)oxalamide (BHEOX) and N-(2-hydroxy ethyl)glycine (HEGly), in addition to four intermediate products formaldehyde, formic acid, glyoxal and oxalic acid.

Rate equations were developed for the reactions, and implemented in the degradation model. The model was thereafter fitted to the experimental data of both experiments, to provide parameters in the rate equations.

The found parameters and rate equations were implemented in an obtained Aspen Plus absorber simulation. Three different absorber cases were created, with two different flue gas compositions. The ammonia emission in the simulation results ranged within reasonable 9.6 - 14.6 ppmv. However, a rough estimation of the degradation rate, showed that the rate in the simulations was much higher than previously measured in pilot plants.

The results showed that the data set used for the modeling was too small to provide a complete degradation model. This resulted in several weaknesses in the model, such as independence of CO₂-loading, temperature, contaminates and instability with respect to the concentration of dissolved ferric. Yet, the results also showed that it was possible to model degradation reactions in detail, and that further development of the model had good potential if more experimental data would become available.

Sammendrag

To forskjellige, tidligere gjennomførte oksidative degraderingsexperimenter ble brukt som basis for modellering av monoetanolamin-degraderingsreaksjoner. Litteratur og tidligere erfaring ble brukt som grunnlag til å konstruere reaksjonslikninger for dannelsen av fem viktige degraderingsprodukter; ammoniakk, N-(2-hydroksetyl)formamide (HEF), N-(2-hydroksetyl)imidazol (HEI), N,N-bis(2-hydroksetyl)oxalamid (BHEOX) og N-(2-hydroksetyl)glycin (HEGly), i tillegg til fire mellomprodukter; formaldehyd, maursyre, glyoksal og glyoksalsyre.

Hastighetslikninger ble utviklet for reaksjonene, og ble implementert i degraderingsmodellen. Modellen ble deretter tilpasset eksperimentelle data fra begge eksperimentene, for å finne parametrene i hastighetslikningene.

Parametrene som ble funnet sammen med hastighetslikningene, ble implementert i en eksternt innhentet Aspen Plus absorber simulering. Tre absorber-case ble laget med to forskjellige eksosgasser. Ammoniakkutslippet i simuleringresultatene varierte mellom fornuftige 9.6 - 14.6 ppmv, men et grovt estimat av degraderingshastigheten viste at reaksjonshastigheten i simuleringene var mye høyere enn tidligere målt i pilotanlegg.

Resultatene viste at datasettet, som ble brukt til modelleringen, var for lite til å lage en fullstendig degraderingsmodell. Det resulterte i flere svakheter i modellen, eksempelvis uavhengighet av CO₂-loading, -temperatur, -forurensninger og ustabilitet med hensyn til konsentrasjon av jernioner. Likevel viste modellen at det var mulig å modellere degraderingsreaksjoner i detalj, og at videre utvikling av modellen hadde potensiale hvis flere eksperimentelle data blir tilgjengelig.

Preface

The work with this master's thesis has been carried out at the Department of Chemical Engineering at the Norwegian University of Science and Technology in cooperation with Technology Centre Mongstad, during the spring of 2012.

I would like to thank my supervisors at NTNU, Hanna Knuutila and Hallvard Svendsen for guidance, academic discussions, advice and making the project possible together with Olav Falck-Pedersen at TCM DA. I would also like to thank my supervisor at TCM DA, Toine Cents, for a lot of help, discussions and insight.

Thanks to Ph.D. Solrun Johanne Vevelstad, at NTNU, for providing unpublished degradation experiment data and help with finding reaction mechanisms of the degradation reactions. Thanks to Andreas Grimstvedt, at SINTEF, for providing additional experimental data, and Eirik Falck da Silva, at SINTEF, for calculating the Henry's law coefficient data for the degradation products.

Thanks to Diego Di Domenico Pinto, at NTNU, for providing MatLab-code and essential help with particle swarm optimization.

Special thanks to my girlfriend and cohabitant, Stine Henriksen, for encouragement, support, and motivation during this work.

The picture on the front page shows the amine absorber at TCM DA, photographed with permission, the 01.11.2011 at Mongstad, by the author.

I declare that this is an independent work according to the exam regulations of the Norwegian University of Science and Technology.

Trondheim, June 15, 2012

Fridtjof Finsnes Henriksen

Contents

Abstract	i
Sammendrag	iii
Preface	v
Nomenclature	xv
1 Introduction	1
1.1 The Absorption Process	2
1.2 Amine Degradation in Industrial Context	3
1.3 Document Structure	4
I Modeling of Degradation Experiments	5
2 Experimental Basis	7
2.1 Laboratory Setups	7
2.1.1 Open Loop Laboratory Setup	7
2.1.2 Closed Loop Laboratory Setup	9
2.2 Experiment 1: Open Loop	9
2.3 Experiment 2: Closed Loop	10
2.4 Experiment 3: Open Loop with Iron Ions	12
3 The Models	13
3.1 Semi Flow Batch Reactor (SFBR) Model	13
3.2 Batch Reactor Model	14
3.3 Gas-Side Mass Transfer Coefficient	15
3.4 The Reaction Rate Expression	15
4 Degradation Reactions	17
4.1 Reaction 1 and -2: Formation of Formate	17
4.1.1 MEA Oxidation Pathway	18
4.1.2 Hydrogen Abstraction Mechanism	18
4.1.3 Modeled Reactions	19
4.2 Reaction 3: Formation of HEF	20
4.3 Reaction 4 and -5: Formation of HEI	20
4.4 Reaction 6 and -7: Formation of BHEOX	21
4.4.1 Modeled Reactions	22
4.5 Reaction 8: Formation of HEGly	23
4.5.1 Oxidation Pathway	23
4.5.2 Reaction with Epoxide	23
4.5.3 Reaction with Glycolic Acid	24

4.5.4	Modeled reactions	24
4.6	Overview of Implemented Reactions	24
4.7	Catalytic Effects	24
5	Parameter Fitting	27
5.1	Program Structure	28
5.2	Methods of Parameter Fitting	29
5.2.1	Manual Trial and Error	29
5.2.2	Simplex Iteration	29
5.2.3	Least-Squares Iteration	30
5.2.4	Particle Swarm Optimization	30
6	Development of the Rate Equations	31
6.1	First Version	31
6.2	Second Version	34
6.3	Third Version	36
6.4	Final (Fourth) Version	39
6.4.1	Ammonia Locked	40
6.4.2	Ammonia Unlocked	42
6.4.3	Deviation Between Model and Experiment	44
6.4.4	The Oxygen Leakage	47
6.4.5	Prediction of an Additional Experiment	47
7	Physical Properties	51
7.1	Mass Transfer Properties of the Experiments	51
7.1.1	Model Sensitivity of the Mass Transfer Parameters	52
7.1.2	Liquid Side Mass Transfer Coefficient of Ammonia	54
7.1.3	Non-volatile Components	55
7.2	Henry's Law Coefficients	56
II	Absorber Simulation	59
8	Implementation in Absorber Model	61
8.1	Rate Equations	61
8.2	Implementing the Rate Expression in Aspen Plus	63
8.3	Implementing the Reaction Equations in Aspen Plus	64
8.4	Charge Balance	66
8.5	User Defined Components	67
9	Case Description	69
9.1	Initial Run Case	69
9.2	Recycle Case	70
9.3	Absorbers in Series	72
9.4	Flow Rates and Compositions	73
9.4.1	Flue Gas Inlet Composition and Condition	73
9.4.2	Flow Rates	74
10	Absorber Simulation Results	75

10.1	Initial Case	75
10.1.1	CHP Results	76
10.1.2	RFCC Results	77
10.2	Recycle Case	79
10.3	Absorber Series Case	81
10.3.1	CHP Results	81
10.3.2	RFCC Results	83
 III Discussion and Conclusions		85
 11 Discussion		87
11.1	Modeling of the Degradation Experiments	87
11.1.1	Deviation Between Model and Experiments	87
11.1.2	Iron Catalyst Dependency	89
11.1.3	The Oxygen Leakage and the Hydrogen Abstraction Mechanism	90
11.1.4	Locked Ammonia Profile	91
11.1.5	Validity of the Experimental Models	92
11.1.6	Over-all Gas Phase Balance for the Closed Loop Experiment Model	93
11.1.7	The Mass Transfer Coefficients	94
11.1.8	Henry's Law Coefficients	94
11.1.9	Minor Assumptions	95
11.2	The Degradation Reactions	96
11.2.1	The General Uncertainty of the Reaction Mechanisms	96
11.2.2	Uncertainty of the Reaction Mechanism of HEGly	96
11.2.3	Charge Balance and Radicals	97
11.2.4	Reversible Reactions	97
11.3	Absorber Simulation	98
11.3.1	Absorber Results	98
11.3.2	Validity of the Simulation Cases	100
11.3.3	Property Estimation	101
11.3.4	The Concentration of Iron Ions	101
11.3.5	Comparison of the Laboratory Experiments and the TCM Absorber	102
11.3.6	No Stripper Conditions	103
 12 Conclusions		105
 13 Further Work		107
 Bibliography		109
 Appendices		A1
 A Reactions as Implemented in Absorber Simulation		A1

B	Use of Aspen Plus	B1
B.1	Adding a User Defined Component	B1
B.2	Implementing Kinetic Reactions	B5
C	Gas Phase Degradation Modeling Results	C1
C.1	Locked Ammonia Profile	C2
C.2	Unlocked Ammonia Profile	C4
D	MatLab Files	D1
D.1	Files for Parameter Search	D1
D.1.1	main.m	D1
D.1.2	SPSO.m	D3
D.1.3	OBJF.m	D7
D.1.4	ANSFIG.m	D10
D.2	Experimental Model Files	D12
D.2.1	RUN.m	D12
D.2.2	SFBRrun.m	D13
D.2.3	SBFRmodel.m	D16
D.2.4	SFBRpicture.m	D18
D.2.5	batchrun.m	D20
D.2.6	batchmodel.m	D22
D.2.7	batchpicture.m	D25
D.2.8	MetalSFBRrun.m	D27
D.2.9	MetalSFBRmodel.m	D29
D.2.10	MetalSFBRpicture.m	D32
D.2.11	reaction.m	D34
D.2.12	watvappres.m	D36
D.2.13	henrys.m	D37
D.2.14	constant.m	D38

The MatLab-code given in appendix D, and the complete Aspen Plus tables for the results presented in chapter 10, were electronically submitted, and may be retrieved on the following web pages; <http://daim.idi.ntnu.no/>.

The confidential Aspen Plus simulation files, in addition to the MatLab-files containing experimental data, were neither included in this document nor in the electronic submission. They were though delivered to Hallvard F. Svendsen by email; hallvard.svendsen@chemeng.ntnu.no.

List of Tables

4.1	Molar quantities of the measured compounds in degradation experiment 1, section 2.3.	18
4.2	Merged Degradation Reactions as Implemented in the Models. . .	26
6.1	Model standard deviations for experiment 1; open loop.	44
6.2	Model standard deviations for experiment 2; closed loop.	44
7.1	Henry's law coefficients.	57
8.1	Overview of the rate coefficients.	62
8.2	Parameters in equation (8.3.4).	66
8.3	Calculated loading in experiment 2; closed loop.	66
8.4	Aspen Plus input properties of HEF, HEI, BHEOX and HEGly. . .	68
9.1	CHP- and RFCC flue gas composition.	74
9.2	Flue gas composition implemented in Aspen Plus.	74
9.3	Flow rates for the two flue gases.	74
10.1	Aspen Plus component IDs.	75
10.2	Initial case results; CHP flue gas.	76
10.3	Initial case results; RFCC flue gas.	77
10.4	Recycle case results; CHP flue gas, 5 % purge.	80
10.5	Absorber holdup; RFCC flue gas.	81
10.6	Absorber in series case results; CHP flue gas.	82
10.7	Absorber holdup; RFCC flue gas.	83
10.8	Absorber in series case results; RFCC flue gas.	84
A.1	Degradation Reactions as Implemented in Absorber Simulation. . .	A2
A.2	Degradation Reactions as Implemented in Absorber Simulation (Continued)	A3
A.3	Degradation Reactions as Implemented in Absorber Simulation (Continued)	A4
A.4	Degradation Reactions as Implemented in Absorber Simulation (Continued)	A5
A.5	Degradation Reactions as Implemented in Absorber Simulation (Continued)	A6
A.6	Degradation Reactions as Implemented in Absorber Simulation (Continued)	A7

List of Figures

1.1	Simplified flow sheet describing the amine plant.	2
2.1	Illustration of the open loop experimental setup.	8
2.2	Illustration of the closed loop experimental setup.	8
2.3	Product concentration profiles in experiment 1; open loop.	9
2.4	Reactant concentration profiles in experiment 1; open loop.	10
2.5	Product concentration profiles in experiment 2; closed loop.	11
2.6	Reactant concentration profiles in experiment 2; closed loop.	11
2.7	Concentration profiles in experiment 3; open loop with iron ions.	12
3.1	Illustration of the semi-flow batch reactor model.	13
3.2	Illustration of the batch reactor model.	14
5.1	Illustration of the program structure for parameter search.	28
6.1	1 st version of the rate equations. Experiment 1; open loop.	32
6.2	1 st version of the rate equations. Experiment 2; closed loop.	32
6.3	2 nd version of the rate equations. Experiment 1; open loop.	34
6.4	2 nd version of the rate equations. Experiment 2; closed loop.	35
6.5	3 rd version of the rate equations. Experiment 1; open loop.	37
6.6	3 rd version of the rate equations. Experiment 2; closed loop.	38
6.7	Final version of the rate equations. Experiment 1; open loop. Locked ammonia profile.	40
6.8	Final version of the rate equations. Experiment 2; closed loop. Locked ammonia profile.	41
6.9	Final version of the rate equations. Experiment 1; open loop. Un- locked ammonia profile.	42
6.10	Final version of the rate equations. Experiment 2; closed loop. Unlocked ammonia profile.	43
6.11	Experimental- versus modeled points for Figure 6.7.	45
6.12	Experimental- versus modeled points for Figure 6.8.	45
6.13	Experimental- versus modeled points for Figure 6.9.	46
6.14	Experimental- versus modeled points for Figure 6.10.	46
6.15	Final version of the rate equations. Experiment 3; open loop with iron ions.	48
7.1	Open loop experiment model, k_L varied.	53
7.2	Closed loop experiment model, k_L varied.	53
7.3	Illustration of the open loop experiment versus the open loop model.	54

7.4	Open loop experiment model, k_{L,NH_3} varied.	55
8.1	N-(2-hydroxyethyl)-formamide (HEF)	67
8.2	1-(2-hydroxyethyl)-imidazole (HEI)	67
8.3	N,N-bis(2-hydroxyethyl)oxalamide (BHEOX)	68
8.4	N-(2-hydroxyethyl) glycine (HEGly)	68
9.1	Screen view in Aspen Plus of the initial absorber case.	69
9.2	Screen view in Aspen Plus of the recycle case.	70
9.3	Screen view in Aspen Plus of the absorber in series case.	72
B.1	The component specifications window, in the data browser.	B1
B.2	The user defined component wizard.	B2
B.3	The conventional component basic data window.	B3
B.4	The molecule editor.	B3
B.5	The molecule structure window.	B4
B.6	The conventional component additional data window.	B4
B.7	The reaction stoichiometry window, in the data browser.	B5
B.8	The select reaction type window.	B6
B.9	The edit reaction window.	B6
B.10	The reaction kinetic window, in the Data Browser.	B7
C.1	Gas phase mole fractions to Figure 6.7.	C2
C.2	Gas phase mole fractions to Figure 6.8.	C3
C.3	Gas phase mole fractions to Figure 6.9.	C4
C.4	Gas phase mole fractions to Figure 6.10.	C5
C.5	Gas phase mole fractions to Figure 6.15.	C6

Nomenclature

LATIN LETTERS		
A	Parameter in the rate equation ¹	$[(kmol/m^3)^{(1-\sum_{j=1}^N n_j)} day^{-1}]$
a	Specific masstransfer area	$[m^2/m^3]$
B	Parameter in the rate equation ¹	$[(kmol/m^3)^{(1-n_{cat}-\sum_{j=1}^N n_j)} day^{-1}]$
C	Concentration	$[kmol/m^3]$
\bar{E}	Average error	
E	Error	
E	Activation energy	$[J]$
G	Gas flow	$[kmol/day]$
H	Henry's law coefficient	$[bar\ m^3/kmol]$
h	Liquid holdup	$[m^3/run]$
K	Over-all mass transfer coefficient	$[kmol/m^2\ day\ bar]$
k	Rate coefficient ¹	$[(kmol/m^3)^{(1-\sum_{j=1}^N n_j)} day^{-1}]$
k	Mass transfer coefficient	$[m/day]$
N	Number of components	
n	Temperature exponent	
P	Pressure	$[bar]$
p	Forward reaction order exponent	
q	Backward reaction order exponent	
R	Gas constant	$[m^3\ bar/K\ kmol]$ or $[J/mol\ K]$
R_{-x}	Backward reaction rate	$[kmol/m^3\ day]$ or $[kmol/m^3\ sec]$
R_x	Reacton rate	$[kmol/m^3\ day]$ or $[kmol/m^3\ sec]$
T	Temperature	$[K]$
t	Time	$[day]$ (24 hrs)
T_0	Reference temperature	$[K]$
V	Volume	$[m^3]$
\dot{V}	Flow rate	$[m^3/hr]$
W	User supplied constant	
X	User supplied constant	
x	Mass fraction	
Y	User supplied constant	
y	Mole fraction	
Z	User supplied constant	
GREEK LETTERS		
α	loading	
τ	Recidence time per run	$[hr/run]$
ν	Stoichiometric coefficient	
SUBSCRIPTS		
0	Initial	
-i	Backward reaction index	

<i>b</i>	Bubble
<i>b</i>	Backward
<i>cat</i>	Catalyst
<i>conv</i>	Conversion
<i>eq</i>	Equilibrium
<i>exp</i>	Experimental
<i>f</i>	Forward
<i>G</i>	Gas
<i>i</i>	Reaction index
<i>in</i>	In
<i>j</i>	Component index
<i>L</i>	Liquid
<i>mod</i>	Modelled
<i>N</i>	Bubble index
<i>out</i>	Out
<i>R</i>	Reaction
<i>sat</i>	Saturation
<i>st</i>	Boiling point of water 1 atm

ABBREVIATIONS

<i>AAD</i>	Absolute average deviation
<i>AD</i>	Average deviation
<i>BHEOX</i>	N,N-bis(2-hydroxyethyl)oxalamide
<i>CCS</i>	Carbon capture and storage
<i>CHP</i>	Combined heat and power plant
<i>CUM</i>	Cubic meter
<i>CW</i>	Cooling water
<i>DCC</i>	Direct contact cooler
<i>DEA</i>	Diethyl amine
<i>HEA</i>	N-(2-hydroxyethyl)acetamide
<i>HEF</i>	N-(2-hydroxyethyl)formamide
<i>HEGly</i>	N-(2-hydroxyethyl)glycine
<i>HEI</i>	N-(2-hydroxyethyl)imidazole
<i>HEOX</i>	Hydroxyethyl oxalamide
<i>HEPO</i>	4-(2-hydroxyethyl)piperazin-2-one
<i>MEA</i>	Monoethyl amine
MEACOO [⊖]	Carbamate
MEA [⊕]	Protonated monoethyl amine
<i>ODE</i>	Ordinary differential equation
<i>OZD</i>	2-oxazolidinone
<i>RFCC</i>	Refinery fluidized catalytic cracker
<i>SFBR</i>	Semi-flow batch reactor
<i>TCM</i>	Technology centre Mongstad
<i>TDE</i>	Thermo data engine

¹n=p, for forward reaction term, n=q for backward reaction term.

Chapter 1

Introduction

TCM DA has just officially opened the world's largest center for testing, verification and development of CCS technologies. The technology center is located at Mongstad, north of Bergen, Norway. The center will test two different capture technologies, where one of them will be based on amine CO_2 absorption.

In the amine technology, a monoethylamine (MEA) solution is circulated between the absorber, where carbon dioxide is captured, and the stripper column, where the amines are regenerated. It has been recognized that over time the amines may degrade by reacting with other components than CO_2 , e.g. oxygen, sulfuric- and nitric compounds in the flue gas, or metal ions in the amine solution.

The degradation causes a decrease in the efficiency of the capture plant, and the degradation products may also leak to the surroundings with the cleaned gas. It was therefore of interest to model the degradation of the amines, and study the extent of the degradation reactions.

Thus, the aim of this master thesis was to implement selected degradation reactions in an already existing absorber model, and study the extent of these reactions. There has already been several attempts on modeling degradation of MEA; e.g. Supap and Idem (2001) [35], Bello and Idem (2006) [8], Uyanga and Idem (2007) [37] and Supap and Idem (2009) [34]. Yet, these have only modeled either the consumption of MEA and/or the formation of NH_3 . This thesis will aim to model the degradation in a more detailed manner. By constructing reaction equations and belonging rate equations for the formation for several degradation products, the model aims to not only explain the consumption of MEA, but also explain the extent of formation of the degradation products.

To construct these reaction- and rate equations, data from conducted degradation experiments had to be studied. A degradation model had to be fitted to the data, obtaining rate equations for the degradation reactions. To investigate the effects of degradation, the found rate equations were to be implemented in an absorber model corresponding to the absorber at TCM. Thus the following objectives:

- Model selected degradation experiments.
- Find proper reaction equations for the degradation reactions.

1 INTRODUCTION

- Fit the corresponding rate equations to the experimental data.
- Implement the found rate equations and reactions in an absorber simulation.

Note that since a model of this level of detail had never been constructed for amine degradation before, it was necessary to make rather large assumptions to reach the stated objectives. Especially the formation reaction mechanisms of several of the degradation products were uncertain, as the following chapters will show.

1.1 The Absorption Process

This section aims to explain typical operation of an amine based CO₂-absorption plant, in a simplified manner.

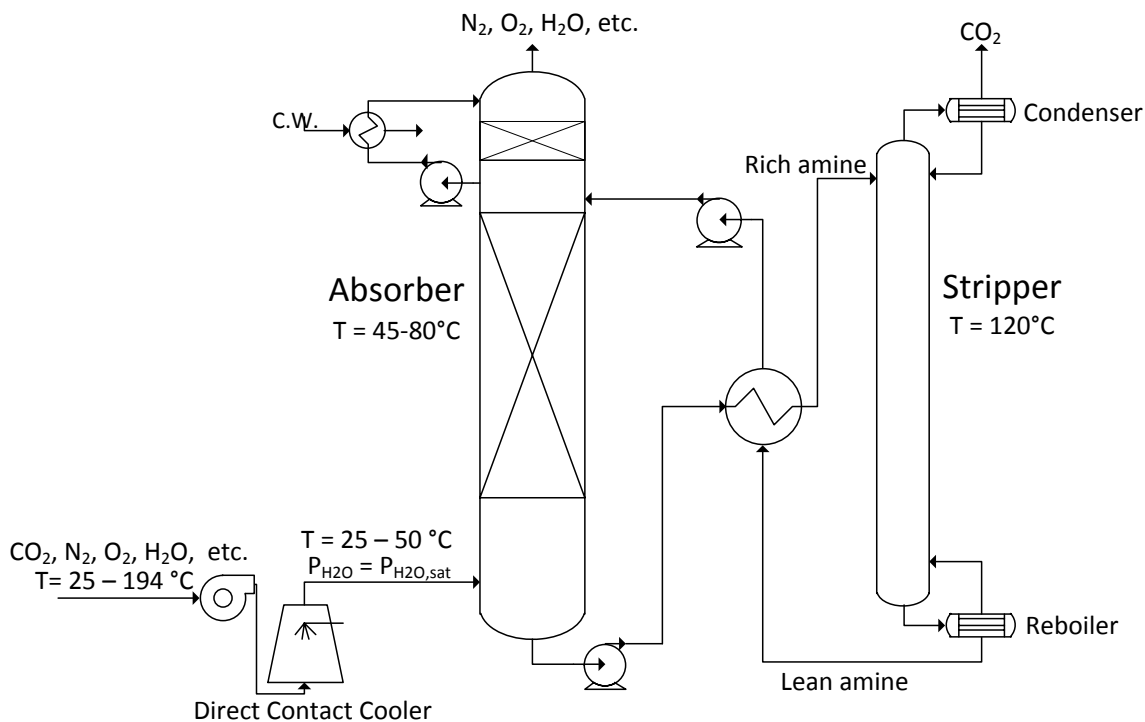


Figure 1.1: Simplified flow sheet describing the amine plant.

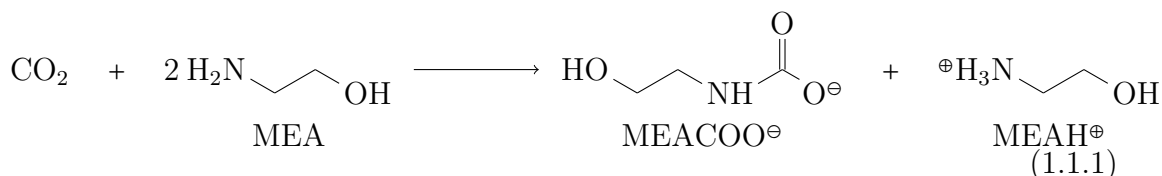
Figure 1.1 shows a simplified flow sheet of the amine plant. On the left hand side of the flow sheet, the flue gas is entering the direct contact cooler (DCC). The flue gas may be one of two types; flue gas from the refinery fluidized catalytic cracker (RFCC), or flue gas from the combined heat and power plant (CHP). The flue gases are described in more detail in section 9.4.1.

In the direct contact cooler, the flue gas is either heated or cooled to a specified temperature between 25 - 50 °C. In addition the gas is saturated with water vapor.

The saturated and cooled flue gas then enters the absorber tower. The temperature here is typically between 45 - 80 °C. In the absorber tower a lean amine solution

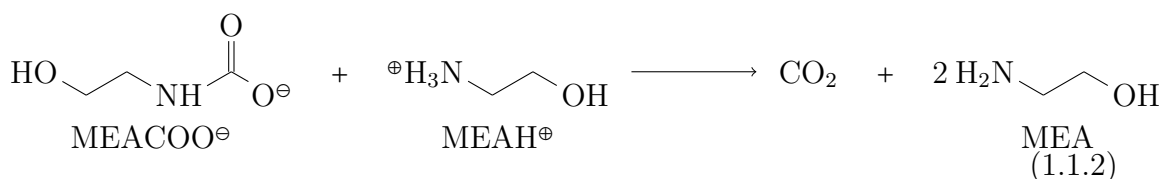
is fed through the top, and flows downwards along on the packing. The packing is designed to give the amine solution a high contact area with the CO₂-rich flue gas which is flowing counter currently in the column.

The alkaline nature of the amine solution, makes the sour CO₂ absorb and react rapidly with the liquid solution. This can be described by the following reaction equation:



The rest of the remaining gas does not participate in the reaction. This cleaned flue gas flows out the top of the column.

The amine solution, now loaded with CO₂, exits the bottom of the column before it is heated by the stream exiting the stripper column. The heated rich amine solution is now pumped in through the top of the stripper column, where the reaction is reversed due to the raised temperature:



This releases the CO₂, and regenerates the amine solution which is heat exchanged with the rich amine solution. Then the regenerated solution is pumped back into the absorber. The concentrated CO₂ would then typically be compressed and sent to storage. Nevertheless, at TCM the CO₂ is released to the atmosphere, since this is a test center for flue gas separating processes.

1.2 Amine Degradation in Industrial Context

Alkanolamines as absorbents for acidic gases such as H₂S and CO₂ was firstly patented by Bottoms (1930) [10], and in the recent years the technology has become increasingly important (Kohl (1997) [20]). Alkanolamines were found to be good absorbents for acidic gases, since the moderate basic strength made the absorption reactions reversible. This makes the acid gas easily stripped off by a temperature shift, as described in section 1.1.

A major disadvantage using alkanolamines, is the tendency for the amines to react with radicals or other components than the acid gas. These kinds of reactions will normally form components that are unable to absorb the gas, in other words a loss of amines, which consequently will lead to a loss in absorption capacity. This tendency is called amine degradation.

1 INTRODUCTION

In a flue gas treating plant, such as the amine plant at TCM, see section 1.1. The degradation reactions can be roughly divided in two categories:

- Oxidative Degradation
- Thermal Degradation

Where the categories corresponds to the degradation in respectively, the absorber, where the flue gas is rich in oxygen (4 - 15 %(mol)), and the stripper, where the temperature can be up to 120°C. These two conditions promote different reactions and degradation products, but since the liquid is circulated between these units, the degradation in the absorber and the stripper can affect each other. Additionally, a number of other factors can affect the degradation, such as CO₂-loading of the amines, catalytic effects of ions in the liquid solution, different contaminants in the flue gas, amine concentration etc.

The mentioned effects create the complete picture of the different degradation reactions. A complex picture which is only partly understood (da Silva et al. (2012) [14]).

This thesis, as mentioned, aims to model the degradation in absorber conditions. That implies, that only the oxidative degradation is studied. For a more complete understanding of the degradation in an amine based CO₂ absorption plant, the thermal degradation also has to be studied. Additionally, the interactions between the oxidative and thermal degradation have to be investigated to provide a full degradation model.

1.3 Document Structure

To fulfill the goals of this study, degradation experiments were modeled and programmed in MatLab where rate equations were fitted to the experimental data. Thereafter, the rate equations found in MatLab were implemented in a simulation of the absorber at TCM in the process simulation software Aspen Plus. The work was in other words divided in two, where the results from the first part were applied to the second part.

To avoid confusion and maintain an orderly overview, this document is divided into three parts:

The first part (I) will review the modeling of the degradation experiments, the degradation reactions and the fitting of the model to the experimental data. In other words, everything connected to the modeling and programming in MatLab.

The second part (II) will apply the results from the first part, by implementing the reaction- and rate equations in the absorber simulations, and present the results from the absorber simulation. This part will thus deal with everything related to Aspen Plus.

The third part (III) will tie parts one and two together, by providing a thorough discussion, conclusion and recommend further work.

Part I

Modeling of Degradation Experiments

Chapter 2

Experimental Basis

To be able to simulate the degradation of amines at TCM, information of the degradation and their rate equations were needed. This information was found in data from degradation experiments performed at NTNU.

This chapter will present the experimental data which was modeled to find the rate equations for the degradation reactions, and the laboratory setup used to obtain these data. Data from in total three MEA degradation experiments was received from Vevelstad (2012) [25] and Grimstvedt (2012) [23].

2.1 Laboratory Setups

Two of the experiments were performed in open loop configurations, and one in a closed loop configuration. These two different laboratory setups will be described in the following sections.

2.1.1 Open Loop Laboratory Setup

The open loop experiments consisted of a small glass batch reactor, where the gas was bubbled through the liquid. This experiment did not involve a packed column, but was similar to an industrial process in terms of being a system open to the environment.

Figure 2.1 shows a simplified illustration of the laboratory setup. CO₂ was mixed with air and bubbled through a water saturation tank, where the gas was saturated with water vapor. The gas was then pumped from the saturation tank to the reactor, which was filled with a loaded MEA solution. The gas was bubbled through the amine solution, while the solution was continuously stirred.

After being bubbled through the reactor, the gas was sent through a condenser, where water vapor was condensed, and returned to the reactor. Before being emitted, the gas was bubbled through an acidic solution to wash off ammonia in the gas.

2 EXPERIMENTAL BASIS

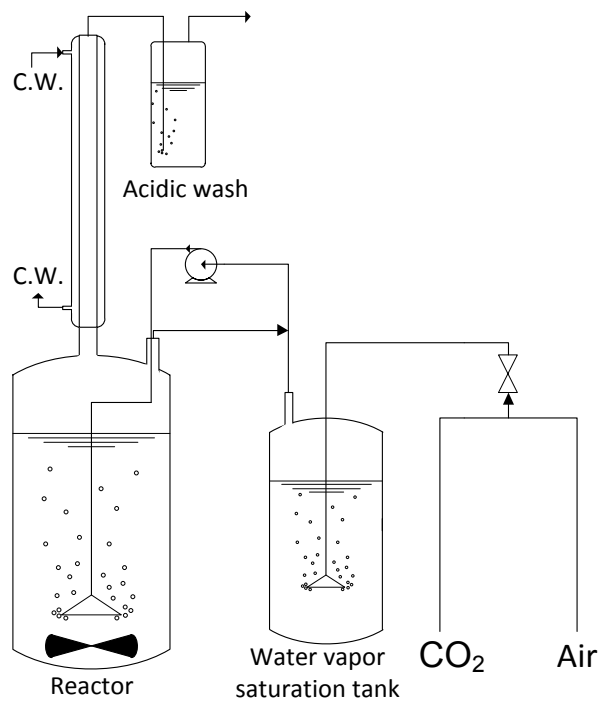


Figure 2.1: Illustration of the open loop experimental setup.

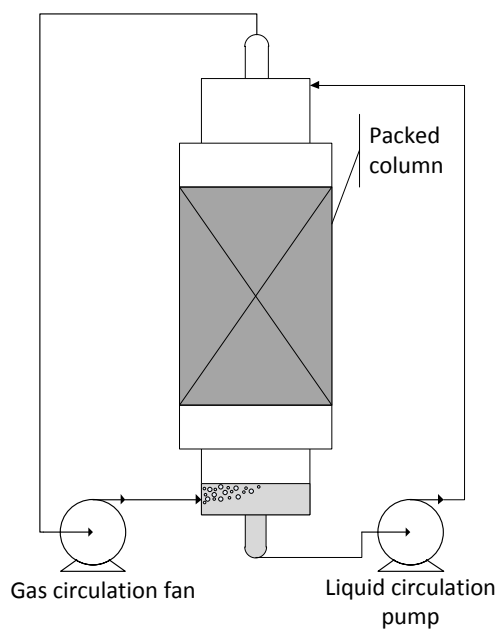


Figure 2.2: Illustration of the closed loop experimental setup.

2.1.2 Closed Loop Laboratory Setup

The closed loop experiment consisted of a setup with a packed absorber where gas and liquid were circulated. The experiment contained a packed column, but was closed from the environment, unlike an industrial absorber.

Figure 2.2 shows an illustration of the laboratory setup. The gas is circulated from the top of the absorber to the bottom, while the liquid is circulated in the opposite direction. The total volume of the absorber was calculated to be approximately 4 liters.

2.2 Experiment 1: Open Loop

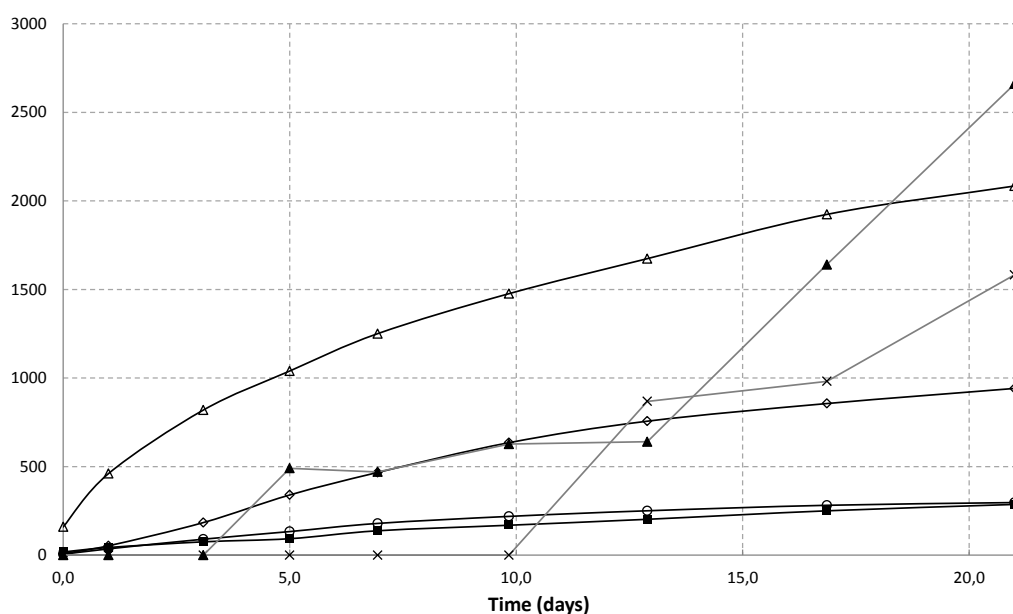


Figure 2.3: Measured products of experiment 1; open loop. HEF (Δ), HEI (\blacksquare), BHEOX (\circ), HEGly (\diamond), formate (\times), ammonia (\blacktriangle) all concentrations in [$\mu\text{g}/\text{mL}$].

These experimental data were retrieved from Vevelstad (2012) [25]. Due to confidentiality agreements, the raw data from this experiment will not be presented in this document.

The experiment was carried out in an open laboratory setup as described in section 2.1.1, and was performed in the time period from 4/2-2011 - 25/2-2011. The reactor initially held 1081 g 30 % (weight) MEA solution, loaded $\alpha = 0.4 \text{ CO}_2$. 350 mL/min air and 7.5 mL/min CO_2 was bubbled through the reactor. The temperature was kept at 55°C , and liquid samples were taken out regularly from the reactor.

The production of HEF, HEI, BHEOX, HEGly, formic acid and ammonia is presented in Figure 2.3. The consumption of MEA is shown Figure 2.4.

Disregarding ammonia, the main degradation product in this experiment was HEF, as shown in Figure 2.3. Thereafter, in declining order; formate, HEGly, BHEOX

and HEI. The terminal concentrations of these products in this experiment were significantly lower than the concentrations which will be presented for the closed loop experiment.

Data from this experiment, together with the closed loop experiment, see section 2.3, was used to find the rate equations. See section 6.

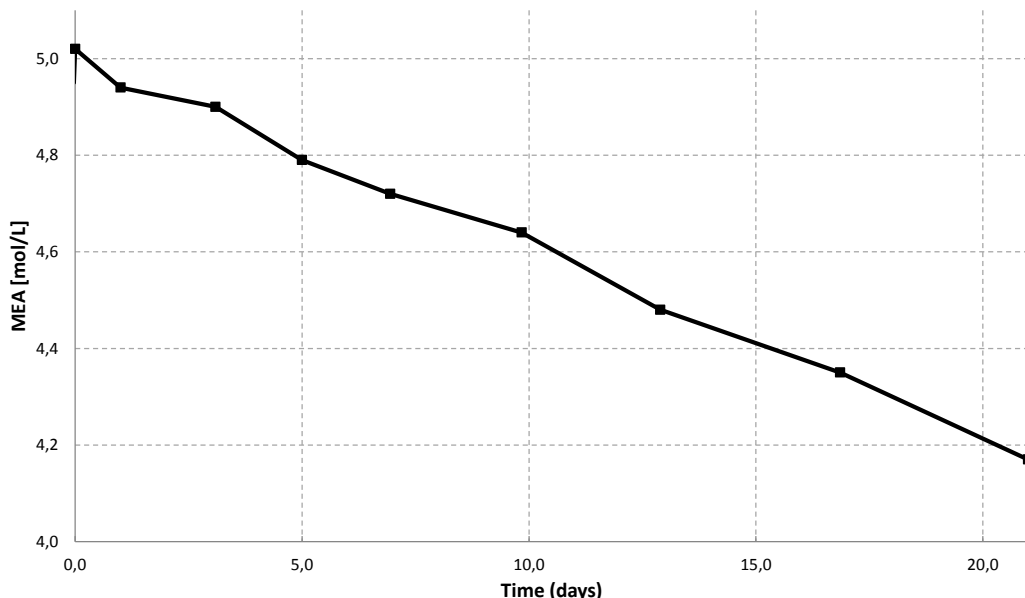


Figure 2.4: Measured reactants of experiment 1; open loop. MEA (■).

2.3 Experiment 2: Closed Loop

As mentioned for experiment 1, in section 2.2, these experimental data were retrieved from Vevelstad (2012) [25]. Due to confidentiality agreements, the raw data from this experiment will not be presented in this document.

This experiment was carried out in a closed loop laboratory setup as described in section 2.1.2, and was performed in the time period 1/6-2011 - 22/6-2011. 0.91 L/min of a 30 % (weight) MEA solution, loaded $\alpha = 0.4$ CO_2 , was circulated through the reactor. 24.6 NL/min air was circulated through the reactor. The temperature was kept between 50 – 55 °C, liquid samples were taken out regularly from the reactor, and CO_2 and O_2 in the gas phase was continuously logged.

The production of HEF, HEI, BHEOX, HEGly, ammonia and formic acid in addition to the aqueous concentration of iron ions are shown in Figure 2.5. The consumption of MEA and the gas phase oxygen profile is shown Figure 2.6. Notice that the unit of the iron ion concentration differs from the units for the other components in Figure 2.5.

In opposite to the open loop experiment, section 2.2, the main degradation product in this experiment, excluding ammonia, was HEI. Thereafter, in declining order; HEF, formate, HEGly and BHEOX. Ammonia was not measured during this experiment, except for one point when the experiment was finished. This point was considered when the rate equations were developed.

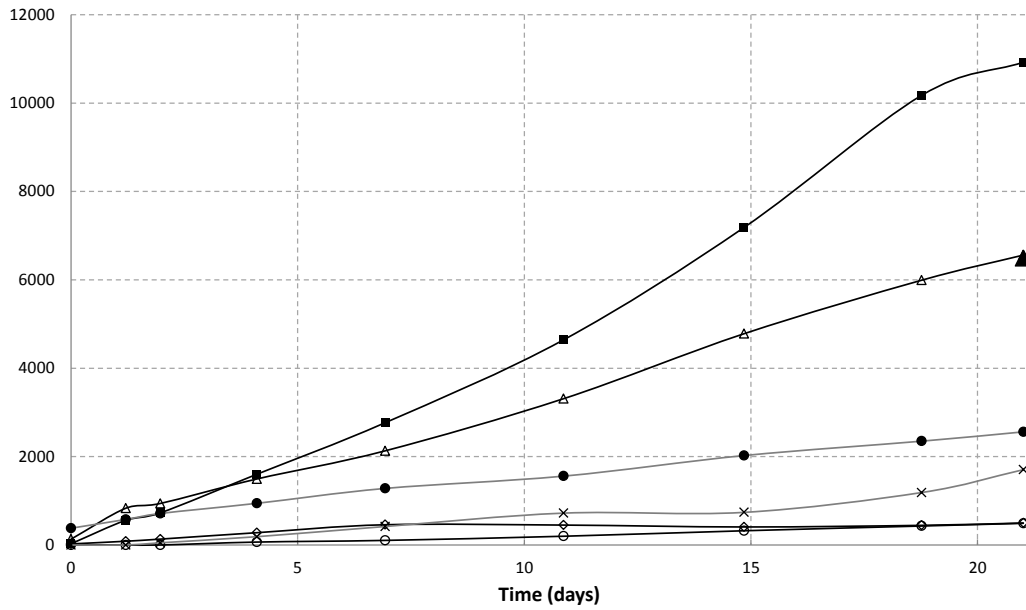


Figure 2.5: Measured products of experiment 2; closed loop. HEF (Δ), HEI (\blacksquare), BHEOX (\circ), HEGly (\diamond), ammonia (\blacktriangle), and formate (\times) in unit [$\mu\text{g/mL}$]. Additionally Fe^{3+} (\bullet) in unit [$\mu\text{g/L}$].

A note to these results is that the experimental setup was opened to the environment at day 8. This is evident from the gas phase profile of oxygen in Figure 2.6, which is showing a peak at day 8. The peak is further commented in section 4.1, and discussed in section 11.1.3.

As mentioned in the previous section, this experiment was one of two used to find the rate equations. See section 6.

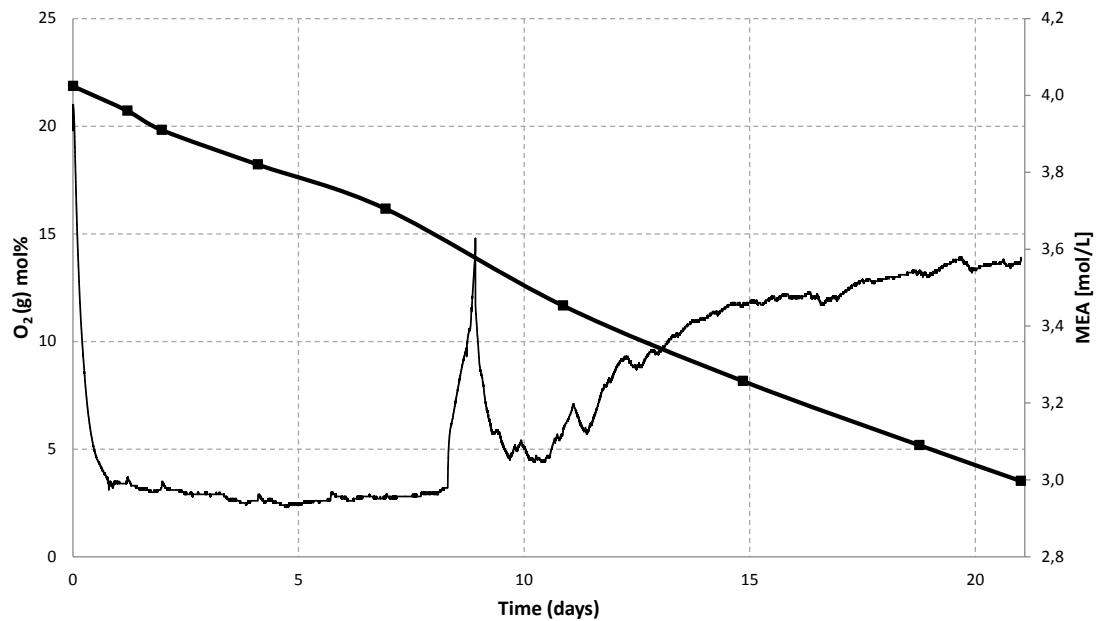


Figure 2.6: Reactants of experiment 2; closed loop. MEA(\blacksquare) and $\text{O}_2(\text{g})$ (—).

2.4 Experiment 3: Open Loop with Iron Ions

These experimental data were retrieved from Grimstvedt (2012) [23]. Due to confidentiality agreements, the raw data form this experiment is not presented in this document.

This experiment was carried out in an open laboratory setup as described in section 2.1.1, in 2009, while the samples were reanalyzed in 2011. The reactor initially held 1082 g 30 % (weight) MEA solution, loaded $\alpha = 0.4 CO_2$, in addition to 1 mM $FeSO_4$. 350 mL/min air and 7.5 mL/min CO_2 was bubbled through the reactor. The temperature was kept at 55 °C, and liquid samples were taken regularly from the reactor.

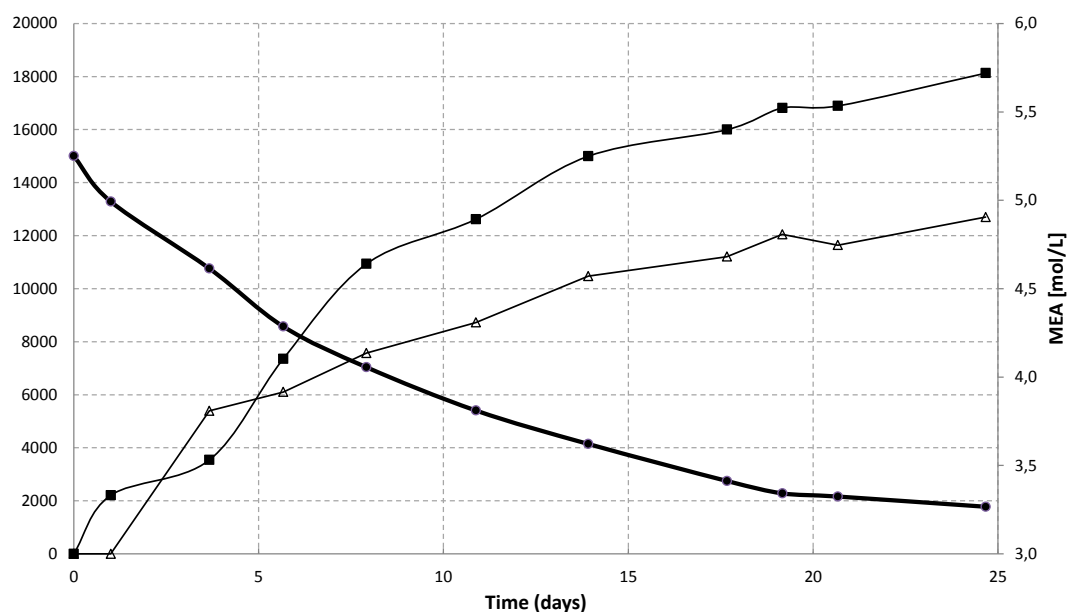


Figure 2.7: Measured products and -reactant of experiment 3; open loop with iron ions. HEF (Δ) and HEI (\blacksquare) concentrations in [ug/mL] on the left axis. MEA(\bullet) concentration in [mol/L] on the right axis.

The production of HEF and HEI, in addition to the consumption of MEA and the aqueous concentration of iron ions in this experiment is presented in Figure 2.7.

This experiment was not used to find rate equations, but was used to test the model developed based on the two previous experiments. See section 6.4.5.

Chapter 3

The Models

This chapter will present the equations used to model the degradation experiments. Two models were applied, one for the open loop- and one for the closed loop laboratory setup presented previously in chapter 2. To make the time spent on fitting the rate equations as short as possible, it was desirable to keep the models simple.

The following sections will firstly present the model applied for the open loop laboratory setup, thereafter present the model used for the closed loop setup.

3.1 Semi Flow Batch Reactor (SFBR) Model

A semi flow batch reactor model was obtained in literature by Schafflein and Russell (1968) [30]. This was used to model the open experiment setup, see section 2.1.1. The liquid was assumed well-mixed batch, and the gas was assumed well-mixed plug flow. An illustration of the model is given in Figure 3.1.

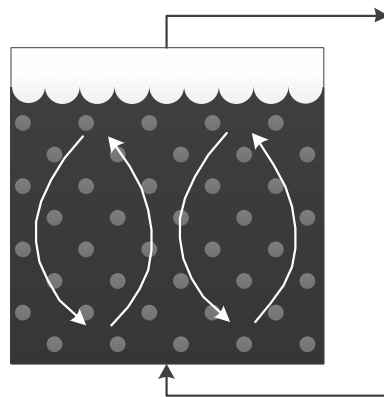


Figure 3.1: Illustration of the semi-flow batch reactor model. Gas enters the bottom of the reactor, gets perfectly mixed and reacts with the liquid, before the gas leaves the top of the reactor.

Gas phase:

$$G_{in}y_{0,j} - G_{out}y_j - K_{G,j}aV_LP(y_j - C_j\frac{H_j}{P}) = 0 \quad (3.1.1)$$

Liquid phase:

$$K_{G,j}aP(y_j - C_j\frac{H_j}{P}) - R_{x,j} = \frac{dC_j}{dt} \quad (3.1.2)$$

Solving equation 3.1.1 for y_j , and substituting y_j in equation 3.1.2 provided equation 3.1.3:

$$K_{G,j}aP\left(\frac{G_{in}y_{0,j} + K_{G,j}aV_LC_jH_j}{G_{out} + K_{G,j}aV_LP} - C_j\frac{H_j}{P}\right) - R_{x,j} = \frac{dC_j}{dt} \quad (3.1.3)$$

The MatLab implementation of this model is shown in appendix D.2.2 and D.2.3.

3.2 Batch Reactor Model

A batch reactor model was obtained in literature by Schaftlein and Russell (1968) [30]. This was used to model the closed loop experiment setup, see section 2.1.2. The liquid and the gas were assumed to be a well-mixed two phase batch. An illustration of the model is given in Figure 3.2.

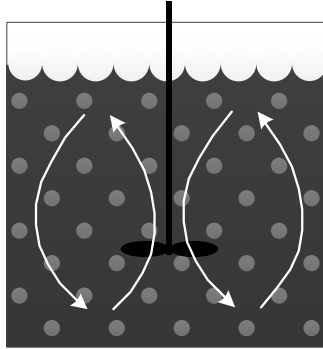


Figure 3.2: Illustration of the batch reactor model. Gas and liquid is perfectly mixed in the reactor. No in- or outflows.

Gas phase:

$$-K_{G,j}aV_LP(y_j - C_j\frac{H_j}{P}) = \frac{d}{dt}\left[(V_LNV_b)\frac{Py_j}{RT}\right] \quad (3.2.1)$$

Where NV_bV_L could be written as:

$$NV_bV_L = V_G \quad (3.2.2)$$

Since the model was to be used on a circulating gas absorber system, the interfacial mass transfer area, a , pressure, P , temperature, T , gas volume, V_G and liquid volume, V_L , were assumed to be independent of time.

These assumptions resulted in the following gas phase equation:

$$-K_{G,j}aRT\frac{V_L}{V_G}\left(y_j - C_j\frac{H_j}{P}\right) = \frac{dy_j}{dt} \quad (3.2.3)$$

And the following equation for the liquid phase:

$$K_{G,j}aP\left(y_j - C_j\frac{H_j}{P}\right) - R_{x,j} = \frac{dC_j}{dt} \quad (3.2.4)$$

Schaftlein and Russell (1968) [30] stated that this model additionally would require an over-all gas phase balance. Unfortunately, due to limitations in the experimental data, it was not possible to provide this balance. This is further discussed in section 11.1.6.

The MatLab implementation of this model is shown in appendix D.2.5 and D.2.6.

3.3 Gas-Side Mass Transfer Coefficient

The inter phase mass transfer coefficient, K_G was defined by the following equation:

$$\frac{1}{K_{G,j}} = \frac{H_j}{k_{L,j}} + \frac{1}{k_{G,j}} \quad (3.3.1)$$

Since the reactions being investigated in this study were progressing in a weekly time scale, see figures in chapter 2, they were considered slow. According to Schaftlein and Russel (1986) [30], for slow reactions, the gas phase mass transfer resistance term, $\frac{1}{k_G}$, was reasonable to neglect. This was due to the reactions being rate limiting, not the gas phase mass transfer resistance.

The expression for the overall interphase mass transfer coefficient, equation 3.3.1, could thus be rewritten to the following form:

$$K_{G,j} = \frac{k_{L,j}}{H_j} \quad (3.3.2)$$

3.4 The Reaction Rate Expression

Since the models were to be used to fit rate equations to the experimental data, it was essential to build a sensible rate equation. Equation (3.4.1) shows the rate equation applied in the models. This is a common way to setup the rate expression; a positive term to count the forward reaction, and a negative term to count the backward reaction and equilibrium effects.

3 THE MODELS

$$R_{x,i} = k_i \prod_{j=1}^N C_j^{p_{i,j}} - k_{-i} \prod_{j=1}^N C_j^{q_{i,j}} \quad (3.4.1)$$

Where k_i was expressed by;

$$k_i = A_i + B_i \cdot C_{cat}^{p_{i,cat}} \quad (3.4.2)$$

,and k_{-i} was analogously expressed by:

$$k_{-i} = A_{-i} + B_{-i} \cdot C_{cat}^{q_{i,cat}} \quad (3.4.3)$$

Equations (3.4.2) and (3.4.3) shows how this rate expression was modified to include the catalytic effects. The motivation for formulating the rate expression like this, and the evolution of the expression is given in chapter 6.

Chapter 4

Degradation Reactions

To provide a reasonable model of the degradation reactions, it was important to start out with reaction equations that were as accurate as possible. Unfortunately, when this study was conducted, several of the reaction mechanisms leading to the degradation products presented in chapter 2, were poorly understood, or not known at all.

As mentioned, it was a lack knowledge regarding the pathways of formation for several of these degradation products. Therefore it would, as this chapter will explain, sometimes become necessary to choose a pathway of formation that could not be further justified. Of this reason, the following sections will aim to present the foundation of the resulting reaction equations as thorough as possible for the pathways in question.

The formation of salts and ions from the degradation products were disregarded in this study. Even though the pH was high in the amine solution, and all acids formed in the solution would be in ionic form, this knowledge served no purpose during the modeling of the reaction rates. It was also of interest to keep the reactions complexity low, because the knowledge of several reactions still was at a sparse level. Additionally, further reactions with formed acids, could be implemented after the rate equations for the formation of the acids were found.

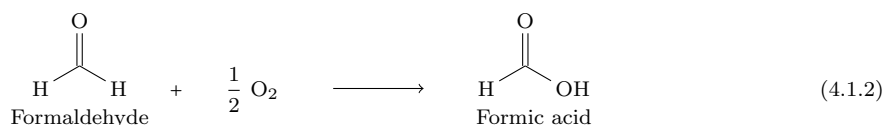
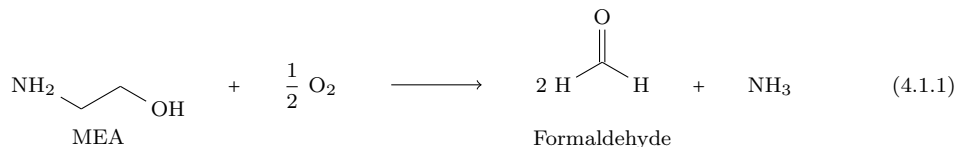
4.1 Reaction 1 and -2: Formation of Formate

The first degradation reaction to be found, was the formation of formaldehyde, and its further reaction to formic acid. Formate was measured in relatively high concentrations in the degradation experiments, and formic acid was known to be a reactant to form HEF (Lepaumier et al. (2011) [21]).

There were two suggested pathways for formation of formic acid, the general oxidation of MEA, and the hydrogen abstraction mechanism.

4.1.1 MEA Oxidation Pathway

The following two reactions were proposed as standard pathways to form formic acid:



To investigate this proposal, the molar quantities of all components in the closed loop experiment were calculated, see Table 4.1.

Table 4.1: Molar quantities of the measured compounds in degradation experiment 1, section 2.3.

	Initial	Terminal
MEA [mol]	2.926	2.183
MEA reacted [mol]	0	0.742
Ammonia [mol]	0	0.278
Oxygen [mol]	0.0226	0.0144
Formate [mol]	0	0.0317
HEF [mol]	0.00108	0.0536
HEI [mol]	0.000184	0.0709

The table shows that the reacted amount of MEA, was 16 times larger than the stoichiometric total amount of oxygen in the gas phase. In addition, the produced amount of ammonia was 6 times greater than the stoichiometric total amount of oxygen in the gas phase. Additionally Table 4.1 shows that less than half of the total amount of oxygen in the system was consumed.

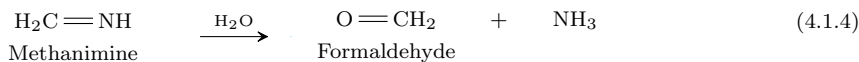
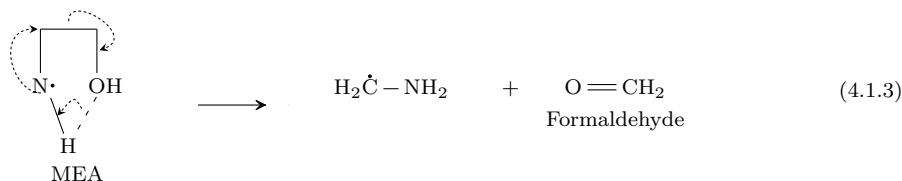
Assuming that the closed loop experiment actually was completely closed, the mechanism proposed above would not occur due to lack of oxygen. Another mechanism was therefore proposed, section 4.1.2. Nevertheless, it will later become clear that air was leaking into the system, this will be discussed in section 4.1.3.

4.1.2 Hydrogen Abstraction Mechanism

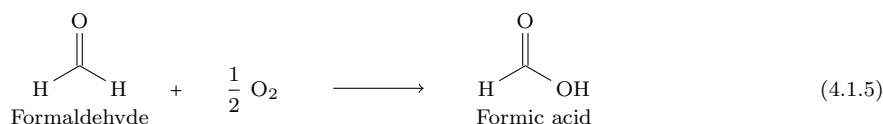
Since the first mechanism demanded more oxygen than assumed present in the system, the hydrogen abstraction mechanism, documented by Petryaev and Pavloc [27] (1984) and Goff and Rochelle [18] (2004), was proposed.

The hydrogen abstraction could possibly attack different atoms in the molecule, assuming the nitrogen was attacked, the mechanism would look like the following:

4.1 Reaction 1 and -2: Formation of Formate



The mechanism would need oxygen as a radical initiator, but not consume oxygen like reaction (4.1.1).



This mechanism would fit better with the assumption of the closed loop experiment being airtight. The total oxygen consumption of reaction (4.1.6) and (4.1.7), was significantly reduced compared to (4.1.1) and (4.1.2), enough for the mentioned assumption to hold.

4.1.3 Modeled Reactions

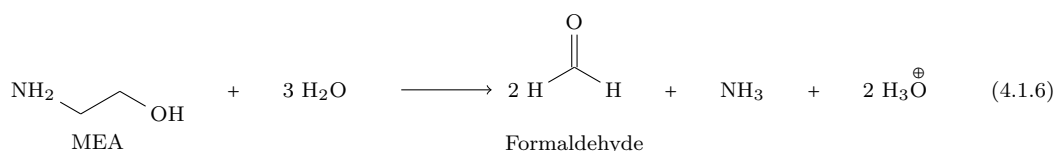
The oxygen profile in the closed loop experiment, shown in Figure 2.2, was showing an odd tendency. This could indicate that an oxygen leakage was present during the experiment. Excluding the peak at day 9, which was caused by opening the apparatus, Figure 2.2 showed a tendency of an increasing oxygen level after day 10. This was most likely caused by a leakage. Additionally, the oxygen level in the experiment never fell below 3%(mol), which would be expected in such an oxygen consuming environment.

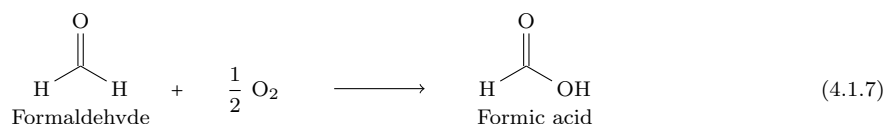
With this tendency taken into account, both the previous stated mechanisms could potentially have taken place during the experiment. With good arguments for both previously stated mechanisms, Figure 2.2 was studied again. It was clear that the oxygen peak at day 9, which was earlier excluded, could indicate which mechanism was taking place.

The oxygen peak was not followed by an increased MEA consumption, which could be expected by a primary degradation reaction as dependent of oxygen as reaction (4.1.1). Anyhow, this did not have to be the case if there never were a shortage for oxygen in the liquid phase.

The hydrogen abstraction mechanism was chosen to represent the formation of formaldehyde in the degradation model. This is further discussed in section 11.1.3.

The following two reactions were implemented in the following simplified and stoichiometric form:

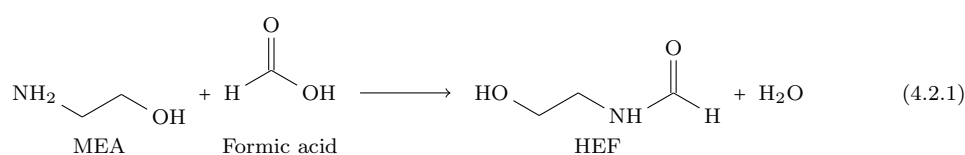




4.2 Reaction 3: Formation of HEF

N-(2-hydroxyethyl)-formamide (HEF) was, as seen in section 2.2 and section 2.3, one of the major degradation products. It was therefore important to model the formation of this product.

The following mechanism was proposed, and is documented by Lepaumier et al. (2011) [21], for the formation of HEF:

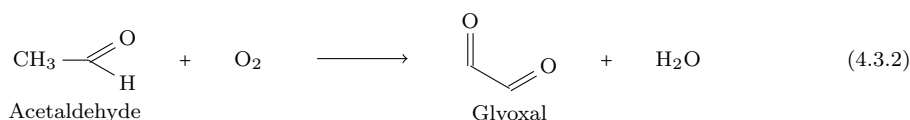
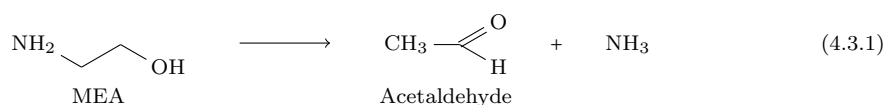


Unlike several of the other degradation reactions, this pathway of formation was well accepted, and was also documented by Supap et al. (2011) [33]. The reaction was therefore implemented in the model as showed in equation (4.2.1).

4.3 Reaction 4 and -5: Formation of HEI

1-(2-hydroxyethyl)-imidazole (HEI) was also a significant degradation product in the degradation experiments, section 2.2 and section 2.3. It was therefore attempted to model this compound.

In addition to formaldehyde, which formation is described in section 4.1, the formation of HEI was believed to consume glyoxal. The following two steps were suggested as likely pathways to glyoxal:

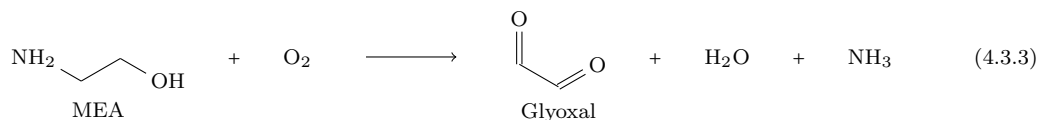


The formation of acetaldehyde (equation (4.3.1)) was suggested to be a radical initiated reaction, described by Petryaev and Pavloc (1984) [27] and Goff and Rochelle (2004) [18], and was therefore not described to consume oxygen.

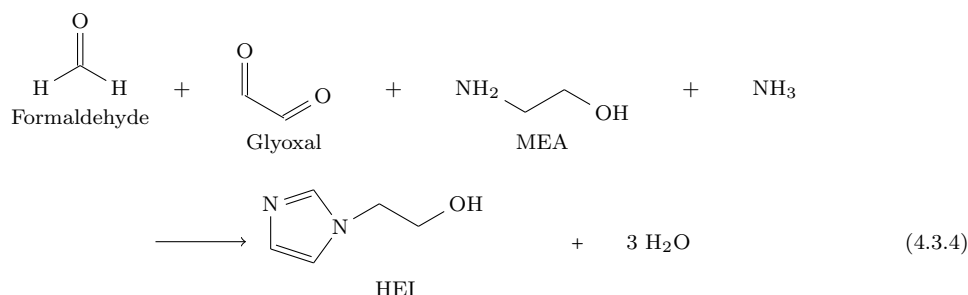
Several other detailed reaction mechanisms for the two reactions were suggested, but the stoichiometric ratio between the reactants and products in these were the same as described above. As long as the stoichiometry, the reactants and products were the same, the selection of mechanism would not influence the model. The mentioned optional mechanisms are therefore not presented in this document, and were not emphasized during this work.

4.4 Reaction 6 and -7: Formation of BHEOX

The concentration profile of acetaldehyde was not recorded in the degradation experiments presented in section 2. Since the role this compound was only as an intermediate in just this reaction, modeling of acetaldehyde served no purpose. Acetaldehyde was therefore assumed to be in pseudo steady-state, and the two reactions (equation (4.3.1) and (4.3.2)) were combined to one reaction, equation (4.3.3):



With the reaction pathways to all reactants, the formation of HEI was suggested according to patent Arduengo et al. (2001) [3]:

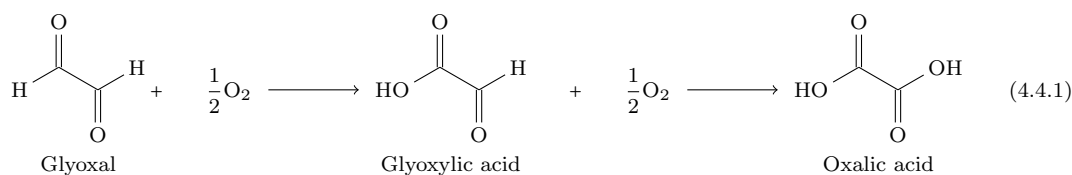


The formation of glyoxal and HEI was modeled as described in equation (4.3.3) and equation (4.3.4).

4.4 Reaction 6 and -7: Formation of BHEOX

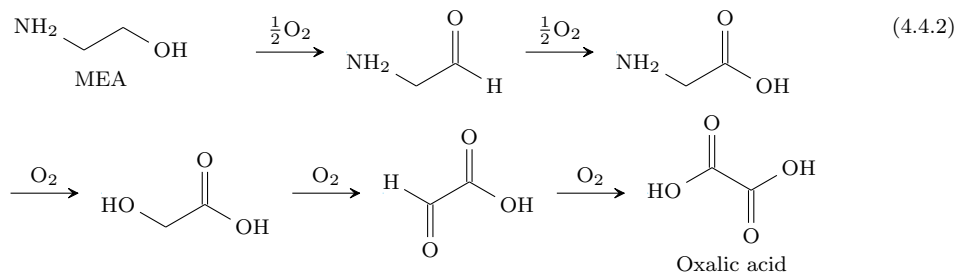
N,N-bis(2-hydroxyethyl)oxalamide (BHEOX) was known to be a degradation product in several degradation experiments (Lepaumier et al. (2011) [21], and da Silva et al. (2012) [14]). The concentrations of this compound were though small in the experiments which were to be modeled, section 2.2 and 2.3. Nevertheless, an attempt of modeling these concentration profiles were made.

To produce BHEOX, oxalic acid was first needed as a reactant. Two different reaction pathways were proposed to form oxalic acid. The first was the oxidation of glyoxal (equation (4.4.1)), as described in atmospheric chemistry literature. Buxton et al. (1997) [12] describes the oxidation of glyoxal via glyoxylic acid to oxalic acid, initiated by $\cdot\text{OH}$ -radicals, in an oxygenated aqueous solution:



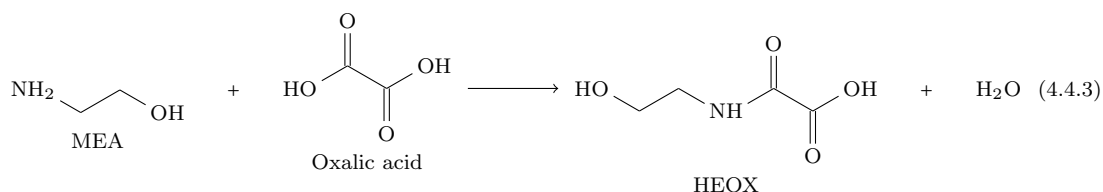
The second proposal was based on direct oxidation of MEA (equation (4.4.2)), documented by Rooney et al. (1998) [29]:

4 DEGRADATION REACTIONS

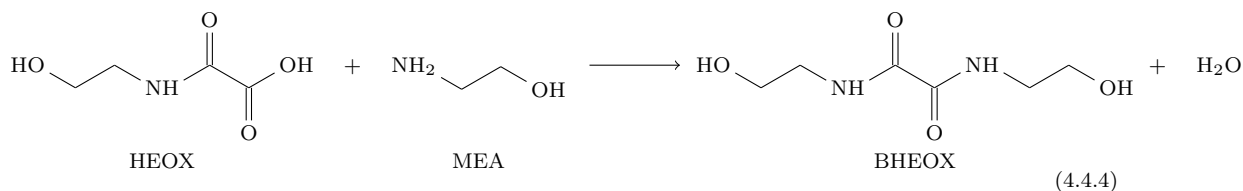


There were no experiments that supported either pathways. Due to the fact that a reaction to form glyoxal already was proposed, and that this reactant was consumed by reaction (4.4.1), this pathway was chosen for the formation of oxalic acid.

After being formed, oxalic acid was proposed to react with MEA to form HEOX. An intermediate which was not quantified in the experiments in chapter 2.



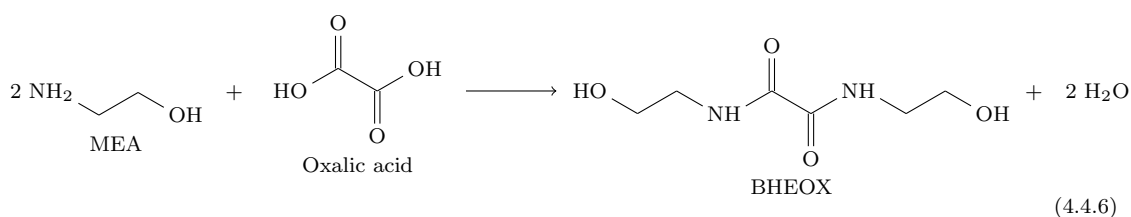
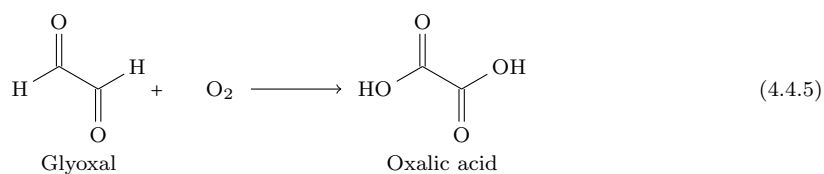
HEOX was then to react with MEA, to form the end product, BHEOX:



This pathway is documented by da Silva et al. (2012) [14] and Lepaumier et al. (2011) [21].

4.4.1 Modeled Reactions

The above reactions were merged into the two following reactions, which were implemented:

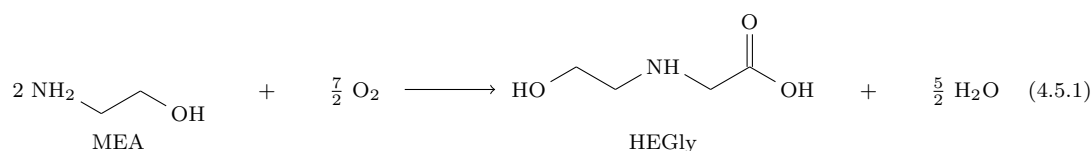


4.5 Reaction 8: Formation of HEGly

2-(2-hydroxyethylamino)acetic acid (HEGly) was the third most abundant degradation product in the degradation experiments presented earlier (see chapter 2), and it was therefore decided to implement the formation of this compound. Nevertheless, the knowledge about the reaction pathway leading to this product was very sparse. Three pathways were proposed:

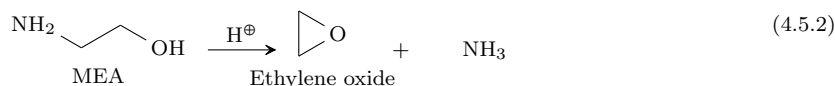
4.5.1 Oxidation Pathway

The general pathway to this product would be a straight forward oxidation of MEA:

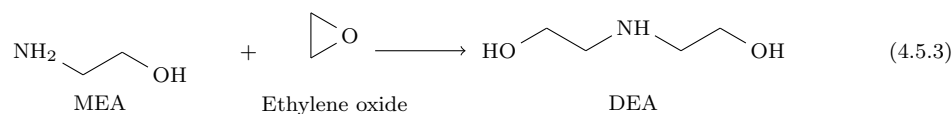


4.5.2 Reaction with Epoxide

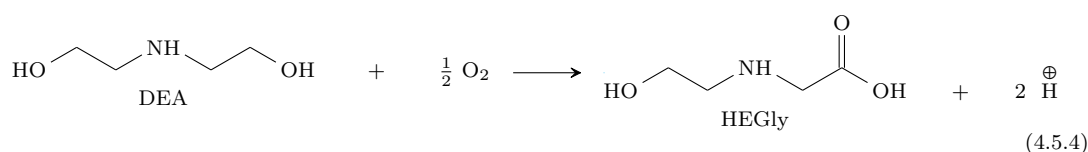
A reaction pathway involving epoxide was proposed. The epoxide was proposed to be formed as described in the following reaction equation, catalyzed by acid impurities as documented by Talzi (2004) [36]:



With the epoxide formed, the reaction would continue to diethanolamie (DEA), also described by Talzi (2004) [36]:



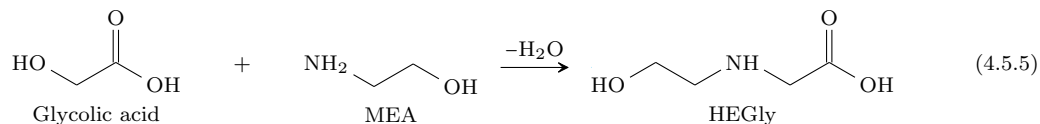
DEA could then be oxidized to form the final product, HEGly:



It is important to note that the pathway to HEGly was very uncertain, as also stated by da Silva et al. (2012) [14]. There were no literature available to support the last step in this pathway, but then again there were no sources to support any other pathways.

4.5.3 Reaction with Glycolic Acid

A third reaction was proposed; the formation of HEGly by a reaction between glycolic acid and MEA:

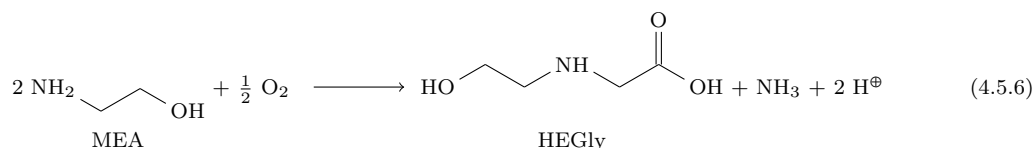


Though from an organic chemistry point of view, this would look like an unlikely reaction. This would be due to an expectation of the double bond with oxygen in glycolic acid to react more easily, than a substitution of the alcohol group. This kind of substitution would consequently produce a different product.

4.5.4 Modeled reactions

At the time of this document being written, it was not known which of these three mechanisms were forming HEGly. Unpublished experiments indicated that HEGly could be formed by several mechanisms at the same time, and that the formation could be initiated by both oxidative-, thermic- and radical conditions. Due to the great uncertainty attached to the formation of HEGly, the epoxy mechanism was chosen to represent the formation of HEGly. This was done bearing in mind that the other mechanisms would be equally good candidates to explain this reaction.

Since neither ethylene oxide- nor DEA concentration were measured in the experiments, they were assumed to be in pseudo steady-state. Equations (4.5.2), (4.5.3) and (4.5.4) were merged to one reaction equations, which was to be implemented:



4.6 Overview of Implemented Reactions

An overview of the degradation reactions, shown as they were implemented in the experimental reactor models, is given in Table 4.2. The reactions are balanced, but it is worth noticing that reaction 1 and -8 were not in charge balance. This was because of the radicals in the hydrogen abstraction mechanisms. The issue is further discussed in section 8.4 and section 11.2.3.

4.7 Catalytic Effects

Chi and Rochelle (2002) [13] and Sexton and Rochelle (2009) [31] among others, showed that some metals dissolved in the amine solution had catalytic effects on the oxidation of MEA. Sexton and Rochelle (2009) [31] showed that the order of metals with catalytic effects would be iron/copper>chromium/nickel>iron>vanadium, in a 7 M MEA solution at 55°C with a gas flow of 98% O₂ and 2% CO₂.

Of the mentioned metals, iron was the metal with highest concentration in the closed loop experiment (section 2.3), and according to Sexton and Rochelle (2009) [31] had the highest catalytic effect of the measured metals in this experiment. It was therefore decided to investigate the effect of iron in the experiments, see chapter 6.

Table 4.2: Merged Degradation Reactions as Implemented in the Models.

Nr.	Product	Reaction
1	Formaldehyde	$\text{NH}_2\text{CH}_2\text{CH}_2\text{OH} + 3\text{H}_2\text{O} \longrightarrow 2\text{HCHO} + \text{NH}_3 + 2\text{H}_3\text{O}^{\oplus} + 2\text{e}^{\ominus}$ <p style="text-align: center;">MEA Formaldehyde</p>
2	Formic acid	$\text{HCHO} + \frac{1}{2}\text{O}_2 \longrightarrow \text{HCOOH}$ <p style="text-align: center;">Formaldehyde Formic acid</p>
3	HEF	$\text{NH}_2\text{CH}_2\text{CH}_2\text{OH} + \text{HCOOH} \rightleftharpoons \text{HOCH}_2\text{CH}_2\text{NHCHO} + \text{H}_2\text{O}$ <p style="text-align: center;">MEA Formic acid HEF</p>
4	Glyoxal	$\text{NH}_2\text{CH}_2\text{CH}_2\text{OH} + \text{O}_2 \longrightarrow \text{OHCCHO} + \text{H}_2\text{O} + \text{NH}_3$ <p style="text-align: center;">MEA Glyoxal</p>
5	HEI	$\text{NH}_2\text{CH}_2\text{CH}_2\text{OH} + \text{HCHO} + \text{OHCCHO} + \text{NH}_3 \rightleftharpoons \text{Imidazole-CH}_2\text{CH}_2\text{OH} + 3\text{H}_2\text{O}$ <p style="text-align: center;">MEA Formaldehyde Glyoxal HEI</p>
6	Oxalic acid	$\text{OHCCHO} + \text{O}_2 \rightleftharpoons \text{HOOC-COOH}$ <p style="text-align: center;">Glyoxal Oxalic acid</p>
7	BHEOX	$2\text{NH}_2\text{CH}_2\text{CH}_2\text{OH} + \text{HOOC-COOH} \rightleftharpoons \text{HOCH}_2\text{CH}_2\text{NHCOCONHCH}_2\text{CH}_2\text{OH} + 2\text{H}_2\text{O}$ <p style="text-align: center;">MEA Oxalic acid BHEOX</p>
8	HEGly	$2\text{NH}_2\text{CH}_2\text{CH}_2\text{OH} + \frac{1}{2}\text{O}_2 + 2\text{H}_2\text{O} \rightleftharpoons \text{HOCH}_2\text{CH}_2\text{NHCH}_2\text{CHO} + \text{NH}_3 + 2\text{H}_3\text{O}^{\oplus} + 2\text{e}^{\ominus}$ <p style="text-align: center;">MEA HEGly</p>

Chapter 5

Parameter Fitting

To fit the experiment models to the experimental data, obtaining the reaction rate parameters, different methods were applied. The methods applied will be presented in the following sections.

The parameters that were to be found, when fitting the models to the experimental data, were mainly of two categories;

- Rate coefficients, k_i
- Reaction orders, q_j and p_j

,in the generalized rate equation:

$$R_{x,i} = (A_i + B_i \cdot C_{cat}^{q_{cat}}) \prod_{j=1}^N C_j^{q_j} - (A_{-i} + B_{-i} \cdot C_{cat}^{p_{cat}}) \prod_{j=1}^N C_j^{p_j} \quad (5.0.1)$$

For the j component in reaction number i , with N number of components.

When fitting these parameters, these two categories of parameters, had very different properties. The rate coefficients could be of large values, and the models would handle major changes in these parameters without problems. This was in contrast to the reaction orders, which would typically be values between -1 and 2, and where small changes that could cause the models to fail.

Additionally the models were calculated using ordinary differential (ODE) solvers. This meant that for each iteration in the parameter search, the ODE-solver had to recalculate all concentration profiles.

With all the parameters in the reactions equations to search for, in addition to a term for oxygen leakage, there were in total a maximum of 64 parameters to find.

These properties of the system made the optimization of the parameters an unstable and time consuming problem.

5.1 Program Structure

Figure 5.1 shows how the MatLab-files were connected to search for the best parameters. This section will go through the structure of the program.

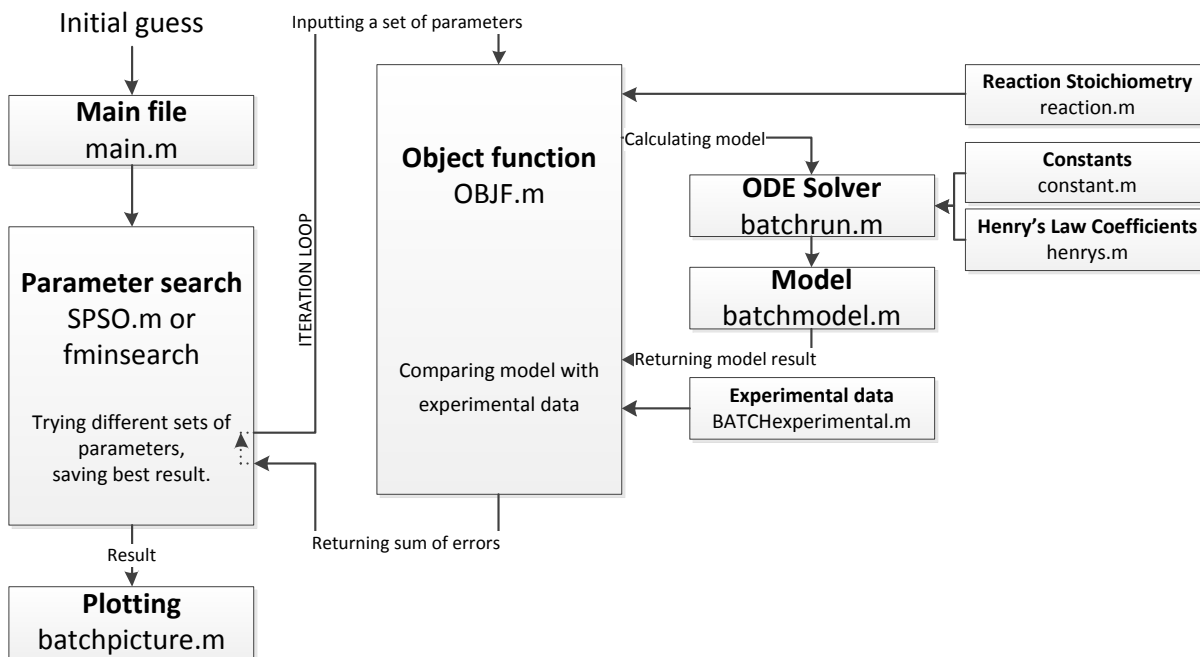


Figure 5.1: Illustration of the program structure for parameter search.

An initial guess was entered in the main file. The initial guess was then structured as a vector or matrix of the range of each parameter, depending on which parameter fitting method to be applied.

The initial guess vector or -matrix was then sent to the parameter fitting routine. The fitting routine could either be the MatLab-routine *fminsearch*, or particle swarm optimization, both described in section 5.2. The parameter fitting routine would generate a set of new parameters, based on the initial guess. The new set of parameters was then sent to the object function.

In the object function the parameter set was received and combined with the reaction stoichiometry and already found parameters in a large vector. This vector was then sent to the file running the ODE-solver.

In the ODE-solver file all necessary experiment specific data was given, such as reactor volume, initial concentrations, temperature, pressure and so on. The reaction stoichiometry was also inputted from a separate file. With all the necessary information available, the model equations, stored in the model file, were solved. The results were then sent back to the object function in a matrix.

Back in the object function, the experimental data was retrieved from a file containing this information. The corresponding modeled values were extracted from

the result matrix. The experimental values and the modeled values were then compared in the following equation:

$$E = \frac{1}{N} \sum_{j=1}^N \frac{|C_{j,Experimental} - C_{j,Modeled}|}{C_{j,Experimental}} \cdot 100 \quad (5.1.1)$$

Where N , was the total number of experimental points, $C_{j,Experimental}$, the experimental value, $C_{j,Modeled}$, the modeled value, and E , the error.

The error was then sent back to the parameter searching routine, which would repeat the operation until the iteration toleration was met. The result of the iteration was then sent to a file plotting the result.

The MatLab files used for the parameter search are presented in appendix D.

5.2 Methods of Parameter Fitting

In Figure 5.1 the program structure was exemplified with the particle swarm optimization file (SPSO.m) calling the object function. Yet, several other optimization functions were also applied during the work with parameter fitting. These methods will be presented in the following sections.

5.2.1 Manual Trial and Error

Manual trial and error was applied to find rate parameters in the models which would fit the experimental points. The method provided reasonable results, but the mutual dependency of some of the reactions made this method time consuming. This method was quickly replaced by automatic fitting routines.

5.2.2 Simplex Iteration

To improve the stability of the iterations, a built-in MatLab function was applied. *fminsearch* is a function searching for the lowest value of an object function, applying simplex iteration. The function is called with the following syntax:

$$X = \text{FMINSEARCH}(\text{FUN}, X0)$$

Where X is the optimized parameters, $X0$ is the initial guess values for the parameters, and FUN is the object function to be minimized.

The output value of the object function was to be a positive integer value, and was defined by equation (5.1.1), which provided percentage of total deviation.

This type of parameter fitting provided good results reasonably fast and was stable in the sense that it was approaching convergence. The disadvantage with the function was its dependency of the initial guess. The function was not able to detect other minimums than the one suggested by the initial guesses. In an attempt where the initial guess was changed to another point than the minimum, the solver was not able to find the minimum detected earlier.

5.2.3 Least-Squares Iteration

Least-squares iteration was provided by the MatLab-functions *fminunc*, and MODFIT, a MatLab-code written by Thor Mejdell, SINTEF, and Terje Herzberg, NTNU, made to fit models to experimental data.

For *fminunc* the object function described in equation (5.1.1) was applied, for MODFIT the program specified values were provided.

Neither of these methods succeeded in completing one iteration within 10 minutes, and of this reason it was decided to not spend more time on these methods.

5.2.4 Particle Swarm Optimization

A code applying particle swarm optimization (PSO) was provided by Diego Di Domenico Pinto, NTNU.

Particle swarm optimization was originally introduced by Kennedy and Eberhart (1995) [19] as a method of optimizing nonlinear functions applying the so-called particle swarm methodology.

The method applies a swarm of entities, or particles, spread out in the search space of the problem. Each particle is then evaluating the object function at its location, comparing it with its previous best location, and adding some random perturbation to determine its future velocity in the search space, for the next iteration. Additionally the particle compares its location with the previously best locations of its neighbor particles. In this way the particles are intended to cooperate as a swarm, to find the best solution. See Poli et al. (2007) [28] for more information.

Within PSO methods, there exist many variations. Most of them apply the global best communication topology, which means that a particle is attracted to the best position in the whole swarm. Ghosh et al. (2012) [17] argued that the described method often would provide false or premature convergence over multimodal fitness landscapes. They therefore argued that a method based on the local best topology, where a particle is attracted to the best location in its neighborhood, would ensure stability and asymptotic convergence.

The latter method is known as standard particle swarm optimization (SPSO), which was applied in this study.

The advantage of this method was its independence of the initial guess, and the fact that it was searching a wide range of parameter combinations to find a solution. The disadvantage was the time consumed due to a large number of iterations.

Chapter 6

Development of the Rate Equations

To clarify the challenges that were met, the choices made, and how the problems were solved, during the development of the rate equations. This chapter will aim to go through four stages in the development of the model, in chronological order. The fourth version will be the result of this development, and the section describing this version will therefore also contain an evaluation of the final rate equations.

6.1 First Version

In the early stages of the model development, only one degradation product was included. Due to the abundance of the compound in the experiments, and the relatively well known formation pathway, this compound was selected to be HEF.

$$\begin{aligned}R_{x,1} &= 5 \cdot 10^{-3}[MEA] \\R_{x,2} &= 380[O_2][CH_2O] \\R_{x,3} &= 2.5 \cdot 10^{-2}[CHOOH][MEA]\end{aligned}\tag{6.1.1}$$

Equation set (6.1.1) shows the reaction parameters that were found for this case, and Figure 6.1 and Figure 6.2 show the results of these parameters.

As equation set (6.1.1) shows, the reactions were assumed to be of first order of the reactants. All reactions were also assumed to be irreversible. As a result of these assumptions, only three parameters needed to be found to fit the model to the experimental data. This made the search for parameters quick and convenient, and the problem was easily solved applying manual trial and error and simple iteration. The problem with a model this simple, is obvious from Figure 6.1 and Figure 6.2. The rate equations were unable to describe the concentration profiles of the products as their concentrations were increasing with time.

When these rate equations were found, it was assumed that the closed loop experiment was completely closed from the environment. This led to the hypothesis that MEA could not be consumed by only oxidation reactions (see section 4.1.1). This was due to the fact that the initial oxygen amount in the system was too low

6 DEVELOPMENT OF THE RATE EQUATIONS

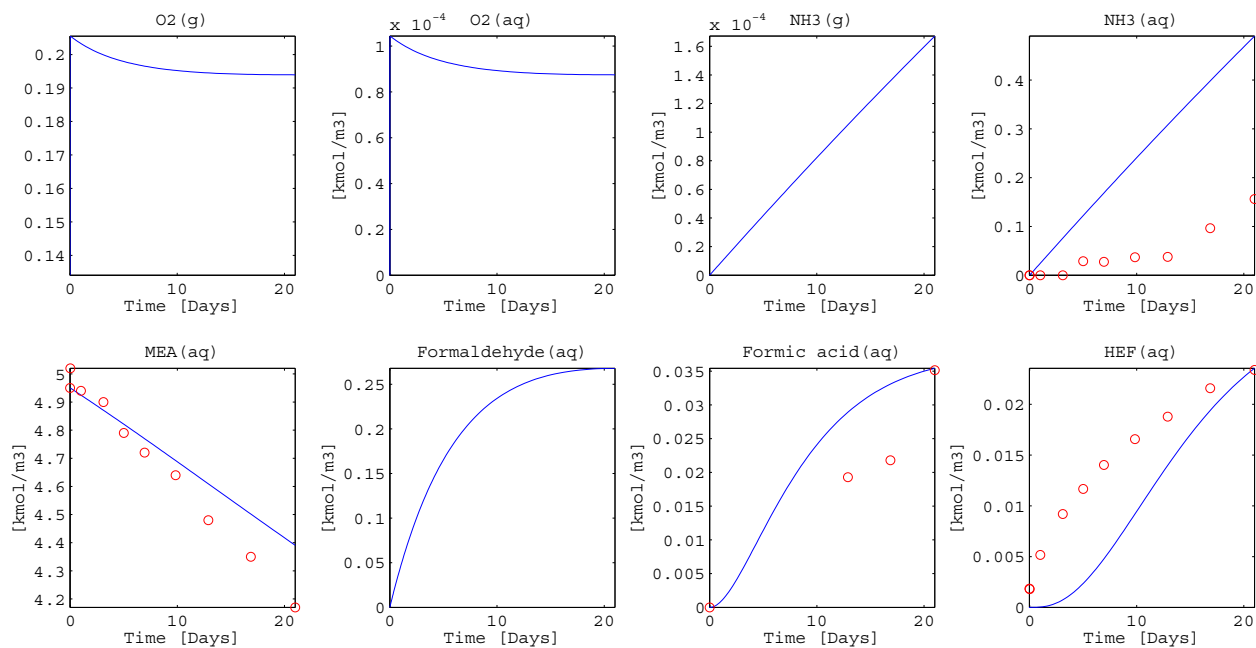


Figure 6.1: Experiment 1; open loop. 1st version of the rate equations. Experimental values (o) and modeled values (—).

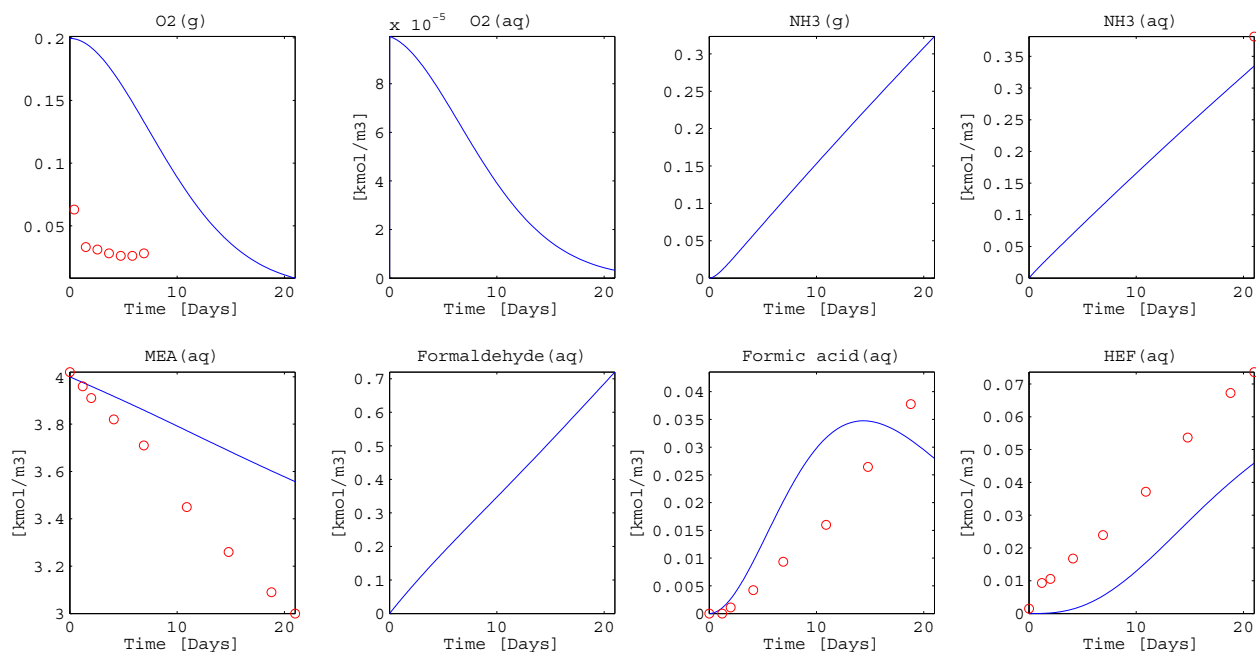


Figure 6.2: Experiment 2; closed loop. 1st version of the rate equations. Experimental values (o) and modeled values (—).

to explain the consumption of MEA, when considering a stoichiometric reaction with oxygen.

For this reason the hydrogen abstraction mechanism (section 4.1.2) was implemented for the MEA consumption and formation of formaldehyde. It was now possible to explain the full MEA consumption in the closed loop experiment, by this reaction. Nevertheless, when applying the rate parameters found for the open loop experiment on the model for the closed loop experiment, as done in Figure 6.2, the MEA consumption was not explained.

At this point in the model development there was also no parameter in the rate equations that differed the reaction rates between the open- and the closed loop experiment. A parameter which was later found to be the concentration of iron.

6.2 Second Version

In the next stage of the model development, the formation of HEI was added. The reaction parameters found for this case are shown in equation set (6.2.1).

$$\begin{aligned}
 R_{x,1} &= 5 \cdot 10^{-3}[MEA] \\
 R_{x,2} &= 900[O_2][CH_2O] \\
 R_{x,3} &= 3 \cdot 10^{-2}[CHOOH][MEA] \\
 R_{x,4} &= 5[O_2][MEA] \\
 R_{x,5} &= 5 \cdot 10^{-2}[MEA][CH_2O][NH_3][Glyoxal] - 100[HEI]
 \end{aligned}
 \tag{6.2.1}$$

In this case the reaction equations from the 1st version (equation set (6.1.1)) were kept, and the reactions leading to HEI was added.

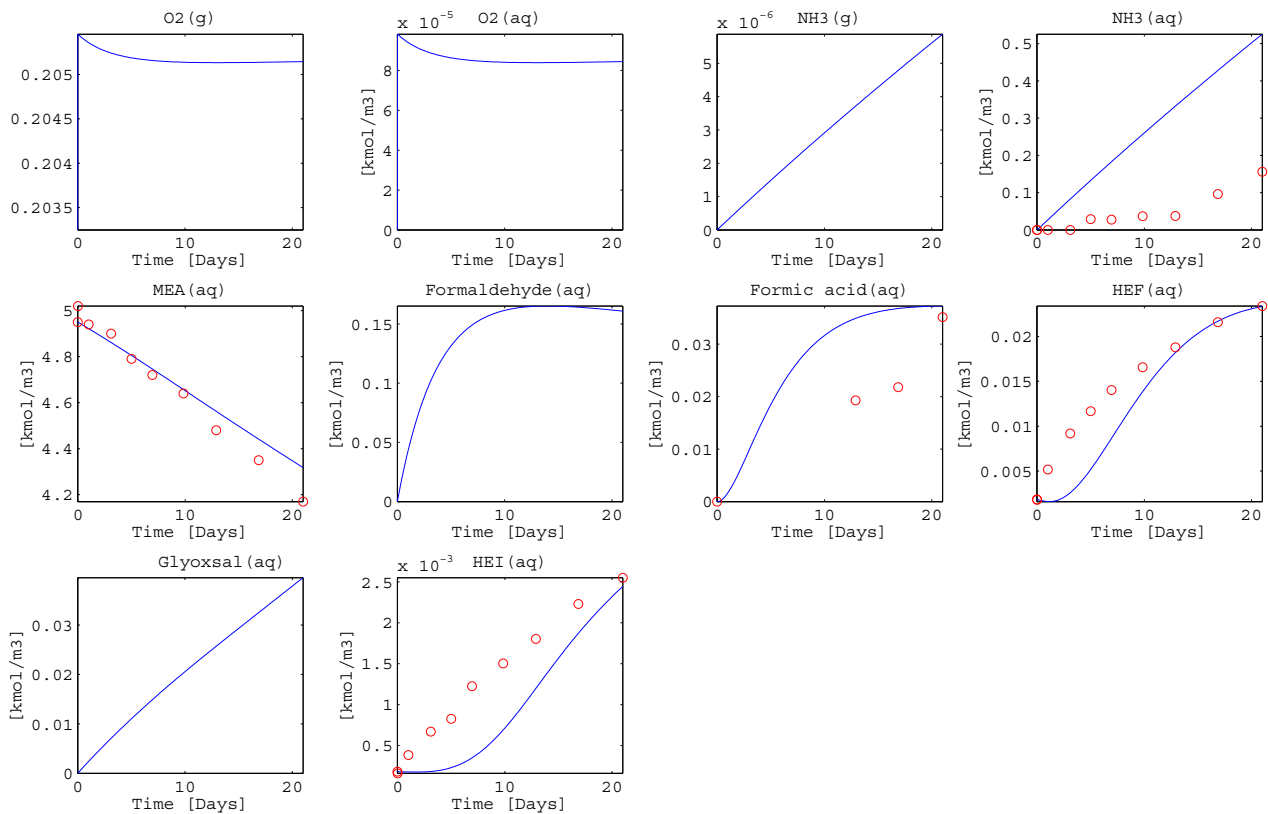


Figure 6.3: Experiment 1; open loop. 2nd version of the rate equations. Experimental values (o) and modeled values (—).

As equation set (6.2.1) is showing, reaction 5 was modeled as a reversible reaction. This was done in an attempt to match the modeled concentration curve, with the experimental points. Evident from the plots, Figure 6.3 and Figure 6.4, the attempt was only partly successful.

For the open loop experiment, Figure 6.3, the modeled profile was hitting three experimental points of HEI, as a result of the reverse nature of the rate equation for HEI. For the closed loop experiment, Figure 6.4, the model barely showed any production of HEI. The lack of HEI production in the closed loop model was mainly caused by lack of oxygen.

This version of the model made it clear that there had to be an oxygen leakage in the closed loop experiment. With several oxygen dependent reaction left to implement, an oxygen shortage after only two degradation products were implemented seemed unreasonable.

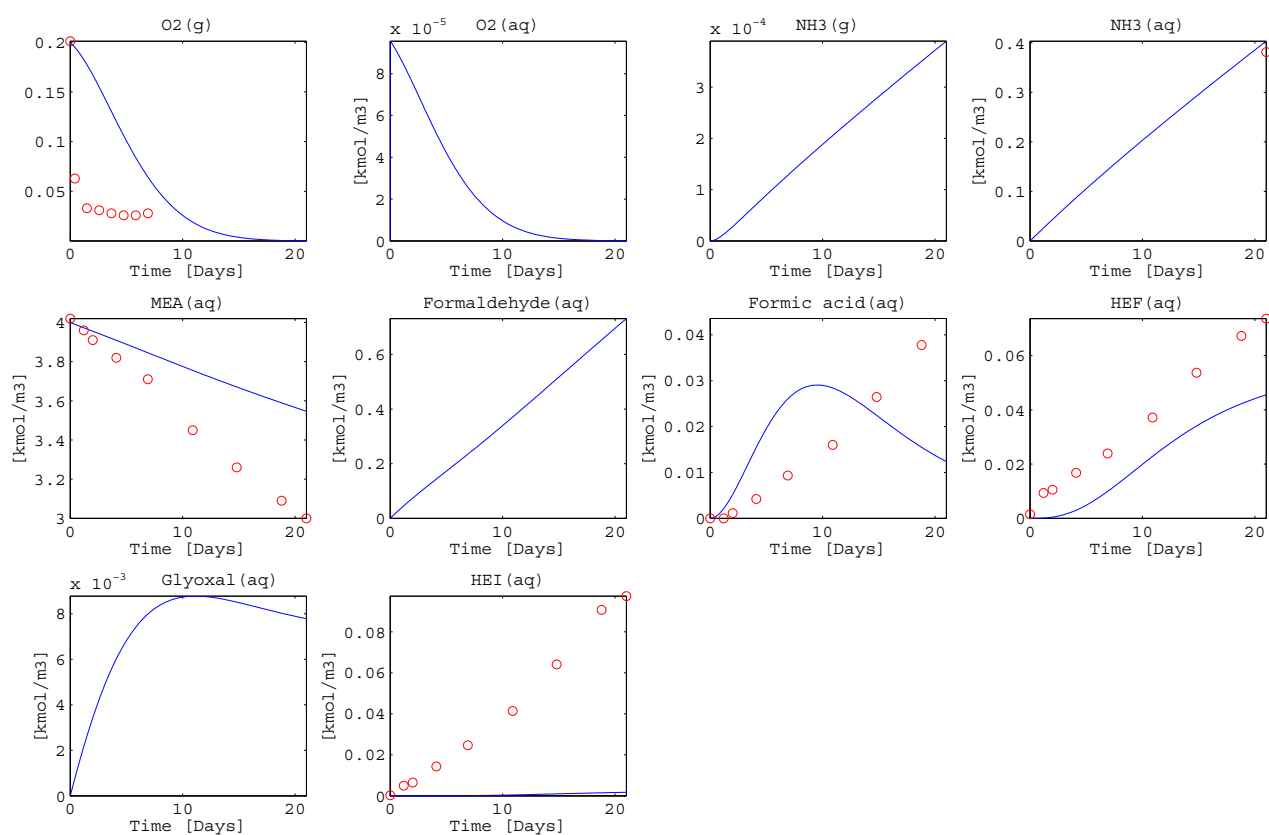


Figure 6.4: Experiment 2; closed loop. 2nd version of the rate equations. Experimental values (○) and modeled values (—).

In addition, it became clear that there had to be a factor involved in the closed loop experiment which allowed the reactions to speed up in this experiment, compared to the open loop experiment. This factor was found to be the concentration of dissolved iron in the closed loop experiment, which was zero in the open loop experiment.

6.3 Third Version

In the third version of the model, several big changes were made. The formation of BHEOX and HEGly was implemented, an oxygen leakage term was added, the catalytic effect of dissolved iron was implemented, and the reaction order of each reactant was included in the search for parameters.

$$\begin{aligned}
R_{x,1} &= 6.19 \cdot 10^{-3} [Fe^{3+}]^{-0.023} [MEA]^{1.2} \\
R_{x,2} &= 42.88 [Fe^{3+}]^{-1.920} [O_2] [CH_2O]^{1.23 \cdot 10^{-9}} \\
R_{x,3} &= 6.05 \cdot 10^2 [Fe^{3+}]^{-0.150} [MEA]^{2.68 \cdot 10^{-5}} [CHOOH]^{0.5} - 5.7 \cdot 10^4 [HEF]^{1.6} \\
R_{x,4} &= 1.31 [Fe^{3+}]^{-2.306} [O_2]^{1.1} [MEA]^{1.0} \\
R_{x,5} &= 1.03 \cdot 10^4 [Fe^{3+}]^{0.391} [MEA]^{8.60 \cdot 10^{-4}} [CH_2O]^{1.0} [NH_3]^{1.15} [Glyoxal]^{0.64} \\
&\quad - 7.97 \cdot 10^{12} [Fe^{3+}]^{1.43} [HEI]^5 \\
R_{x,6} &= 9.45 \cdot 10^4 [Fe^{3+}]^{-0.152} [O_2]^{0.7} [Glyoxal]^{1.2} - 7.9 \cdot 10^{-4} [Fe^{2/3+}]^{0.042} [Oxalic] \\
R_{x,7} &= 4.78 \cdot 10^{-3} [Fe^{3+}]^{-0.150} [MEA]^{2.4} [Oxalic]^{0.8} - 0.87 [BHEOX]^{1.4} \\
R_{x,8} &= 0.21 [Fe^{3+}]^{-1.699} [O_2] [MEA]^{1.9} - 3.2 \cdot 10^{-2} C_{Fe}^{0.1} [HEGly]
\end{aligned} \tag{6.3.1}$$

For convenience, the concentration profiles for ammonia were locked to the experimental points. This implied that time dependent equations, independent of reaction and mass transfer between the phases, was used to describe the experimental points of the liquid ammonia concentrations. As a consequence, the ammonia dependent rate equations, when the model was fitted to the experimental points, would describe the reaction rates as functions of the actual ammonia concentration, regardless of the ammonia concentration being modeled correctly or not. In this way the mass transfer of ammonia could be adjusted later, without affecting the rate equations. This is further discussed in section 11.1.4.

Equation set (6.3.1) shows the reaction equations found for this case, and Figure 6.5 and Figure 6.6 are showing the resulting plots. As the figures are showing, the model was now matching the experimental points much better than in the previous versions.

With the newly added terms for effect of iron, oxygen leakage and reaction orders, one set of equations could now describe most of the tendencies in both experiments. But this increased number of variables to be searched for, also caused the search for parameters to be a time consuming process.

Including the oxygen leakage term, which is not shown in equation set (6.3.1), the number of variables now became 47. This was a large number of variables compared to the previous version, where there were six variables to be searched for. The parameter search was done applying particle swarm optimization and simplex iteration (see section 5.2.2 and 5.2.4), in combination with manual trial and error.

The parameter search was done by firstly finding the rate coefficients and all reaction orders, except for iron, for the open loop experiment. Once these were

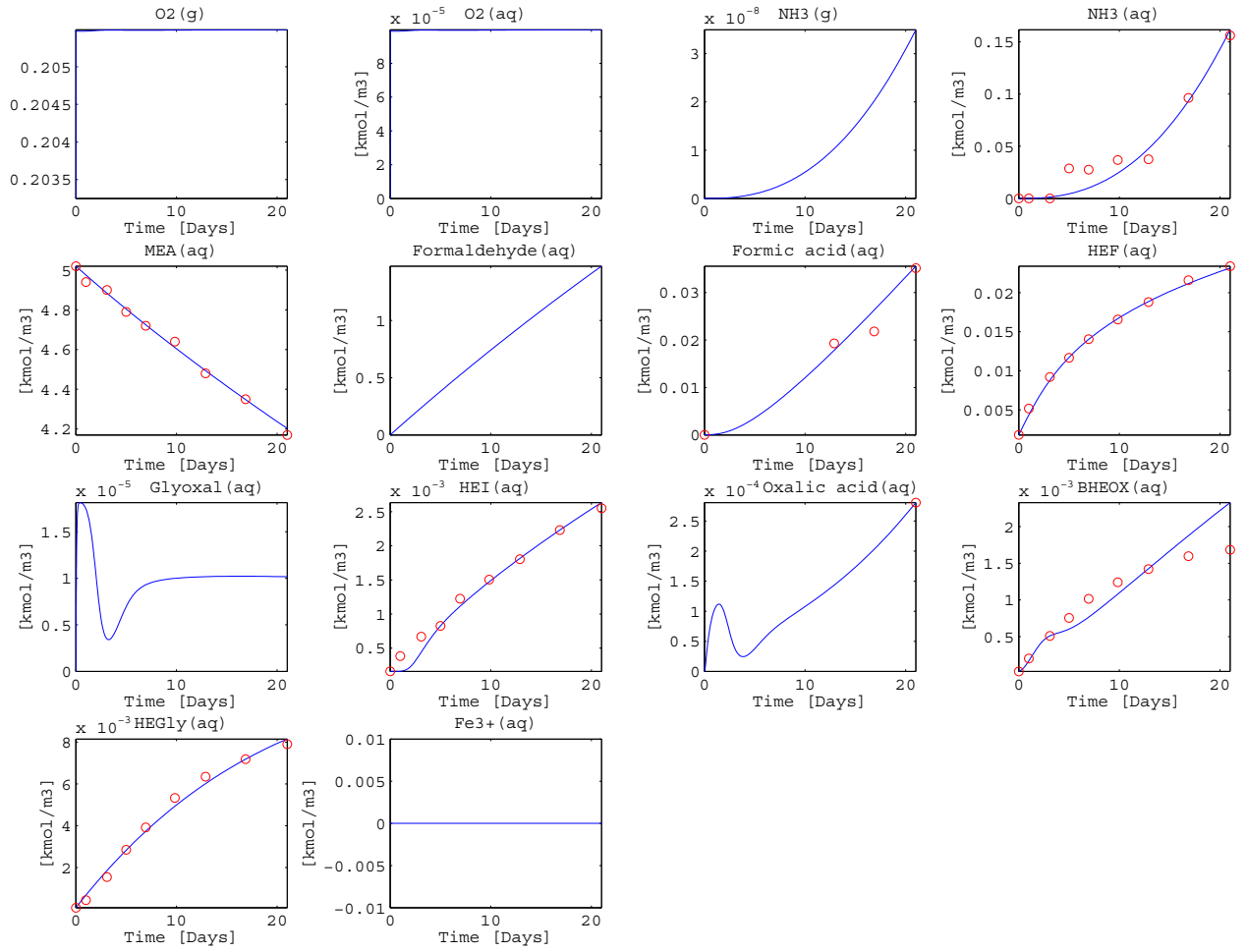


Figure 6.5: Experiment 1; open loop. 3rd version of the rate equations. Experimental values (o) and modeled values (—).

6 DEVELOPMENT OF THE RATE EQUATIONS

determined, the found parameters were applied to the closed loop experiment, where the oxygen leakage term and the reaction orders for iron were found.

On a closer look at the rate equations, equations (6.3.1), a problem was discovered with the found reaction orders of iron. For many of these exponents the value was negative. This resulted in that an increase of iron concentration would decrease the reaction rate, a tendency which was not believed to represent the reality.

The reason for this odd tendency, was that the concentrations of iron were less than a value of 1 [$kmol/m^3$]. For the reactions where the reaction rate had to be increased, the exponent for iron consequently had to be negative. This problem was solved in the next version.

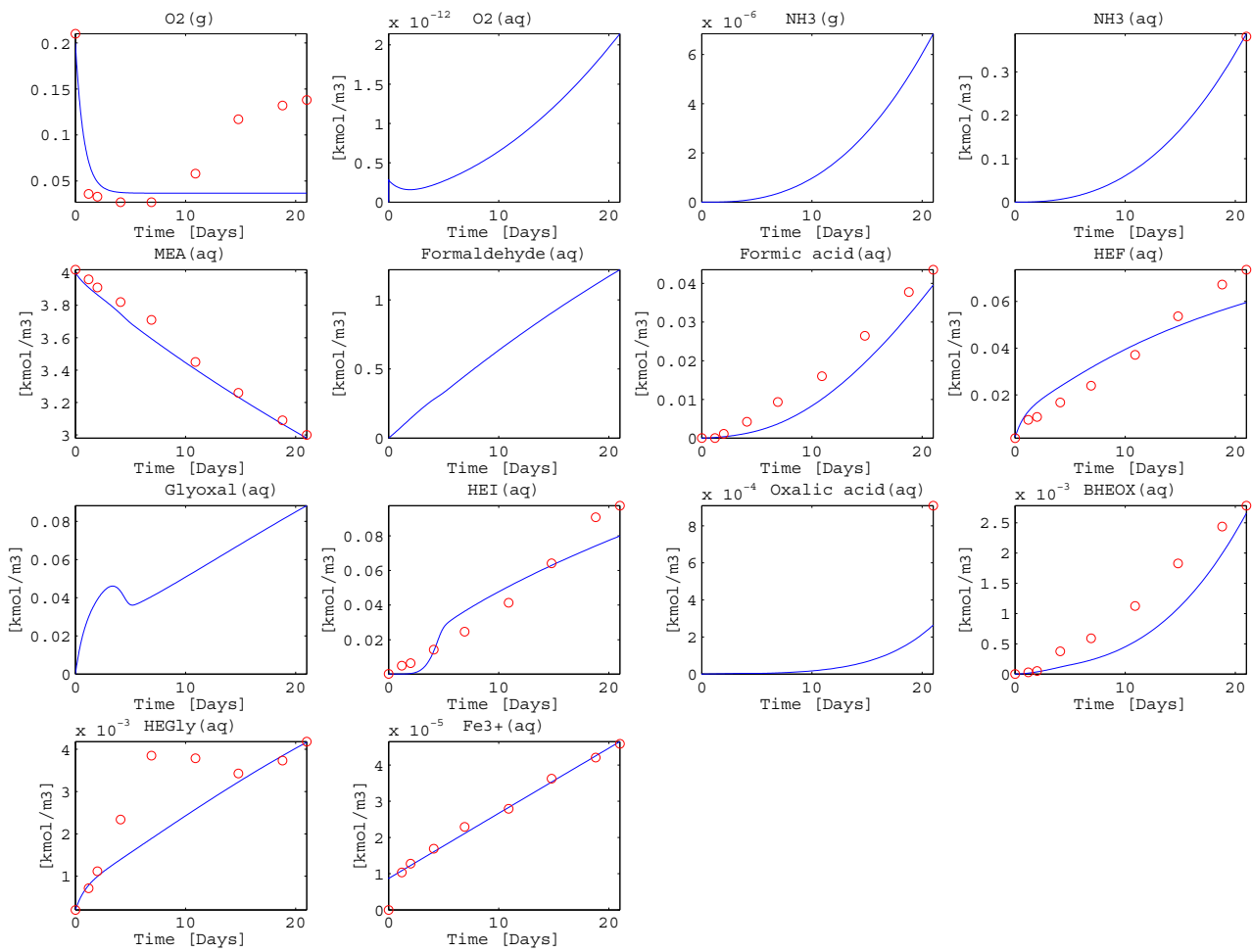


Figure 6.6: Experiment 2; closed loop. 3rd version of the rate equations. Experimental values (o) and modeled values (—).

6.4 Final (Fourth) Version

This version of the rate equations was the final one, and was considered as the result of the modeling of degradation experiments. Therefore, the rate equations will be thoroughly tested and deviation between model and experiment data will be analyzed in the following sections.

In this final version the rate expressions were redesigned to provide more realistic tendencies.

$$\begin{aligned}
R_{x,1} &= (6.2 \cdot 10^{-3} + 92.8[Fe^{3+}]^{1.1}) [MEA]^{1.2} \\
R_{x,2} &= (42.9 + 1.3 \cdot 10^{17}[Fe^{3+}]^3) [O_2][CH_2O]^{1.2 \cdot 10^{-9}} \\
R_{x,3} &= (6.0 \cdot 10^2 + 9.4 \cdot 10^5[Fe^{3+}]^{0.7}) [MEA]^{2.7 \cdot 10^{-5}} [CHOOH]^{0.5} \\
&\quad - (5.7 \cdot 10^4 - 5.9 \cdot 10^{12}[Fe^{3+}]^{1.9}) [HEF]^{1.6} \\
R_{x,4} &= (1.3 + 1.7 \cdot 10^{10}[Fe^{3+}]^{1.6}) [O_2]^{1.1} [MEA] \\
R_{x,5} &= (5 \cdot 10^4 + 1.2 \cdot 10^{27}[Fe^{3+}]^{3.8}) [MEA]^{8.6 \cdot 10^{-4}} [CH_2O][NH_3]^{1.15} [Glyoxal]^{0.64} \\
&\quad - (1.5 \cdot 10^{14} - 3.0 \cdot 10^{22}[Fe^{3+}]^2) [HEI]^5 \\
R_{x,6} &= (0.09 + 1.2 \cdot 10^9[Fe^{3+}]^2) [O_2]^{0.7} [Glyoxal]^{0.1} - 7.9 \cdot 10^{-4} [Oxalic] \\
R_{x,7} &= (0.07 + 2.0 \cdot 10^{11}[Fe^{3+}]^3) [MEA]^{2.4} [Oxalic]^{0.7} \\
&\quad - (50.0 - 4.6 \cdot 10^{10}[Fe^{3+}]^{2.2}) [BHEOX]^{1.4} \\
R_{x,8} &= (0.21 + 1.3 \cdot 10^7[Fe^{3+}]^{1.4}) [O_2][MEA]^{1.9} - 3.2 \cdot 10^{-2} [HEGly]
\end{aligned} \tag{6.4.1}$$

Equation (6.4.1) shows the found reaction parameters, while Figure 6.7 and Figure 6.8 are showing the resulting plot, where the modeled ammonia concentrations still were locked to the experimental data points.

In difference to the rate equations in the 3rd version, section 6.3, the iron concentrations factors were moved to be a part of the rate coefficient. An additional variable was added to be multiplied with the iron concentrations. This resulted in a tendency where, when the iron concentrations were increased, the reaction rate would also increase. A tendency which seemed to be representing the reality in a better way than the rate equations in the 3rd version.

6.4.1 Ammonia Locked

Figure 6.7 and Figure 6.8, shows the results for the open- and closed loop experiment models applying rate equation set (6.4.1). With the ammonia profile locked to the experimental points as described in section 6.3 and further discussed in section 11.1.4.

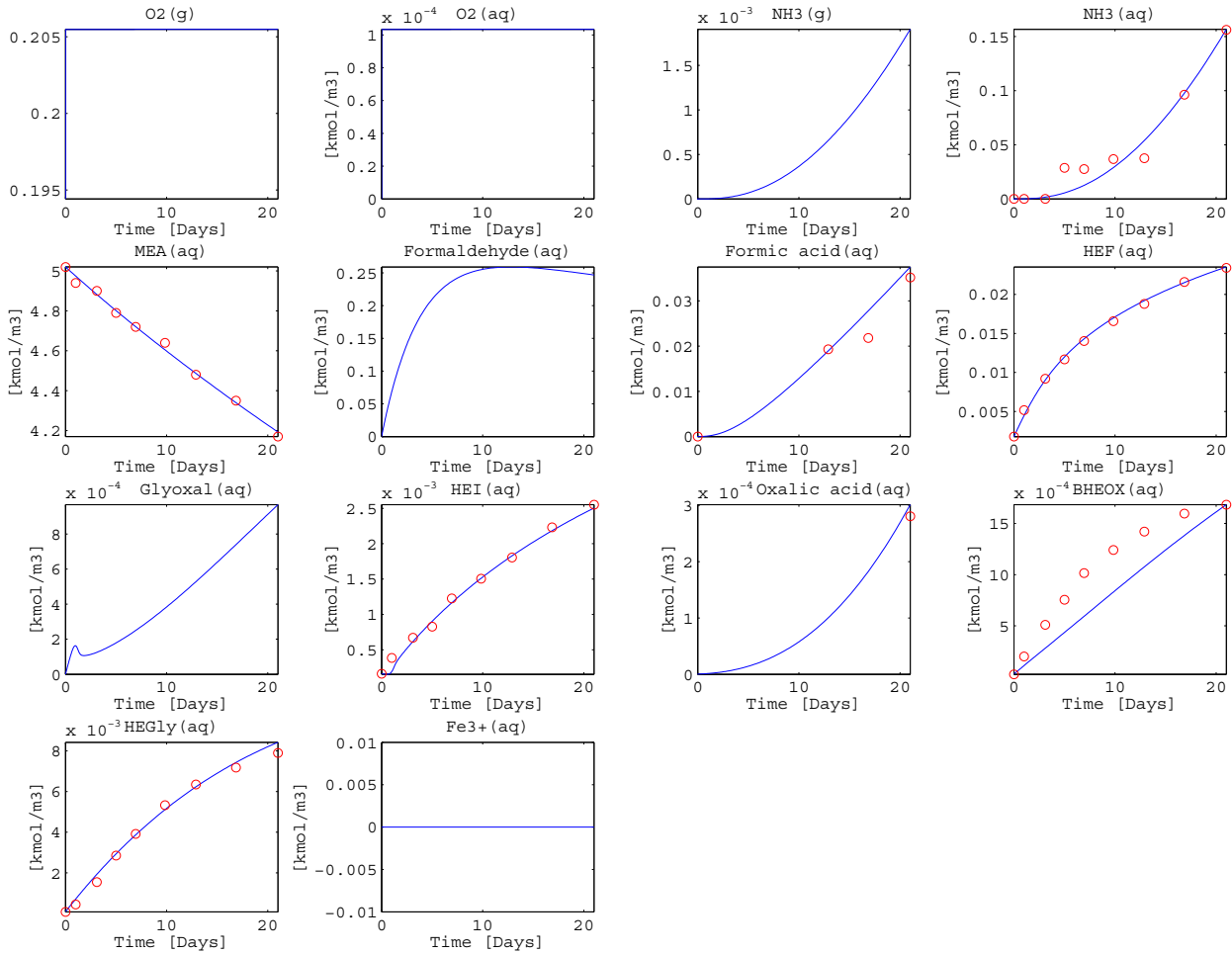


Figure 6.7: Experiment 1; open loop. Locked ammonia profile. Final version of the rate equations. Experimental values (o) and modeled values (—).

As the figures show, the models were now providing a very good description of the experimental data, with some exceptions. These are discussed in section 11.1.1.

Despite some deviations, these rate equations were considered to give the best possible result within the time limit for the study. It was therefore investigated how the model would behave with the ammonia profile unlocked.

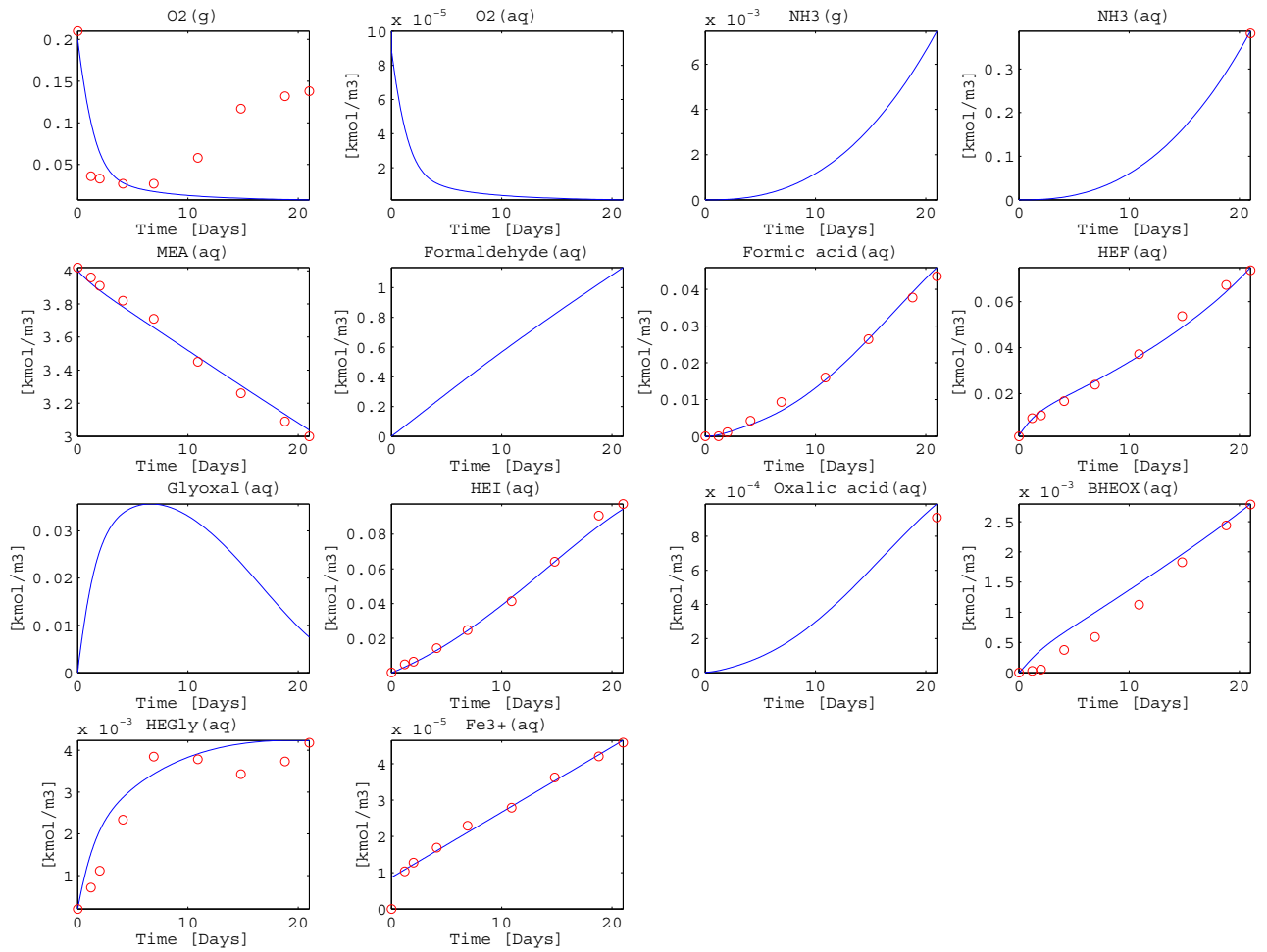


Figure 6.8: Experiment 2; closed loop. Locked ammonia profile. Final version of the rate equations. Experimental values (o) and modeled values (—).

6.4.2 Ammonia Unlocked

Figure 6.9 and Figure 6.10 shows the open- and closed loop models, with the ammonia profile unlocked. This implies that the ammonia concentration now was calculated by the model in the same way as all other components.

It is important to notice that the liquid mass transfer coefficient, k_{L,NH_3} , for ammonia had to be adjusted for the open loop model to hit the last experimental point for ammonia, and that the model underestimated the ammonia concentration when k_L for the other components were applied to ammonia. This is explained in section 7.1.2.

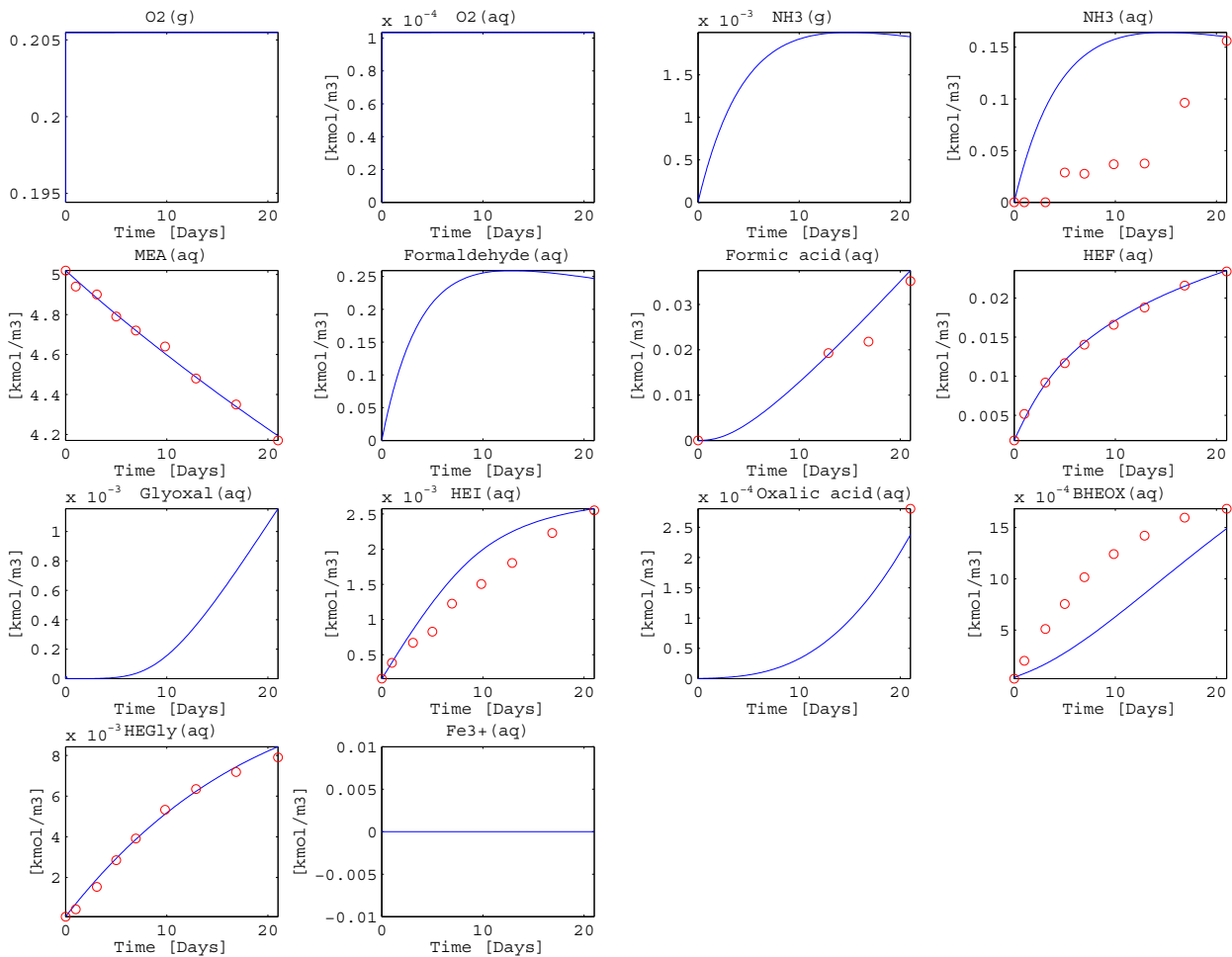


Figure 6.9: Experiment 1; open loop. Unlocked ammonia profile. Final version of the rate equations. Experimental values (o) and modeled values (—).

The consequences of the unlocking of the ammonia profile were minor, after adjusting k_{L,NH_3} . As seen in Figure 6.9, the increased ammonia concentration at the middle time points, led to an overestimation of the HEI formation at the same points in time. This overestimation of HEI caused increased consumption of glyoxal. Lower availability of glyoxal led to underestimation of oxalic acid formation,

this in turn led to underestimation of BHEOX. See Table 4.2 in section 4.6 for an overview of the reactions.

For the closed loop model, Figure 6.10, the ammonia concentration was overestimated when unlocking the ammonia profile. However, since there was only one experimental point for aqueous ammonia, experimental error could also be a contributing factor causing the model to miss the experimental point. As for the consequences of the overshooting of the ammonia concentration, the only difference between Figure 6.8 and Figure 6.10, was a slightly overshooting HEI profile and a slightly underestimation BHEOX profile, in the unlocked closed loop results.

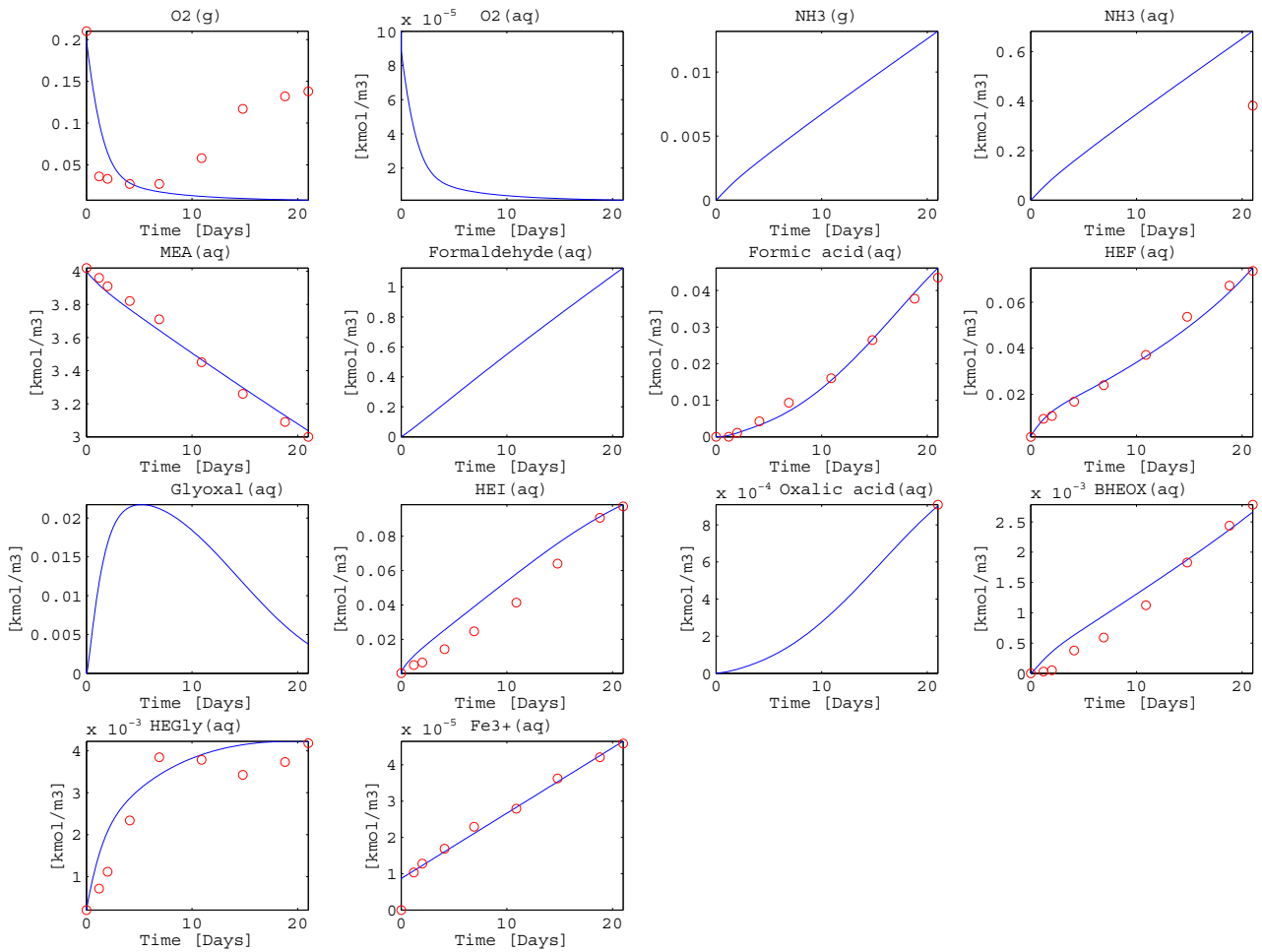


Figure 6.10: Experiment 2; closed loop. Unlocked ammonia profile. Final version of the rate equations. Experimental values (o) and modeled values (—).

6.4.3 Deviation Between Model and Experiment

Both the absolute average deviation (AAD) and the average deviation (AD) were calculated for the final version of the rate equations. These deviations were defined the following way:

- AAD-absolute average deviation: $\frac{1}{N} \sum_{j=1}^N |E_j - \bar{E}|$
- AD-average deviation: $\frac{1}{N} \sum_{j=1}^N |E_j|$

Where $E_j = \frac{C_{j,model} - C_{j,exp}}{C_{j,exp}} \cdot 100$. Table 6.1 presents the model deviation from the experimental data of the open loop experiment with locked and unlocked ammonia profiles, Figure 6.7 and Figure 6.10, respectively.

Table 6.1: Standard deviations between final version of the rate equations and experiment 1; open loop.

	LOCKED		UNLOCKED	
	AAD%	AD%	AAD%	AD%
MEA (aq)	0.3	0.3	0.3	0.3
NH ₃ (aq)	27	30	166	164
Formic acid (aq)	20	9	10	9
HEF (aq)	3	3	3	3
HEI (aq)	10	9	15	20
BHEOX (aq)	19	30	23	45
HEGly (aq)	14	12	14	12

Table 6.2 presents the deviation between the model and experiment data for the closed loop experiment with locked and unlocked ammonia profile, Figure 6.8 and Figure 6.9 respectively.

Table 6.2: Standard deviations between final version of the rate equations, and experiment 2; closed loop.

	LOCKED		UNLOCKED	
	ADD%	AD%	AAD%	AD%
O ₂ (g)	73	75	73	76
MEA (aq)	1	1	1	1
Formic acid (aq)	9	8	8	8
HEF (aq)	9	9	9	9
HEI (aq)	9	10	43	51
BHEOX (aq)	25	21	23	18
HEGly (aq)	32	30	32	30

In addition to calculate the deviations, the experiment data and the corresponding model results were normalized by dividing every data point with the highest experimental value of each component. The resulting normalized model- and experimental data was plotted on each axis to get a clear picture of how well the model was describing the experiments. In case of a perfect description, the points should be on the diagonal guide line.

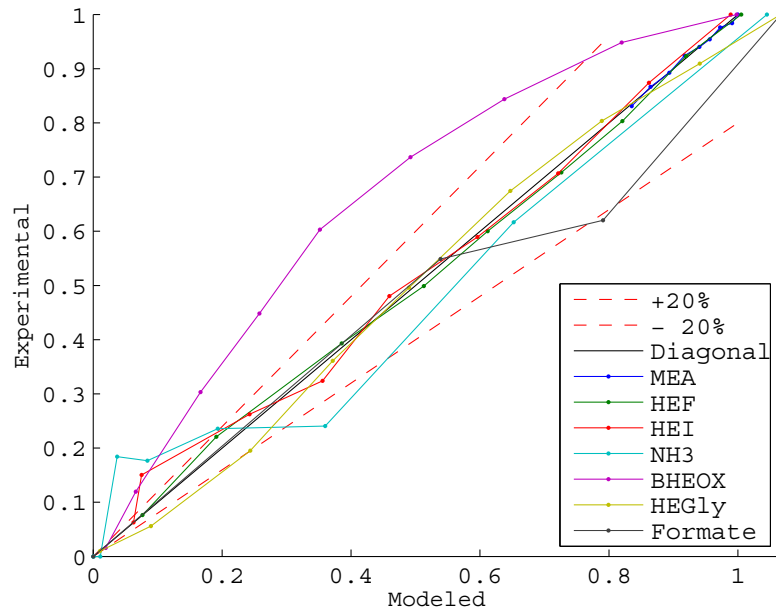


Figure 6.11: Dimensionless experimental value plotted versus dimensionless modeled value. Open loop experiment, locked ammonia profile, see Figure 6.7.

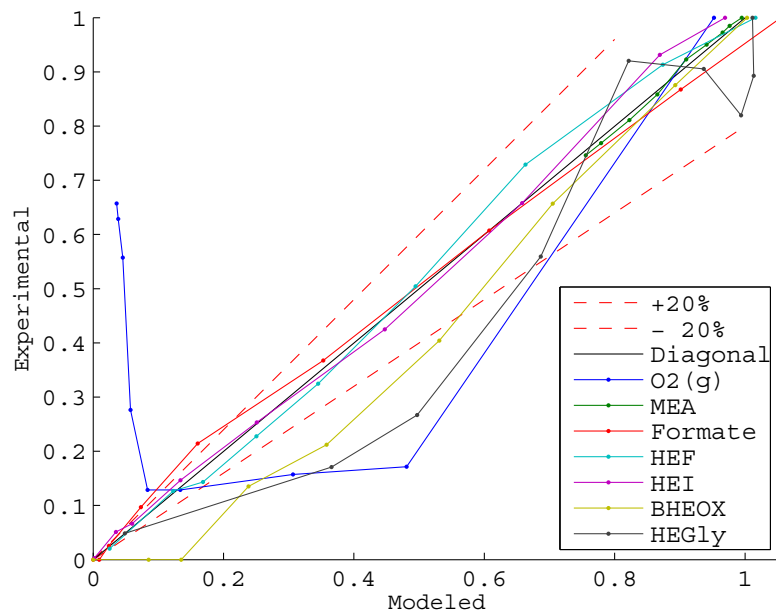


Figure 6.12: Dimensionless experimental value plotted versus dimensionless modeled value. Closed loop experiment, locked ammonia profile, see Figure 6.8.

6 DEVELOPMENT OF THE RATE EQUATIONS

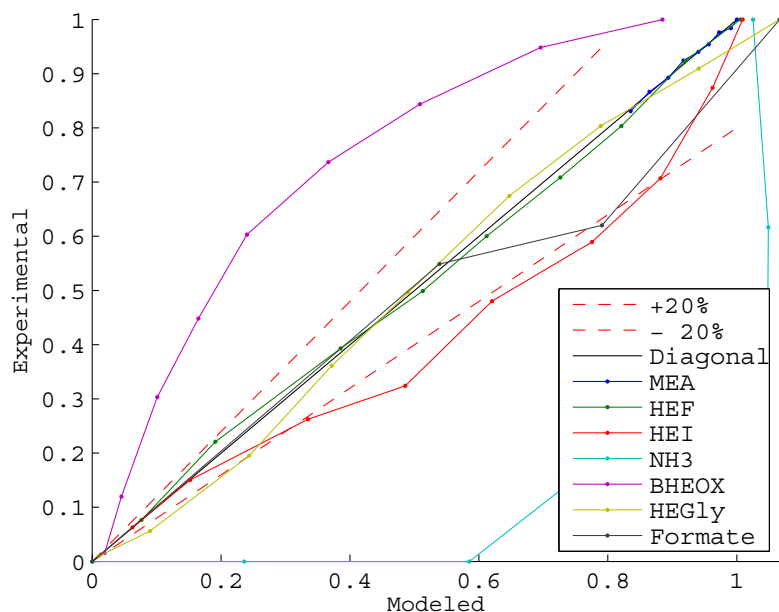


Figure 6.13: Dimensionless experimental value plotted versus dimensionless modeled value. Open loop experiment, unlocked ammonia profile, see Figure 6.9.

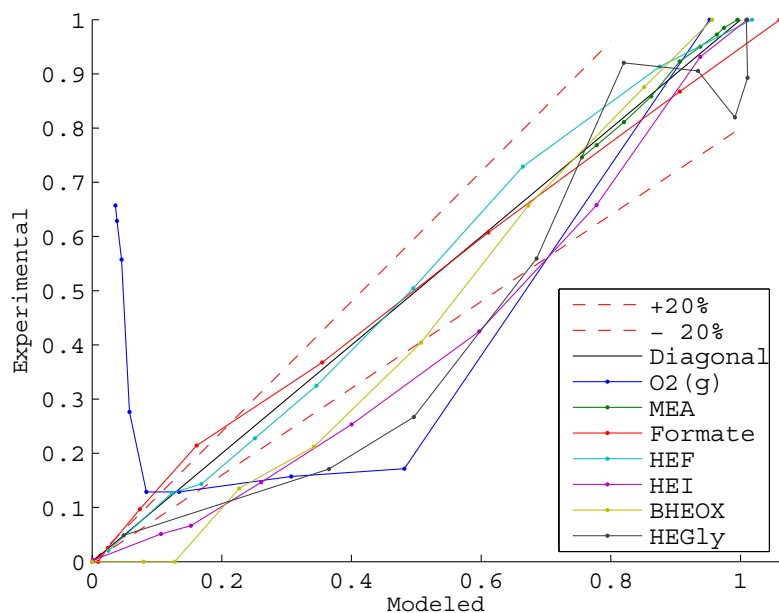


Figure 6.14: Dimensionless experimental value plotted versus dimensionless modeled value. Closed loop experiment, unlocked ammonia profiles, see Figure 6.10.

Figure 6.11 and Figure 6.12 are showing these plots for the open- and closed loop experiments, with locked ammonia profile in the models. Figure 6.13 and Figure 6.14 are showing the equivalent plots for the cases with unlocked ammonia profiles.

6.4.4 The Oxygen Leakage

The oxygen leakage term found by the parameter search resulted with the value of $0.033 [kmolO_2/m^3-day]$. To evaluate this result, the leakage was to be calculated as a fraction of the gas circulating rate in the closed loop experiment of 24.6 NL/min, and a gas volume of 4 L.

$$\frac{0.033 \left[\frac{kmolO_2}{m^3day} \right] \cdot \frac{1}{0.21} \left[\frac{Air}{O_2} \right] \cdot 4 \cdot 10^{-3} [m^3]}{24.6 \left[\frac{NL}{min} \right] \cdot 10^{-3} \left[\frac{m^3}{L} \right] \cdot \frac{101300 [Pa]}{8.314 \left[\frac{m^3Pa}{molK} \right] 293.15 [K]} \cdot 1 \cdot 10^{-3} \left[\frac{kmol}{mol} \right] \cdot 1440 \left[\frac{min}{day} \right]} = 0.017\% \quad (6.4.2)$$

The air leakage was thus 0.017%(mol) air per mole of gas circulated.

6.4.5 Prediction of an Additional Experiment

To fully test the model, an attempt was made to predict a third degradation experiment. This open loop experiment, described in section 2.4, was a combination of the properties found in the two previous experiments: The same experimental setup as the first open loop experiment, section 2.2, and an iron concentration as found in the closed loop experiment, section 2.3.

The experiment would look like the perfect combination of parameters to put the rate equations to the test. The only problem was that its initial iron concentration was around 100 times higher than the initial iron concentration in the closed loop experiment. More specific, a concentration of $1 \cdot 10^{-3} [kmol/m^3]$ compared with $1 \cdot 10^{-5} [kmol/m^3]$ in the closed loop experiment.

This caused problems for the rate equations. They were not designed to handle this high iron concentrations, and when attempting to predict the experiment with the existing models, the ordinary differential equation (ODE) solver failed, and was unable to give any reasonable results.

The initial iron concentration in the model was lowered until the ODE solver was able to provide results. At that point the iron concentration was lowered from $1 \cdot 10^{-3} [kmol/m^3]$ to $1.6 \cdot 10^{-5} [kmol/m^3]$, these results are shown in Figure 6.15.

As the results show, the consumption of MEA and the formation of HEF, was almost perfectly described. Yet, the production of HEI was grossly underestimated.

Yet, the rate equations described the degradation to some extent, with a modeled iron concentration of almost a hundredth of the actual concentration. This could indicate that the catalytic effect of the iron ions would decrease with increasing iron ion concentration. And that the catalytic effect could reach a maximum, at

6 DEVELOPMENT OF THE RATE EQUATIONS

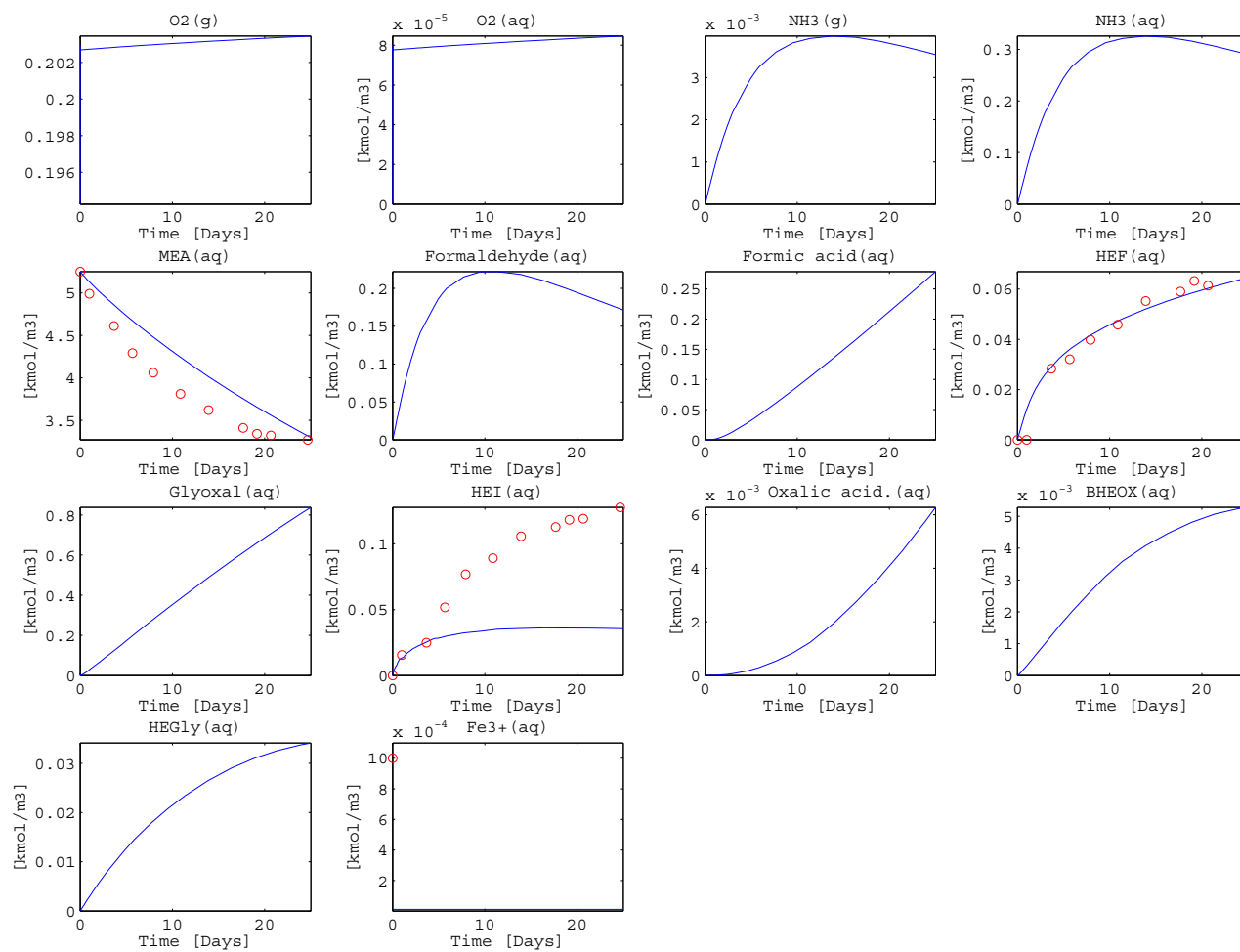


Figure 6.15: Experiment 3; open loop with iron ions. Final version of the rate equations. Experimental values (o) and modeled values (—).

a certain iron ion concentration, after which the catalytic effect would no longer increase even if the iron ion concentration was further increased.

Anyhow, these results showed that the rate equations had major weaknesses. That further development and more experiments were necessary to improve the understanding of the degradation, and to produce a more complete model of the degradation. This is further discussed in section 11.1.2.

6 DEVELOPMENT OF THE RATE EQUATIONS

Chapter 7

Physical Properties

This chapter will review the physical properties used in the model developed in the previous chapter. Since this chapter contains model sensitivity analysis of the mass transfer properties, this chapter was placed after the chapter describing the development of the model.

The equations for modeling of the experiments, equations (3.1.1), (3.1.2), (3.2.1) and (3.2.2), demanded values for the following physical parameters:

- G_1 and G_2 , the gas flow in- and out of the SFBR reactor.
- K_G , the gas side mass transfer coefficient
- a , the mass transfer area per unit volume of continuous phase
- V_L and V_G , the gas- and liquid volume.
- P , the pressure.
- H , Henry's law coefficient for all components.
- T , the temperature.

Several of these values; T , P , V_L , V_G and G_1 , could easily be obtained from the experiment records, chapter 2. The remaining parameters would prove to be less trivial to obtain, these parameters are discussed in the following sections.

7.1 Mass Transfer Properties of the Experiments

K_G and a were essential parameters for description of the mass transfer between the gas- and liquid phase.

The specific area, a , is commonly given for a packing by the manufacturer. It was therefore attempted to obtain this value from, Sulzer DX, the producer of the packing used in the closed loop experiment (section 2.3). Unfortunately the manufacturer had no knowledge of this parameter, apart from that it had a higher value than normal packing, e.g. Mellapak.

According to Billet and Schultes (1999) [9], Mellapak 250Y had a specific area of $250 \text{ m}^2/\text{m}^3$, due to the lack of a better value, this value was used for a in the

closed loop experiment.

For the open loop experiment, the specific area between the gas- and liquid phase would be the surface area of all bubbles in the continuous phase. Since there was no way of determining this area, the value of a was set to $200 \text{ m}^2/\text{m}^3$. There was no way of justifying this number, except that the specific area was assumed to be lower for the bubbles in the open loop experiment than the packing in the closed loop experiment.

For k_L there was no documentation, so a value of 10 (m/day) was chosen. This value was found by trial and error to provide reasonable results.

Due to the major uncertainties associated to the chosen mass transfer values, the impact of these parameters was investigated:

7.1.1 Model Sensitivity of the Mass Transfer Parameters

In section 3.3 it was shown that the gas side mass transfer coefficient, k_G , could be neglected. After this assumption the liquid side mass transfer coefficient, k_L , and the specific area, a , were the only parameters determining the mass transfer, in addition to the Henry's law coefficients. The values of these parameters were uncertain, and the model sensitivity to these was therefore to be investigated.

Since the gas side mass transfer coefficient was neglected, as mentioned above, the liquid equations could be rewritten:

$$K_{G,j}aP(y_j - C_j \frac{H_j}{P}) - R_{x,j} = \frac{dC_j}{dt} \quad (7.1.1)$$

Substituting $K_{G,j}$, with $\frac{k_{L,j}}{H_j}$, provided:

$$k_{L,j}a(P \frac{y_j}{H_j} - C_j) - R_{x,j} = \frac{dC_j}{dt} \quad (7.1.2)$$

This shows that the sensitivity of either k_L or a , could be investigated by only varying one of them. Varying them one by one, would provide the same results since the parameters were to be multiplied.

The sensitivity of the liquid side mass transfer coefficient for all components except ammonia, was investigated by varying its value over a range of 10^4 [$\text{kmol}/\text{m}^2\text{-day-bar}$]. The result of this variation is shown in Figure 7.1 and Figure 7.2. As explained in section 6.4.2, and discussed in section 11.1.7, the liquid side mass transfer coefficient for ammonia had to be independently adjusted to account for simplifications in the model.

The variation in the gas side mass transfer coefficient was only affecting the mass transfer of oxygen into the solution, and consequently affecting all reaction dependent of oxygen. Due to the main reaction consuming MEA (reaction 1, see section 4.6) being independent of oxygen, the change of the mass transfer coefficient is not affecting the MEA consumption significantly.

7.1 Mass Transfer Properties of the Experiments

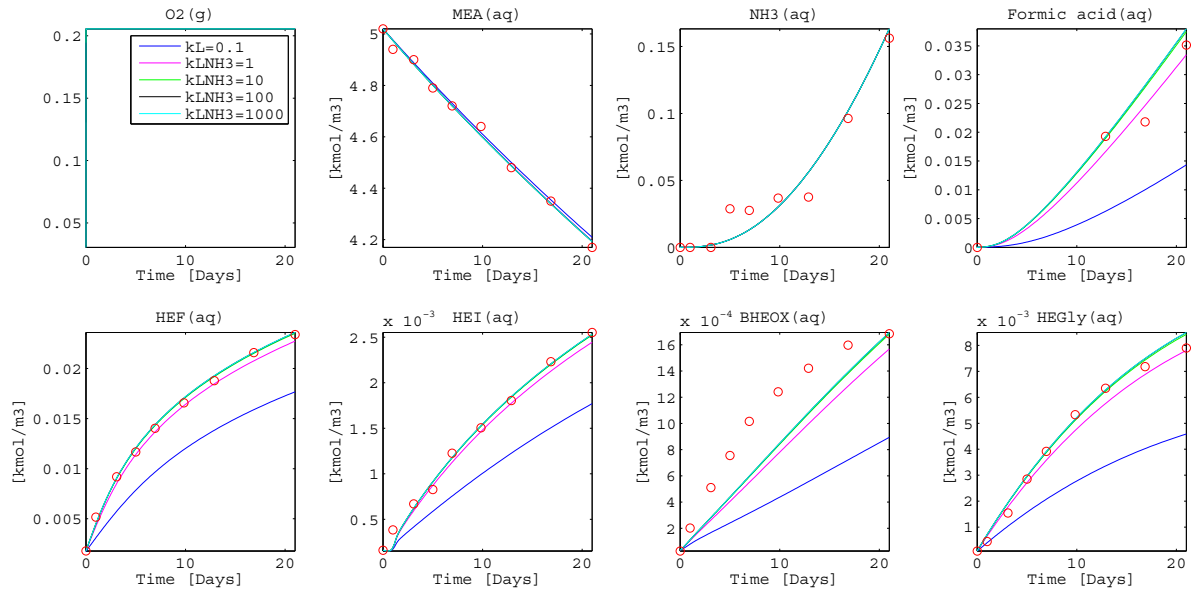


Figure 7.1: Experiment 1; open loop. Locked ammonia profile. Final version of the rate equations. The liquid side mass transfer coefficient, k_L [m/day], is varied.

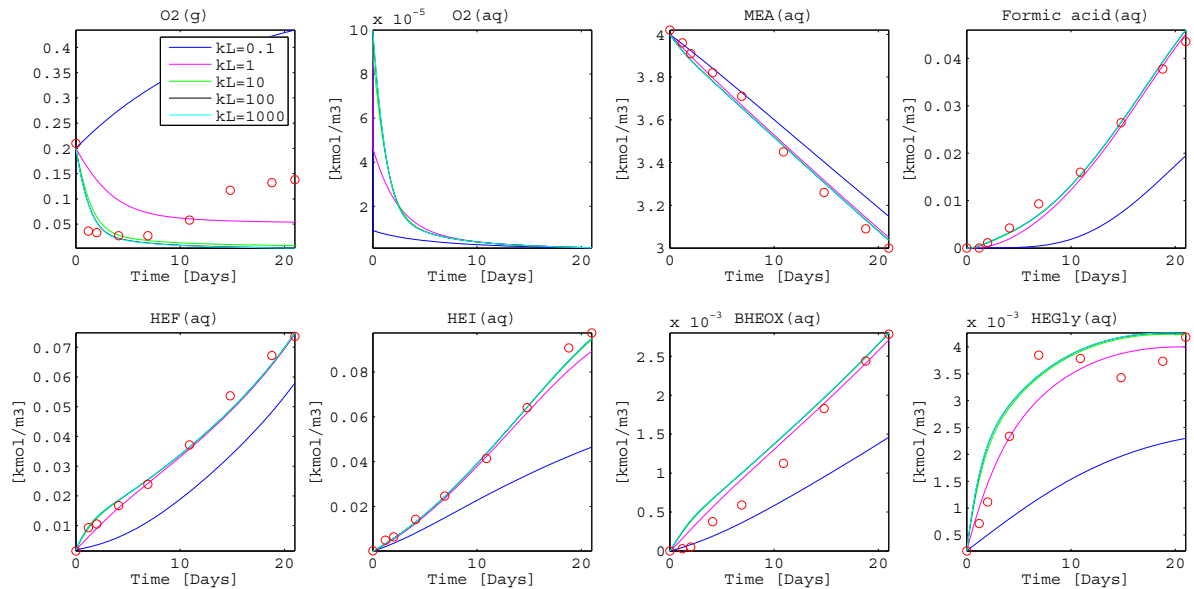


Figure 7.2: Experiment 2; closed loop. Locked ammonia profile. Final version of the rate equations. The liquid side mass transfer coefficient, k_L [m/day], is varied.

The figures, Figure 7.1 and Figure 7.2, show that with values of k_L above 10 [m/day], the gas side mass transfer is not rate limiting, and values above this limit are barely affecting the modeling results. This is further discussed in section 11.1.7.

7.1.2 Liquid Side Mass Transfer Coefficient of Ammonia

Even though the gas outflow, from the open loop experiment, was circulated back into the reactor, as seen in Figure 2.1, the open loop model assumed that the gas outflow was leaving the system, see section 3.1.

The main reason for this assumption was that the circulation ratio in the open loop experiment was unknown. Secondly, this model worked well for the description of the oxygen in gas phase. Figure 7.3 illustrates a comparison of the open loop experiment and the open loop model.

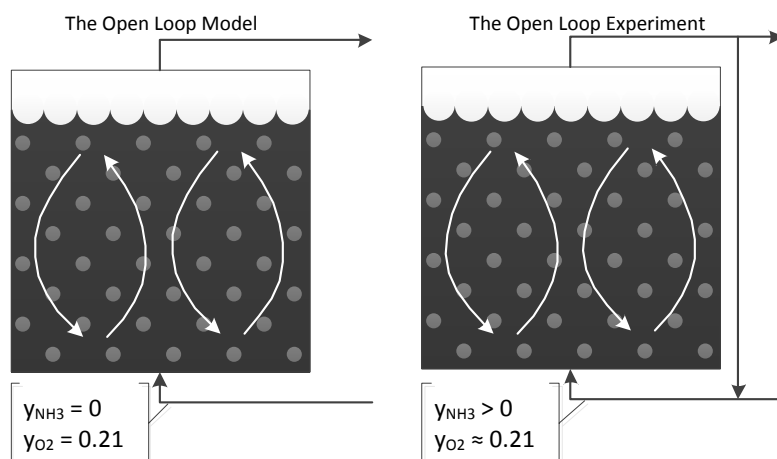


Figure 7.3: Illustration of the open loop experiment versus the open loop model.

As Figure 7.3 illustrates, the gas phase oxygen concentration would enter the system at 21%(mol), then bubble through the liquid, before some of the gas would be returned to the inlet, and the rest would be released to the environment. Since the reactions were slow, compared to the gas flow, and fresh air would be supplemented continuously to the gas phase, the gas phase concentration of oxygen was not likely to decrease drastically. The modeled assumption of no gas circulation, was in other words not affecting the oxygen concentration much.

For the gas phase ammonia, the situation was quite different. Since all of the ammonia in the system were products of the reactions, no ammonia was found in the inlet gas stream in the system. In the open loop experiment the gas circulation would cause the formed ammonia to build up in the gas phase. This elevated gas phase concentration would cause elevated liquid concentration of ammonia.

For the fitting of the rate equations this was no problem. In these procedures the modeled ammonia profile was locked to the liquid experimental points, so that

the ammonia dependent reactions were fitted to the actual ammonia concentration. When the ammonia profile later was released, a measure had to be taken to account for the simplification of the open loop model. The liquid side mass transfer coefficient for ammonia was therefore adjusted to keep more ammonia in the liquid phase, and provide reasonable results.

Figure 7.4 shows k_{L,NH_3} varied over a range of 10^4 [m/day]. This illustrates how the concentration profiles behaved, when the mass transfer coefficient for ammonia was varied. As seen in the figure, the HEI profile was the most sensitive to the concentration of ammonia. The figure also shows that if k_{L,NH_3} was kept at a value of 0.003 [m/day], the last experimental point of ammonia was hit. If the value was lower than this, the ammonia profile was overestimated. If the value was increased, the profile was slightly underestimated, but the ammonia profile was far less sensitive to an increase in the mass transfer coefficient, than a decrease.

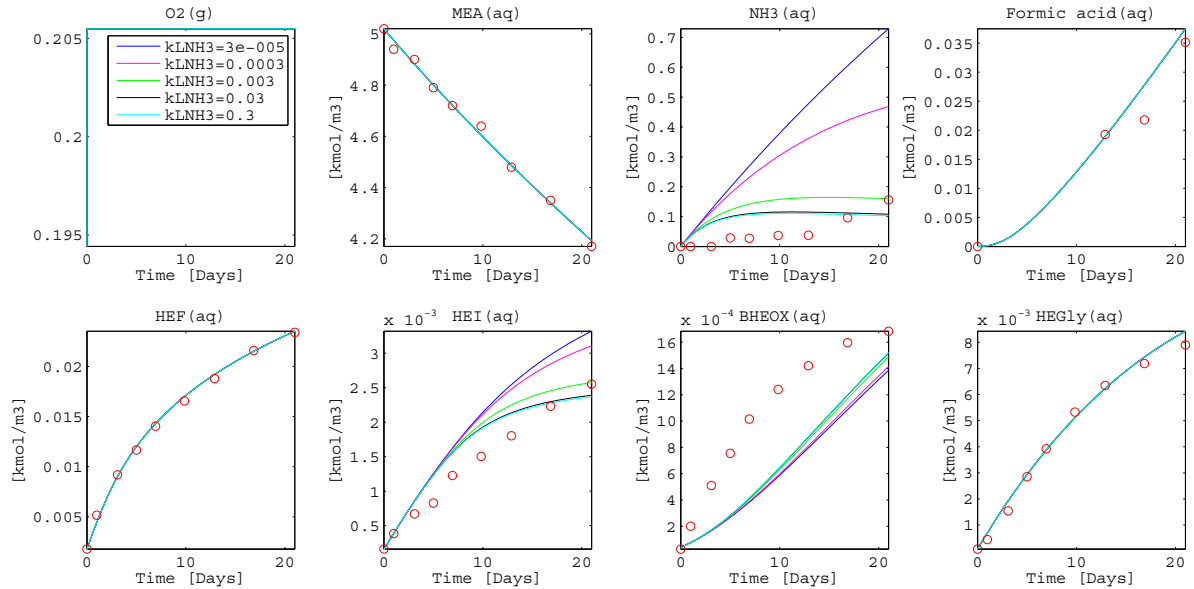


Figure 7.4: Experiment 1; open loop. Unlocked ammonia profile. Final version of the rate equations. The liquid side mass transfer coefficient for ammonia, k_{L,NH_3} [m/day], is varied.

7.1.3 Non-volatile Components

As described in section 3.3 the overall interphase mass transfer coefficient was defined by the following equation:

$$K_G = \frac{k_L}{H} \quad (7.1.3)$$

While Henry's law coefficient was defined by:

$$H = \frac{P_{gas,interphase}}{C_{liq,interphase}} \quad (7.1.4)$$

The Henry's law coefficient could be simplified and rewritten to a dimensionless unit:

$$H = \frac{C_{gas}}{C_{liq}} \quad (7.1.5)$$

As equation (7.1.5) shows, for a component with low volatility, Henry's law coefficient would be a small number. When inserting this small number into equation (7.1.3), K_G would approach infinite with decreasing component volatility.

According to the batch model, equations (3.2.3) and (3.2.4), infinite K_G would mean infinitely fast transfer from the gas phase to the liquid phase. But since all reactions were taking place in the liquid phase, no components with low volatility would be formed in the gas phase. The term for transferring these components from the gas phase to the liquid phase was therefore unnecessary.

Nevertheless, perturbations and minor errors during solving of the ordinary differential equations in the model, could cause minor gas phase concentrations of these components. Perturbations like this would consequently lead to very steep gradients, with high values for K_G , and even worse, if K_G was equal to infinite. Steep gradients and infinite numbers are known to cause ODE-solvers to fail.

To avoid this problem, K_G was set to be zero for the following components with low volatility:

- Formic acid
- $\text{H}_3\text{O}^\oplus$
- HEF
- Glyoxal
- HEI
- $\text{Fe}^{2+/3+}$
- Oxalic acid
- BHEOX
- HEGly

As mentioned, this measure would not compromise the accuracy of the model. Yet, the stability of ODE-solver would increase significantly.

7.2 Henry's Law Coefficients

The Henry's law coefficients, H , was needed in the experimental reactor models, see section 3. These coefficients were collected from two sources, and are presented in Table 7.1. The models were very sensitive on the Henry's law coefficient for ammonia, this is further discussed in section 11.1.8.

Table 7.1: Henry's law coefficients for the components in the degradation reactions.

Compound	Alt. name	Mw [g/mol]	SMILES	Henry's law coefficient [M gas/M liq]	
				EPIWIN ^a	Comp Chem ^b
Carbon dioxide	-	44.01	O=C=O	6.210·10 ⁻¹	-
Oxygen	-	32.00	$exp(3.71814 + (5.59617 \cdot 10^3/T) - (1.049668 \cdot 10^6/(T^2))) \cdot \frac{PMW}{\rho RT}$ ^c		
Ammonia	-	17.03	-	Not organic	7.085·10 ⁻⁴
Nitrate	-	62.00	-	Not organic	Not volatile
Nitrite	-	46.01	-	Not organic	Not volatile
Methylamine	-	31.06	NC	3.100·10 ⁻⁴	4.488·10 ⁻⁴
2-Ethanolamine	MEA	61.08	OCCN	1.500·10 ⁻⁸	2.468·10 ⁻⁷
Ethanolaminocarbamate	MEACOO-	104.08	-	-	Not volatile
Protonated ethanolamine	MEAH+	62.09	-	-	Not volatile
Methanal	Formaldehyde	30.03	O=C	3.800·10 ⁻³	5.572·10 ⁻³
Formic acid	Formate	45.02	O=CO	3.070·10 ⁻⁵	Not volatile
1-(2-hydroxyethyl)-imidazole	HEI	112.13	N1=C[N](CCO)C=C1	1.590·10 ⁻⁷	1.909·10 ⁻¹¹
N-(2-hydroxyethyl)-formamide	HEF	89.09	C(=O)NCCO	6.5757·10 ⁻¹⁶	3.044·10 ⁻⁹
2-oxazolidinone	OZD	87.08	O(CC1)C(=O)N1	1.570·10 ⁻⁶	3.843·10 ⁻⁸
4-(2-hydroxyethyl)piperazine-2-one	HEPO	144.17	N1C-C[N](CCO)C-C1(=O)	2.130·10 ⁻¹³	4.740·10 ⁻¹⁰
2-(2-hydroxyethylamino)acetic acid	HeGly	119.12	OCCNCC(=O)O	4.900·10 ⁻¹²	2.607·10 ⁻⁴⁹
N,N-bis(2-hydroxyethyl)oxalamide	BHEOX	176.17	O=C(C(=O)NCCO)NCCO	7.400·10 ⁻¹⁵	1.734·10 ⁻¹²
N-(2-hydroxyethyl)acetamide	HEA	103.12	O=C(NCCO)C	4.870·10 ⁻¹¹	7.088·10 ⁻⁹
Oxalic acid	Oxalate	88.02	O=C(C(=O)O)O	9.850·10 ⁻¹⁰	Not volatile

^aBond contribution method obtained from EPI Suite (2008) [22](HenryWin v3.20).

^bCalculated with computational chemistry retrieved from da Silva (2012) [24].

^cHenry's law coefficient for oxygen retrieved from Rooney and Daniels (1998) [29].

Part II

Absorber Simulation

Chapter 8

Implementation in Absorber Model

With the degradation reactions and the belonging rate equations sorted out, the degradation reactions were ready to be implemented in the Aspen Plus absorber simulation obtained from TCM. The following chapters will go through the implementation of the rate equations in Aspen Plus.

8.1 Rate Equations

The reaction rate equations found in the final version of the degradation experiment models section 6.4, were recalculated to the unit of $[kmol/m^3 - sec]$, and split to forward and backward reactions, see equation set 8.1.1. Now the rate equations would correspond to the reaction equations in appendix A, and the reactions could easily be implemented in Aspen Plus.

$$\begin{aligned}R_{x,1} &= (7.16 \cdot 10^{-8} + 1.07 \cdot 10^{-3}[Fe^{3+}]^{1.1}) [MEA]^{1.2} \\R_{x,2} &= (4.96 \cdot 10^{-4} + 1.51 \cdot 10^{12}[Fe^{3+}]^3) [O_2][CH_2O]^{1.2 \cdot 10^{-9}} \\R_{x,3} &= (7.00 \cdot 10^{-3} + 10.9[Fe^{3+}]^{0.7}) [MEA]^{2.7 \cdot 10^{-5}} [CHOOH]^{0.5} \\R_{x,-3} &= (0.661 - 6.81 \cdot 10^7[Fe^{3+}]^{1.9}) [HEF]^{1.6} \\R_{x,4} &= (1.51 \cdot 10^{-5} + 1.95 \cdot 10^5[Fe^{3+}]^{1.6}) [O_2]^{1.1}[MEA] \\R_{x,5} &= (0.579 + 1.39 \cdot 10^{22}[Fe^{3+}]^{3.8}) [MEA]^{8.6 \cdot 10^{x-4}} [CH_2O][NH_3]^{1.15} [Glyoxal]^{0.64} \\R_{x,-5} &= (1.74 \cdot 10^9 - 3.47 \cdot 10^{17}[Fe^{3+}]^2) [HEI]^5 \\R_{x,6} &= (1.04 \cdot 10^{-6} + 1.41 \cdot 10^4[Fe^{3+}]^2) [O_2]^{0.7} [Glyoxal]^{0.1} \\R_{x,-6} &= 9.20 \cdot 10^{-9} [Oxalic] \\R_{x,7} &= (8.10 \cdot 10^{-7} + 2.31 \cdot 10^6[Fe^{3+}]^3) [MEA]^{2.4} [Oxalic]^{0.7} \\R_{x,-7} &= (5.79 \cdot 10^{-4} - 5.30 \cdot 10^5[Fe^{3+}]^{2.2}) [BHEOX]^{1.4} \\R_{x,8} &= (2.48 \cdot 10^{-6} + 1.5 \cdot 10^2[Fe^{3+}]^{1.4}) [O_2][MEA]^{1.9} \\R_{x,-8} &= 3.72 \cdot 10^{-7} [HEGly]\end{aligned}\tag{8.1.1}$$

Table 8.1 shows the rate coefficients calculated for two cases from equation set 6.4.1. The table also gives an overview of what reaction equation numbers (Rx.Nr)

in Table 4.2 were corresponding to the reaction numbers in the absorber simulation (Sim.Rx.Nr), see appendix A.

Table 8.1: Overview of the rate coefficients for $C_{Fe^{3+}} = 0$, and $C_{Fe^{3+}} = 5 \cdot 10^{-5}$.

Rate Coefficient	Rx. Nr. ^a	Sim. Rx. Nr ^b	No Iron Ions	With Iron Ions ^c
$k_1[kmol/m^3day]$	1	20, 21, 22	$7.16259001 \cdot 10^{-8}$	$1.00550599 \cdot 10^{-7}$
$k_2[kmol/m^3day]$	2	30	$4.96284562 \cdot 10^{-4}$	$1.89079263 \cdot 10^{-1}$
$k_3[kmol/m^3day]$	3	40, 41, 42	$7.00038714 \cdot 10^{-3}$	$2.31751358 \cdot 10^{-2}$
$k_{-3}[kmol/m^3day]$	3	45, 46, 47	$6.60983904 \cdot 10^{-1}$	$3.03706298 \cdot 10^{-1}$
$k_4[kmol/m^3day]$	4	50, 51, 52	$1.51152524 \cdot 10^{-5}$	$2.93758793 \cdot 10^{-2}$
$k_5[kmol/m^3day]$	5	60, 61, 62	$5.78870370 \cdot 10^{-1}$	$6.29149592 \cdot 10^5$
$k_{-5}[kmol/m^3day]$	5	65, 66, 67	$1.73689972 \cdot 10^9$	$8.68844166 \cdot 10^8$
$k_6[kmol/m^3day]$	6	70	$1.04166667 \cdot 10^{-6}$	$3.62633164 \cdot 10^{-5}$
$k_{-6}[kmol/m^3day]$	6	75	$9.19564100 \cdot 10^{-9}$	$9.19564100 \cdot 10^{-9}$
$k_7[kmol/m^3day]$	7	80, 81, 82	$8.10185185 \cdot 10^{-7}$	$1.09953704 \cdot 10^{-6}$
$k_{-7}[kmol/m^3day]$	7	85, 86, 87	$5.78703704 \cdot 10^{-4}$	$3.59679487 \cdot 10^{-4}$
$k_8[kmol/m^3day]$	8	90, 91, 92	$2.47820980 \cdot 10^{-6}$	$9.45112111 \cdot 10^{-5}$
$k_{-8}[kmol/m^3day]$	8	95, 96, 97	$3.71830054 \cdot 10^{-7}$	$3.71830054 \cdot 10^{-7}$

^aRelated reaction number in the experiment models.

^bRelated reaction numbers in absorber simulation.

^cConcentration of iron, $C_{Fe^{3+}} = 5 \cdot 10^{-5}$.

In Table 8.1 the rate coefficients were calculated for an iron ion concentration of $5 \cdot 10^{-5}[kmol/m^3]$, this was the terminal concentration of iron ions in the closed loop experiment, see Figure 2.5 in section 2.3. This value was used because there was no information about the iron ion concentration in the absorber at TCM, and the closed loop experiment was the only experiment containing data indicating the amount of iron ions that could dissolve from a packing into the liquid.

Only the rate coefficients calculated with iron ions were used in the absorber simulations. However, the corresponding rate coefficients for zero catalyst were calculated to show how the reactions were affected by catalyst.

8.2 Implementing the Rate Expression in Aspen Plus

The absorption column was modeled with a model called RadFrac in Aspen Plus. The RadFrac allowed two different reaction model types, REAC-DIST or USER see Aspen Plus Help (2011) [5]. Since the USER model demanded the rate expression to be coded in FORTRAN programming language, the REAC-DIST model was chosen for convenience. Additionally the absorption reactions and -equilibriums were already implemented in the REACT-DIST model, when the simulation was obtained from TCM.

The REACT-DIST model offered three built-in reaction types, see Aspen Plus Help (2011) [6]; kinetic, equilibrium and conversion , equation (8.2.1), (8.2.2) and (8.2.3), respectively:

$$R_x = k \left(\frac{T}{T_o} \right)^n e^{-(E/R)(1/T-1/T_o)} \prod_{j=1}^N C_j^{p_j} \quad (8.2.1)$$

$$\begin{aligned} \ln K_{eq} &= W + X/T + Y \ln T + Z \cdot T \\ K_{eq} &= \prod_{j=1}^N (C_j)^{\nu_j} \end{aligned} \quad (8.2.2)$$

$$R_{x,conv} = W + X/T + Y \ln T + Z \cdot T \quad (8.2.3)$$

The rate expression from the experimental modeling was, as presented in section 3.4, however on the following form:

$$R_{x,i} = \left(A_i + B_i \cdot C_{cat}^{p_{i,cat}} \right) \prod_{j=1}^N C_j^{p_{i,j}} - \left(A_{-i} + B_{-i} \cdot C_{cat}^{q_{i,cat}} \right) \prod_{j=1}^N C_j^{q_{i,j}} \quad (8.2.4)$$

The rate expression found during the development, chapter 6, was to be implemented in the kinetic reaction type, equation (8.2.1). This was because this type was most similar to the found rate expression, compared to equilibrium- and conversion type. However, even though these expressions were similar, there were some differences. Of that reason the found rate expression had to be modified to fit Aspen Plus.

To implement the found rate expression (equation 8.2.4) in the kinetic reaction type (equation (8.2.1)), some modifications had to be done on the found rate expression. First of all the rate equation, now expressed for a single reaction, had to be split into two equations:

$$\begin{aligned}
R_x &= R_f - R_b \\
R_{x,f} &= (A_f + B_f \cdot C_{cat}^{p_{cat}}) \prod_{j=1}^N C_j^{p_j} \\
R_{x,b} &= (A_b + B_b \cdot C_{cat}^{q_{cat}}) \prod_{j=1}^N C_j^{q_j}
\end{aligned} \tag{8.2.5}$$

Secondly, the rate coefficients were collected:

$$\begin{aligned}
R_{x,f} &= k_{x,f} \prod_{j=1}^N C_j^{p_j} \\
R_{x,b} &= k_{x,b} \prod_{j=1}^N C_j^{q_j} \\
k_{x,f} &= A_f + B_f \cdot C_{cat}^{p_{cat}} \\
k_{x,b} &= A_b + B_b \cdot C_{cat}^{q_{cat}}
\end{aligned} \tag{8.2.6}$$

By inserting $n = 0$, $E = 0$, and $T_o = 298$ (to avoid dividing by zero) into Aspen Plus' kinetic reaction type, equation (8.2.1), the following expression was obtained;

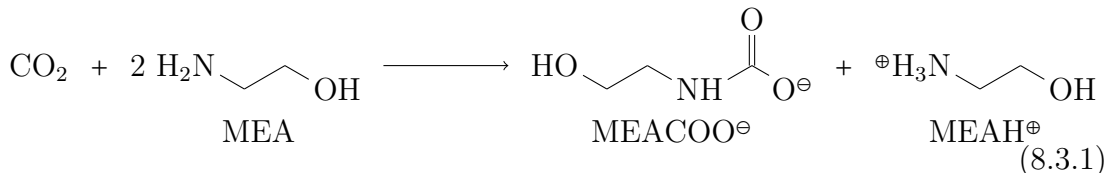
$$R_x = k \prod_i C_i^{q_i} \tag{8.2.7}$$

,fully compatible with equation (8.2.6).

Rewriting the rate expression in this way, had two consequences. First of all, the reversible reactions had to be implemented twice. Once for the forward reaction, and once for the reverse reaction. Additionally, as described in equation 8.2.6, and presented in Table 8.1, the catalyst concentration had to be predefined to generate the rate coefficients, before inserting the coefficients in Aspen. This implied that the reaction rates were independent of the catalyst concentration during the absorber simulation, and that new rate coefficients had to be calculated externally from Aspen when changing the catalyst concentration.

8.3 Implementing the Reaction Equations in Aspen Plus

As presented in section 1.1, CO₂ reacts by the following reaction equation, in the absorption reaction:



To characterize the amount of absorbed carbon dioxide, the loading, α , is defined by the following equation:

$$\alpha = \frac{[CO_2]_{Absorbed}}{[MEA]_{Total}} \quad (8.3.2)$$

In the degradation experiments, chapter 2, the loading was, $\alpha = 0.4$. This would imply that the most of MEA, would be of the form of $MEACOO^\ominus$ and $MEAH^\oplus$. Nevertheless, the amine concentration in the experiments was measured as total amine:

$$MEA_{Total} = MEA_{Free} + MEACOO^\ominus + MEAH^\oplus \quad (8.3.3)$$

In other words, there were no direct measurements of the loading in the experiments.

For the implementation in Aspen Plus, the case was the opposite, thus both the products of MEA were specified, in addition to pure MEA.

From a modeling point of view, there were thus two options: Either to use the existing rate equations as functions of total MEA, which was measured in the experiments. Or calculating the amount of free MEA, protonated MEA and carbamate for each time step in the experiment, and redesign the rate equations to be functions of each of the three MEA species. The latter option would consequently add uncertainty to the experimental data, which was not desirable. It would however make the implementation in Aspen Plus more convenient. But most importantly, if the rate of degradation was significantly higher for one of the three MEA species, it would have been necessary to build separate rate expressions for each of them.

In order to decide which option to choose, the CO_2 -loading during the experiments were to be investigated. If the loading was more or less constant throughout the experiment, one could assume that the rate of disappearance was equal for all MEA species. Either due to equal degradation reactions for these, or due to equilibrium between the species.

A relationship between the CO_2 -loading, and the partial pressure of CO_2 was obtained from Bruder et al. (2012) [11]:

$$\ln P_{CO_2} = A \ln \alpha + k_1 + \frac{B}{1 + k_2 \exp(-k_3 \ln \alpha)} \quad (8.3.4)$$

The equation was applied to calculate the loading of each time point in experiment 2; closed loop (section 2.3).

Table 8.3 gives a rough estimate of the loading during the time of experiment 2; closed loop. The initial measured loading was $\alpha = 0.4$. With this variation between measured and estimated loading, it is not unreasonable to assume the loading to be constant, and it could be concluded that the loading would not decrease.

Table 8.2: Parameters in equation (8.3.4).

	5 M MEA
A	1,8
B	10
k1	$-9155.95 * (1/T) + 28.03$
k2	$\exp (-6146.18 * (1/T) + 15)$
k3	$7527.04 * (1/T) - 16.94$

Table 8.3: Calculated loading in experiment 2; closed loop.

Time (days)	MEA_{Total} (l) [mol/l]	Experimental CO_2 (g) [mol]	$\alpha_{Calculated}$ ^a
0.0	4.024	3.54E-04	0.33
1.2	3.96	9.09E-04	0.38
2.0	3.91	1.11E-03	0.39
4.1	3.82	1.23E-03	0.40
6.9	3.705	1.60E-03	0.41
10.9	3.453	1.54E-03	0.41
14.8	3.257	2.19E-03	0.42
18.8	3.09	2.61E-03	0.43
21.0	2.997	2.89E-03	0.43

^aAssuming atmospheric pressure, 55 °C, 4 l gas volume, and equation (8.3.4) to be valid in the current MEA concentration range.

This finding showed that the disappearance rate for free MEA, protonated MEA and carbamate, was roughly the same. Meaning that the same reaction rates could be applied for the consumption of these three. The reaction equations had though to be balanced out, to account for either release of CO_2 or H^{\oplus} . The reaction equations in Table 4.2 were therefore rewritten to account for all three forms of MEA, to make the reactions implementable. The result is shown in appendix A.

8.4 Charge Balance

As discussed in section 4.6, some of the reactions implemented in the experimental modeling, were not in charge balance. This is further discussed in section 11.2.3.

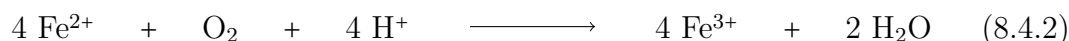
Nevertheless, the Aspen Plus absorber simulation demanded charge balance for all reactions. According to Chi and Rochelle (2002) [13], either ferric, Fe^{3+} , or a radical, $R\cdot$, could react with MEA to produce radicals. Since Aspen Plus was unable to handle radicals, reaction 8.4.1 was used to balance the charge in reaction 1 and -8. The balanced reactions, as they were implemented in Aspen Plus, are showed in Table A.1 to Table A.6.

It is important to notice that there was no evidence of iron ions reacting as described in these tables, and that the ions where only included to balance the charge and make it possible to simulate the degradation reactions.



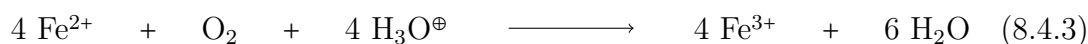
In the simulation a ferric level equal to the maximum level of iron ions in the closed loop experiment ($5 \cdot 10^{-5} [kmol/m^3]$), section 2.3, was inputted in the liquid inlet stream. This value was used, because this was the only indication on the value of the iron ion concentration in the absorber.

To prevent consumption of all the Fe^{3+} , the following oxidation reaction was implemented in the absorber simulation.



This autooxidation was described to occur in amine flue gas CO_2 capture by Bedell (2011) [7].

Since the absorber simulation applied H_3O^{\oplus} , instead of H^{\oplus} for the hydrogen ion, the reaction was rewritten to fit the implementation:



This rate of this reaction was set to an arbitrary high value of $R_x = 4000 [kmol/m^3 s]$, chosen for the simulations to converge.

8.5 User Defined Components

Four of the degradation products, HEF, HEI, BHEOX and HEGly, were not included in the component data base in Aspen Plus. It was therefore necessary to estimate the properties of these components, using estimation methods found in Aspen Plus. The procedure of adding user defined components like this is described in appendix B.1.

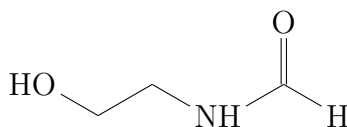


Figure 8.1: N-(2-hydroxyethyl)-formamide (HEF)

As described in the mentioned appendix the molecular weight, the normal boiling point and the specific gravity were properties that were needed to estimate the remaining parameters. These properties were found from different sources and are presented in Table 8.4. In other words; the values found in Table 8.4 were inputs to the estimation methods in Aspen Plus.

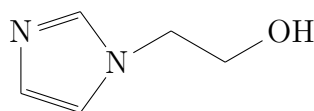


Figure 8.2: 1-(2-hydroxyethyl)-imidazole (HEI)

Notice that the table contains some blank fields. This means that these values were not found. For the components where this was the case, the value was assumed to be equal to $1[g/cm^3]$, in lack of a better value.

The structures of the user defined components were also needed, they are showed in Figure 8.1, Figure 8.2, Figure 8.3 and Figure 8.4 for HEF, HEI, BHEOX and HEGly respectively.

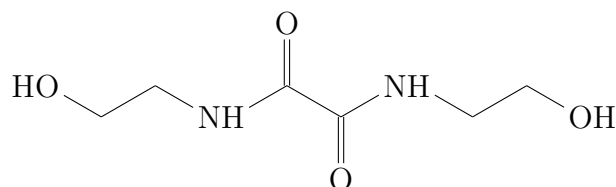


Figure 8.3: N,N-bis(2-hydroxyethyl)oxalamide (BHEOX)

HEF, BHEOX and HEGly were all estimated using bond contribution- in combination with the Aspen Plus property estimation method. This worked well for the mentioned components, but failed when it was attempted to estimate the properties of HEI. The reason why HEI was more difficult to estimate for the property estimation routines, could be due to the imidazole group it contained. The method was based on group contribution, and the imidazole was most likely an unknown group to this method. Of this reason HEI was estimated using the TDE estimation method, see appendix B.1.

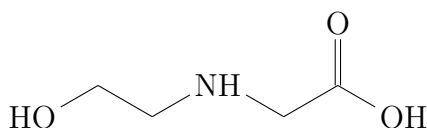


Figure 8.4: N-(2-hydroxyethyl) glycine (HEGly)

The TDE estimation method estimated most of the properties of HEI, but failed to estimate its heat capacity properties. Since Aspen was unable to simulate the absorber without this property, and since the concentration of this component most likely would be too low to affect the temperature profile in the absorber, the heat capacity of HEI was assumed to be equal to HEF. The assumption would probably be incorrect, but it was believed that it would not have any impact on the simulation.

Table 8.4: Aspen Plus input properties of HEF, HEI, BHEOX and HEGly. Retrieved from ChemSpider (2012) [1].

	HEF ^a	HEI	BHEOX	HEGly	Unit
Molecular weight	89.09318	112.1313	176.17	119.1192	$[g/mol]$
Normal boiling point	262.80	316.487	451.35	339.27	$[^{\circ}C]$
Specific gravity at 60°F		1.157		1.247	$[g/cm^3]$

^aEstimated with U.S. Environmental Protection Agency's EPI Suite (2008) [22].

Chapter 9

Case Description

To provide a thorough investigation of the degradation reaction in the simulated absorber, three cases were made. Firstly, a simple case with a single run through the absorber was made to show the initial degradation in the absorber. Secondly, a case where the liquid was circulated was made to emulate degradation at a later point in time. Thirdly, a case with three absorbers in series was made to calculate the degradation gradient. This would provide a rough estimate of time that had to be spent to achieve 1% degradation.

The three cases will be presented in the following sections.

9.1 Initial Run Case

An absorber simulation was retrieved from TCM DA (Cents (2012) [26]). The simulation already contained all reactions for CO₂ absorption, was connected with the proper streams, and was dimensioned similar to the absorber at TCM.

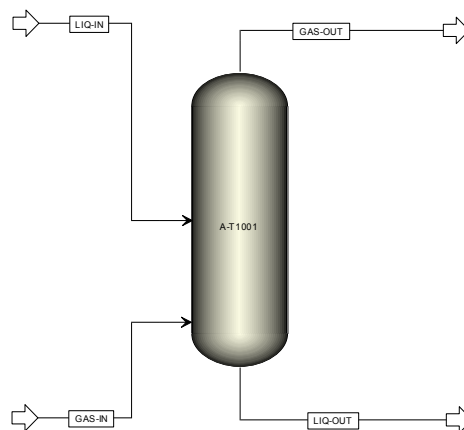


Figure 9.1: Screen view in Aspen Plus of the initial absorber case.

The absorber was packed with 12 meters of packing, with a diameter of 3 meter. The packing type in the simulation, same as used at TCM, was confidential, and

is therefore not presented in this document.

The user defined components, presented in section 8.5 were firstly implemented in the absorber as described in appendix B.1. Thereafter the reactions equations, see appendix A, and the belonging rate equations, see 8.1, were implemented as described in appendix B.2.

Figure 9.1 shows the screen view in Aspen Plus of the initial run case. As the figure shows, the absorber was fed with a fresh and unloaded MEA solution. The liquid was then degraded, while the CO_2 was absorbed. There were no stripper connected to the simulation, and liquid was not recirculated. This case would show how Aspen Plus handled the initial stages of degradation.

9.2 Recycle Case

It was of interest to investigate how the absorber simulation, with the implemented degradation reactions, would handle recycling of the liquid, and how the degradation products would accumulate in the system.

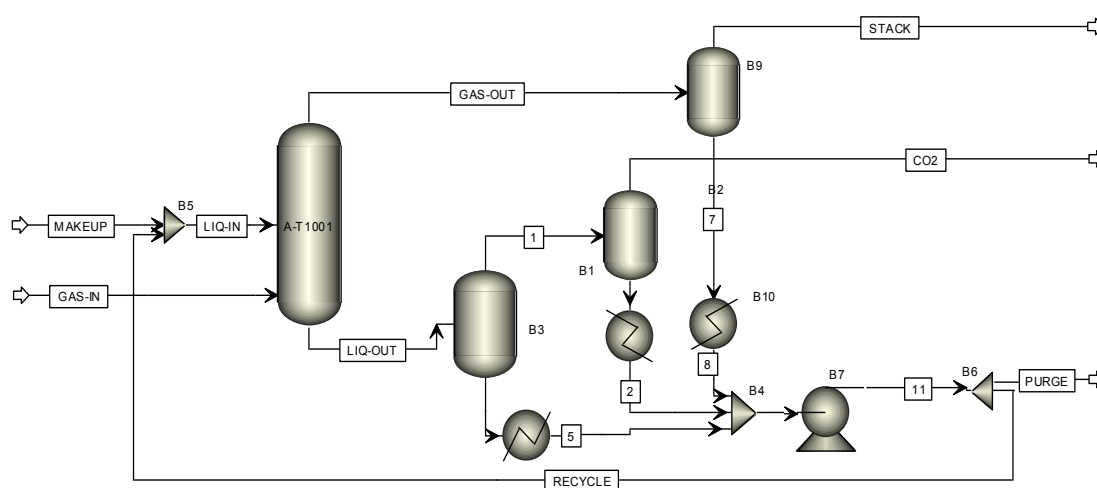


Figure 9.2: Screen view in Aspen Plus of the recycle case.

To examine this, a case was made where the liquid was recycled while a fraction of the liquid was purged out, and fresh liquid was added. This was done to avoid all MEA being consumed, which was a possibility since this was a steady-state simulation.

Figure 9.2 shows the screen view in Aspen Plus of the recycle case. The same absorber as presented in section 9.1, was applied. To recycle the liquid, the CO_2 had to be stripped off the solution. As described in section 1.1, this is usually done with a stripper. But since the stripping conditions were of no interest in this study, a series of flash tanks were substituting the stripper. This would create a more convenient simulation with decreased calculation time.

As shown in Figure 9.2, after the liquid had absorbed the carbon dioxide in addition to being slightly degraded in the absorber, the liquid entered a flash tank (B3, Figure 9.2). In B3, the temperature was kept at approximately 100 °C. This reversed the absorption reactions, and the CO₂ and water vapor would leave through the top stream of the flash tank, while the lean amine solution would leave the tank through the bottom stream.

The lean amine, would then be cooled in a heat exchanger before it was sent to be recycled. The CO₂ and water vapor stream leaving B3, would then be sent to another flash tank (B1, Figure 9.2) with a temperature of approximately 3 °C. Here the water vapor was condensed out, and sent to recycle to maintain the water balance in the system. The carbon dioxide would then leave the system via the stream named "CO2" in Figure 9.2.

To maintain the overall water balance, it had to be assured that the correct amount of water vapor was leaving the system. A flash tank (B9, Figure 9.2) was therefore inserted to condense out some water from the cleaned flue gas leaving the absorber. A design specification was entered in Aspen Plus, to keep the temperature in B9 at a level so that the water flow in the inlet gas stream, "GAS-IN", was equal to the sum of the two outlet gas streams, "STACK" and "CO2". Maintaining the water balance was essential to avoid accumulation of water, or drying of the system. Both which would be unfavorable for the process.

To maintain the overall mass balance, another design specification was entered in Aspen Plus. The liquid inlet stream, "MAKEUP", was regulated such that the sum of mass flow of all inlet streams, "MAKEUP" and "GASIN", was equal to the sum of all outlet streams, "STACK", "CO2" and "PURGE".

9.3 Absorbers in Series

In addition to the latter two cases, it was of interest to calculate a rough estimate of the degradation rate in the absorber, simulated in Aspen Plus. This was done by calculating the total residence time of the liquid needed to achieve 1%(weight) degradation products in the liquid. The total residence time could indicate if the simulated degradation was of a reasonable rate, compared to experience from pilot plants.

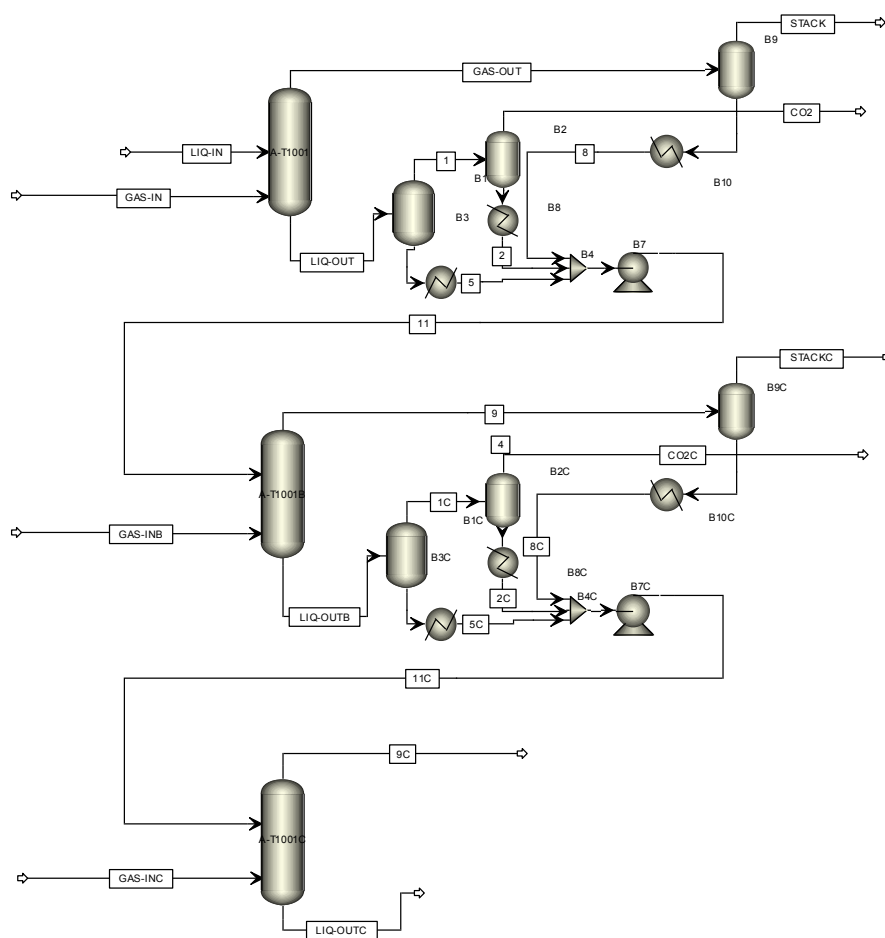


Figure 9.3: Screen view in Aspen Plus of the absorber in series case.

The estimate was calculated by finding the increase of degradation products during one run through the absorber. Thereafter, this value was combined with the total holdup in the column. This would provide the increase in degradation, per time. This gradient was then extrapolated to 1%(weight) degradation products in the liquid, which would provide the total residence time.

It is important to notice that this calculation would only provide a ball park estimate, or a rough order of magnitude, of the time it would take to achieve this degradation. The estimation would only extrapolate the initial degradation

gradient in a straight line to the desired concentration. As shown in section 6.4, none of the degradation products behaved linearly. Additionally the calculation would neglect the equilibrium effects of the reactions with reversible reaction rate terms.

Anyhow, the simulation was set up as shown in Figure 9.3. This case was equal to the recycle case in terms of conditions. The only difference was that no streams were purged or added, and that the liquid was sent to a new absorber with the exact same specification as the previous, instead of being recycled.

The liquid was sent through three absorbers. The first absorber and the flash tanks belonging to it, were used to initialize the liquid. In this way it was certain that the only variation between the next two absorbers, was the amount of degradation.

The increase in degradation was measured as the difference in the liquid out stream of the second and third absorber.

9.4 Flow Rates and Compositions

In addition to the three different simulation cases mentioned, there were two different flue gases, each with its flow rates and compositions. The compositions of the flue gases are presented in the following sections, in addition to the liquid- and gas flow rates for the two gases.

The liquid composition is not discussed in these sections, this was because the composition was already implemented in the simulation, when it was retrieved from TCM (Cents (2012) [26]). The composition can be seen in the result tables in Table 10.2.

9.4.1 Flue Gas Inlet Composition and Condition

The compositions and states of the flue gases when entering the flue gas pipes were found in Masterplan Mongstad (2009) [32], as shown in Table 9.1.

The concentration of the components in Table 9.1 which were already implemented in Aspen Plus, were extracted from this table. So the mole fractions of nitrogen, argon, oxygen, carbon dioxide, water vapor and ammonia were retrieved from Table 9.1. These were then normalized, and the mole fraction of water vapor, assuming the gas was saturated with water at 25°C, was calculated by use of the Goff-Gratch equation (equation (9.4.1)). The resulting flue gas compositions are presented in Table 9.2.

$$\begin{aligned} \log_{10} P_{sat} = & -7.90298 \frac{T_{st}}{T} - 1 + 5.02808 \log_{10} \frac{T_{st}}{T} \\ & - 1.3816 \cdot 10^{-7} (10^{11.344(\frac{T_{st}}{T}-1)} - 1) \\ & + 8.1328 \cdot 10^{-3} (10^{-3.49159(\frac{T_{st}}{T}-1)} - 1) \\ & + \log_{10} P_{st}^* \end{aligned} \tag{9.4.1}$$

Table 9.1: CHP- and RFCC flue gas composition.

<i>Component</i>	<i>CHP</i>	<i>RFCC</i>
N_2 (vol%)	75.1-74.8	79.5
Ar (vol%)	0.9	0.9
O_2 (vol%)	13.8-12.8	4.2
CO_2 (vol%)	3.4-3.9	12.9
H_2O (vol%)	6.8-7.7	2.5
SO_2 (ppmv)	0.3	10-30
SO_3 (ppmv)	Not defined	0.9
NO_X (ppmv)	5	70-100
NO_2 (ppmv)	0.5	5-10
N_2O (ppmv)	Not defined	0.8
NH_3 (ppmv)	Average 2, Max 5	Max 0.2
HCl (ppmv)	Not defined	0.5
Particulates (mg/ Nm^3)	Not defined	5-20
Temperature (°C)	194	15-25
Pressure (barg)	0.02	0.025

The gas was assumed saturated with water vapor, because the flue gas had been cooled in the direct contact coolers (DCC), before entering the absorber. See Figure 1.1 in section 1. The temperature was chosen for convenience, since the degradation reactions were independent of temperature in the simulation.

Table 9.2: Flue gas composition (mole fraction), saturated with water vapor at 25°C, as implemented in absorber simulations.

	CHP	RFCC
N_2	0.784398	0.791911
Ar	0.009419	0.008965
O_2	0.139193	0.041837
CO_2	0.0382	0.128499
H_2O	0.028788	0.028788
NH_3	$2.09 \cdot 10^{-6}$	$1.99 \cdot 10^{-7}$

The resulting flue gas compositions, after the implemented species were extracted from Table 9.1, saturated with water vapor, and normalized, are shown in Table 9.2.

9.4.2 Flow Rates

The flow rates for the two flue gases were retrieved from Cents (2012) [26].

Table 9.3: Flow rates for the two flue gases.

	RFCC	CHP
Gas flow [kmol/hr]	2 000	2 300
Liquid Flow [kg/hr]	180 000	70 000

The flow rates are presented in Table 9.3.

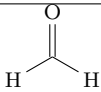
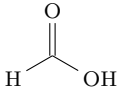
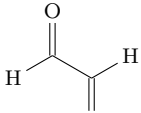
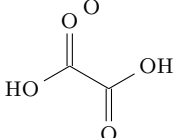
Chapter 10

Absorber Simulation Results

This chapter will present the results from the absorber simulations cases, presented in chapter 9. The results were exported from Aspen Plus, and the component names in the following tables are therefore different from the rest of the document.

Four of the component IDs given by Aspen Plus were very similar, and can possibly be misunderstood. Closer descriptions of these are therefore given in Table 10.1.

Table 10.1: Aspen Plus' component IDs of formaldehyde, formic acid, glyoxal and oxalic acid.

Component	Aspen Comp.ID	Structure
Formaldehyde	CH2O	
Formic Acid	CH2O2	
Glyoxal	C2H2O-01	
Oxalic Acid	C2H2O-02	

10.1 Initial Case

This case addressed the the initial degradation of amine. An unloaded and un-degraded MEA solution was fed to the absorber, where both CO₂-absorption and degradation would take place. Figure 9.1 shows the screen view of the simulation, with the names of the inlet- and outlet streams.

10.1.1 CHP Results

Table 10.2 shows the results from the simulation of CHP gas.

Table 10.2: Initial case results; CHP flue gas.

	GAS-IN	GAS-OUT	LIQ-IN	LIQ-OUT
	Mole Fraction			
H2O	0.028788	0.073552	0.886975	0.882689
NH3	2.09E-06	1.38E-05	0	8.58E-07
CO2	0.0382	0.005815	3.49E-09	1.08E-06
H3O+	0	0	1.54E-12	2.42E-11
OH-	0	0	6.45E-06	4.85E-07
NH4+	0	0	0	0
NH2COO-	0	0	0	0
HCO3-	0	0	0.000208	0.000673
CO3-2	0	0	0.000628	0.000308
N2	0.784398	0.77394	0	3.96E-06
O2	0.139193	0.137323	0	1.26E-06
CO	0	0	0	0
H2	0	0	0	0
AR	0.009419	0.009293	0	1.01E-07
H2SO4	0	0	0	0
HSO4-	0	0	0	0
SO4-	0	0	0	0
AMMON(S)	0	0	0	0
SALT1	0	0	0	0
MEA	0	5.61E-05	0.062593	0.012609
MEAH+	0	0	0.025527	0.052496
MEACOO-	0	0	0.024062	0.051209
HEF	0	1.20E-11	0	3.35E-06
HEI	0	7.79E-19	0	5.38E-15
BHEOX	0	1.08E-21	0	2.35E-09
HEGLY	0	3.93E-15	0	1.26E-07
CH2O	0	9.96E-44	0	1.62E-32
CH2O2	0	1.80E-12	0	9.90E-12
C2H2O-01	0	7.61E-06	0	2.45E-06
C2H2O-02	0	8.38E-15	0	4.84E-08
FE+2	0	0	0	2.37E-08
FE+3	0	0	1.13E-06	1.15E-06
	Physical Properties			
Total Flow kmol/hr	2300	2331.066	2923.677	2818.337
Total Flow kg/hr	66708.8	65342.67	70000.19	71366.32
Total Flow cum/hr	51789.49	59064.31	65.96461	64.8468
Temperature C	25	44.02941	25	28.73088
Pressure bara	1.1	1.04	1.1	1.047952
Vapor Frac	1	1	0	0
Liquid Frac	0	0	1	1
Solid Frac	0	0	0	0
Enthalpy J/kmol	-2.2E+07	-2E+07	-3E+08	-3.1E+08
Enthalpy J/kg	-759143	-697454	-1.2E+07	-1.2E+07
Enthalpy Watt	-1.4E+07	-1.3E+07	-2.4E+08	-2.4E+08
Entropy J/kmol-K	4244.838	4447.68	-259161	-327813
Entropy J/kg-K	146.3544	158.6687	-10824.3	-12945.7
Density kmol/cum	0.044411	0.039467	44.3219	43.46147
Density kg/cum	1.288076	1.106297	1061.178	1100.537
Average MW	29.00383	28.03124	23.94252	25.32214
Liq Vol 60F cum/hr	120.8319	118.7596		

The simulation of the CHP flue gas converged quite easily, opposite to the RFCC gas which will be discussed later. The simulation calculated 84.7%(mol) removal of CO₂ through the absorber. While the degradation caused 13.8 ppmv of NH₃ in the outflow of gas. A study by Fluor and Statoil (2005) [16], expected an NH₃ emission of 23 ppmv, with a similar flue gas as this case.

The main degradation products were HEF, with HEGly, BHEOX and HEI in declining order. Note that there was an absolute error in the mass balance of

$1 \cdot 10^{-4} [kg/hr]$, which caused an apparent production of Fe^{3+} through the absorber.

10.1.2 RFCC Results

Table 10.3 shows the results from the simulation of RFCC gas.

Table 10.3: Initial case results; RFCC flue gas.

	GAS-IN	GAS-OUT	LIQ-IN	LIQ-OUT
	Mole fraction			
H2O	0.028788	0.134714	0.886975	0.881379
NH3	1.99E-07	9.58E-06	0	1.62E-07
CO2	0.128499	0.017395	3.49E-09	1.71E-05
H3O+	0	0	1.54E-12	1.34E-10
OH-	0	0	6.45E-06	6.35E-15
NH4+	0	0	0	0
NH2COO-	0	0	0	0
HCO3-	0	0	0.000208	0.002842
CO3-2	0	0	0.000628	0.000395
N2	0.791911	0.796607	0	3.32E-06
O2	0.041837	0.042073	0	2.80E-07
CO	0	0	0	0
H2	0	0	0	0
AR	0.008965	0.009018	0	7.67E-08
H2SO4	0	0	0	0
HSO4-	0	0	0	0
SO4-	0	0	0	0
AMMON(S)	0	0	0	0
SALT1	0	0	0	0
MEA	0	0.000182	0.062593	0.006137
MEAH+	0	0	0.025527	0.056425
MEACOO-	0	0	0.024062	0.052795
HEF	0	5.03E-11	0	2.81E-06
HEI	0	2.82E-19	0	8.59E-19
BHEOX	0	2.03E-20	0	7.64E-10
HEGLY	0	5.78E-15	0	2.19E-08
CH2O	0	2.44E-11	0	6.79E-20
CH2O2	0	6.09E-18	0	7.77E-12
C2H2O-01	0	2.58E-06	0	5.75E-07
C2H2O-02	0	1.57E-14	0	1.13E-08
FE+2	0	0	0	6.11E-07
FE+3	0	0	1.13E-06	5.50E-07
	Physical properties			
Total Flow kmol/hr	2000	1988.18	7518.026	7307.571
Total Flow kg/hr	60109.78	54130.43	180000.5	185979.8
Total Flow cum/hr	45021.04	52646.83	169.6233	168.4028
Temperature C	25	58.40177	25	40.39355
Pressure bara	1.1	1.04	1.1	1.050493
Vapor Frac	1	1	0	0
Liquid Frac	0	0	1	1
Solid Frac	0	0	0	0
Enthalpy J/kmol	-5.8E+07	-3.9E+07	-3E+08	-3.1E+08
Enthalpy J/kg	-1915722	-1414138	-1.2E+07	-1.2E+07
Enthalpy Watt	-3.2E+07	-2.1E+07	-6.2E+08	-6.3E+08
Entropy J/kmol-K	4422.671	2752.772	-259161	-330552
Entropy J/kg-K	147.1531	101.1078	-10824.3	-12988.1
Density kmol/cum	0.044424	0.037764	44.3219	43.39341
Density kg/cum	1.335149	1.02818	1061.178	1104.375
Average MW	30.05489	27.22613	23.94252	25.45029
Liq Vol 60F cum/hr	105.0712	96.97461		

Unlike the CHP case, the RFCC case gas was not trivial to converge. This was due to the high CO_2 content in the gas. The problem was solved by changing the flow model. The absorber was first solved using a "mixed"-flow model, assuming the bulk properties for each phase was the same as the outlet conditions for that phase leaving that cell (stage for a tray column). When the simulation did converge, the flow model was changed to the counter-current flow model, without initializing the

10 ABSORBER SIMULATION RESULTS

simulation. In the counter-current flow model, the bulk properties of each phase was the average of the inlet and outlet properties, the recommended assumption for a packed column.

The simulation provided reasonable results as seen in Table 10.3. The simulation calculated 86.4%(mol) removal of CO₂ through the absorber. While the degradation caused 9.58 ppm(mol) of NH₃ in the outflow of gas. Like for the CHP case the main degradation products were HEF, with HEGly, BEHOX and HEI in declining order. The absolute error in the mass balance was $1.01 \cdot 10^{-2} [kg/hr]$.

10.2 Recycle Case

The details of this case are presented in section 9.2, and the case was a request from TCM DA. The objective of the case was to achieve 1 - 2%(weight) of degradation products in the liquid, and find the ammonia emission at this degree of degradation. This was to be achieved by decreasing the purge- and makeup stream, and let the degradation products accumulate in the system until the desired fraction of degradation products was reached.

Convergence proved to be very tough to reach in this case, and the calculations were very time consuming. When the calculation finally converged, it unfortunately became clear that the iterations diverged if the purge was decreased to values less than 900 kg/hr. The fraction of degradation products was at this purge flow, far less than the desired 1 - 2%(weight).

The simulation seemed to be unable to reach the goal for CHP flue gas. Of this reason the RFCC gas case, which had proved to be hard to converge in the initial case, Table 10.3, was not simulated for this case.

Table 10.4 shows the results of the recycle case for CHP flue gas, with 5% purge, which converged.

10 ABSORBER SIMULATION RESULTS

Table 10.4: Recycle case results; CHP flue gas, 5 % purge.

	CO2	GAS-IN	GAS-OUT	LIQ-IN	MAKEUP	PURGE	STACK
	Mole Fraction						
H2O	0.007695	0.028788	0.064757	0.886614	0.886975	0.886586	0.029548
NH3	1.05E-06	2.09E-06	1.46E-05	1.37E-06	0	1.46E-06	1.44E-05
CO2	0.992039	0.0382	0.012784	8.81E-09	3.49E-09	9.44E-09	0.013236
H3O+	0	9.84E-10	0	2.63E-12	1.54E-12	2.73E-12	0
OH-	0	1.43E-14	0	3.94E-06	6.45E-06	3.80E-06	0
NH4+	0	0	0	0	0	0	0
NH2COO-	0	0	0	0	0	0	0
HCO3-	0	9.84E-10	0	0.000343	0.000208	0.000356	0
CO3-2	0	1.77E-15	0	0.000746	0.000628	0.000753	0
N2	0.000196	0.784398	0.775491	2.60E-07	0	2.78E-07	0.80474
O2	6.25E-05	0.139193	0.137599	9.07E-08	0	9.69E-08	0.142789
CO	0	0	0	0	0	0	0
H2	0	0	0	0	0	0	0
AR	5.00E-06	0.009419	0.009312	6.73E-09	0	7.19E-09	0.009663
H2SO4	0	0	0	0	0	0	0
HSO4-	0	0	0	0	0	0	0
SO4-	0	0	0	0	0	0	0
AMMON(S)	0	0	0	0	0	0	0
SALT1	0	0	0	0	0	0	0
MEA	4.51E-12	0	3.17E-05	0.045217	0.062593	0.044026	2.68E-09
MEAH+	0	0	0	0.034428	0.025527	0.03504	0
MEACOO-	0	0	0	0.032591	0.024062	0.033176	0
HEF	7.38E-14	0	1.83E-09	4.66E-05	0	4.98E-05	1.74E-13
HEI	0	0	1.00E-35	0	0	0	0
BHEOX	0	0	3.61E-18	2.64E-07	0	2.82E-07	0
HEGLY	9.76E-20	0	4.39E-13	1.74E-06	0	1.86E-06	1.54E-19
CH2O	1.03E-13	0	4.11E-14	1.02E-14	0	7.18E-15	4.23E-14
CH2O2	9.43E-10	0	2.12E-09	2.50E-08	0	2.67E-08	1.30E-09
C2H2O-01	1.55E-06	0	1.04E-05	3.46E-06	0	3.69E-06	9.76E-06
C2H2O-02	1.46E-18	0	7.39E-13	4.10E-07	0	4.38E-07	2.27E-18
FE+2	0	0	0	2.22E-08	0	2.38E-08	0
FE+3	0	0	0	1.11E-06	1.13E-06	1.11E-06	0
	Physical Properties						
Total Flow kmol/hr	56.91582	2300	2326.402	2877.193	185.1889	184.7118	2241.846
Total Flow kg/hr	2493.247	66708.8	65677.2	70017.07	4433.889	4500	64148.89
Total Flow cum/hr	1298.726	47372.86	58464.23	65.05745	4.178271	4.177289	55284.24
Temperature C	3	25	41.43396	25.15166	25	25.16951	23.65144
Pressure bara	1	1.2	1.04	1.1	1.1	1.1	1
Vapor Frac	1	0.997932	1	0	0	0	1
Liquid Frac	0	0.002068	0	1	1	1	0
Solid Frac	0	0	0	0	0	0	0
Enthalpy J/kmol	-3.9E+08	-2.2E+07	-2E+07	-3E+08	-3E+08	-3E+08	-1.2E+07
Enthalpy J/kg	-8979227	-762306	-716867	-1.2E+07	-1.2E+07	-1.2E+07	-433801
Enthalpy Watt	-6218730	-1.4E+07	-1.3E+07	-2.4E+08	-1.5E+07	-1.5E+07	-7729954
Entropy J/kmol-K	187.2223	3215.075	4709.081	-280870	-259161	-282362	4160.755
Entropy J/kg-K	4.27391	110.85	166.804	-11541.7	-10824.3	-11590.1	145.4082
Density kmol/cum	0.043824	0.048551	0.039792	44.22543	44.3219	44.21811	0.040551
Density kg/cum	1.919764	1.408165	1.123374	1076.235	1061.178	1077.254	1.160347
Average MW	43.80587	29.00383	28.23123	24.3352	23.94252	24.36227	28.61431
Liq Vol 60F cum/hr	3.032735		119.2481				117.7162

10.3 Absorber Series Case

The details of this case is presented in section 9.3, the aim for the case was to calculate the total absorber residence time needed to give 1%(weight) of degradation products in the liquid phase.

10.3.1 CHP Results

Table 10.6 shows the mass fraction of the streams "LIQ-OUTB" and "LIQ-OUTC", shown in Figure 9.3. The total mass fractions of liquid phase degradation products were summed up for these streams. The difference between these two mass fractions, would represent the degradation during the time of a single run through the absorber.

Table 10.5: Absorber holdup; RFCC flue gas.

Stage	Liquid holdup [m^3]
1	0.18440813
2	0.1732027
3	0.17367606
4	0.17110427
5	0.16985174
6	0.16847324
7	0.16758018
8	0.1671213
9	0.16715543
10	0.16768768
11	0.16875186
12	0.17053256
Sum	2.04954515

To find the time of a single run through the absorber, the liquid holdups were summed in Table 10.5. Together with the data of the volumetric flow rate, the retention time for a single run through the absorber could now be calculated.

Equation (10.3.1) shows how the residence time per run was calculated.

$$\tau = \frac{h}{\dot{V}} = \frac{2.05 [m^3/run]}{65.3 [m^3/hr]} = 0.031 [hr/run] \quad (10.3.1)$$

The residence time needed to extrapolate the degradation gradient to 1%(weight), was then calculated in equation (10.3.2):

$$t_{goal} = \frac{x_{deg,goal} - x_{deg,init}}{\Delta x_{deg}} \cdot \tau = \frac{0.01 - 3.21 \cdot 10^{-5}}{1.22504 \cdot 10^{-5} [\frac{1}{run}]} \cdot 0.031 [hr/run] = 25.54 [hr] \quad (10.3.2)$$

10 ABSORBER SIMULATION RESULTS

Table 10.6: Absorber in series case results; CHP flue gas. Mass fractions of the streams to be compared.

Mass Frac	LIQ-OUTB	LIQ-OUTC	LIQ-OUTB	LIQ-OUTC
	All components		Degradation products	
H2O	0.6258385	0.6258338		
NH3	6.19E-07	6.20E-07	6.19E-07	6.2E-07
CO2	7.10E-06	7.29E-06		
H3O+	4.32E-24	4.36E-24		
OH-	1.58E-07	1.57E-07		
NH4+	0	0		
NH2COO-	0	0		
HCO3-	2.50E-03	2.53E-03		
CO3-2	5.95E-04	5.94E-04		
N2	4.40E-06	4.40E-06		
O2	1.61E-06	1.61E-06		
CO	0	0		
H2	0	0		
AR	1.60E-07	1.60E-07		
H2SO4	0	0		
HSO4-	0	0		
SO4-	0	0		
AMMON(S)	0	0		
SALT1	0	0		
MEA	0.0136464	0.0134414		
MEAH+	0.1358907	0.1359692		
MEACOO-	0.2214776	0.2215756		
HEF	2.31E-05	3.45E-05	2.31E-05	3.45E-05
HEI	6.29E-27	2.15E-20	6.29E-27	2.15E-20
BHEOX	5.28E-08	1.03E-07	5.28E-08	1.03E-07
HEGLY	1.16E-06	1.73E-06	1.16E-06	1.73E-06
CH2O	1.33E-13	1.03E-13	1.33E-13	1.03E-13
CH2O2	9.68E-11	2.23E-10	9.68E-11	2.23E-10
C2H2O-01	6.87E-06	6.94E-06	6.87E-06	6.94E-06
C2H2O-02	3.19E-07	4.60E-07	3.19E-07	4.6E-07
FE+2	5.39E-08	5.39E-08		
FE+3	2.50E-06	2.50E-06		
Total Flow kmol/hr	2840.21	2840.551		
Total Flow kg/hr	72213.16	72223.54		
Total Flow cum/hr	65.28692	65.292		
Temperature C	26.71462	26.68174		
Pressure bara	1.047688	1.047679		
SUM			3.21E-05	4.43E-05

10.3.2 RFCC Results

Table 10.8 shows the mass fraction of the streams "LIQ-OUTB" and "LIQ-OUTC", shown in Figure 9.3. As for the corresponding CHP case, the total mass fractions of liquid phase degradation products were summed up for these streams. The difference between these two mass fractions, would be the degradation during the time of a single run through the absorber.

Table 10.7: Absorber holdup; RFCC flue gas.

Stage	Liquid holdup [m^3]
1	0.36342469
2	0.36045585
3	0.35713729
4	0.35345352
5	0.34941756
6	0.3450923
7	0.34060976
8	0.33618277
9	0.33210747
10	0.32877257
11	0.32672365
12	0.32692119
Sum	4.12029862

Table 10.7 shows the liquid holdup for RFCC case.

Analogous to the CHP case, the total residence time needed to achieve 1%(weight) of degradation products in the liquid phase was calculated by equation (10.3.3) and (10.3.4):

$$\tau = \frac{h}{\dot{V}} = \frac{4.12 [m^3/run]}{171.2 [m^3/hr]} = 0.024063524 [hr/run] \quad (10.3.3)$$

$$t_{goal} = \frac{x_{deg,goal} - x_{deg,init}}{\Delta x_{deg}} \cdot \tau = \frac{0.01 - 1.636 \cdot 10^{-5}}{7.420 \cdot 10^{-6} [\frac{1}{run}]} \cdot 0.02406 [hr/run] = 32.3 [hr] \quad (10.3.4)$$

10 ABSORBER SIMULATION RESULTS

Table 10.8: Absorber in series case results; RFCC flue gas. Mass fractions of the streams to be compared.

Mass Frac	LIQ-OUTB	LIQ-OUTC	LIQ-OUTB	LIQ-OUTC
	All components		Degradation products	
H2O	0.630133	0.630203		
NH3	1.54E-07	1.54E-07	1.54E-07	1.54E-07
CO2	3.54E-05	3.54E-05		
H3O+	7.19E-11	7.19E-11		
OH-	2.15E-07	2.15E-07		
NH4+	0	0		
NH2COO-	0	0		
HCO3-	5.03E-03	5.03E-03		
CO3-2	5.71E-04	5.71E-04		
N2	3.70E-06	3.70E-06		
O2	3.77E-07	3.77E-07		
CO	0	0		
H2	0	0		
AR	1.22E-07	1.22E-07		
H2SO4	0	0		
HSO4-	0	0		
SO4-	0	0		
AMMON(S)	0	0		
SALT1	0	0		
MEA	0.013454	0.013448		
MEAH+	0.134999	0.134972		
MEACOO-	0.215751	0.215708		
HEF	1.33E-05	2.00E-05	1.33E-05	2.00E-05
HEI	2.24E-13	6.27E-13	2.24E-13	6.27E-13
BHEOX	9.96E-09	1.95E-08	9.96E-09	1.95E-08
HEGLY	1.66E-07	2.50E-07	1.66E-07	2.50E-07
CH2O	1.19E-33	1.19E-33	1.19E-33	1.19E-33
CH2O2	3.31E-11	6.28E-11	3.31E-11	6.28E-11
C2H2O-01	2.62E-06	3.22E-06	2.62E-06	3.22E-06
C2H2O-02	5.92E-08	8.82E-08	5.92E-08	8.82E-08
FE+2	2.35E-07	2.35E-07		
FE+3	2.27E-06	2.27E-06		
Total Flow kmol/hr	7463.631	7465.53		
Total Flow kg/hr	1.89E+05	1.89E+05		
Total Flow cum/hr	171.6703	171.7039		
Temperature C	42.47476	42.47144		
Pressure bara	1.047618	1.047617		
Sum			1.64E-05	2.38E-05

Part III

Discussion and Conclusions

Chapter 11

Discussion

The following chapter will discuss the assumptions, actions and results of the two previous parts. First the degradation modeling will be discussed, thereafter the degradation reactions, and last the absorber simulations.

11.1 Modeling of the Degradation Experiments

The following sections will discuss assumptions and results in the final version of the rate equations, during the modeling of the closed- and open loop experiments.

11.1.1 Deviation Between Model and Experiments

As shown in section 6.4.3, there were large deviations between the degradation model and -experiments for some of the components, and low deviations for other components. The deviations also varied between the open- and closed loop experiment, and between the cases with locked- and unlocked ammonia profile.

There were two main sources of error: Experimental error; uncertainty and errors in the experimental data, and model error; uncertainty and errors in the found rate equations, reaction equations, physical parameters, or the model in general. In this study, the author had no control over the experimental errors, in contrast to the model errors which the author was fully responsible for.

The standard deviations for some of the components calculated in section 6.4.3, showed large deviations. The figures in the same section showed similar tendencies. Still, it is of importance to note that the aim of the model fitting was not necessarily to minimize the deviation at all costs. Even though it seemingly would be optimal to explain the experimental data perfectly with the model, the main emphasis was laid on explaining the tendencies that the experimental data showed.

An example of this can be seen in Figure 6.8, for the concentration profile of HEGly. In this case it was obvious that the standard deviation would become quite large. This was due to the modeled profile almost not hitting any of the experimental points. Still, if the experimental points of this component were studied, it would become clear that there were several ways to interpret these data.

11 DISCUSSION

The first option would be to force the model to strictly follow the experimental data. This would provide a function which would look like a logarithmic function with a dip at day 15. The model would then provide the lowest standard deviation for HEGly in the closed loop experiment. Yet, it would be practically impossible to explain the experimental points of HEGly in the open loop experiment, Figure 6.7, with the same equation.

The second option was to assume that the fourth and fifth experimental point in the closed loop experiment, were outliers. This would provide a very similar HEGly profile in the closed- and open loop model, but the standard deviations would become large for the closed loop experiment. Still, it was generally not believed that two subsequent points with some of the largest values in the experimental data for this component, would both contain such large experimental errors. Mainly because the largest values were values the furthest away from the detection limit of the analyzer used in the experiments.

The third, and chosen, option, was to think of the closed loop HEGly profile as a function with a steep gradient in the initial days of the experiment, which would later flatten out when it was reaching some kind of equilibrium. As Figure 6.8 shows, this option resulted in a modeled profile which was a compromise between the experimental points of HEGly. The profile gave rather large standard deviations for the closed loop model, but the profile also looked realistic.

This example shows that it was not trivial to fit the model to the experimental data, and that it was not always directly of interest to minimize the standard deviations. The requirement for the same equations to describe both the closed- and the open loop experiment, sometimes resulted in that the same rate equation had to describe opposite tendencies for each of the two experiments (see the BHEOX profile in Figure 6.7 and Figure 6.8). Additionally there was no ways to determine if an experimental tendency was just unexpected, or a result of experimental error. This made the fitting even more demanding.

The calculated standard deviations also emphasized the deviation at low experimental values, due to the way the errors where calculated. In section 6.4.3 it is shown that every error was divided by its experimental value, for some components this value was $\ll 1$, which resulted in large standard deviations for some components.

Figure 6.11 shows a plot of the deviations for the open loop model with locked ammonia profile. A conspicuous tendency in this plot was the BHEOX profile, which showed systematic errors. The reason for this, as mentioned in section 6.4 and earlier in this section, was that the experimental BHEOX profile in the closed loop experiment, Figure 6.8, showed an opposite tendency compared with the profile in the open loop experiment, Figure 6.7. The modeled profile was therefore a compromise which undershot the experimental points in the open loop-, and overshot the experimental point in the closed loop experiments.

Another profile which showed large deviations in Figure 6.11, was the ammonia profile. Even though the ammonia profile was locked to the experimental points. The reason for this deviation can easily be seen in Figure 6.7. Two pairs of experimental points for ammonia had the same value which made it impossible

for the modeled profile to hit all the points. These errors were most likely results of experimental error. Additionally, the formic acid profile had a point with error of more than 20%, from Figure 6.7, which also looked like experimental error.

Figure 6.12 shows a plot of the deviations for the closed loop model with locked ammonia profile. An important trend in Figure 6.12, is the large deviations for the gas phase concentration of oxygen. The experimental gas phase oxygen profile in the closed loop, Figure 6.8, was not described correctly by the model, even though an oxygen leakage term was added in the modeling. Some of the reason for the difficulties in describing the experimental oxygen profile was most likely inconsistency in the experimental data. Figure 2.2 in section 2.3, shows that the experimental data for oxygen had a peak at day 8, because the closed loop system was opened at that point. Additionally the oxygen level began increasing after day 12. This might be explained by the reactions that would consume less oxygen as equilibrium was approached, while the leakage would proceed and cause the increase of oxygen level. Nevertheless, the model was not able to describe these tendencies.

Figure 6.13 and Figure 6.14 shows plots of the deviation for respectively the open- and the closed loop model, with unlocked ammonia profiles. These figures contain more or less the same tendencies as was shown for the locked profiles, Figure 6.11 and Figure 6.12. The exception was, as expected, the deviation for the ammonia profiles, in addition to some ammonia dependent products, especially HEI. The deviation for the ammonia profile is further discussed in section 11.1.4.

To sum up, the deviation presented in section 6.4.3, was mostly expected and could be justified. The exception was the deviation of the gas phase profile of oxygen in the closed loop model, which revealed weaknesses in the model.

11.1.2 Iron Catalyst Dependency

The concentration of iron ions ranged from zero, in the open loop experiment, to a low value, for the closed loop experiment. The dependency of this parameter was therefore utilized, during the fitting of the rate parameters, to obtain rate equations that would describe both experiments. Chapter 6 showed how this made it possible to describe two different sets of experimental data, with the same rate equations.

Nevertheless, as shown in section 6.4.5, the resulting degradation model failed when it attempted to predict the degradation in a third experiment, see section 2.4. The main issue was that this experiment contained a concentration of iron ions about 100 times larger than in the closed loop experiment, section 2.3, which the model was fitted to. In comparison, the terminal concentrations of HEF and HEI were approximately the same in the closed loop experiment and the third experiment.

This indicated that the catalytic effect of iron ions would reach a maximum, at a concentration which was much lower than the iron ion concentration in the third experiment. This was evident when the iron concentration in the model of the third experiment was lowered to a level the model could handle, see Figure 6.15. As the figure shows, the model was then able to predict both the MEA consumption

and the HEF formation, with surprisingly accuracy. The HEI concentration was underestimated though.

The phenomena described above showed that the model had obvious weaknesses in the handling of the iron ion concentration. For future work a separate function to handle the catalytic effects could be added to solve the problem, or the model could be viewed as a binary system of equations. One set of equations for systems without catalyst, and another set for systems with iron concentrations, see chapter 13.

Anyhow, the prediction of the third experiment, did not only show weaknesses with the degradation model, but also that it was possible to predict amine degradation with a model of this kind. That this model could be one step in the direction of obtaining the complete overview of the degradation reactions.

11.1.3 The Oxygen Leakage and the Hydrogen Abstraction Mechanism

As mentioned in section 4.1 and 6.2, it was believed in the early stages of this study, that the closed loop experimental setup (section 2.1.2) was completely closed from the environment. Except, of course, at day 8 in the experiment, Figure 2.6, when the system was opened. As described in section 4.1.1, the total stoichiometric amount of oxygen in the system, was too low to account for the consumed MEA. This motivated the search for alternative reaction mechanisms which were not consuming oxygen, which resulted in the hydrogen abstraction mechanism, section 4.1.2.

It later became clear, as mentioned in section 4.1 and 6.2, that even if reaction 1, Table 4.2, did not consume oxygen, there would still not be enough oxygen available in the system for the remaining reactions to take place. This led to the assumption that there had been an oxygen leakage in the closed loop setup. Therefore, an oxygen leakage term was added in the gas phase equation for oxygen in the closed loop model, section 6.3.

In section 6.4.4, the found air leakage to gas circulation ratio was calculated to 0.017%(mol). This was a very small leakage, and was most likely caused by the gas circulation fan, see Figure 2.2. The fact that the leakage necessary to feed all the oxygen consuming reactions, was this small, made the assumption of a leakage probable.

The problem was now that the hydrogen abstraction mechanism had been chosen on the basis, and consequence, of the assumption that the closed loop experiment was completely closed. This assumption was found to be false, which meant that the formation pathway of formaldehyde could just as well be by the oxidation mechanism, section 4.1.1. Nevertheless, if the oxidation pathway was applied in the degradation model, the liquid phase would have consumed significantly larger amounts of oxygen. The formaldehyde formation was modeled as the main MEA consuming reaction.

About 0.04 [$kmol/m^3$] formate, 0.075 [$kmol/m^3$] HEF, and 0.10 [$kmol/m^3$] HEI, was produced by the most abundant reactions. These reactions were already im-

plemented, and consuming oxygen, see Figure 2.5 and Figure 2.6. In addition to about 1 [$kmol/m^3$] of MEA which was to be consumed in the closed loop experiment. With the formaldehyde formation as the main MEA consuming reaction, and if the hydrogen abstraction mechanism was applied, oxygen would not be consumed by this reaction. But if the oxidation mechanism was applied, the oxygen consumption would look different: The oxidation mechanism for formaldehyde would stoichiometrically consume 0.5 mole O_2 per mole MEA reacted, so would the formation of formate and HEF, while HEI would consume 1 mole O_2 per mole HEF formed. This meant that the oxygen consumption would increase by roughly four times, if the oxidation mechanism was implemented.

The current oxygen leak was quite low, and a leak of four times the current would probably not be unreasonable. Still, if the reaction actually was this dependent of the oxygen concentration, one would expect an increase in the MEA consumption when the closed loop setup was opened in the middle of the experiment, see Figure 2.6. As previously mentioned, the oxygen concentration had a peak at day 8. Figure 2.6 shows that MEA was consumed steadily, apparently unaffected by the oxygen peak.

On the other hand, the reason for the MEA consumption being this steady, could also be due to that the reactions were rate limiting, and not the mass transfer of oxygen. This meant that both pathways to formaldehyde were equally likely to be correct. Yet, Goff and Rochelle (2004) [18], assumed that the mass transfer of oxygen was rate limiting in MEA degradation, and obtained equal or less degradation rates as reported in literature. This could indicate that the reaction rate was not rate limiting, and that an increased MEA consumption should be observed, when the oxygen level peaked, if MEA was consumed by the oxidation mechanism.

The reality could be that both pathways were participating in the formation of formaldehyde. But for the degradation model, a single pathway was to be chosen to keep the simplicity at a reasonable level.

When fitting the degradation model to the experimental data, as described in chapter 5, an attempt was made to fit the oxidation pathway to the experimental data (not shown in this report). This attempt was unsuccessful, and was consuming the oxygen faster than the mass transfer was able to provide oxygen in the liquid phase. Due to this, the hydrogen abstraction mechanism was applied in the further fitting of the model. This does not necessarily tell anything about which mechanism was taking place, due to the uncertainty in the parameters describing the mass transfer. Nevertheless, as mentioned earlier, one of the pathways had to be chosen. In this case the hydrogen abstraction mechanism was chosen. It would be a part of the further work, chapter 13, to investigate which of these that is actually taking place, if not both.

11.1.4 Locked Ammonia Profile

It was suspected during the development of the model that the gas-liquid mass transfer of ammonia was unreliable. The reason for this suspicion was that the models seemed to incorrectly predict the ammonia content in the liquid phase.

Later, during the development of the model, it was found that the mass transfer parameters were not to blame for this. One of the main reasons the ammonia seemed incorrectly predicted was due to the recycle loop in the open loop experiment, explained in section 7.1.2. But during the development of the model, the mass transfer properties of the components were also continuously updated to more accurate values.

Since the rate equations were sensitive to the ammonia concentration, an incorrect estimation of this concentration profile would transfer to an incorrect estimation of the rate equations depending on ammonia. To be certain that the rate equations would become a function of the actual ammonia concentration, the liquid ammonia profile was locked to the experimental points, during the model development, as explained in section 6.3.

A "Locked concentration profile" implied that a time dependent function of concentration derivative, was found which described the experimental point as good as possible. This made the profile of the component, in this case ammonia, independent of reactions and mass transfer.

The obtained rate parameters, fitted to the locked ammonia profile, would then be dependent of the actual experimental ammonia profile. After the rate parameters were obtained, the ammonia profile could be unlocked. The mass transfer parameters could then be adjusted so that the ammonia profile would hit the experiment points, as done in section 7.1.2, to compensate for the lack of recycle loop in the model.

The latter step would not affect the absorber simulations in Aspen Plus. As long the rate equations were fitted to the experimental ammonia profile, the simulation software would provide the remaining properties.

This reasoning would also apply to other volatile components, especially formaldehyde. Nevertheless, there were no experimental data to substitute the concentration profile of formaldehyde. It was therefore reasonable to believe that the found rate equations could be incorrectly dependent of the formaldehyde concentration. Yet, the lack of experimental data for this component made it impossible to validate this hypothesis.

11.1.5 Validity of the Experimental Models

As mentioned in chapter 3, it was of interest to keep the degradation models as simple as possible. This was done to keep the calculation time low, and make it possible to fit the models to the experimental data by performing large numbers of iterations. Of this reason both experimental setups, see section 2.1.1 and 2.1.2, were modeled as bubble reactors, see section 3.1 and 3.2.

As discussed in section 11.1.4, and in section 7.1.2, the experiment model for the open loop experiment was not suitable for the volatile degradation products, but worked fine for oxygen and non-volatile components. This was, as mentioned, due to that the unknown recycle ratio in the open loop experiment was not modeled. Also the closed loop model had to be modified, since the closed loop experiment was leaking air into the system, as discussed in section 11.1.3.

One might argue that the models were too simple to describe the experiments which, as previously discussed, and in some manner they were. But the frequent lack of physical data, e.g. the recycle ratio of the open loop experiment, or the rate of leakage in the closed loop experiment, forced the author to accept the simplifications and assumptions needed to run the model without these data. It was obvious that when the degradation experiments were designed, it was not intended for the experiments to be modeled.

Additionally, even with models of this simplicity, it was one of the most time consuming processes during this study to fit the rate parameters to the experiment data. An increase in the model complexity, would also increase the time spent on fitting.

11.1.6 Over-all Gas Phase Balance for the Closed Loop Experiment Model

According to Schaftlein et al (1968) [30], an over-all gas phase balance was needed in addition to the equations presented in 3.2, to describe a two-phase batch reactor. For implementing such a balance for this case, either a pressure model, or data for the pressures was needed. This requirement would prove to be hard to fulfill, since the total pressure in the closed loop system was unknown.

Before the rate equations were fitted to the experimental data, the gas phase leakage (see section 11.1.3) in the closed loop experimental setup was unknown. Yet, it was evident from the closed loop experimental data, section 2.3, that the gas phase fraction of oxygen had significantly decreased during the experiment. In an actual closed system, such a decrease of one of the gas phase components, would consequently have decreased the total pressure in the system. The production of volatile components, like ammonia and formaldehyde, would though have compensated for some of this pressure loss. Nevertheless, even considering such compensation, a drastic decrease of total pressure would be expected in such a case.

When the conductor of these experiments, Velvelstad (2012) [25], was consulted with this problem, it became clear that a water trap that had been connected to the closed loop setup during the experiments. The water trap had provided an indication of the approximate pressure difference between the environment and the closed loop experiment. Velvelstad (2012) [25] reported that only minor pressure differences had been observed during the closed loop experiment. This indicated that the apparatus had been leaking.

It was thus known, before the fitting of the rate equations, that the closed loop contained a leakage, but the size of the leak was unknown. It was therefore not possible to provide an accurate gas phase balance for the system.

Due to these aspects, it came to a choice between adding an over-all gas phase balance, which would describe the gas phase balance incorrectly, or not to add an over-all gas phase balance at all. The latter option was chosen, due to a belief that no information was better than incorrect information. As a consequence of this choice, it became important to control the resulting gas phase composition of

the model, to be realizable.

Appendix C shows the gas phase results for the final version of the model. The results showed reasonable mole fractions for the different gas phase components. It could therefore be assumed that the model was realizable.

11.1.7 The Mass Transfer Coefficients

In section 3.3 the gas side mass transfer was assumed to be negligible. This was done under the assumption that the degradation reactions were slow. As seen in the figures in section 2.2 and 2.3, approximately one mole of MEA was consumed during three weeks. The assumption of slow reactions was in other words reasonable.

The liquid side mass transfer coefficient was unknown in the experiments. Of this reason a sensitivity analysis was made by varying this parameter over a range of $10^4[m/day]$, see section 7.1.1. The sensitivity analysis showed that as long as the liquid side mass transfer coefficient was held at a value above $k_L = 10[m/day] = 1.16 \cdot 10^{-4}[m/s]$, the reactions were not affected by this parameter. Thus, this value was chosen. Alves et al. (2004) [2] measured liquid side mass transfer coefficients in the range of $k_L = 0.87 - 3.19 [10^{-4}m/s]$, in stirred bubble tanks filled with water. This showed that the selection of k_L for the models, were reasonable.

This was, as earlier mentioned, not true for the liquid side mass transfer coefficient for ammonia. Even though this coefficient usually is independent of components, the coefficient for ammonia was used to compensate for assumptions made in the modeling, see section 7.1.2.

11.1.8 Henry's Law Coefficients

Two sets of estimated Henry's law coefficients were available for use in the modeling: Either calculated by da Silva (2012) [24] for infinite dilution in water by use of computational chemistry, or obtained from U.S. Environmental Protection Agency's EPI Suite (2008) [22], also for infinite dilution in water. This applied to all components except for oxygen, which for a temperature dependent function by Rooney and Daniels (1998) [29] for solubility of oxygen in MEA solutions was applied.

Except for oxygen, the Henry's law coefficient had to be assumed equal for water and the MEA water solution. This assumption was not necessarily true, especially considering that the MEA solution could be up to 30%(weight) MEA in the experiments. Nevertheless, no better data was found for Henry's law coefficient, and the assumption was accepted. Still, this could be a source of error in the modeling of the experiments.

Of the two sources of Henry's law coefficients, the ones estimated applying computational chemistry were used in this study. This was because EPI Suite (2008) [22] was using group contribution methods to estimate the coefficients, when empirical data was unavailable. Computational chemistry, in contrast, applied an electrostatic term, in addition to the empirical terms, which was considered to

provide a more rigorous estimation than the group contribution method (da Silva (2012) [24]).

11.1.9 Minor Assumptions

During the implementation of the models, chapter 3, in MatLab, see appendix D, several common minor assumptions were made to complete the models. These assumptions will be commented in this section:

Where it was necessary, the gas phase was assumed to behave as ideal gas. This was reasonable considering the ambient temperature and pressure in the experiments.

The volume of the liquid phase was assumed to be constant, even though mass transfer was occurring between the gas- and liquid phase. Still, the mass transfer was small compared to the volume of the liquids. There were also no data on the volumetric change in the liquid phase. The assumption was therefore considered to be reasonable.

For the open loop experiment, it was assumed that the volumetric gas flow was approximately the same in- and out flow of the reactor. This was done due to the lack of measurements of the volumetric out flow. The assumption was strictly speaking not true, due to the mass transfer of oxygen to the liquid phase, and the mass transfer of volatile degradation products to the gas phase. The degradation was considered to consume reactants, and produce products, in a slow compared to the gas flow. The assumption was therefore also considered to be reasonable.

When Henry's law coefficient for oxygen was recalculated from mass- to mole basis, the liquid density was assumed to be equal to water at 4 °C ($1000 \text{ [kg/m}^3\text{]}$). The same assumption was made when Henry's law coefficient was calculated for water. This assumption was not necessarily correct, since 30%weight of the liquid was MEA. It was though considered to be unnecessary to implement a density function, since the use of this parameter in the model was limited. In addition, there were several larger uncertainties associated with the model. The deviation of the density was therefore considered to be very small in comparison to the general uncertainty.

11.2 The Degradation Reactions

This section will discuss the uncertainties in the reaction equations for the degradation. In addition the charge balance in the reactions will be discussed, before the section is ended with a discussion of reversible reactions.

11.2.1 The General Uncertainty of the Reaction Mechanisms

The details of the degradation reactions, as presented in chapter 4, were uncertain in different degrees. The hydrogen abstraction mechanism, as already discussed in section 11.1.3, and the reaction mechanism to HEGly, see section 11.2.2, were cases where the uncertainty in the reaction mechanisms played a larger role than for the other reactions. Generally it was rather the rule than the exception, that there were uncertainty connected with the formation pathway of the different degradation products.

The reason for this uncertainty was that a large part of the details in the degradation reactions were still unknown (da Silva et al. (2012) [14]), at the time this study was done. Nevertheless, to model the degradation, the reaction stoichiometry was needed. An effort was therefore made to find the most probable reactions, as seen in chapter 4, even though it was impossible to conclude on several pathways with available knowledge and research.

From a modeling perspective it would be optimal to have a correct stoichiometry, but since all rate equations were to be fitted to the experimental data, the model would to some extent be able to describe the concentration profiles even with incorrect stoichiometry. As long as the rate equations were applied with the stoichiometry they were fitted for, the rate equations would describe the tendencies in the fitted experiments. Nevertheless, wrong stoichiometry could provide incorrect concentration profiles for intermediate components with no experimental measurements. This could be the case for formaldehyde and glyoxal, see Figure 6.7. Still, since there were no experimental measurements of these components, there were no way to conclude if these predicted concentration profiles were realizable or not.

11.2.2 Uncertainty of the Reaction Mechanism of HEGly

As mentioned, there was some degree of uncertainty associated with all the reaction mechanisms, but in contrast, the formation pathway of HEGly was practically unknown. There was no evidence to back up any formation pathway of this product. At the point this model was made, a pathway was more or less randomly chosen between two suggested options, see section 4.5. This was to investigate if it was possible to describe the formation of this product.

Due to the high uncertainty associated with the formation of HEGly, some measures were taken to prevent the uncertainty of this mechanism to affect the rest of the model. As shown in Table 4.2, the formation of HEGly was implemented independent of the remaining reactions. In this way the formation of HEGly could

be removed, resulting in nothing else than a slightly lower oxygen- and MEA consumption.

The modeling results, section 6.4, showed that the formation of HEGly could be described using the proposed reaction equation. This can be seen of the modeled profiles which described the experimental point in a reasonable manner.

11.2.3 Charge Balance and Radicals

Due to the radical mechanism in reaction 1, section 4.1.2, and oxidation in reaction 8, section 4.5.2, these reactions presented in the reaction overview, Table 4.2, were apparently producing electrons. These electrons were only included to balance the reactions, and would typically be substituted with radicals or metals to account for the charge balance.

When the reactions were implemented in Aspen Plus, there was no opportunity to implement radicals or electrons in the liquid phase. Due to this the electrons, in reaction 1 and -8, were substituted with the reduction of ferric, equation (8.4.1). The resulting reaction equations are shown in appendix A.

It is important to notice that the reactions only were consuming ferric to fulfill Aspen Plus' demand of charge balance for all reactions. The reactions could just as well be balanced out with radicals.

It is also important to notice the difference between the catalytic effect of the iron ions included in the degradation model, and the charge balancing iron ions included in the reactions in Aspen Plus. The latter can be viewed more as a representative for the radical effects. There was no connection between these effects included in the simulation.

11.2.4 Reversible Reactions

As presented in the reaction overview, Table 4.2, the formation of HEF, HEI, oxalic acid, BHEOX and HEGLY, were illustrated as reversible reactions. The remaining three reactions, were illustrated as irreversible. This was corresponding to the rate equations, see equation set (6.4.1), where the equations for the reactions illustrated as reversible, had backward rate terms.

Documentation on which of the reactions that was reversible was not found in literature. The reason to why some of the reactions were implemented with this term, was just due to the fitting of the rate parameters. For the degradation products which, during the fitting process, seemed to be indescribable without the backward term, a backward term was added. For the reactions where the backward term was found to be zero, the term was removed.

As mentioned, no sources were found to confirm that some of the reactions were reversible. Nevertheless, the found rate equations were describing the formation of the degradation products in a satisfactory manner.

11.3 Absorber Simulation

This section will discuss the absorber simulation results, the validity of the simulation cases, problems in the property estimation, and the iron ion concentration in the absorber simulation. Then the laboratory experiments will be discussed in comparison to the TCM absorber, before the section is ended with a comment on the stripper degradation.

11.3.1 Absorber Results

The following sections will discuss the results from the absorber simulation, the validity of the simulation cases, and weaknesses in the simulations.

The Initial Cases

For both the CHP and RFCC gas in the initial cases, Table 10.2 and Table 10.3, the order of liquid degradation products concentrations values was found to be:

HEF > NH₃ > HEGly > BHEOX > Formic Acid > HEI

This order of degradation products was not unlike the order found in the open loop experiment, see Figure 6.7:

NH₃ > Formic acid > HEF > HEGly > HEI > BHEOX

If formic acid and ammonia was excluded from this comparison, the only difference between the degradation products order, would be the placement of HEI. As will be discussed in section 11.3.3, the volatility of HEI was incorrectly estimated by Aspen Plus. This explains why so little HEI was seen in the liquid phase in the simulations.

As for ammonia and formic acid, the pH was probably different in the absorber simulation, and the degradation experiments. This would be due to no lean amine in the experiments. Difference in pH, would result in different solubility of basic- and acidic components, and could be the reason for the differences in the degradation product orders between the experiment and absorber simulations. Additionally, the simulation conditions were a combination of the conditions found in the open- and closed loop experiments. The oxygen concentrations were also lower for the absorber simulations. Identical order of the degradation products was therefore not expected.

The absolute concentrations of the degradation products were slightly lower for the RFCC- than the CHP flue gas. This was expected, since the oxygen concentration in the CHP case was higher than in the RFCC flue gas. The increased flow rate for the RFCC flue gas would additionally increase this difference, since the increased volumetric flow rate would decrease the liquid residence time for the RFCC flue gas. This is the opposite of what would be expected in reality for the RFCC gas, which contained higher amounts of impurities SO_x and NO_x. The degradation model constructed in this study, was though not dependent of these parameters, see section 11.3.5. With this in mind, the difference in degradation product concentrations, between the RFCC- and CHP results, seemed reasonable.

The gas phase ammonia emission was 13.8 ppmv for the CHP flue gas, and 9.58 ppmv for the RFCC flue gas. This was not unlike the ammonia emission expected by Fluor and Statoil (2005) [16], of 23 ppmv, with a similar flue gas as the CHP flue gas.

The Recycle Case

The recycle case was only calculated for the CHP flue gas. The reason for this, was that the recycle case did not provide the desired results of 1%(weight) degradation products in the liquid. Additionally, the RFCC case was known from the initial cases, to be nontrivial to convergence even without a recycle loop. It was therefore decided to not spend time on the RFCC recycle case. In section 10.2, the recycle case is presented for 5% purge, for CHP flue gas, to show how it compared to the initial case of CHP.

The order of the degradation products in the liquid phase were: HEF >HEGly >NH₃ >BHEOX >Formic Acid >Formaldehyde >HEI.

The difference of this order compared to the CHP initial case, was that HEGly now had changed place with ammonia in the liquid phase. A more peculiar result was that the liquid phase HEI concentration was zero, and all the produced HEI was found in the gas phase. This is further discussed in section 11.3.3.

Compared to the initial case, the concentrations of the degradation products in the liquid phase was significantly higher. This showed that there had been some accumulation of degradation products in the absorber loop. Despite this accumulation, the ammonia emission was 14.6 ppmv, virtually the same as in the initial case.

The Absorber Series Case

The absorber series case was made to give a ball park estimate of the absorber residence time needed to provide 1%(weight) degradation products in the liquid, see section 10.3. As described in section 9.3, the result of these calculations would provide very rough estimates, since the calculation only would extrapolate the initial degradation gradient.

The calculations of residence time needed to provide 1%(weight) degradation products in the liquid, resulted in 25.5 hours for the CHP gas, and 32.3 hours for the RFCC case. This result showed that the degradation in the simulation was much faster than measured in pilot plants. da Silva (2012) [14] measured approximately 0.9%(weight) of the degradation products, in lean and rich MEA solution after 11 weeks at the Esbjerg pilot plant. This fraction of degradation products measured was OZD, HEA, BHEOX, HEF, HEGly, HEI and HEPO. Even though this number was based on different degradation products, than accounted for in the mentioned calculation, it shows that the rate of degradation rate in the simulation was too fast.

There were several possible reasons to why the degradation rate was over estimated this much. First of all, this way of calculating the degradation time did not take into account the backward reactions of reaction 3, -5, -6, -7 and -8, see

Table 4.2. These backward reactions would have slowed down the reactions when the products had reached a certain concentration.

Secondly, the rate equations were designed on a basis of experiments with initial oxygen concentration in the gas phase of approximately 21%(mol). A much higher concentration than in the flue gases at TCM DA. This difference seemed to result in too high degradation rates.

Thirdly, it could seem as if the absorber model in Aspen Plus was not coping well with the slow degradation reactions. The help file of Aspen Plus Dynamics (2011) [4] stated the following: "Since the actual holdup used for hydraulics is not calculated in the steady-state run, the holdup that is used for calculating the reaction rate is likely to be different from the actual holdup." This could indicate that the holdup used for calculation of the reaction rate was wrong. Yet, it was not clear if the holdup given by Aspen Plus, presented in section 10.3 was the actual holdup or not. Too little was known about the equations applied in Aspen Plus to conclude if this was a source of error or not.

The calculation of the degradation time also showed an expected result. The degradation time of CHP, relative to RFCC, was lower. This tendency was also seen in the initial case, discussed earlier in this section, and was due to the lower oxygen content in the RFCC flue gas.

11.3.2 Validity of the Simulation Cases

During the work with the absorber simulation in Aspen Plus, it became clear that none of the cases presented in chapter 9, and discussed in section 11.3.1, were optimal to simulate the transient nature of the degradation reactions: The initial case did only find the degradation after one liquid run through the absorber. In the recycle case, there was no way of determining the time a corresponding process without purge, would need to achieve the found amount of degradation. For the absorbers in series case, the time needed to achieve a certain amount of degradation was found. But the estimate was so rough, that most of the tendencies the rate equations were able to explain in the experiment models, were neglected.

The weaknesses of the latter case, could be one of the reasons that the residence calculated time needed to achieve 1%(weight) degradation products in the liquid, was as underestimated as presented in section 10.3.

To provide a more accurate picture of the transient nature of the degradation reactions, transient simulations were needed. Since it was possible to convert a simulation from Aspen Plus, to the dynamic process simulator Aspen Dynamics, it was attempted to simulate the degradation in the absorber dynamically: A simulation where the liquid was fully recycled was set up in Aspen Dynamics. Unfortunately this attempt was unsuccessful, since Aspen Dynamics was demanding steady-state before the dynamic simulations could begin. Of this reason, this attempt is not presented in this document.

Other process configurations were also attempted in Aspen Dynamics: Firstly, it was tested to achieve steady-state with a valve blocking the flow in the system, before opening the valve once the dynamic simulation had begun. Secondly, it was

attempted to only run water in the system to achieve steady-state, then adding the MEA from a storage tank. None of these attempts were successful, due to limitations in Aspen softwares.

The problem seemed to be that the simulation software always demanded the simulations to be in steady-state. Theoretically it should have been possible to achieve steady-state for the degradation, at a point in time where all degradation reactions had reached equilibrium, if the liquid circulation loop was completely closed. Nevertheless, the simulations would not converge when the purge was removed from the recycle case. And still, if convergence was found in such a simulation, the time a process like that would need to achieve steady-state would be unknown.

11.3.3 Property Estimation

The properties of the HEF, HEI, BHEOX and HEGly were estimated by Aspen Plus as explained in section 8.5. This seemed to work well for three of the components, but for HEI, which was estimated using a different estimation routine than the other components, a strange tendency was seen in the results.

For the initial cases results, section 10.1, the main fraction of the produced HEI was found in the gas phase. For the recycle case, section 10.2, and absorber series cases, section 10.3, all produced HEI was found in the gas phase. From these results it was obvious that the solubility and volatility of HEI was incorrectly estimated.

11.3.4 The Concentration of Iron Ions

Section 8.1 explains that the concentration of ferric in TCM's absorber was assumed to be equal to the terminal iron ion concentration from the closed loop experiment. As also explained in the mentioned section, this was done due to lack of other information of the iron ion concentration in the absorber.

The alternative would have been to assume that there were no iron ions in the absorber. This seemed unlikely since the packing material in the absorber was made of metal, most likely steel, and the pipes were built of similar materials. Dissolved ferric were therefore likely to be found in the liquid in the TCM absorber.

As explained in section 8.2, the rate equations became independent of the catalyst amount once the rate coefficients were entered in Aspen Plus. This was an obvious weakness with the implementation, but nevertheless necessary to implement the reactions. An alternative could be to implement the rate expressions in a FORTRAN code, which would communicate with Aspen Plus. With this procedure it might have been possible to make the rate equations directly dependent of the iron concentration.

Nevertheless, there were no information of the amount of iron ions in the TCM absorber, and there could also be that other species were catalyzing the degradation reactions. As discussed in section 11.1.2, the understanding of the ferric dependency, was incomplete. Due to the sparse knowledge about these effects, and concentrations, it was considered better to simplify the implementation of the

ferric dependency. The alternative would be using time on implementing a more complex and possibly less accurate dependency.

11.3.5 Comparison of the Laboratory Experiments and the TCM Absorber

Because the rate equations were found from two degradation experiments, the rate equations would strictly speaking only be valid for this kind of experiments. Since the same rate equations were applied in the absorber simulation, it was of interest to discuss the differences between the experiments and the absorber conditions:

Both flue gases which were to be utilized at TCM, section 9.4.1, contained considerably less oxygen than the initial gas composition in all the laboratory experiments, section 2.2, 2.3 and 2.4. As explained in chapter 4, the all these degradation reactions were found to be either directly dependent on oxygen concentration, or dependent of radicals which were most likely to be formed by oxygen. The dependency on oxygen is also evident in literature by Supap and Idem (2009) [34] and Bello and Idem (2006) [8], which described increased degradation with increased oxygen concentration in the flue gas. The degradation reactions were in other words well known to be dependent of oxygen, and the oxygen content was considerably higher in the experiments. The degradation in the absorber simulations was therefore expected to be overestimated, see section 11.3.1.

Since all three degradation experiments were conducted at a temperature of 55 °C, the found rate equations were only valid for this temperature. Yet, the found rate equations were to be applied in the absorber simulation, with quite different conditions than in the experiments. The liquid phase temperature interval in the absorber simulations were 25 - 29 °C, for the CHP flue gas (Table 10.2), and 25 - 40 °C, for the RFCC flue gas (Table 10.3). Temperatures less than the 55 °C in the experiments. Since degradation of MEA is known to increase with increased temperature, Davis and Rochelle (2009) [15], Bello and Idem (2006) [8], one would again expect the rate equations in the absorber simulation to over predict the degradation.

Bello and Idem (2006) [8] also stated that increased CO_2 -loading would act as an inhibitor on the degradation, and Uyanga and Idem (2007) [37] concluded that presence of SO_2 would increase the degradation rate. No literature was found about how the NO_X concentration would affect the system. The loading of CO_2 in the absorber simulation varied between $\alpha = 0.216$ and $\alpha = 0.450$, in the degradation experiments the loading was more or less constant, $\alpha = 0.40$, through the experiment. The loading, in the experiments the rate equations were based on, was thus between the limits in the absorber simulation. This could mean that the difference in loading between the experiments and the absorber simulation would not be a large source of error. On the other hand, a consequence of that the loading dependency not was included in the rate equations at all, was that the absorber simulations would become simplified. In reality differences in the CO_2 -loading through the absorber column, could affect the concentration gradients for the degradation products through the column. Changes in the concentration gradients could influence the further degradation in the absorber, when the liquid

was circulated.

In addition to the already mentioned differences between the experiments and the absorber simulation, there were several other differences between the two. Sizing of the equipment, materials, flow regimes, and absorber structure, would be just some of the additional differences. However, when comparing the closed loop experiment with the absorber, the differences would be smaller, than if the open loop setup was to be compared. The closed loop contained a structured packing for mass transfer like the absorber at TCM. Nevertheless, the similarities ended at this point. The TCM absorber was not closed to the environment, like the closed loop experimental setup, in some extent, was. The flow rates and the sizing of the TCM absorber were also hugely different than in the laboratory setups.

To sum up, there were several differences between the degradation experiments and the conditions in the absorber at TCM, which could lead the rate equations to overestimate the degradation in the absorber. This could explain that the degradation seen in the absorber, discussed in 11.3.1, was much faster than expected.

11.3.6 No Stripper Conditions

An important note to the simulations, is that this study only considered the absorber conditions. This means that no stripper effects was considered, consequently the effects the stripper conditions could have on the degradation in the absorber, were disregarded.

This means that results presented in chapter 10, not necessarily were valid for a flue gas treating plant, since degradation products of the stripper could decrease or increase the degradation in the absorber.

11 DISCUSSION

Chapter 12

Conclusions

Two different previously conducted oxidative degradation experiments, were used as a basis of modeling monoethanolamine-degradation reactions. Literature and previous experience was used to construct reaction equations for the formation of five main degradation products; ammonia, N-(2-hydroxyethyl)formamide (HEF), N-(2-hydroxy ethyl)imidazole (HEI), N,N-Bis(2-hydroxy ethyl)oxalamide (BHEOX) and N-(2-hydroxy ethyl)glycine (HEGly), in addition to four intermediate products formaldehyde, formic acid, glyoxal and oxalic acid.

Rate equations were developed for the reactions, and implemented in the degradation model. The model was thereafter fitted to the experimental data of both experiments, to provide parameters in the rate equations.

The found parameters and rate equations were implemented in an obtained Aspen Plus absorber simulation. Three different absorber cases were created, with two different flue gas compositions. The ammonia emission in the simulation results ranged within reasonable 9.6 - 14.6 ppmv. However, a rough estimation of the degradation rate, showed that the rate in the simulations was much higher than previously measured in pilot plants.

The results showed that the data set used for the modeling was too small to provide a complete degradation model. This resulted in several weaknesses in the model, such as independence of CO₂-loading, temperature, contaminates and instability with respect to the concentration of dissolved ferric. Yet, the results also showed that it was possible to model degradation reactions in detail, and that further development of the model had good potential if more experimental data would become available.

12 CONCLUSIONS

Chapter 13

Further Work

For further work on MEA degradation in the absorber, the most important task would be to improve the rate equations. Experiments designed to be modeled, where the mass transfer properties is well known, should be performed to investigate especially the oxygen dependency of the different reactions. Additionally the dependency of ferric in the solution would be important to understand. The second priority would be to investigate the degradation reactions dependency of CO₂-loading, and flue gas impurities as NO_x and SO_x.

For the implementation in Aspen Plus a FORTRAN-function which would calculate the degradation in the liquid as a function of time, flue gas, and other properties, externally of the absorber block would make the simulation more convenient for the user. This way the user could decide a point in time, the FORTRAN-function would calculate the degradation products in the liquid, and Aspen Plus could run a steady-state simulation of that time point. This would also be necessary if the degradation reactions were to be implemented in a full simulation of the absorber and stripper, since Aspen Plus and Aspen Dynamics both require initial steady-state, which degradation reactions would never be.

For full understanding of the degradation, degradation in the stripper should also be modeled. The interaction of the degradation in the stripper with the degradation in the absorber, should also be investigated. For the best model, a full absorber and stripper model should be fitted to pilot plant data to provide rate equations.

13 FURTHER WORK

Bibliography

- [1] ACD/Labs ACD/PhysChem Suite. ChemSpider. Website, 2012.
HEI:<http://www.chemspider.com/Chemical-Structure.66778.html?rid=f1bb12b7-755f-40d9-a606-f84cc33e10c7>
BHEOX:<http://www.chemspider.com/Chemical-Structure.67213.html?rid=737707b5-8e6e-44c7-aa45-765ab46ad3fa>
HEGLY:<http://www.chemspider.com/Chemical-Structure.196451.html?rid=36b33f74-623b-4811-89c9-ba4e6c26fb5> URLs retrieved 14. June 2012.
- [2] Alves, S.S., Maia, C.I. and Vasconcelos, J.M.T. Gas-liquid Mass Transfer Coefficient in Stirred Tanks Interpreted through Bubble Contamination Kinetics. *Chemical Engineering and Processing: Process Intensification*, 43(7):823 – 830, 2004.
- [3] Arduengo, A. J., Gentry, Jr. F. P., Taverkere, P. K., and Simmons, H. E. Process for Manufacture of Imidazoles. Patent, 01 2001. US 6177575.
- [4] Aspen Dynamics Help V7.3. RadFrac Hydraulics and Reactions, 2011. Also found: http://www.cadfamily.com/online-help/adref210_web%5Cimage/radfrachydraulicsandreaactions.htm URL retrieved 14. June 2012.
- [5] Aspen Plus Help V7.3. Reactive Distillation, 2011. Also found: http://www.cadfamily.com/online-help/apunitop_web%5Chtml/reactivedistillationrad.htm URL retrieved 14. June 2012.
- [6] Aspen Plus Help V7.3. Reactive Distillation Form, 2011. Search for *Reactive Distillation Form* in Aspen Plus Help.
- [7] Bedell, S. A. Amine Sutoxidation in Flue Gas CO₂ capture Mechanistic Lessons Learned from other Gas Treating Processes. *International Journal of Greenhouse Gas Control*, 5(1):1 – 6, 2011.
- [8] Bello, A. and Idem, R.O. Comprehensive Study of the Kinetics of the Oxidative Degradation of CO₂ Loaded and Concentrated Aqueous Monoethanolamine (MEA) with and without Sodium Metavanadate during CO₂ Absorption from Flue Gases. *Industrial & Engineering Chemistry Research*, 45(8):2569–2579, 2006.
- [9] Billet, R. and Schultes, M. Prediction of Mass Transfer Columns with Dumped and Arranged Packings: Updated Summary of the Calculation

BIBLIOGRAPHY

- Method of Billet and Schultes. *Chemical Engineering Research and Design*, 77(6):498 – 504, 1999.
- [10] Bottoms, R.R. Process for Separating Acidic Gases. Patent, 10 1930. US 1783901.
- [11] Bruder P., Lauritsen K.G., Mejdell T., and Svendsen H.F. CO₂ capture into aqueous solutions of 3-methylaminopropylamine activated dimethyl-monoethanolamine. *Chemical Engineering Science*, 75(0):28 – 37, 2012.
- [12] Buxton, G. V., Malone, T. N. and Salmon, G. A. Oxidation of Glyoxal Initiated by OH in Oxygenated Aqueous Solution. *J. Chem. Soc., Faraday Trans.*, 93, 1997.
- [13] Chi, S. and Rochelle, G. T. Oxidative Degradation of Monoethanolamine. *Industrial & Engineering Chemistry Research*, 41(17):4178–4186, 2002.
- [14] da Silva, E.F., Lepaumier, H., Einbu, A., Grimstvedt, A., Vernstad, K., Vevelstad, S. J., Svendsen, H.F. and Zahlsen, K. Understanding MEA Degradation in Postcombustion CO₂ Capture. *Ind. Eng. Chem. Res.*, 2012. Submitted, not published.
- [15] Davis, J. and Rochelle, G.T. Thermal Degradation of Monoethanolamine at Stripper Conditions. *Energy Procedia*, 1(1):327 – 333, 2009. Greenhouse Gas Control Technologies 9, Proceedings of the 9th International Conference on Greenhouse Gas Control Technologies (GHGT-9), 1620 November 2008, Washington DC, USA.
- [16] Fluor and Statoil. Study and Estimate for CO₂ Capture Facilities for the Proposed 800 MW Combined Cycle Power Plant - Tjeldbergodden, Norway. Website, 2005. <http://www.ipt.ntnu.no/~jsg/undervisning/naturgass/dokumenter/TjeldbergoddenFluorStatoil2005.pdf> URL retrieved 14. June 2012.
- [17] Ghosh, S., Das, S., Kundu, D., Suresh, K. and Abraham, A. Inter-particle Communication and Search-dynamics of lbest Particle Swarm Optimizers: An Analysis. *Information Sciences*, 182(1):156 – 168, 2012. Nature-Inspired Collective Intelligence in Theory and Practice.
- [18] Goff, G. S. and Rochelle, G. T. Monoethanolamine Degradation: O₂ Mass Transfer Effects under CO₂ Capture Conditions. *Industrial & Engineering Chemistry Research*, 43(20):6400–6408, 2004.
- [19] Kennedy, J. and Eberhart, R. Particle swarm optimization. In *Neural Networks, 1995. Proceedings., IEEE International Conference on*, volume 4, pages 1942 –1948, nov/dec 1995.
- [20] Kohl, A. L. and Nielsen, R. B. *Gas Purification*. Gulf Publishing Company, 5th edition, 1997. 41 – 46.
- [21] Lepaumier, H., da Silva, E. F., Einbu, A., Grimstvedt, A., Knudsen, J. N., Zahlsen, K. and Svendsen, H. F. . Comparison of MEA Degradation in Pilot-Scale with Lab-Scale Experiments. *Energy Procedia*, 4(0):1652 – 1659, 2011. 10th International Conference on Greenhouse Gas Control Technologies.

- [22] U.S. Environmental Protection Agency's (EPA) Office of Pollution Prevention Toxics and Syracuse Research Corporation (SRC). EPI Suite. Retrieved from Website; 2012, Published 2008. <http://www.epa.gov/oppt/exposure/pubs/episuitedl.htm>.
- [23] Personal communication with Andreas Grimstvedt, Research Scientist, Process Technology, SINTEF Materials and Chemistry, 2012. andreas.grimstvedt@sintef.no.
- [24] Personal communication with Eirik Falck da Silva, Senior Scientist, Process Technology, SINTEF Materials and Chemistry, 2012. Eirik.FalckdaSilva@sintef.no.
- [25] Personal communication with Solrun Johanne Vevelstad, Ph.D. Candidate, Department of Chemical Engineering, Norwegian University of Technology and Science, 2012. solrun.vevelstad@chemeng.ntnu.no.
- [26] Personal communication with Toine Cents, Senior Process Engineer, Research and Simulation at CO2 Technology Centre Mongstad, 2012. tcen@tcmda.com.
- [27] Petryaev, E.P. and Pavloc, A.V. Homolytic Deamination of Amino Alcohols. *Zh. Org. Khim*, pages 29–34, 1984.
- [28] Poli, R., Kennedy, J. and Blackwell, T. Particle Swarm Optimization. *Swarm Intelligence*, 1:33–57, 2007. 10.1007/s11721-007-0002-0.
- [29] Rooney, P.C., DuPart, M.S. and Bacon, T.R. Oxygen's Role In Alkanolamine Degradation. *Hydrogen Processing*, 77:109–113, 1998.
- [30] Schaftlein, R. W. and Russell, T. W. F. Two-Phase Reactor Design. Tank-Type Reactors. *Industrial & Engineering Chemistry*, 60(5):12–27, 1968.
- [31] Sexton, A. J. and Rochelle, G. T. Catalysts and Inhibitors for MEA Oxidation. *Energy Procedia*, 1(1):1179 – 1185, 2009. Greenhouse Gas Control Technologies 9 Proceedings of the 9th International Conference on Greenhouse Gas Control Technologies (GHGT-9), 1620 November 2008, Washington DC, USA.
- [32] Statoil. CO₂ Masterplan Mongstad. Website, 2011. <http://www.statoil.com/no/NewsAndMedia/News/2009/Downloads/CO2%20Masterplan%20Mongstad%20norsk.pdf> URL retrieved 14. June 2012.
- [33] Supap, T., Idem, R. and Tontiwachwuthikul, P. Mechanism of Formation of Heat Stable Salts (HSS) and their Roles in Further Degradation of Monoethanolamine during CO₂ Capture from Flue Gas Streams. *Energy Procedia*, 4(0):591 – 598, 2011. 10th International Conference on Greenhouse Gas Control Technologies.
- [34] Supap, T., Idem, R., Tontiwachwuthikul, P. and Saiwan, C. Kinetics of Sulfur Dioxide- and Oxygen-induced Degradation of Aqueous Monoethanolamine Solution during CO₂ Absorption from Power Plant Flue Gas Streams. *International Journal of Greenhouse Gas Control*, 3(2):133 – 142, 2009.

BIBLIOGRAPHY

- [35] Supap, T., Idem, R., Veawab, A., Aroonwilas, A., Tontiwachwuthikul, P., Chakma, A. and Kybett, B. D. Kinetics of the Oxidative Degradation of Aqueous Monoethanolamine in a Flue Gas Treating Unit. *Industrial & Engineering Chemistry Research*, 40(16):3445–3450, 2001.
- [36] Talzi, V.P. NMR Determination of the Total Composition of Commercial Absorbents Based on Monoethanolamine. *Russian Journal of Applied Chemistry*, 77:430–434, 2004. 10.1023/B:RJAC.0000031284.10428.e6.
- [37] Uyanga, I.J. and Idem, R.O. Studies of SO₂- and O₂-Induced Degradation of Aqueous MEA during CO₂ Capture from Power Plant Flue Gas Streams. *Industrial & Engineering Chemistry Research*, 46(8):2558–2566, 2007.

Appendices

Appendix A

Reactions as Implemented in Absorber Simulation

Table A.1: Degradation Reactions as Implemented in Absorber Simulation.

Rx.nr.	As.Nr.	Reaction
1	20	$\text{NH}_2\text{CH}_2\text{CH}_2\text{OH} + 3 \text{H}_2\text{O} + 2 \text{Fe}^{3+} \longrightarrow 2 \text{H}-\overset{\text{O}}{\parallel}{\text{C}}-\text{H} + \text{NH}_3 + 2 \text{H}_3\text{O}^{\oplus} + 2 \text{Fe}^{2+}$ <p>MEA Formaldehyde</p>
1	21	$\text{O}^{\ominus}-\overset{\text{O}}{\parallel}{\text{C}}-\text{NH}-\text{CH}_2\text{CH}_2\text{OH} + 2 \text{H}_2\text{O} + 2 \text{Fe}^{3+} \longrightarrow 2 \text{H}-\overset{\text{O}}{\parallel}{\text{C}}-\text{H} + \text{NH}_3 + \text{H}_3\text{O}^{\oplus} + \text{CO}_2 + 2 \text{Fe}^{2+}$ <p>MEACOO[⊖] Formaldehyde</p>
1	22	$\text{NH}_3^{\oplus}\text{CH}_2\text{CH}_2\text{OH} + 4 \text{H}_2\text{O} + 2 \text{Fe}^{3+} \longrightarrow 2 \text{H}-\overset{\text{O}}{\parallel}{\text{C}}-\text{H} + \text{NH}_3 + 3 \text{H}_3\text{O}^{\oplus} + 2 \text{Fe}^{2+}$ <p>MEA[⊕]H Formaldehyde</p>
2	30	$\text{H}-\overset{\text{O}}{\parallel}{\text{C}}-\text{H} + \frac{1}{2} \text{O}_2 \longrightarrow \text{H}-\overset{\text{O}}{\parallel}{\text{C}}-\text{OH}$ <p>Formaldehyde Formic acid</p>
3	40	$\text{NH}_2\text{CH}_2\text{CH}_2\text{OH} + \text{H}-\overset{\text{O}}{\parallel}{\text{C}}-\text{OH} \longrightarrow \text{HOCH}_2\text{CH}_2\text{NH}-\overset{\text{O}}{\parallel}{\text{C}}-\text{H} + \text{H}_2\text{O}$ <p>MEA Formic acid HEF</p>
3	41	$\text{O}^{\ominus}-\overset{\text{O}}{\parallel}{\text{C}}-\text{NH}-\text{CH}_2\text{CH}_2\text{OH} + \text{H}-\overset{\text{O}}{\parallel}{\text{C}}-\text{OH} \longrightarrow \text{HOCH}_2\text{CH}_2\text{NH}-\overset{\text{O}}{\parallel}{\text{C}}-\text{H} + \text{OH}^{\ominus} + \text{CO}_2$ <p>MEACOO[⊖] Formic acid HEF</p>
3	42	$\text{NH}_3^{\oplus}\text{CH}_2\text{CH}_2\text{OH} + \text{H}-\overset{\text{O}}{\parallel}{\text{C}}-\text{OH} \longrightarrow \text{HOCH}_2\text{CH}_2\text{NH}-\overset{\text{O}}{\parallel}{\text{C}}-\text{H} + \text{H}_3\text{O}^{\oplus}$ <p>MEA[⊕]H Formic acid HEF</p>

Table A.2: Degradation Reactions as Implemented in Absorber Simulation (Continued)

Rx.nr.	As.Nr.	Reaction
3	45	$\text{HO-CH}_2\text{-CH}_2\text{-NH-C(=O)-H} + \text{H}_2\text{O} \longrightarrow \text{NH}_2\text{-CH}_2\text{-CH}_2\text{-OH} + \text{H-C(=O)-OH}$ <p style="text-align: center;">HEF MEA Formic acid</p>
3	46	$\text{HO-CH}_2\text{-CH}_2\text{-NH-C(=O)-H} + \text{OH}^\ominus + \text{CO}_2 \longrightarrow \text{O}^\ominus\text{-C(=O)-NH-CH}_2\text{-CH}_2\text{-OH} + \text{H-C(=O)-OH}$ <p style="text-align: center;">HEF MEACOO[⊖] Formic acid</p>
3	47	$\text{HO-CH}_2\text{-CH}_2\text{-NH-C(=O)-H} + \text{H}_3\text{O}^\oplus \longrightarrow \text{NH}_3^\oplus\text{-CH}_2\text{-CH}_2\text{-OH} + \text{H-C(=O)-OH}$ <p style="text-align: center;">HEF MEAH[⊕] Formic acid</p>
4	50	$\text{NH}_2\text{-CH}_2\text{-CH}_2\text{-OH} + \text{O}_2 \longrightarrow \text{H-C(=O)-CH}_2\text{-CHO} + \text{H}_2\text{O} + \text{NH}_3$ <p style="text-align: center;">MEA Glyoxal</p>
4	51	$\text{O}^\ominus\text{-C(=O)-NH-CH}_2\text{-CH}_2\text{-OH} + \text{O}_2 \longrightarrow \text{H-C(=O)-CH}_2\text{-CHO} + \text{OH}^\ominus + \text{NH}_3 + \text{CO}_2$ <p style="text-align: center;">MEACOO[⊖] Glyoxal</p>
4	52	$\text{NH}_3^\oplus\text{-CH}_2\text{-CH}_2\text{-OH} + \text{O}_2 \longrightarrow \text{H-C(=O)-CH}_2\text{-CHO} + \text{H}_3\text{O}^\oplus + \text{NH}_3$ <p style="text-align: center;">MEAH[⊕] Glyoxal</p>

Table A.3: Degradation Reactions as Implemented in Absorber Simulation (Continued)

Rx.nr.	As.Nr.	Reaction
5	60	$\text{NH}_2\text{CH}_2\text{CH}_2\text{OH} + \text{HCHO} + \text{OHCCHO} + \text{NH}_3 \longrightarrow \text{HEI} + 3\text{H}_2\text{O}$ <p>MEA Formaldehyde Glyoxal HEI</p>
5	61	$\text{MEACOO}^- + \text{HCHO} + \text{OHCCHO} + \text{NH}_3 \longrightarrow \text{HEI} + 2\text{H}_2\text{O} + \text{CO}_2 + \text{OH}^-$ <p>MEACOO⁻ Formaldehyde Glyoxal HEI</p>
5	62	$\text{MEAH}^+ + \text{HCHO} + \text{OHCCHO} + \text{NH}_3 \longrightarrow \text{HEI} + 2\text{H}_2\text{O} + \text{H}_3\text{O}^+$ <p>MEAH⁺ Formaldehyde Glyoxal HEI</p>
5	65	$\text{HEI} + 3\text{H}_2\text{O} \longrightarrow \text{MEA} + \text{HCHO} + \text{OHCCHO} + \text{NH}_3$ <p>HEI MEA Formaldehyde Glyoxal</p>
5	66	$\text{HEI} + 2\text{H}_2\text{O} + \text{CO}_2 + \text{OH}^- \longrightarrow \text{MEACOO}^- + \text{HCHO} + \text{OHCCHO} + \text{NH}_3$ <p>HEI MEACOO⁻ Formaldehyde Glyoxal</p>
5	67	$\text{HEI} + 2\text{H}_2\text{O} + \text{H}_3\text{O}^+ \longrightarrow \text{MEAH}^+ + \text{HCHO} + \text{OHCCHO} + \text{NH}_3$ <p>HEI MEAH⁺ Formaldehyde Glyoxal</p>

Table A.4: Degradation Reactions as Implemented in Absorber Simulation (Continued)

Rx.nr.	As.Nr.	Reaction
6	70	$ \begin{array}{c} \text{H} \quad \text{O} \quad \text{H} \\ \parallel \quad \parallel \\ \text{C} \quad \text{C} \\ \backslash \quad / \\ \text{H} \quad \text{H} \\ \text{Glyoxal} \end{array} + \text{O}_2 \longrightarrow \begin{array}{c} \text{O} \\ \parallel \\ \text{HO} \text{---} \text{C} \text{---} \text{C} \text{---} \text{OH} \\ \parallel \\ \text{O} \\ \text{Oxalic acid} \end{array} $
6	75	$ \begin{array}{c} \text{O} \\ \parallel \\ \text{HO} \text{---} \text{C} \text{---} \text{C} \text{---} \text{OH} \\ \parallel \\ \text{O} \\ \text{Oxalic acid} \end{array} \longrightarrow \begin{array}{c} \text{H} \quad \text{O} \quad \text{H} \\ \parallel \quad \parallel \\ \text{C} \quad \text{C} \\ \backslash \quad / \\ \text{H} \quad \text{H} \\ \text{Glyoxal} \end{array} + \text{O}_2 $
7	80	$ \begin{array}{c} 2 \text{NH}_2 \text{---} \text{CH}_2 \text{---} \text{CH}_2 \text{---} \text{OH} \\ \text{MEA} \end{array} + \begin{array}{c} \text{O} \\ \parallel \\ \text{HO} \text{---} \text{C} \text{---} \text{C} \text{---} \text{OH} \\ \parallel \\ \text{O} \\ \text{Oxalic acid} \end{array} \longrightarrow \begin{array}{c} \text{O} \\ \parallel \\ \text{HO} \text{---} \text{CH}_2 \text{---} \text{NH} \text{---} \text{C} \text{---} \text{C} \text{---} \text{NH} \text{---} \text{CH}_2 \text{---} \text{CH}_2 \text{---} \text{OH} \\ \parallel \\ \text{O} \\ \text{BHEOX} \end{array} + 2 \text{H}_2\text{O} $
7	81	$ \begin{array}{c} \text{O} \\ \parallel \\ 2 \text{O}^- \text{---} \text{C} \text{---} \text{NH} \text{---} \text{CH}_2 \text{---} \text{CH}_2 \text{---} \text{OH} \\ \text{MEACOO}^- \end{array} + \begin{array}{c} \text{O} \\ \parallel \\ \text{HO} \text{---} \text{C} \text{---} \text{C} \text{---} \text{OH} \\ \parallel \\ \text{O} \\ \text{Oxalic acid} \end{array} \longrightarrow \begin{array}{c} \text{O} \\ \parallel \\ \text{HO} \text{---} \text{CH}_2 \text{---} \text{NH} \text{---} \text{C} \text{---} \text{C} \text{---} \text{NH} \text{---} \text{CH}_2 \text{---} \text{CH}_2 \text{---} \text{OH} \\ \parallel \\ \text{O} \\ \text{BHEOX} \end{array} + 2 \text{OH}^- + 2 \text{CO}_2 $
7	82	$ \begin{array}{c} 2 \text{NH}_3^+ \text{---} \text{CH}_2 \text{---} \text{CH}_2 \text{---} \text{OH} \\ \text{MEA}^+ \text{H} \end{array} + \begin{array}{c} \text{O} \\ \parallel \\ \text{HO} \text{---} \text{C} \text{---} \text{C} \text{---} \text{OH} \\ \parallel \\ \text{O} \\ \text{Oxalic acid} \end{array} \longrightarrow \begin{array}{c} \text{O} \\ \parallel \\ \text{HO} \text{---} \text{CH}_2 \text{---} \text{NH} \text{---} \text{C} \text{---} \text{C} \text{---} \text{NH} \text{---} \text{CH}_2 \text{---} \text{CH}_2 \text{---} \text{OH} \\ \parallel \\ \text{O} \\ \text{BHEOX} \end{array} + 2 \text{H}_3\text{O}^+ $

Table A.5: Degradation Reactions as Implemented in Absorber Simulation (Continued)

Rx.nr.	As.Nr.	Reaction
7	85	$\text{HO-CH}_2\text{-CH}_2\text{-NH-CO-CO-NH-CH}_2\text{-CH}_2\text{-OH} + 2 \text{H}_2\text{O} \longrightarrow 2 \text{NH}_2\text{-CH}_2\text{-CH}_2\text{-OH} + \text{HO-CO-CO-OH}$ <p style="text-align: center;">BHEOX MEA Oxalic acid</p>
7	86	$\text{HO-CH}_2\text{-CH}_2\text{-NH-CO-CO-NH-CH}_2\text{-CH}_2\text{-OH} + 2 \text{OH}^\ominus + 2 \text{CO}_2 \longrightarrow 2 \text{O}^\ominus\text{-C(=O)-NH-CH}_2\text{-CH}_2\text{-OH} + \text{HO-CO-CO-OH}$ <p style="text-align: center;">BHEOX MEACOO[⊖] Oxalic acid</p>
7	87	$\text{HO-CH}_2\text{-CH}_2\text{-NH-CO-CO-NH-CH}_2\text{-CH}_2\text{-OH} + 2 \text{H}_3\text{O}^\oplus \longrightarrow 2 \text{NH}_3^\oplus\text{-CH}_2\text{-CH}_2\text{-OH} + \text{HO-CO-CO-OH}$ <p style="text-align: center;">BHEOX MEAH[⊕] Oxalic acid</p>
8	90	$2 \text{NH}_2\text{-CH}_2\text{-CH}_2\text{-OH} + \frac{1}{2} \text{O}_2 + 2 \text{H}_2\text{O} + 2 \text{Fe}^{3+} \longrightarrow \text{HO-CH}_2\text{-CH}_2\text{-NH-CH}_2\text{-COOH} + \text{NH}_3 + 2 \text{H}_3\text{O}^\oplus + 2 \text{Fe}^{2+}$ <p style="text-align: center;">MEA HEGly</p>
8	91	$2 \text{O}^\ominus\text{-C(=O)-NH-CH}_2\text{-CH}_2\text{-OH} + \frac{1}{2} \text{O}_2 + 2 \text{Fe}^{3+} \longrightarrow \text{HO-CH}_2\text{-CH}_2\text{-NH-CH}_2\text{-COOH} + \text{NH}_3 + 2 \text{CO}_2 + 2 \text{Fe}^{2+}$ <p style="text-align: center;">MEACOO[⊖] HEGly</p>
8	92	$2 \text{NH}_3^\oplus\text{-CH}_2\text{-CH}_2\text{-OH} + \frac{1}{2} \text{O}_2 + 4 \text{H}_2\text{O} + 2 \text{Fe}^{3+} \longrightarrow \text{HO-CH}_2\text{-CH}_2\text{-NH-CH}_2\text{-COOH} + \text{NH}_3 + 4 \text{H}_3\text{O}^\oplus + 2 \text{Fe}^{2+}$ <p style="text-align: center;">MEAH[⊕] HEGly</p>

Table A.6: Degradation Reactions as Implemented in Absorber Simulation (Continued)

Rx.nr.	As.Nr.	Reaction
8	95	$ \begin{array}{c} \text{O} \\ \parallel \\ \text{HO}-\text{CH}_2-\text{CH}_2-\text{NH}-\text{CH}_2-\text{C}-\text{OH} \\ \text{HEGly} \end{array} + \text{NH}_3 + 2 \text{H}_3\text{O}^\oplus + 2 \text{Fe}^{2+} \longrightarrow 2 \text{NH}_2-\text{CH}_2-\text{CH}_2-\text{OH} + \frac{1}{2} \text{O}_2 + 2 \text{H}_2\text{O} + 2 \text{Fe}^{3+} $
8	96	$ \begin{array}{c} \text{O} \\ \parallel \\ \text{HO}-\text{CH}_2-\text{CH}_2-\text{NH}-\text{CH}_2-\text{C}-\text{OH} \\ \text{HEGly} \end{array} + \text{NH}_3 + 2 \text{CO}_2 + 2 \text{Fe}^{2+} \longrightarrow 2 \begin{array}{c} \text{O} \\ \parallel \\ \text{O}^\ominus-\text{C}-\text{NH}-\text{CH}_2-\text{CH}_2-\text{OH} \\ \text{MEACOO}^\ominus \end{array} + \frac{1}{2} \text{O}_2 + 2 \text{Fe}^{3+} $
8	97	$ \begin{array}{c} \text{O} \\ \parallel \\ \text{HO}-\text{CH}_2-\text{CH}_2-\text{NH}-\text{CH}_2-\text{C}-\text{OH} \\ \text{HEGly} \end{array} + \text{NH}_3 + 4 \text{H}_3\text{O}^\oplus + 2 \text{Fe}^{2+} \longrightarrow 2 \begin{array}{c} \oplus \\ \text{NH}_3-\text{CH}_2-\text{CH}_2-\text{OH} \\ \text{MEAH}^\oplus \end{array} + \frac{1}{2} \text{O}_2 + 4 \text{H}_2\text{O} + 2 \text{Fe}^{3+} $
-	100	$ 4 \text{Fe}^{2+} + \text{O}_2 + 4 \text{H}_3\text{O}^\oplus \longrightarrow 4 \text{Fe}^{3+} + 6 \text{H}_2\text{O} $

Appendix B

Use of Aspen Plus

B.1 Adding a User Defined Component

- From the "Data menu", click "Components".
- In the left pane of the "Data Browser", click "Specifications".
- Find a blank spot in the component list, and click "User Defined". See Figure B.1.

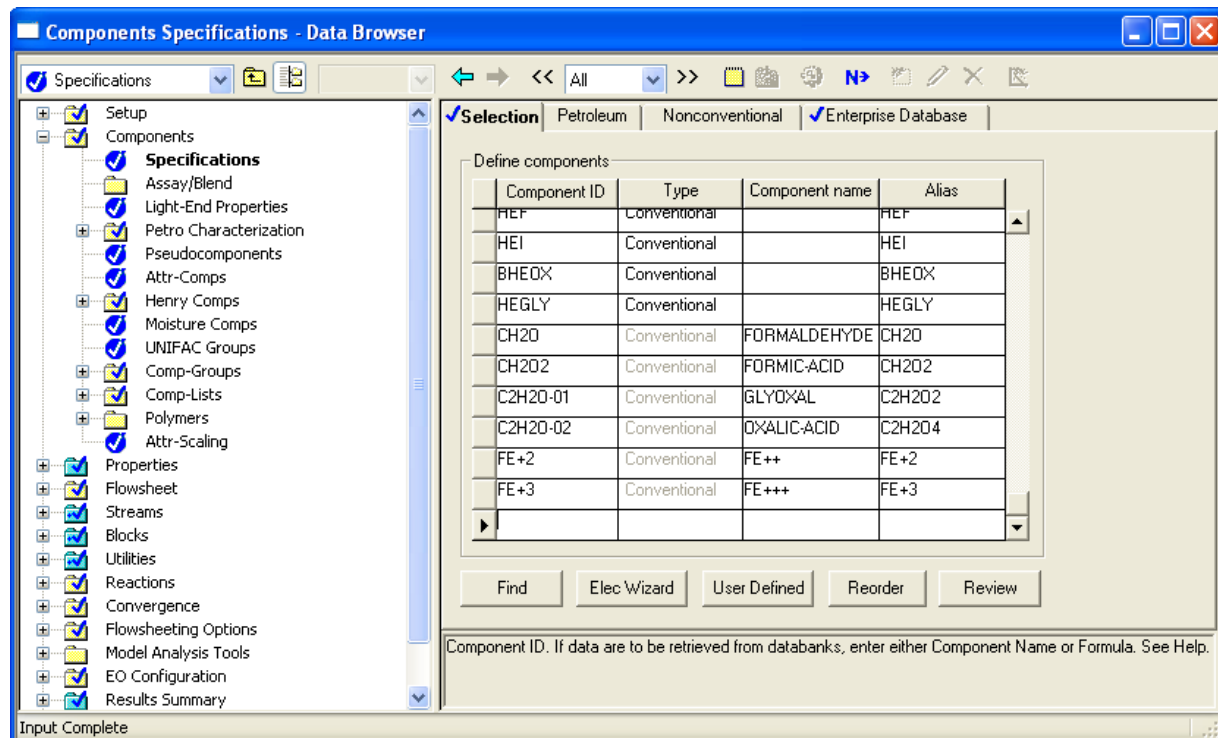


Figure B.1: The component specifications window, in the data browser.

- In the "User Defined Component Wizard", Figure B.2, enter component ID and alias. Enter Conventional in the type box. Click "Next".

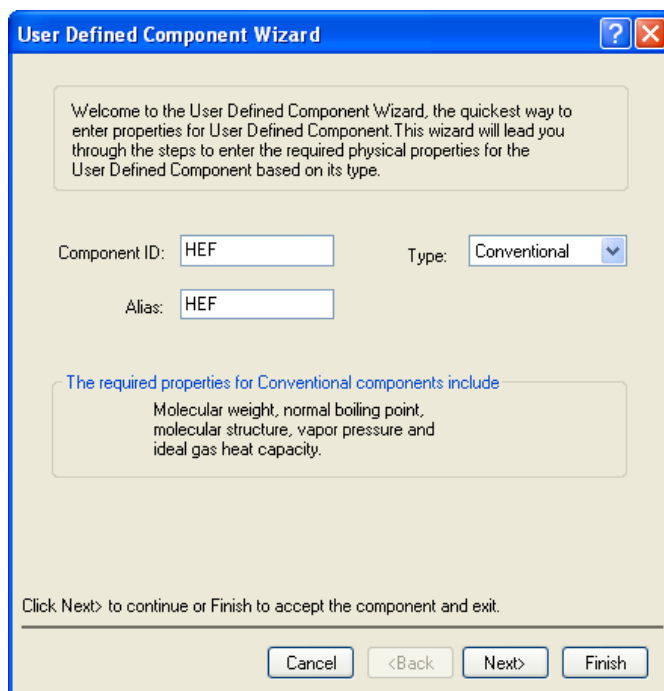
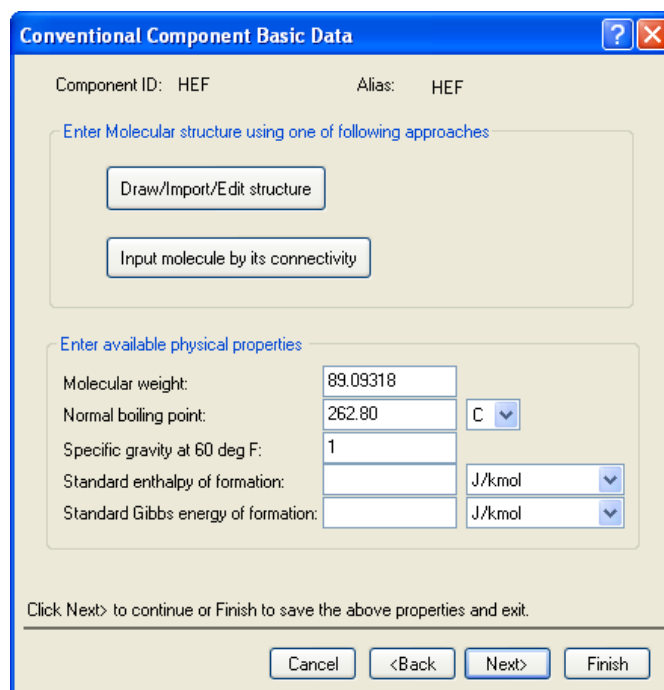


Figure B.2: The user defined component wizard.

- In the "Conventional Component Basic Data", Figure B.3, enter molecular weight, normal boiling point and specific gravity of the component. These parameters are essential for the estimation of the component properties. Click "Draw/Import/Edit structure".
- In the "Molecule Editor", Figure B.4, draw the chemical structure of the component you are adding. Close the "Molecule Editor"-window when finished.
- In the "Conventional Component Basic Data", Figure B.3, click "Input molecule by its connectivity".
- In the "Molecular Structure"-window, Figure B.5 click the "Structure"-tab and click "Calculate Bonds". When the calculation is finished, the window should look like Figure B.5.
- Close the "Molecular Structure"-window, and click "Next" in the "Conventional Component Basic Data"-window, Figure B.3.
- In the "Conventional Component Additional Data"-window, Figure B.6, select either to evaluate the new component using TDE, or Aspen Plus property estimate system.
- For the simulation described in this study, the Aspen Plus property estimate system was applied for all components except HEI, which the estimate system failed for. Of this reason HEI was estimated using TDE, which did not estimate the heat capacity data (CPIG in Aspen Plus) for HEI. Therefore the CPIG data for HEF was used for HEI.

B.1 Adding a User Defined Component



The image shows a software window titled "Conventional Component Basic Data". At the top, it displays "Component ID: HEF" and "Alias: HEF". Below this, there are two options for entering molecular structure: "Draw/Import/Edit structure" and "Input molecule by its connectivity". The second section, "Enter available physical properties", contains several input fields: "Molecular weight" (89.09318), "Normal boiling point" (262.80) with a unit dropdown set to "C", "Specific gravity at 60 deg F" (1), "Standard enthalpy of formation" (empty) with a unit dropdown set to "J/kmol", and "Standard Gibbs energy of formation" (empty) with a unit dropdown set to "J/kmol". At the bottom, there are four buttons: "Cancel", "<Back", "Next>", and "Finish". A note at the bottom of the window reads: "Click Next> to continue or Finish to save the above properties and exit."

Figure B.3: The conventional component basic data window.

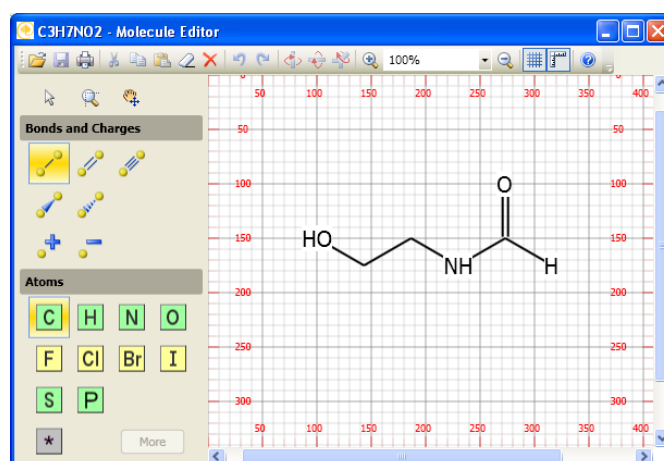


Figure B.4: The molecule editor.

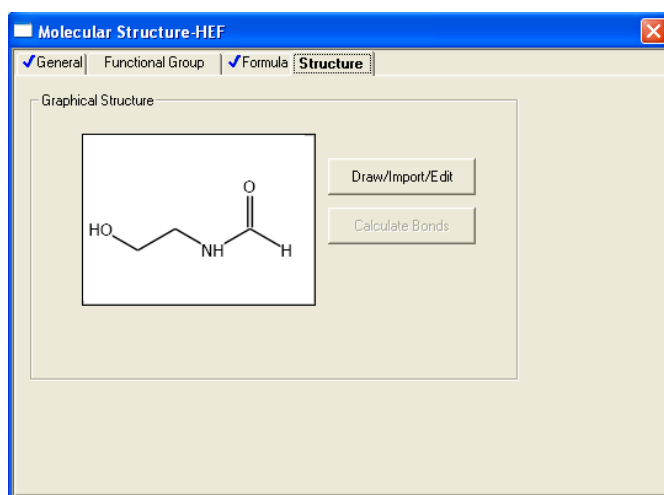


Figure B.5: The molecule structure window.

The screenshot shows a software window titled "Conventional Component Additional Data" with a blue title bar and standard window controls. The window contains a list of five numbered buttons (1-5) for entering additional properties or data:

- 1 Liquid volume
- 2 Vapor pressure data
- 3 Extended Antoine vapor pressure coefficients
- 4 Ideal gas heat capacity data
- 5 Ideal gas heat capacity polynomial coefficients

Below the list, there are two radio button options:

- Evaluate using TDE
- Estimate using Aspen Plus property estimate system

At the bottom of the window, there are four buttons: "Cancel", "<Back", "Next>", and "Finish".

Figure B.6: The conventional component additional data window.

B.2 Implementing Kinetic Reactions

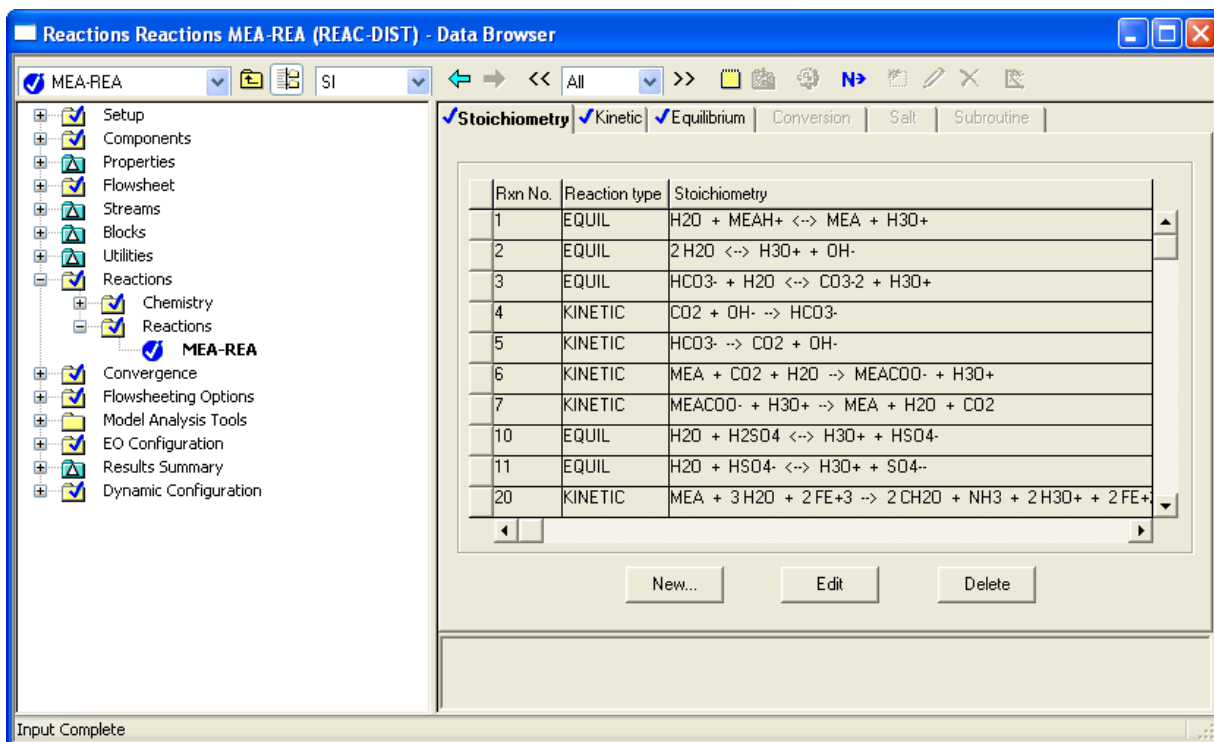


Figure B.7: The reaction stoichiometry window, in the data browser.

- From the "Data menu", click "Reaction" and "Reactions"
- Choose the current reaction set, in this case "MEA-REA"
- Click "New", under the reaction list, Figure B.7.
- Choose "Kinetic/Equilibrium/Conversion", in the "Select Reaction Type"-window, Figure B.8, and enter a reaction number.
- In the "Edit Reaction"-window, Figure B.9, select "Kinetic" in the reaction type tab. Then select all reactants and products for the reactions to be implemented, and input stoichiometry, in the "Coefficient"-column. At last input the reaction order in the "Exponent"-column. Click the blue "next" ("N->") button.
- In the Data browser, Figure B.7, click the "Kinetic" tab, Figure B.10. Locate the reaction number inputed previously. Enter the rate coefficient, k , with unit selected in the $[C_i]$ basis, and seconds. If the reaction rate equations are independent of temperature, as in this study, enter zero for n , and E .

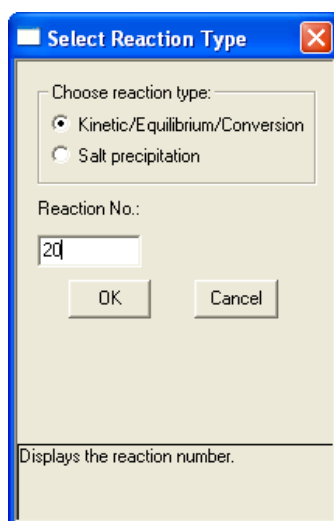


Figure B.8: The select reaction type window.

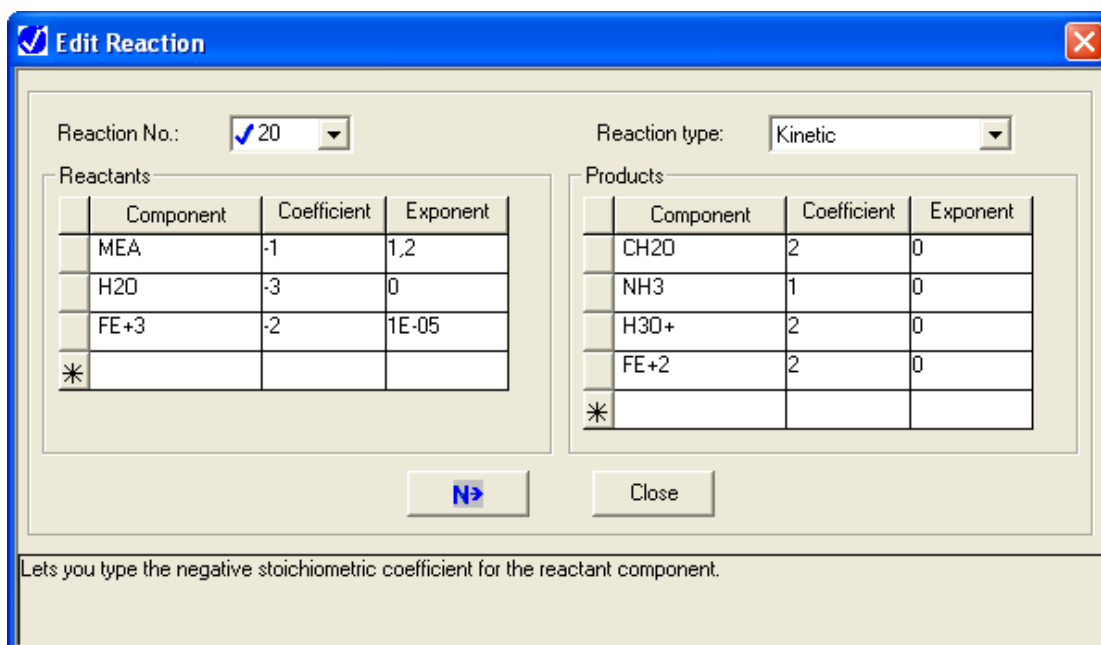


Figure B.9: The edit reaction window.

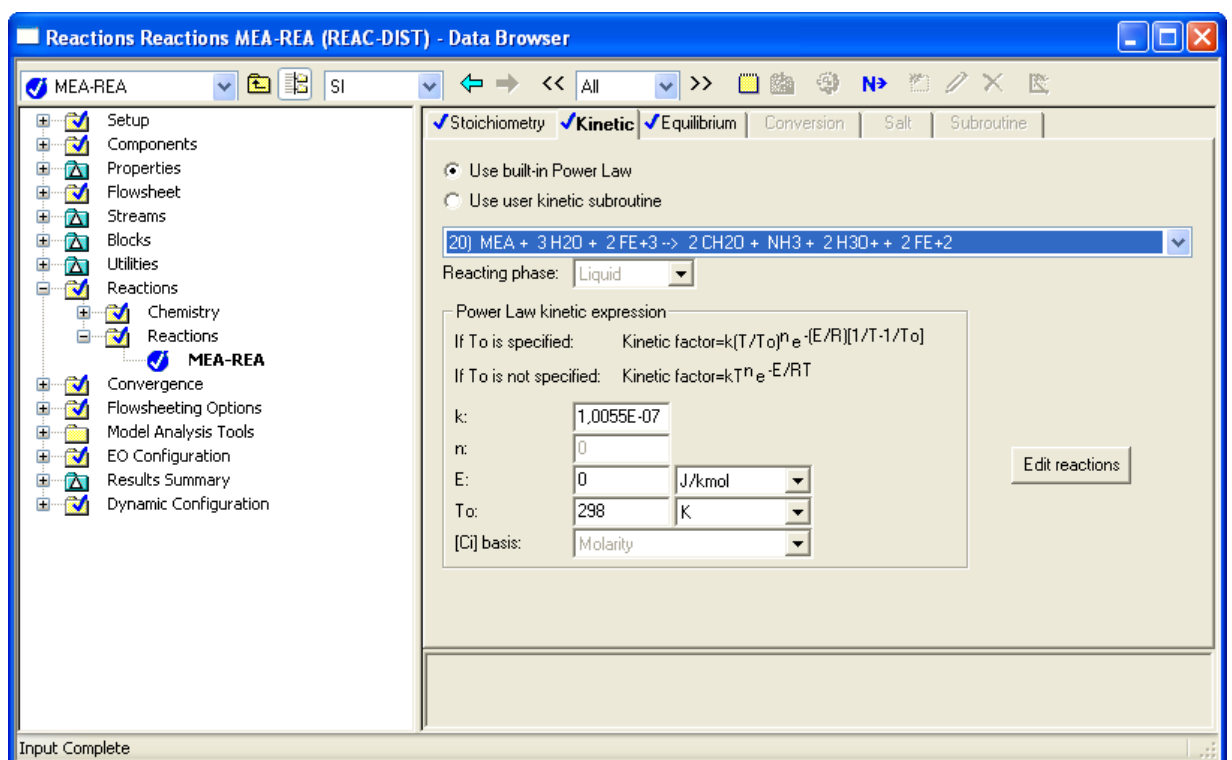


Figure B.10: The reaction kinetic window, in the Data Browser.

Appendix C

Gas Phase Degradation Modeling Results

C.1 Locked Ammonia Profile

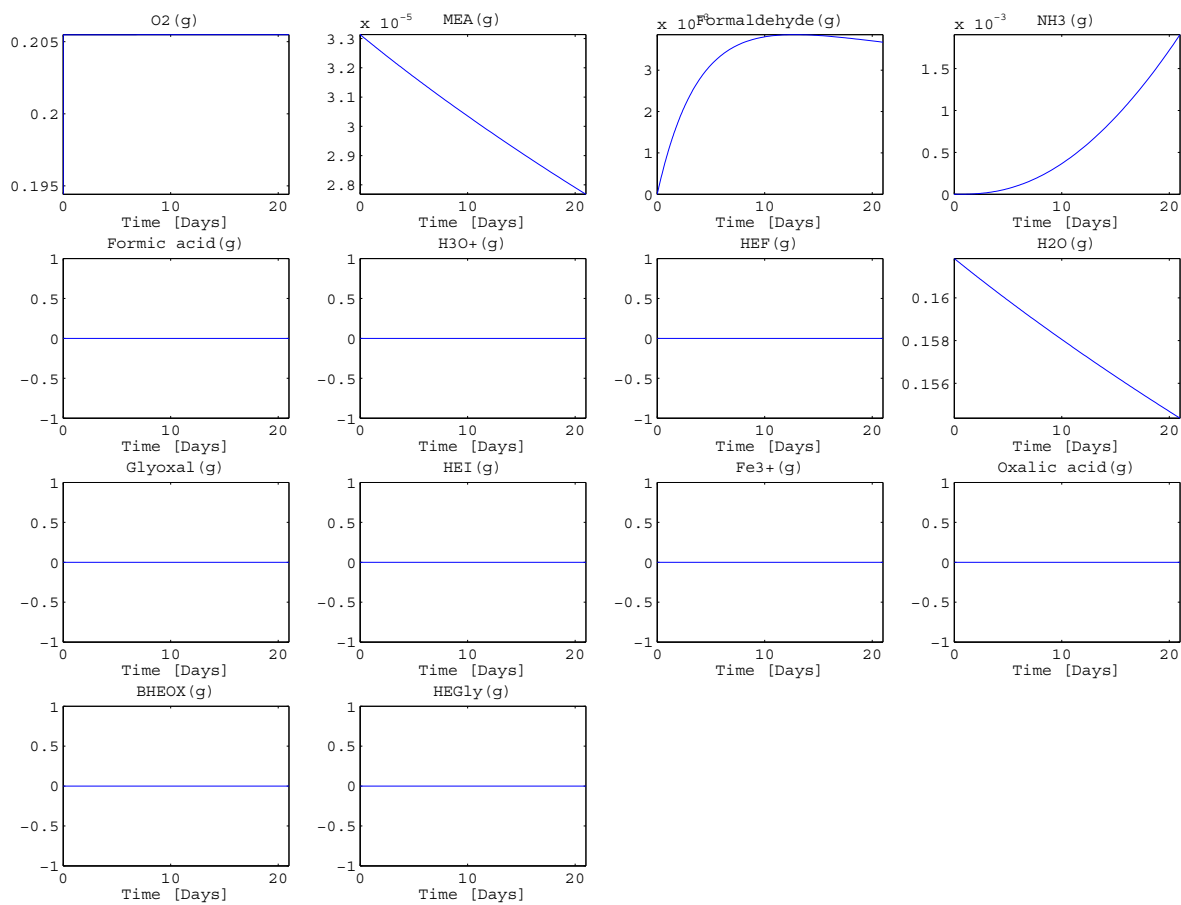


Figure C.1: Gas phase mole fractions to Figure 6.7.

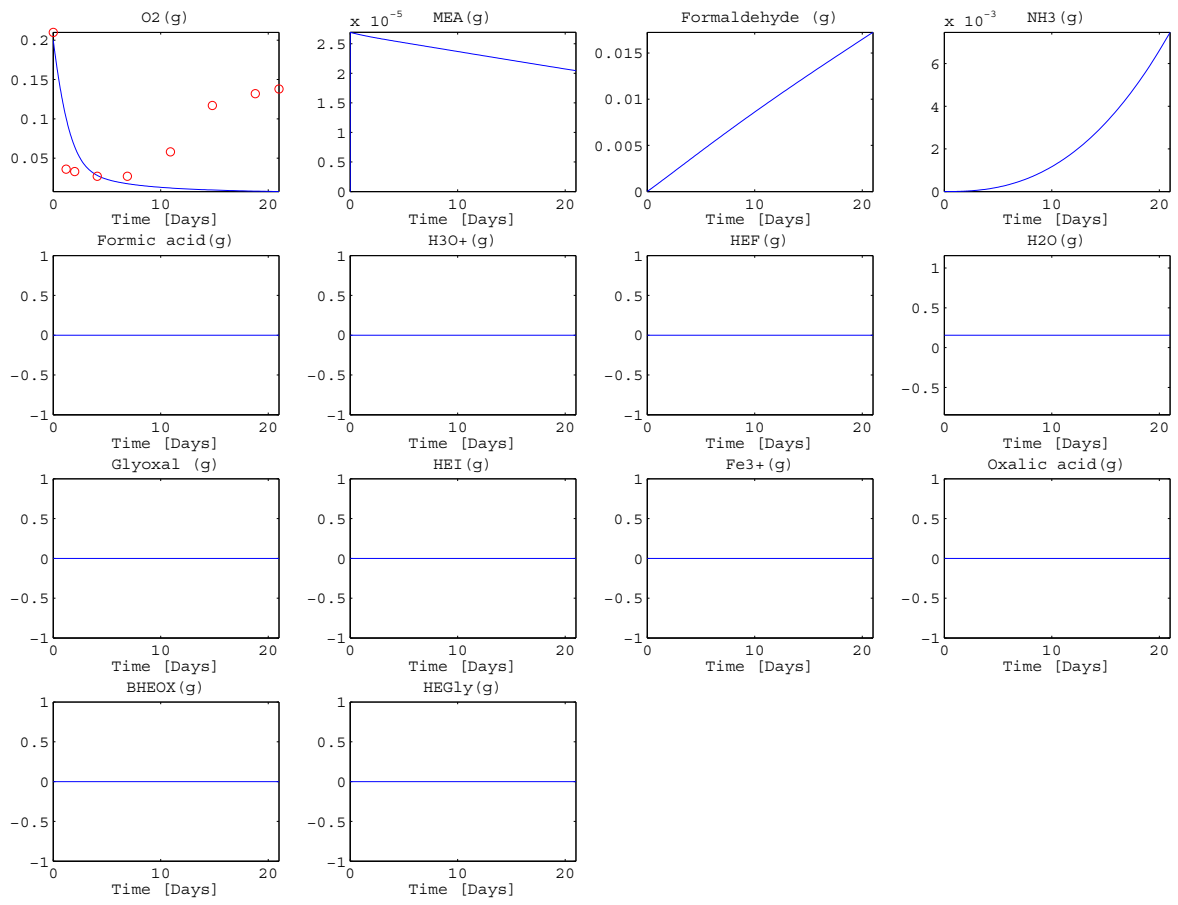


Figure C.2: Gas phase mole fractions to Figure 6.8.

C.2 Unlocked Ammonia Profile

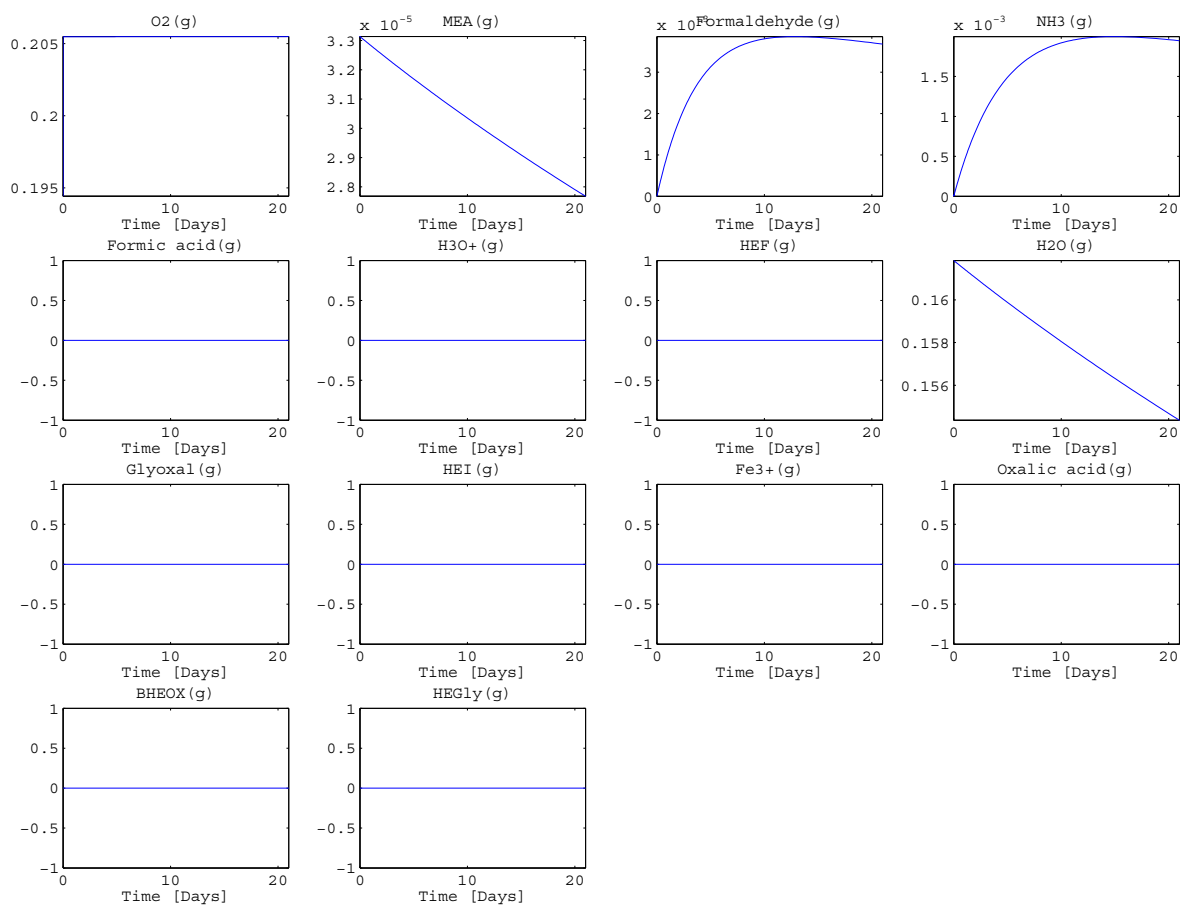


Figure C.3: Gas phase mole fractions to Figure 6.9.

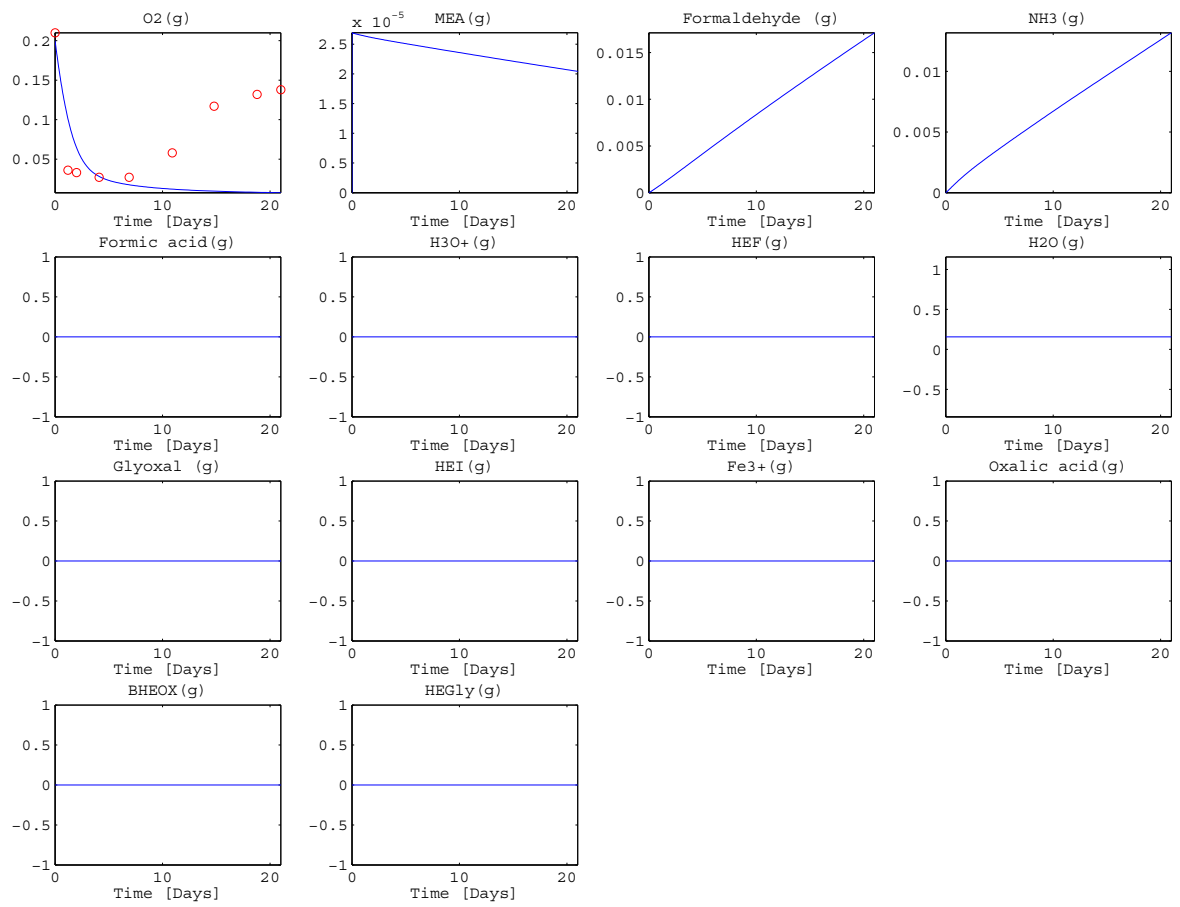


Figure C.4: Gas phase mole fractions to Figure 6.10.

C GAS PHASE DEGRADATION MODELING RESULTS

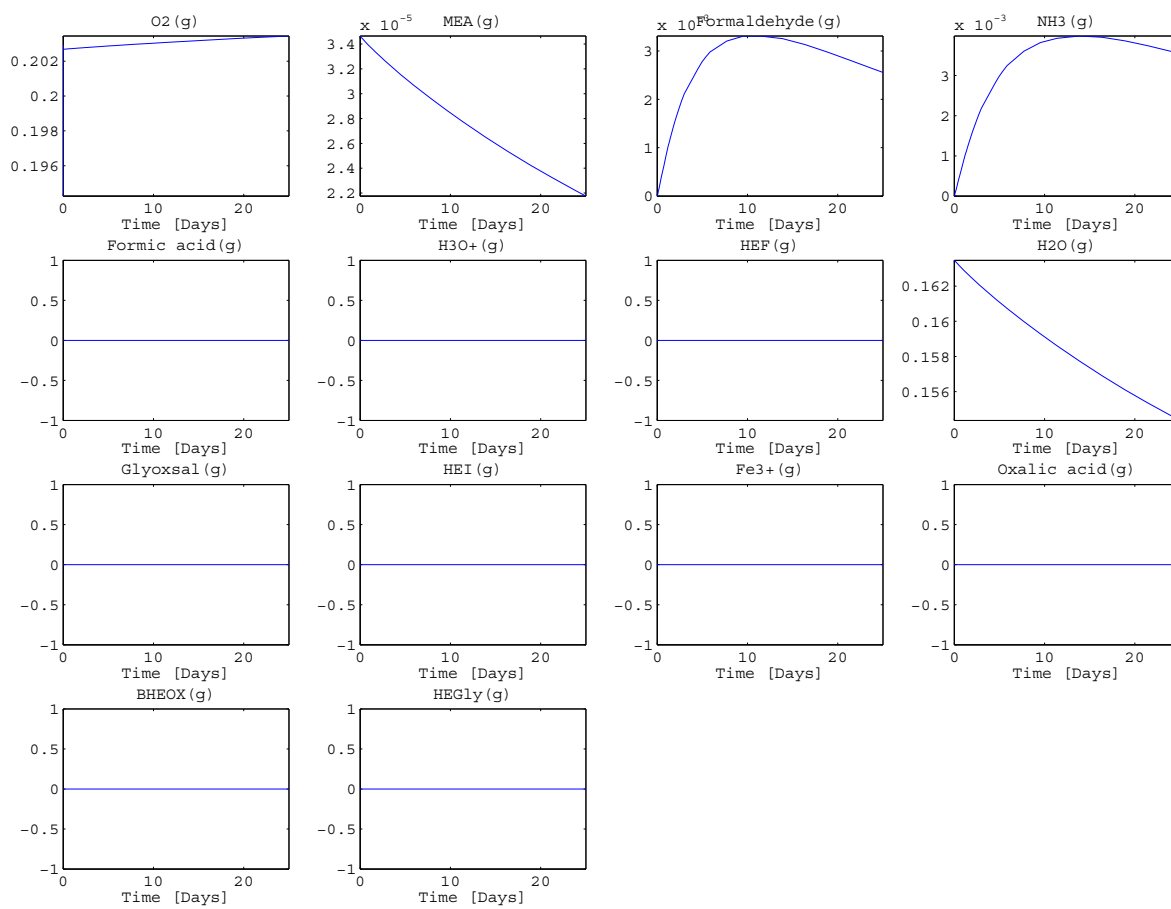


Figure C.5: Gas phase mole fractions to Figure 6.15.

Appendix D

MatLab Files

D.1 Files for Parameter Search

D.1.1 main.m

```
1 %%%%%%%%%%%%%%%%%%%%%%%%%%%%%%%%%%%%%%%%%%%%%%%%%%%%%%%%%%%%%%%%%%%%%%%%%%
2 %
3 %           MAIN FILE FOR PARAMETER SEARCH
4 %
5 %%%%%%%%%%%%%%%%%%%%%%%%%%%%%%%%%%%%%%%%%%%%%%%%%%%%%%%%%%%%%%%%%%%%%%%%%%
6 clc
7 clear all
8 close all
9
10 N=14;           %Number of components
11 reaction;      %Initalizing vectors and providing stoichiometry
12               %(Reaction orders are later overwritten)
13
14 %Initial guesses
15 %-----
16 O2LEAK        =    0.03304691883076794;
17 k1B           =    92.82974568284675;
18 k2B           =    1.303485549781516e+017;
19 k3B           =    939660.1545803259;
20 k_3B         =    -5881186764867.572;
21 k4B           =    16811801063.91369;
22 k5B           =    12e26 ;
23 k_5B         =    -3e22 ;
24 k6B           =    1217260213.673329;
25 k_6B         =    0;
26 k7B           =    200000000000;
27 k_7B         =    -45788508727.30507;
28 k8B           =    12924091.47118291;
29 k_8B         =    0;
30
31
32 ro1(11)       =    1.0625139958739;
33 ro2(11)       =    3;
34 ro3(11)       =    0.6574284605700789;
35 ro_3          =    1.925107576931437;
```

D MATLAB FILES

```
36 ro4(11)      = 1.585976650797294;
37 ro5(11)      = 3.8;
38 ro_5         = 2;
39 ro6(11)      = 2;
40 ro_6         = 1.034924998879484;
41 ro7(11)      = 3;
42 ro_7         = 2.181744984670027;
43 ro8(11)      = 1.44405937688007;
44 ro_8         = 1.551686018256;
45
46 X0=[O2LEAK;k1B;k2B;k3B;k_3B;k4B;k5B;k_5B;k6B;k_6B;k7B;k_7B;k8B;...
47 k_8B;ro1(11);ro2(11);ro3(11);ro_3;ro4(11);ro5(11);ro_5;ro6(11);...
48 ro_6;ro7(11);ro_7;ro8(11);ro_8];
49
50 %Selecting upper and lower range of initial guesses for SPSO
51 for i=1:length(X0)
52     Xmin(i)=X0(i)-0.1*X0(i);
53 end
54 for i=1:length(X0)
55     Xmax(i)=X0(i)+0.1*X0(i);
56 end
57
58 %Matrix of initial guesses for SPSO
59 A=[Xmin' Xmax'];
60
61 %Swarm parameters
62 swsz         = 20;
63 itermax      = 600;
64 lp           = 10;
65
66 warning off
67
68 %OPTIMIZATION ROUTINE (Select by uncommenting)
69 %-----
70 [Xopt,Fval,iter] = SPSO('OBJF',length(X0),swsz,itermax,A,lp);
71 % [Xopt]=fminsearch('OBJF',X0,optimset('Display','iter',...
72 %'TolFun',1e-2,'Maxiter',30000));
73
74 save Best_parameters Xopt
75
76 %Re-assigning the newly found parameters for plotting
77 %-----
78 O2LEAK       = Xopt(1);
79 k1B          = Xopt(2);
80 k2B          = Xopt(3);
81 k3B          = Xopt(4);
82 k_3B         = Xopt(5);
83 k4B          = Xopt(6);
84 k5B          = Xopt(7);
85 k_5B         = Xopt(8);
86 k6B          = Xopt(9);
87 k_6B         = Xopt(10);
88 k7B          = Xopt(11);
89 k_7B         = Xopt(12);
90 k8B          = Xopt(13);
91 k_8B         = Xopt(14);
92
93
```

```

94 ro1(11)      = Xopt(15);
95 ro2(11)      = Xopt(16);
96 ro3(11)      = Xopt(17);
97 ro_3         = Xopt(18);
98 ro4(11)      = Xopt(19);
99 ro5(11)      = Xopt(20);
100 ro_5         = Xopt(21);
101 ro6(11)      = Xopt(22);
102 ro_6         = Xopt(23);
103 ro7(11)      = Xopt(24);
104 ro_7         = Xopt(25);
105 ro8(11)      = Xopt(26);
106 ro_8         = Xopt(27);
107
108
109 RX_in=[O2LEAK k1A k2A k3A k_3A k4A k5A k_5A k6A k_6A k7A k_7A k8A...
110        k_8A ro1 ro2 ro3 ro4 ro5 ro6 ro7 ro8 rs1 rs2 rs3 rs4...
111        rs5 rs6 rs7 rs8 ro_3 ro_5 ro_6 ro_7 ro_8 k1B k2B k3B ...
112        k_3B k4B k5B k_5B k6B k_6B k7B k_7B k8B k_8B];
113
114 tc=[0 21];
115
116 [to,Co,yo]=batchrun(RX_in,to);
117
118 h=batchpicture(tc,Cc,yc);

```

D.1.2 SPSO.m

File obtained from Diego.

```

1 function [Xopt,Fval,iter] = SPSO(func,npar,varargin)
2 VMAX = 1e10*ones(1,npar);
3 % Default values for parameters:
4
5 if nargin == 2
6     swsz = 50; % swarm size
7     itermax = 100; % Max number of iterations
8     a = -ones(npar,1); % Lower boundary
9     b = ones(npar,1); % Upper boundary
10    lp = 30;
11    tol = 1e-6;
12    prob = 0.5;
13    w = 0.7298;
14    phi1 = 1.49618;
15    phi2 = 1.49618;
16 elseif nargin == 3
17     swsz = varargin{1};
18     itermax = 100;
19     a = -ones(npar,1);
20     b = ones(npar,1);
21     lp = 30;
22     tol = 1e-6;
23     prob = 0.5;
24     w = 0.7298;
25     phi1 = 1.49618;
26     phi2 = 1.49618;
27 elseif nargin == 4

```

D MATLAB FILES

```
28     swsz     =     varargin {1};
29     itermax  =     varargin {2};
30     a       =     -ones (npar ,1);
31     b       =     ones (npar ,1);
32     lp      =     30;
33     tol     =     1e-6;
34     prob    =     0.5;
35     w       =     0.7298;
36     phi1    =     1.49618;
37     phi2    =     1.49618;
38 elseif nargin == 5
39     swsz     =     varargin {1};
40     itermax  =     varargin {2};
41     A       =     varargin {3};
42     a       =     A (: ,1);
43     b       =     A (: ,2);
44     lp      =     30;
45     tol     =     1e-6;
46     prob    =     0.5;
47     w       =     0.7298;
48     phi1    =     1.49618;
49     phi2    =     1.49618;
50 elseif nargin == 6
51     swsz     =     varargin {1};
52     itermax  =     varargin {2};
53     A       =     varargin {3};
54     a       =     A (: ,1);
55     b       =     A (: ,2);
56     lp      =     varargin {4};
57     tol     =     1e-6;
58     prob    =     0.5;
59     w       =     0.7298;
60     phi1    =     1.49618;
61     phi2    =     1.49618;
62 elseif nargin == 7
63     swsz     =     varargin {1};
64     itermax  =     varargin {2};
65     A       =     varargin {3};
66     a       =     A (: ,1);
67     b       =     A (: ,2);
68     lp      =     varargin {4};
69     tol     =     varargin {5};
70     prob    =     0.5;
71     w       =     0.7298;
72     phi1    =     1.49618;
73     phi2    =     1.49618;
74 elseif nargin == 8
75     swsz     =     varargin {1};
76     itermax  =     varargin {2};
77     A       =     varargin {3};
78     a       =     A (: ,1);
79     b       =     A (: ,2);
80     lp      =     varargin {4};
81     tol     =     varargin {5};
82     prob    =     varargin {6};
83     w       =     0.7298;
84     phi1    =     1.49618;
85     phi2    =     1.49618;
```

```

86 elseif nargin == 9
87     swsz = varargin{1};
88     itermax = varargin{2};
89     A = varargin{3};
90     a = A(:,1);
91     b = A(:,2);
92     lp = varargin{4};
93     tol = varargin{5};
94     prob = varargin{6};
95     w = varargin{7};
96     phi1 = 1.49618;
97     phi2 = 1.49618;
98 elseif nargin == 10
99     swsz = varargin{1};
100    itermax = varargin{2};
101    A = varargin{3};
102    a = A(:,1);
103    b = A(:,2);
104    lp = varargin{4};
105    tol = varargin{5};
106    prob = varargin{6};
107    w = varargin{7};
108    phi1 = varargin{8};
109    phi2 = 1.49618;
110 elseif nargin == 11
111    swsz = varargin{1};
112    itermax = varargin{2};
113    A = varargin{3};
114    a = A(:,1);
115    b = A(:,2);
116    lp = varargin{4};
117    tol = varargin{5};
118    prob = varargin{6};
119    w = varargin{7};
120    phi1 = varargin{8};
121    phi2 = varargin{9};
122 end
123
124 disp('Iteration      min f(x)      Loop      Time(s)      Clock')
125 Fval = 1e100;
126 FV = 1e100;
127 fg = FV;
128
129 iter = zeros(lp,1);
130
131
132 for kp = 1 : lp
133
134     swpos = zeros(swsz, npar);
135     p = prob*ones(swsz,1); % Probability treshold
136
137     for k = 1 : npar
138         swpos(:,k) = a(k) + (b(k) - a(k)).*rand(swsz,1);
139     end
140 % swpos(1,:)=pg;
141
142     pbest = fg*ones(swsz,1);
143

```

D MATLAB FILES

```

144 %     swvlc   =   rand(swsz ,npar);
145 swvlc   =   zeros(swsz ,npar);
146 swpos   =   swpos + swvlc;
147 Pb     =   swpos;
148
149 psw     =   zeros(swsz ,1);
150
151 while FV > tol && iter(kp) < itermax
152
153     iter(kp)   =   iter(kp) + 1;
154
155     tini     =   tic;
156     for k2   =   1 : swsz
157
158         % Function Evaluation
159
160         psw(k2) = feval(func ,swpos(k2 ,:));
161
162         FV = psw(k2);
163
164         % Searching and Updating best positions
165
166         if psw(k2) < pbest(k2)
167             pbest(k2)   =   psw(k2);
168             Pb(k2 ,:)   =   swpos(k2 ,:);
169         end
170
171         % Updating best values
172
173         if FV < fg
174             fg = FV;           % Global k so far
175             pg = swpos(k2 ,:); % Updating best position so far
176
177
178             save ALLnew15 pg fg
179             ANSFIG(pg);
180 %             pause;
181         end
182
183     end
184
185     mp = rand(swsz ,swsz);
186
187     for k2 = 1 : swsz
188
189         m     =   mp(:,k2);
190         mpos  =   m < p(k2);
191         mpos(k2)= 1;
192 %         F     =   find(min(psw(mpos)) == psw);
193 %         pl    =   swpos(F(1) ,:);
194         F     =   find(min(pbest(mpos)) == pbest);
195         pl    =   Pb(F(1) ,:);
196         if F == k2
197             % Updating velocities
198             swvlc_x   =   w*swvlc(k2 ,:) + phi1*rand*(Pb(k2 ,:) ...
199 - swpos(k2 ,:));
200             swvlc_x(abs(swvlc_x)>VMAX)   =   sign(swvlc_x(abs...
(swvlc_x)>VMAX)).*VMAX(abs(swvlc_x)>VMAX);

```



```

201         %velocity restriction ...
202         swvlc(k2,:) = swvlc_x;
203     else
204         % Updating velocities
205         swvlc_x = w*swvlc(k2,:) + phi1*rand*(Pb(k2, :)...
206 - swpos(k2, :)) + phi2*rand*(p1 - swpos(k2, :));
207         swvlc_x(abs(swvlc_x)>VMAX) = sign(swvlc_x(abs...
208 (swvlc_x)>VMAX)).*VMAX(abs(swvlc_x)>VMAX);
209         swvlc(k2,:) = swvlc_x;
210
211     end
212 end
213 % Updating positions
214 swpos = swpos + swvlc;
215 tfinal=toc(tini);
216 tfinal=round(tfinal);
217 CK = clock;
218
219     fprintf(' %5.0f      %12.6g      %5.0f      %5.0f ...
220 %5.0f %5.0f\n', iter(kp), fg, kp, tfinal, CK(4), CK(5))
221
222 end
223
224 if fg < Fval
225     Xopt = pg;
226     Fval = fg;
227 end
228
229 end

```

D.1.3 OBJF.m

```

1  %%%%%%%%%%%%%%%%%%%%%%%%%%%%%%%%%%%%%%%%%%%%%%%%%%%%%%%%%%%%%%%%%%%%%%%%%%%
2  %
3  % OBJECT FUNCTION
4  % Calling the model-file , comparing model with experimental
5  % points , calculating the error.
6  %
7  %%%%%%%%%%%%%%%%%%%%%%%%%%%%%%%%%%%%%%%%%%%%%%%%%%%%%%%%%%%%%%%%%%%%%%%%%%%
8  function [D sigma]=OBJF(x)
9
10 global tini
11
12
13 N=14;
14 reaction;
15 constant;
16
17 % Previously found parameters for the open loop experiment
18 %-----
19 k1A = 0.006188477768123002;
20 k2A = 42.87898612739161;
21 k3A = 604.8334491505484;
22 k_3A = 57109.00927412349;
23 k4A = 1.305957805794899;
24 k5A = 50000;
25 k_5A = 150068135985528.371;

```

D MATLAB FILES

```
26 k6A          = 0.09;
27 k_6A        = 0.0007945033825119468;
28 k7A         = 70e-3;
29 k_7A        = 50;
30 k8A         = 0.2141173268358577;
31 k_8A        = 0.03212611664751086;
32
33 ro1(2)      = 1.164662723731612;
34 ro2(1)      = 1.049367576169141;
35 ro2(3)      = 0;
36 ro3(5)      = 0.4865419595890305;
37 ro3(2)      = 0;
38 ro3(7)      = 1.638724147587275;
39 ro4(1)      = 1.094956970302114;
40 ro4(2)      = 0.9780589604174879;
41 ro5(2)      = 0;
42 ro5(3)      = 0.9972061576948763;
43 ro5(4)      = 1.150624321997112;
44 ro5(8)      = 0.0002335071682050042;
45 ro5(9)      = 0.6420418490615194;
46 ro5(10)     = 4.976339480090978;
47 ro6(1)      = 0.6627231174779569;
48 ro6(9)      = 0.1;
49 ro6(12)     = 0.9506938500142967;
50 ro7(2)      = 2.386339988618684;
51 ro7(12)     = 0.7;
52 ro7(13)     = 1.383401735222115;
53 ro8(1)      = 0.9719254581424652;
54 ro8(2)      = 1.92710691179245;
55 ro8(4)      = 1.36332398240264;
56 ro8(14)     = 1.021624123492898;
57
58
59
60 %Assigning the parameters to be optimized
61 %-----
62 O2LEAK      = x(1);
63 k1B         = x(2);
64 k2B         = x(3);
65 k3B         = x(4);
66 k_3B        = x(5);
67 k4B         = x(6);
68 k5B         = x(7);
69 k_5B        = x(8);
70 k6B         = x(9);
71 k_6B        = x(10);
72 k7B         = x(11);
73 k_7B        = x(12);
74 k8B         = x(13);
75 k_8B        = x(14);
76
77
78 ro1(11)     = x(15);
79 ro2(11)     = x(16);
80 ro3(11)     = x(17);
81 ro_3        = x(18);
82 ro4(11)     = x(19);
83 ro5(11)     = x(20);
```

```

84         ro_5           =   x(21);
85         ro6(11)       =   x(22);
86         ro_6           =   x(23);
87         ro7(11)       =   x(24);
88         ro_7           =   x(25);
89         ro8(11)       =   x(26);
90         ro_8           =   x(27);
91
92
93     RX_in=[O2LEAK k1A k2A k3A k_3A k4A k5A k_5A k6A k_6A k7A k_7A k8A ...
94           k_8A ro1 ro2 ro3 ro4 ro5 ro6 ro7 ro8 rs1 rs2 rs3 rs4 ...
95           rs5 rs6 rs7 rs8 ro_3 ro_5 ro_6 ro_7 ro_8 k1B k2B k3B ...
96           k_3B k4B k5B k_5B k6B k_6B k7B k_7B k8B k_8B ];
97
98     % SFBExperimental;
99     BATCHexperimental;
100
101     try
102         tini=tic;
103         % [to,Co,yo]=SFBRun(RX_in,toexp);
104         [tc,Cc,yc]=batchrun(RX_in,tcexp);
105
106
107     %Batch Model result
108     %-----
109         ycO2mod=yc(1:5,1); %ONLY 5 FIRST POINTS
110         CcMEAmod=Cc(:,2);
111         CcNH3mod=Cc(:,4);
112         CcFORMmod=Cc(:,5);
113         CcHEFmod=Cc(:,7);
114         CcHEImod=Cc(:,10);
115         CcBHEOXmod=Cc(:,13);
116         CcHEGLymod=Cc(:,14);
117         CcOXALICmod=Cc(:,12);
118
119         ycO2exp=ycO2exp(1:5);%ONLY 5 FIRST POINTS
120
121     %WEIGHTED ERRORS
122     %-----
123         D = 0;
124         D = D + 0.1*sum(abs(ycO2mod - ycO2exp)./ycO2exp)/...
125         length(ycO2exp);
126         D = D + 4*sum(abs(CcMEAmod - CcMEAexp)./CcMEAexp)...
127         /length(CcMEAexp);
128         D = D + (10)*sum(abs(CcFORMmod - CcFORMexp2)./...
129         [1; 1; CcFORMexp2(3:length(CcFORMexp2))])/length(CcFORMexp2);
130         D = D + 10*sum(abs(CcHEFmod - CcHEFexp2)./...
131         CcHEFexp2)/length(CcHEFexp2);
132         D = D + 4*sum(abs(CcHEImod - CcHEIexp2)./...
133         CcHEIexp2)/length(CcHEIexp2);
134         D = D + 10*sum(abs(CcOXALICmod - 9.088946705e-4)./...
135         9.088946705e-4)/1;
136         D = D + 1*sum(abs(CcBHEOXmod - CcBHEOXexp2)./...
137         CcBHEOXexp2)/length(CcBHEOXexp2);
138         D = D + sum(abs(CcHEGLymod - CcHEGLyexp2)./...
139         CcHEGLyexp2)/length(CcHEGLyexp2);
140         D = D*100;
141

```

D MATLAB FILES

```
142     if isnan(D)==1
143         D=1e100;
144         'Is NaN'
145     elseif isinf(D)==1
146         D=1e100;
147         'Is Inf'
148     end
149 catch
150     D=1e100;
151 end
```

D.1.4 ANSFIG.m

```
1 %PLOTING OF THE BEST PARAMETERS AS THE SPSO.m-FILE UPDATES THEM
2 function [] = ANSFIG(Xopt)
3
4
5     N=14;
6     reaction;
7
8 % Previously found parameters for the open loop experiment
9 %-----
10 k1A      = 0.006188477768123002;
11 k2A      = 42.87898612739161;
12 k3A      = 604.8334491505484;
13 k_3A     = 57109.00927412349;
14 k4A      = 1.305957805794899;
15 k5A      = 50000;
16 k_5A     = 150068135985528.371;
17 k6A      = 0.09;
18 k_6A     = 0.0007945033825119468;
19 k7A      = 70e-3;
20 k_7A     = 50;
21 k8A      = 0.2141173268358577;
22 k_8A     = 0.03212611664751086;
23
24 ro1(2)   = 1.164662723731612;
25 ro2(1)   = 1.049367576169141;
26 ro2(3)   = 0;
27 ro3(5)   = 0.4865419595890305;
28 ro3(2)   = 0;
29 ro3(7)   = 1.638724147587275;
30 ro4(1)   = 1.094956970302114;
31 ro4(2)   = 0.9780589604174879;
32 ro5(2)   = 0;
33 ro5(3)   = 0.9972061576948763;
34 ro5(4)   = 1.150624321997112;
35 ro5(8)   = 0.0002335071682050042;
36 ro5(9)   = 0.6420418490615194;
37 ro5(10)  = 4.976339480090978;
38 ro6(1)   = 0.6627231174779569;
39 ro6(9)   = 0.1;
40 ro6(12)  = 0.9506938500142967;
41 ro7(2)   = 2.386339988618684;
42 ro7(12)  = 0.7;
43 ro7(13)  = 1.383401735222115;
44 ro8(1)   = 0.9719254581424652;
```

```

45 ro8(2)      =      1.92710691179245;
46 ro8(4)      =      1.36332398240264;
47 ro8(14)     =      1.021624123492898;
48
49 %Newly found parameters to be plotted
50 %-----
51 O2LEAK      =      Xopt(1);
52 k1B         =      Xopt(2);
53 k2B         =      Xopt(3);
54 k3B         =      Xopt(4);
55 k_3B        =      Xopt(5);
56 k4B         =      Xopt(6);
57 k5B         =      Xopt(7);
58 k_5B        =      Xopt(8);
59 k6B         =      Xopt(9);
60 k_6B        =      Xopt(10);
61 k7B         =      Xopt(11);
62 k_7B        =      Xopt(12);
63 k8B         =      Xopt(13);
64 k_8B        =      Xopt(14);
65
66
67 ro1(11)     =      Xopt(15);
68 ro2(11)     =      Xopt(16);
69 ro3(11)     =      Xopt(17);
70 ro_3        =      Xopt(18);
71 ro4(11)     =      Xopt(19);
72 ro5(11)     =      Xopt(20);
73 ro_5        =      Xopt(21);
74 ro6(11)     =      Xopt(22);
75 ro_6        =      Xopt(23);
76 ro7(11)     =      Xopt(24);
77 ro_7        =      Xopt(25);
78 ro8(11)     =      Xopt(26);
79 ro_8        =      Xopt(27);
80
81
82 RX_in=[O2LEAK k1A k2A k3A k_3A k4A k5A k_5A k6A k_6A k7A k_7A k8A ...
83        k_8A ro1 ro2 ro3 ro4 ro5 ro6 ro7 ro8 rs1 rs2 rs3 rs4 ...
84        rs5 rs6 rs7 rs8 ro_3 ro_5 ro_6 ro_7 ro_8 k1B k2B k3B ...
85        k_3B k4B k5B k_5B k6B k_6B k7B k_7B k8B k_8B];
86
87 %Plotting
88 %-----
89 to=[0 21];
90 % [t,Co,yo]=SFBRrun(RX_in,to);
91 % h=SFBRpicture(t,Co,yo);
92
93
94 [tc,Cc,yc]=batchrun(RX_in,to);
95 h=batchpicture(tc,Cc,yc);

```

D.2 Experimental Model Files

D.2.1 RUN.m

Runs all files to provide the results.

```

1 %%%%%%%%%%%%%%%%%%%%%%%%%%%%%%%%%%%%%%%%%%%%%%%%%%%%%%%%%%%%%%%%%%%%%%%%%%
2 %
3 %                               RUN-FILE
4 %       Running the model-files with the found parameters
5 %
6 %%%%%%%%%%%%%%%%%%%%%%%%%%%%%%%%%%%%%%%%%%%%%%%%%%%%%%%%%%%%%%%%%%%%%%%%%%
7 close all
8 clc
9 clear all
10 N=14;
11 reaction;
12
13 %Found Rate Parameters (Final Version)
14 %-----
15 k1A      =    0.006188477768123002;
16 k2A      =    42.87898612739161;
17 k3A      =    604.8334491505484;
18 k_3A     =    57109.00927412349;
19 k4A      =    1.305957805794899;
20 k5A      =    50000;
21 k_5A     =    150068135985528.371;
22 k6A      =    0.09;
23 k_6A     =    0.0007945033825119468;
24 k7A      =    70e-3;
25 k_7A     =    50;
26 k8A      =    0.2141173268358577;
27 k_8A     =    0.03212611664751086;
28
29 ro1(2)   =    1.164662723731612;
30 ro2(1)   =    1.049367576169141;
31 ro2(3)   =    0;
32 ro3(5)   =    0.4865419595890305;
33 ro3(2)   =    0;
34 ro3(7)   =    1.638724147587275;
35 ro4(1)   =    1.094956970302114;
36 ro4(2)   =    0.9780589604174879;
37 ro5(2)   =    0;
38 ro5(3)   =    0.9972061576948763;
39 ro5(4)   =    1.150624321997112;
40 ro5(8)   =    0.0002335071682050042;
41 ro5(9)   =    0.6420418490615194;
42 ro5(10)  =    4.976339480090978;
43 ro6(1)   =    0.6627231174779569;
44 ro6(9)   =    0.1;
45 ro6(12)  =    0.9506938500142967;
46 ro7(2)   =    2.386339988618684;
47 ro7(12)  =    0.7;
48 ro7(13)  =    1.383401735222115;
49 ro8(1)   =    0.9719254581424652;
50 ro8(2)   =    1.92710691179245;
51 ro8(4)   =    1.36332398240264;

```

```

52 ro8(14) = 1.021624123492898;
53
54 O2LEAK = 0.03304691883076794;
55 k1B = 92.82974568284675;
56 k2B = 1.303485549781516e+017;
57 k3B = 939660.1545803259;
58 k_3B = -5881186764867.572;
59 k4B = 16811801063.91369;
60 k5B = 12e26;
61 k_5B = -3e22;
62 k6B = 1217260213.673329;
63 k_6B = 0;
64 k7B = 200000000000;
65 k_7B = -45788508727.30507;
66 k8B = 12924091.47118291;
67 k_8B = 0;
68
69
70 ro1(11) = 1.0625139958739;
71 ro2(11) = 3;
72 ro3(11) = 0.6574284605700789;
73 ro_3 = 1.925107576931437;
74 ro4(11) = 1.585976650797294;
75 ro5(11) = 3.8;
76 ro_5 = 2;
77 ro6(11) = 2;
78 ro_6 = 1.034924998879484;
79 ro7(11) = 3;
80 ro_7 = 2.181744984670027;
81 ro8(11) = 1.44405937688007;
82 ro_8 = 1.551686018256;
83
84 RX_in=[O2LEAK k1A k2A k3A k_3A k4A k5A k_5A k6A k_6A k7A k_7A k8A ...
85 k_8A ro1 ro2 ro3 ro4 ro5 ro6 ro7 ro8 rs1 rs2 rs3 rs4 ...
86 rs5 rs6 rs7 rs8 ro_3 ro_5 ro_6 ro_7 ro_8 k1B k2B k3B ...
87 k_3B k4B k5B k_5B k6B k_6B k7B k_7B k8B k_8B];
88
89 %RUNNING MODELS AND PLOTTING
90 %-----
91 to=[0 21];
92 [to,Co,yo]=SFBRrun(RX_in,to);
93 h=SFBRRpicture(to,Co,yo);
94
95 tc=[0 21];
96 [tc,Cc,yc]=batchrun(RX_in,tc);
97 h=batchpicture(tc,Cc,yc);
98
99 tm=[0 25];
100 [tm,Cm,ym]=MetalSFBRrun(RX_in,tm);
101 h=MetalSFBRpicture(tm,Cm,ym);

```

D.2.2 SFBRrun.m

```

1 %%%%%%%%%%%%%%%%%%%%%%%%%%%%%%%%%%%%%%%%%%%%%%%%%%%%%%%%%%%%%%%%%%%%%%%%%%%
2 %
3 %           SEMI-FLOW BATCH REACTOR
4 %           Well-mixed gas-well-mixed batch liquid

```

D MATLAB FILES

```

5 %
6 %
7 %
8 %
9 %
10 %
11 %
12 %
13 %
14 %
15 %
16 %
17 %
18 %
19 %
20 %
21 function [t,C,y]=SFBRrun(RX_in,to)
22
23 global KG a P VG VL H y0 N T GASCONST G1 G2
24
25 N=14;          %Total number of components
26 constant;
27 reaction;
28
29 %%%%%%%%%%%%%%%%%%%%%%%%%%%%%%%%%%%%%%%%%%%%%%%%%%%%%%%%%%%%%%%%%%%%%%%%%
30 % EXPERIMENTAL PROPERTIES
31 %%%%%%%%%%%%%%%%%%%%%%%%%%%%%%%%%%%%%%%%%%%%%%%%%%%%%%%%%%%%%%%%%%%%%%%%%
32 kL=1e1*ones(N,1);%Liquid mass transfer ...
33                   %coefficient [kmol/m2-Days-bar]
34 kL(4)=3e-3;      %Liquid mass transfer coefficient NH3 ...
35                   %(found to fit experimental data)
36
37
38 a=200;          %Mass transfer area per unit volume of ...
39                   %continous phase [m2/m3]
40 P=1.02;         %Total pressure [bar]
41 VL=1.08142e-3; %Volume of liquid phase [m3]
42 T=273.15+55;
43
44 G1=0.01911461; %Molar gas flow rate [kmol/Days] @ reactor inlet
45 G2=0.01911461; %Molar gas flow rate [kmol/Days] @ reactor outlet
46
47 [H]=henrys(MWO2,rhoL,N,T,GASCONST2);
48
49 KG=kL./H'; %Over-all gas-phase mass transfer coefficient, vector
50
51 % NO MASS TRANSFER OF THE FOLLOWING COMPONENTS:
52 %(Either due to low concentrations or low volatility)
53 %(Values set zero, to avoid infinite values)
54 KG(5)=0; %Formic acid
55 KG(6)=0; %H3O+
56 KG(7)=0; %HEF
57 KG(9)=0; %Glyoxal
58 KG(10)=0;%HEI
59 KG(11)=0;%Fe2+/3+
60 KG(12)=0;%Oxalic acid
61 KG(13)=0;%BHEOX
62 KG(14)=0;%HEGly

```



```

63
64 %%%%%%%%%%%%%%%%%%%%%%%%%%%%%%%%%%%%%%%%%%%%%%%%%%%%%%%%%%%%%%%%%%%%%%%%%%
65 % INITIAL CONCENTRATIONS
66 %%%%%%%%%%%%%%%%%%%%%%%%%%%%%%%%%%%%%%%%%%%%%%%%%%%%%%%%%%%%%%%%%%%%%%%%%%
67     Psat=watvappres(T); %Calculating the saturation pressure of
68                          %water vapor to determine the initial
69                          %concentraion of gas phase water
70
71 %GAS MOLE FRACTIONS [-]
72 y0(1)=0.2055944; %Mol-fraction of component in gas phase ...
73                  %@ reactor inlet
74
75 y0(2)=0;
76 y0(3)=0;
77 y0(4)=0;
78 y0(5)=0;
79 y0(6)=0;
80 y0(7)=0;
81 y0(8)=(Psat/100000)/P; %Gas is saturated with water
82 y0(9)=0;
83 y0(10)=0;
84 y0(11)=0;
85 y0(12)=0;
86 y0(13)=0;
87 y0(14)=0;
88
89 %LIQUID CONCENTRATIONS [kmol/m3]
90 C0(1)=0;
91 C0(2)=5.02;
92 C0(3)=0;
93 C0(4)=0;
94 C0(5)=0;
95 C0(6)=0;
96 C0(7)=159.49e-3/MWHEF;
97 C0(8)=51;
98 C0(9)=0;
99 C0(10)=17.95e-3/MWHEI;
100 C0(11)=1e-15;
101 C0(12)=0;
102 C0(13)=5.8e-3/MWBHEOX;
103 C0(14)=9.8e-3/MWHEGly;
104
105 C0=C0';
106 %%%%%%%%%%%%%%%%%%%%%%%%%%%%%%%%%%%%%%%%%%%%%%%%%%%%%%%%%%%%%%%%%%%%%%%%%%
107 % ODE SOLVER
108 %%%%%%%%%%%%%%%%%%%%%%%%%%%%%%%%%%%%%%%%%%%%%%%%%%%%%%%%%%%%%%%%%%%%%%%%%%
109     RTOL=1E-9;
110     ATOL=1E-9;
111
112 [t,C]=ode15s(@SFBRmodel,to,C0,odeset('RelTol',RTOL,'AbsTol',ATOL),...
113 RX.in);
114
115 %GAS PHASE EQUATION (Not time dependant)
116 for i=1:N
117     y(:,i)=((G1*y0(i) + KG(i)*a*VL.*C(:,i)*H(i))./(G2 + KG(i)*a*VL*P));
118 end

```

D.2.3 SBFmodel.m

```

1 function t_der=SBFmodel(t,C,RX_in)
2 global KG a P VG VL H y0 N T GASCONST G1 G2 tini
3
4 %%%%%%%%%%%%%%%%%%%%%%%%%%%%%%%%%%%%%%%%%%%%%%%%%%%%%%%%%%%%%%%%%%%%%%%%%%
5 %ODE CALCULATION TIME LIMITER
6 %Used in combination with OBJF.m when iterating
7 %%%%%%%%%%%%%%%%%%%%%%%%%%%%%%%%%%%%%%%%%%%%%%%%%%%%%%%%%%%%%%%%%%%%%%%%%%
8 % if toc(tini)>10
9 %     t_der=NaN;
10 %     return
11 % end
12
13 %%%%%%%%%%%%%%%%%%%%%%%%%%%%%%%%%%%%%%%%%%%%%%%%%%%%%%%%%%%%%%%%%%%%%%%%%%
14 % ASSIGNING RATE COEFFICIENTS
15 %%%%%%%%%%%%%%%%%%%%%%%%%%%%%%%%%%%%%%%%%%%%%%%%%%%%%%%%%%%%%%%%%%%%%%%%%%
16 O2LEAK=RX_in(1);
17 k1A=RX_in(2);
18 k2A=RX_in(3);
19 k3A=RX_in(4);
20 k_3A=RX_in(5);
21 k4A=RX_in(6);
22 k5A=RX_in(7);
23 k_5A=RX_in(8);
24 k6A=RX_in(9);
25 k_6A=RX_in(10);
26 k7A=RX_in(11);
27 k_7A=RX_in(12);
28 k8A=RX_in(13);
29 k_8A=RX_in(14);
30
31 q=14; %Number scalar values before the vectors
32      %(Not always equal to number of components)
33
34 ro1=RX_in(q+1:q+N);
35 ro2=RX_in(q+N+1:q+(2*N));
36 ro3=RX_in(q+(2*N)+1:q+(3*N));
37 ro4=RX_in(q+(3*N)+1:q+(4*N));
38 ro5=RX_in(q+(4*N)+1:q+(5*N));
39 ro6=RX_in(q+(5*N)+1:q+(6*N));
40 ro7=RX_in(q+(6*N)+1:q+(7*N));
41 ro8=RX_in(q+(7*N)+1:q+(8*N));
42
43 rs1=RX_in(q+(8*N)+1:q+(9*N));
44 rs2=RX_in(q+(9*N)+1:q+(10*N));
45 rs3=RX_in(q+(10*N)+1:q+(11*N));
46 rs4=RX_in(q+(11*N)+1:q+(12*N));
47 rs5=RX_in(q+(12*N)+1:q+(13*N));
48 rs6=RX_in(q+(13*N)+1:q+(14*N));
49 rs7=RX_in(q+(14*N)+1:q+(15*N));
50 rs8=RX_in(q+(15*N)+1:q+(16*N));
51
52 ro_3=RX_in(q+(16*N)+1);
53 ro_5=RX_in(q+(16*N)+2);
54 ro_6=RX_in(q+(16*N)+3);
55 ro_7=RX_in(q+(16*N)+4);
56 ro_8=RX_in(q+(16*N)+5);

```

```

57 |
58 | k1B=RX_in(q+(16*N)+6);
59 | k2B=RX_in(q+(16*N)+7);
60 | k3B=RX_in(q+(16*N)+8);
61 | k_3B=RX_in(q+(16*N)+9);
62 | k4B=RX_in(q+(16*N)+10);
63 | k5B=RX_in(q+(16*N)+11);
64 | k_5B=RX_in(q+(16*N)+12);
65 | k6B=RX_in(q+(16*N)+13);
66 | k_6B=RX_in(q+(16*N)+14);
67 | k7B=RX_in(q+(16*N)+15);
68 | k_7B=RX_in(q+(16*N)+16);
69 | k8B=RX_in(q+(16*N)+17);
70 | k_8B=RX_in(q+(16*N)+18);
71 |
72 |
73 | %%%%%%%%%%%%%%%%%%%%%%%%%%%%%%%%%%%%%%%%%%%%%%%%%%%%%%%%%%%%%%%%%%%%%%%%%
74 | % DETERMINING HENRYS LAW COEFFICIENT FOR WATER
75 | %%%%%%%%%%%%%%%%%%%%%%%%%%%%%%%%%%%%%%%%%%%%%%%%%%%%%%%%%%%%%%%%%%%%%%%%%
76 | Psat=watvappres(T);
77 | H(8)=(Psat/100000)/C(8); %Henrys constant water vapor
78 |
79 | %%%%%%%%%%%%%%%%%%%%%%%%%%%%%%%%%%%%%%%%%%%%%%%%%%%%%%%%%%%%%%%%%%%%%%%%%
80 | % CALCULATING THE RATE COEFFICIENTS
81 | % Dependant on Fe-concentration
82 | %%%%%%%%%%%%%%%%%%%%%%%%%%%%%%%%%%%%%%%%%%%%%%%%%%%%%%%%%%%%%%%%%%%%%%%%%
83 | k1      =   k1A;
84 | k2      =   k2A;
85 | k3      =   k3A ;
86 | k_3     =   k_3A;
87 | k4      =   k4A;
88 | k5      =   k5A;
89 | k_5     =   k_5A;
90 | k6      =   k6A;
91 | k_6     =   k_6A;
92 | k7      =   k7A;
93 | k_7     =   k_7A;
94 | k8      =   k8A;
95 | k_8     =   k_8A;
96 |
97 | %%%%%%%%%%%%%%%%%%%%%%%%%%%%%%%%%%%%%%%%%%%%%%%%%%%%%%%%%%%%%%%%%%%%%%%%%
98 | % CALCULATING THE REACTION RATES
99 | %%%%%%%%%%%%%%%%%%%%%%%%%%%%%%%%%%%%%%%%%%%%%%%%%%%%%%%%%%%%%%%%%%%%%%%%%
100 | Rx1=k1*(C(1)^ro1(1))*(C(2)^ro1(2));
101 | Rx2=k2*(C(1)^ro2(1))*(C(3)^ro2(3));
102 | Rx3=k3*(C(2)^ro3(2))*(C(5)^ro3(5)) - k_3*(C(7)^ro3(7));
103 | Rx4=k4*(C(1)^ro4(1))*(C(2)^ro4(2));
104 | Rx5=k5 *(C(2)^ro5(2))*(C(3)^ro5(3))*(C(4)^ro5(4))*(C(9)^ro5(9))...
105 | - k_5*(C(10)^ro5(10));
106 | Rx6=k6*(C(1)^ro6(1))*(C(9)^ro6(9)) - k_6*(C(12)^ro6(12));
107 | Rx7=k7*(C(2)^ro7(2))*(C(12)^ro7(12)) - k_7*(C(13)^ro7(13));
108 | Rx8=k8*(C(1)^ro8(1))*(C(2)^ro8(2)) - k_8*(C(14)^ro8(14));
109 |
110 | %%%%%%%%%%%%%%%%%%%%%%%%%%%%%%%%%%%%%%%%%%%%%%%%%%%%%%%%%%%%%%%%%%%%%%%%%
111 | % ASSIGNING THE REACTION STOICHIOMETRY FOR EACH COMPONENT
112 | %%%%%%%%%%%%%%%%%%%%%%%%%%%%%%%%%%%%%%%%%%%%%%%%%%%%%%%%%%%%%%%%%%%%%%%%%
113 | %A O2
114 | R(1)=-rs2(1)*Rx2 - rs4(1)*Rx4 - rs6(1)*Rx6 - rs8(1)*Rx8;

```

D MATLAB FILES

```

115 %B MEA
116 R(2)=-rs1(2)*Rx1 - rs3(2)*Rx3 - rs4(2)*Rx4 - rs5(2)*Rx5...
117 - rs7(2)*Rx7 - rs8(2)*Rx8;
118 %C Formaldehyde
119 R(3)=rs1(3)*Rx1 - rs2(3)*Rx2 - rs5(3)*Rx5;
120 %D NH3
121 R(4)= 2.4e-4*t^1.75;%rs1(4)*Rx1 + rs4(4)*Rx4 - rs5(4)*Rx5 ...
122 %+ rs8(4)*Rx8; % Locked/Unlocked ammonia profile
123 %E Formic acid
124 R(5)=rs2(5)*Rx2 - rs3(5)*Rx3;
125 %F H+
126 R(6)=rs1(6)*Rx1 + rs3(6)*Rx3 + rs4(6)*Rx4 + rs5(6)*Rx5 + rs8(6)*Rx8;
127 %G HEF
128 R(7)=rs3(7)*Rx3;
129 %H H2O
130 R(8)=-rs1(8)*Rx1 - rs3(8)*Rx3 + rs7(8)*Rx7 - rs8(8)*Rx8;
131 %I Glyoxal
132 R(9)=rs4(9)*Rx4 - rs5(9)*Rx5 - rs6(9)*Rx6;
133 %J HEI
134 R(10)=rs5(10)*Rx5;
135 %K Fe3+
136 R(11)=0;
137 %L Oxalic acid
138 R(12)=rs6(12)*Rx6 - rs7(12)*Rx7;
139 %M BHEOX
140 R(13)=rs7(13)*Rx7;
141 %N HEGly
142 R(14)=rs8(14)*Rx8;
143
144 %%%%%%%%%%%%%%%%%%%%%%%%%%%%%%%%%%%%%%%%%%%%%%%%%%%%%%%%%%%%%%%%%%%%%%%%%%
145 % CALCULATING THE TIME DERIVATIVES FOR LIQUID CONCENTRATION
146 %%%%%%%%%%%%%%%%%%%%%%%%%%%%%%%%%%%%%%%%%%%%%%%%%%%%%%%%%%%%%%%%%%%%%%%%%%
147 for i=1:N
148     t_der(i,1)=KG(i)*a*P*(((G1*y0(i) + KG(i)*a*VL*C(i)*H(i))/...
149 (G2 + KG(i)*a*VL*P)) - (C(i)*H(i)/P)) + R(i);
150 end

```

D.2.4 SFBRpicture.m

```

1 function h=SFBRpicture(t,C,y);
2 h=4;
3 l=4;
4 SFBRexperimental
5
6 figure(1)
7
8 subplot(h,l,1)
9 plot(t,y(:,1))
10 title('O2(g)')
11 xlabel('Time [Days]')
12 axis tight
13
14 subplot(h,l,2)
15 plot(t,C(:,1))
16 title('O2(aq)')
17 xlabel('Time [Days]')
18 ylabel('[kmol/m3]')

```

```
19 axis tight
20
21
22 subplot(h,1,3)
23 plot(t,y(:,4))
24 title('NH3(g)')
25 xlabel('Time [Days]')
26 axis tight
27
28 subplot(h,1,4)
29 plot(t,C(:,4),toexp,CoNH3exp2,'ro')
30 title('NH3(aq)')
31 xlabel('Time [Days]')
32 ylabel('[kmol/m3]')
33 axis tight
34
35
36 subplot(h,1,5)
37 plot(t,C(:,2),toexp,CoMEAexp,'ro')
38 title('MEA(aq)')
39 xlabel('Time [Days]')
40 ylabel('[kmol/m3]')
41 axis tight
42
43 subplot(h,1,6)
44 plot(t,C(:,3))
45 title('Formaldehyde(aq)')
46 xlabel('Time [Days]')
47 ylabel('[kmol/m3]')
48 axis tight
49
50
51 subplot(h,1,7)
52 plot(t,C(:,5),toFORMexp,CoFORMexp2,'ro')
53 title('Formic acid(aq)')
54 xlabel('Time [Days]')
55 ylabel('[kmol/m3]')
56 axis tight
57
58 subplot(h,1,8)
59 plot(t,C(:,7),toexp,CoHEFexp2,'ro')
60 title('HEF(aq)')
61 xlabel('Time [Days]')
62 ylabel('[kmol/m3]')
63 axis tight
64
65 subplot(h,1,9)
66 plot(t,C(:,9))
67 title('Glyoxal(aq)')
68 xlabel('Time [Days]')
69 ylabel('[kmol/m3]')
70 axis tight
71
72 subplot(h,1,10)
73 plot(t,C(:,10),toexp,CoHEIexp2,'ro')
74 title('HEI(aq)')
75 xlabel('Time [Days]')
76 ylabel('[kmol/m3]')
```

D MATLAB FILES

```
77 axis tight
78
79 subplot(h,1,11)
80 plot(t,C(:,12),21,2.806212295e-4,'ro')
81 title('Oxalic acid(aq)')
82 xlabel('Time [Days]')
83 ylabel('[kmol/m3]')
84 axis tight
85
86 subplot(h,1,12)
87 plot(t,C(:,13),toexp,CoBHEOXexp2,'ro')
88 title('BHEOX(aq)')
89 xlabel('Time [Days]')
90 ylabel('[kmol/m3]')
91 axis tight
92
93 subplot(h,1,13)
94 plot(t,C(:,14),toexp,CoHEGlyexp2,'ro')
95 title('HEGly(aq)')
96 xlabel('Time [Days]')
97 ylabel('[kmol/m3]')
98 axis tight
99
100 subplot(h,1,14)
101 plot(t,C(:,11))
102 title('Fe3+(aq)')
103 xlabel('Time [Days]')
104 ylabel('[kmol/m3]')
105 axis([0 21 -0.01 0.01])
106 set(gca,'DataAspectRatioMode','auto')
107 set(gca,'Plotboxaspectratiomode','auto')
```

D.2.5 batchrun.m

```
1 %%%%%%%%%%%%%%%%%%%%%%%%%%%%%%%%%%%%%%%%%%%%%%%%%%%%%%%%%%%%%%%%%%%%%%%%%
2 %
3 %           BATCH REACTOR
4 %       Well mixed gas batch, well mixed liquid batch
5 %
6 %           %-----%
7 %           % O O O %
8 %           % O O O O% LIQUID BATCH (VL)
9 %           % O o O % GAS BATCH (VG)
10 %           % o o o %
11 %           % o o o %
12 %           %%%%%%%%%%
13 %%%%%%%%%%%%%%%%%%%%%%%%%%%%%%%%%%%%%%%%%%%%%%%%%%%%%%%%%%%%%%%%%%%%%%%%%
14 function [t,C,y]=batchrun(RX_in,tc);
15
16 global KG a P VG VL H N T GASCONST tini
17
18 N=14;           %Total number of components
19 constant;
20 % reaction;
21
22 %%%%%%%%%%%%%%%%%%%%%%%%%%%%%%%%%%%%%%%%%%%%%%%%%%%%%%%%%%%%%%%%%%%%%%%%%
23 % EXPERIMENTAL PROPERTIES
```

```

24 %%%%%%%%%%%%%%%%%%%%%%%%%%%%%%%%%%%%%%%%%%%%%%%%%%%%%%%%%%%%%%%%%%%%%%%%%%
25 kL=1e1*ones(N,1);%Liquid mass transfer coefficient ...
26 % [kmol/m2-Days-bar]
27 kL(4)=3e-3; %Liquid mass transfer coefficient NH3 (found ...
28 %to fit experimental data)
29
30 a=250; %Mass transfer area per unit volume of ...
31 % continous phase [m2/m3]
32 P=1; %Total pressure [bar]
33 VG=4e-3; %Volume of gas phase [m3]
34 VL=7.6186e-4; %Volume of liquid phase [m3]
35 T=328; %Temperature [K]
36
37 [H]=henrys(MWO2,rhoL ,N,T,GASCONST2);
38
39 KG=kL./H'; %Over-all gas-phase mass transfer coefficient , vector
40
41 % NO MASS TRANSFER OF THE FOLLOWING COMPONENTS:
42 %(Either due to low concentrations or low volatility)
43 %(Values set zero, to avoid infinite values)
44 KG(5)=0; %Formic acid
45 KG(6)=0; %H3O+
46 KG(7)=0; %HEF
47 KG(9)=0; %Glyoxal
48 KG(10)=0;%HEI
49 KG(11)=0;%Fe2+/3+
50 KG(12)=0;%Oxalic acid
51 KG(13)=0;%BHEOX
52 KG(14)=0;%HEGly
53
54 %%%%%%%%%%%%%%%%%%%%%%%%%%%%%%%%%%%%%%%%%%%%%%%%%%%%%%%%%%%%%%%%%%%%%%%%%%
55 % INITIAL CONCENTRATIONS
56 %%%%%%%%%%%%%%%%%%%%%%%%%%%%%%%%%%%%%%%%%%%%%%%%%%%%%%%%%%%%%%%%%%%%%%%%%%
57 Psat=watvappres(T); %Calculating the saturation pressure of ..
58 %water vapor
59 %to determine the inital concentraion of gas
60 %phase water
61
62 %GAS MOLE FRACTIONS [-]
63 y0(1)=0.2; %Mol-fraction of component in gas phase...
64 % @ reactor inlet
65
66 y0(2)=0;
67 y0(3)=0;
68 y0(4)=0;
69 y0(5)=0;
70 y0(6)=0;
71 y0(7)=0;
72 y0(8)=(Psat/100000)/P;
73 y0(9)=0;
74 y0(10)=0;
75 y0(11)=0;
76 y0(12)=0;
77 y0(13)=0;
78 y0(14)=0;
79
80 %LIQUID CONCENTRATIONS [kmol/m3]
81 C0(1)=0.0001;
82 C0(2)=4;

```

D MATLAB FILES

```
82     C0(3)=0;
83     C0(4)=0;
84     C0(5)=0;
85     C0(6)=0;
86     C0(7)=164.6e-3/MWHEF;
87     C0(8)=51;
88     C0(9)=0;
89     C0(10)=20.18e-3/MWHEI;
90     C0(11)=484.27e-6/MWFe;
91     C0(12)=0;
92     C0(13)=0;
93     C0(14)=24.2e-3/MWHEGly;
94
95     C0=C0';
96     y0=y0';
97
98     X0=[C0;y0];
99
100     %%%%%%%%%%%%%%%%%%%%%%%%%%%%%%%%%%%%%%%%%%%%%%%%%%%%%%%%%%%%%%%%%%%%%%%%%%
101     % ODE SOLVER
102     %%%%%%%%%%%%%%%%%%%%%%%%%%%%%%%%%%%%%%%%%%%%%%%%%%%%%%%%%%%%%%%%%%%%%%%%%%
103     RTOL=1E-9;
104     ATOL=1E-9;
105
106     tini=tic; %Initilating ODE time limiter
107
108     [t,X]=ode15s(@batchmodel,tc,X0,odeset('RelTol',RTOL,'AbsTol',ATOL)...
109     ,RX_in);
110
111
112     C=X(:,1:N); %Storing modeling results in seperate matixes
113     y=X(:,N+1:2*N);
```

D.2.6 batchmodel.m

```
1 function t_der=batchmodel(t,X,RX_in)
2 global KG a P VG VL H N T GASCONST tini
3
4 %%%%%%%%%%%%%%%%%%%%%%%%%%%%%%%%%%%%%%%%%%%%%%%%%%%%%%%%%%%%%%%%%%%%%%%%%%
5 %ODE CALCULATION TIME LIMITER
6 %Used in combination with OBJF.m when iterating
7 %%%%%%%%%%%%%%%%%%%%%%%%%%%%%%%%%%%%%%%%%%%%%%%%%%%%%%%%%%%%%%%%%%%%%%%%%%
8 if toc(tini)>10
9     t_der=NaN;
10    return
11 end
12
13 % Assigning the vaiables
14 C=X(1:N,:);
15 y=X(N+1:2*N,:);
16
17 %Routine to prevent negative concentrations when
18 %searching for rate coefficients
19 for i=1:N
20     if C(i)<0
21         C(i)=0;
22     else
```



```

23     end
24 end
25
26 %%%%%%%%%%%%%%%%%%%%%%%%%%%%%%%%%%%%%%%%%%%%%%%%%%%%%%%%%%%%%%%%%%%%%%%%%
27 % ASSIGNING RATE COEFFICIENTS
28 %%%%%%%%%%%%%%%%%%%%%%%%%%%%%%%%%%%%%%%%%%%%%%%%%%%%%%%%%%%%%%%%%%%%%%%%%
29 O2LEAK=RX_in ( 1 );
30 k1A=RX_in ( 2 );
31 k2A=RX_in ( 3 );
32 k3A=RX_in ( 4 );
33 k_3A=RX_in ( 5 );
34 k4A=RX_in ( 6 );
35 k5A=RX_in ( 7 );
36 k_5A=RX_in ( 8 );
37 k6A=RX_in ( 9 );
38 k_6A=RX_in ( 10 );
39 k7A=RX_in ( 11 );
40 k_7A=RX_in ( 12 );
41 k8A=RX_in ( 13 );
42 k_8A=RX_in ( 14 );
43
44 q=14; %Number scalar values before the vectors
45      %(Not always equal to number of components)
46
47 ro1=RX_in (q+1:q+N);
48 ro2=RX_in (q+N+1:q+(2*N));
49 ro3=RX_in (q+(2*N)+1:q+(3*N));
50 ro4=RX_in (q+(3*N)+1:q+(4*N));
51 ro5=RX_in (q+(4*N)+1:q+(5*N));
52 ro6=RX_in (q+(5*N)+1:q+(6*N));
53 ro7=RX_in (q+(6*N)+1:q+(7*N));
54 ro8=RX_in (q+(7*N)+1:q+(8*N));
55
56 rs1=RX_in (q+(8*N)+1:q+(9*N));
57 rs2=RX_in (q+(9*N)+1:q+(10*N));
58 rs3=RX_in (q+(10*N)+1:q+(11*N));
59 rs4=RX_in (q+(11*N)+1:q+(12*N));
60 rs5=RX_in (q+(12*N)+1:q+(13*N));
61 rs6=RX_in (q+(13*N)+1:q+(14*N));
62 rs7=RX_in (q+(14*N)+1:q+(15*N));
63 rs8=RX_in (q+(15*N)+1:q+(16*N));
64
65 ro_3=RX_in (q+(16*N)+1);
66 ro_5=RX_in (q+(16*N)+2);
67 ro_6=RX_in (q+(16*N)+3);
68 ro_7=RX_in (q+(16*N)+4);
69 ro_8=RX_in (q+(16*N)+5);
70
71 k1B=RX_in (q+(16*N)+6);
72 k2B=RX_in (q+(16*N)+7);
73 k3B=RX_in (q+(16*N)+8);
74 k_3B=RX_in (q+(16*N)+9);
75 k4B=RX_in (q+(16*N)+10);
76 k5B=RX_in (q+(16*N)+11);
77 k_5B=RX_in (q+(16*N)+12);
78 k6B=RX_in (q+(16*N)+13);
79 k_6B=RX_in (q+(16*N)+14);
80 k7B=RX_in (q+(16*N)+15);

```

D MATLAB FILES

```

81 k_7B=RX_in(q+(16*N)+16);
82 k8B=RX_in(q+(16*N)+17);
83 k_8B=RX_in(q+(16*N)+18);
84
85 %%%%%%%%%%%%%%%%%%%%%%%%%%%%%%%%%%%%%%%%%%%%%%%%%%%%%%%%%%%%%%%%%%%%%%%%%%%
86 % DETERMINING HENRYS LAW COEFFICIENT FOR WATER
87 %%%%%%%%%%%%%%%%%%%%%%%%%%%%%%%%%%%%%%%%%%%%%%%%%%%%%%%%%%%%%%%%%%%%%%%%%%%
88 Psat=watvappres(T);
89 H(8)=(Psat/100000)/C(8); %Henrys constant water vapor
90
91 %%%%%%%%%%%%%%%%%%%%%%%%%%%%%%%%%%%%%%%%%%%%%%%%%%%%%%%%%%%%%%%%%%%%%%%%%%%
92 % CALCULATING THE RATE COEFFICIENTS
93 % Dependant on Fe-concentration
94 %%%%%%%%%%%%%%%%%%%%%%%%%%%%%%%%%%%%%%%%%%%%%%%%%%%%%%%%%%%%%%%%%%%%%%%%%%%
95 k1      = k1A  + k1B*(abs(C(11))^ro1(11));
96 k2      = k2A  + k2B*(abs(C(11))^ro2(11));
97 k3      = k3A  + k3B*(abs(C(11))^ro3(11));
98 k_3     = k_3A + k_3B*(abs(C(11))^ro_3);
99 k4      = k4A  + k4B*(abs(C(11))^ro4(11));
100 k5      = k5A  + k5B*(abs(C(11))^ro5(11));
101 k_5     = k_5A + k_5B*(abs(C(11))^ro_5);
102 k6      = k6A  + k6B*(abs(C(11))^ro6(11));
103 k_6     = k_6A + k_6B*(abs(C(11))^ro_6);
104 k7      = k7A  + k7B*(abs(C(11))^ro7(11));
105 k_7     = k_7A + k_7B*(abs(C(11))^ro_7);
106 k8      = k8A  + k8B*(abs(C(11))^ro8(11));
107 k_8     = k_8A + k_8B*(abs(C(11))^ro_8);
108
109
110 %%%%%%%%%%%%%%%%%%%%%%%%%%%%%%%%%%%%%%%%%%%%%%%%%%%%%%%%%%%%%%%%%%%%%%%%%%%
111 % CALCULATING THE REACTION RATES
112 %%%%%%%%%%%%%%%%%%%%%%%%%%%%%%%%%%%%%%%%%%%%%%%%%%%%%%%%%%%%%%%%%%%%%%%%%%%
113 Rx1=k1*(C(1)^ro1(1))*(C(2)^ro1(2));
114 Rx2=k2*(C(1)^ro2(1))*(C(3)^ro2(3));
115 Rx3=k3*(C(2)^ro3(2))*(C(5)^ro3(5)) - k_3*(C(7)^ro3(7));%*(C(8)^ro3(8))
116 Rx4=k4*(C(1)^ro4(1))*(C(2)^ro4(2));
117 Rx5=k5*(C(2)^ro5(2))*(C(3)^ro5(3))*(C(4)^ro5(4))*(C(9)^ro5(9))...
118 - k_5*(C(10)^ro5(10));
119 Rx6=k6*(C(1)^ro6(1))*(C(9)^ro6(9)) - k_6*(C(12)^ro6(12));
120 Rx7=k7*(C(2)^ro7(2))*(C(12)^ro7(12)) - k_7*(C(13)^ro7(13));
121 Rx8=k8*(C(1)^ro8(1))*(C(2)^ro8(2)) - k_8*(C(14)^ro8(14));
122
123 %%%%%%%%%%%%%%%%%%%%%%%%%%%%%%%%%%%%%%%%%%%%%%%%%%%%%%%%%%%%%%%%%%%%%%%%%%%
124 % ASSIGNING THE REACTION STOICHIOMETRY FOR EACH COMPONENT
125 %%%%%%%%%%%%%%%%%%%%%%%%%%%%%%%%%%%%%%%%%%%%%%%%%%%%%%%%%%%%%%%%%%%%%%%%%%%
126 %A O2
127 R(1)=-rs2(1)*Rx2 - rs4(1)*Rx4 - rs6(1)*Rx6 - rs8(1)*Rx8;
128 %B MEA
129 R(2)=-rs1(2)*Rx1 - rs3(2)*Rx3 - rs4(2)*Rx4 - rs5(2)*Rx5...
130 - rs7(2)*Rx7 - rs8(2)*Rx8;
131 %C Formaldehyde
132 R(3)=rs1(3)*Rx1 - rs2(3)*Rx2 - rs5(3)*Rx5;
133 %D NH3
134 R(4)=4.80e-4*t^1.5;% rs1(4)*Rx1 + rs4(4)*Rx4 - rs5(4)*Rx5 ...
135 %+ rs8(4)*Rx8; %Locked/Unlocked Ammonia Profile
136 %E Formic acid
137 R(5)=rs2(5)*Rx2 - rs3(5)*Rx3;
138 %F H+

```

```

139 R(6)=rs1(6)*Rx1 + rs3(6)*Rx3 + rs4(6)*Rx4 + rs5(6)*Rx5 + rs8(6)*Rx8 ;
140 %G HEF
141 R(7)=rs3(7)*Rx3;
142 %H H2O
143 R(8)=-rs1(8)*Rx1 - rs3(8)*Rx3 + rs7(8)*Rx7 - rs8(8)*Rx8;
144 %I Glyoxal
145 R(9)=rs4(9)*Rx4 - rs5(9)*Rx5 - rs6(9)*Rx6;
146 %J HEI
147 R(10)=rs5(10)*Rx5;
148 %K Fe3+
149 R(11)=1.8e-6;
150 %L Oxalic acid
151 R(12)=rs6(12)*Rx6 - rs7(12)*Rx7;
152 %M BHEOX
153 R(13)=rs7(13)*Rx7;
154 %N HEGly
155 R(14)=rs8(14)*Rx8;
156
157 %%%%%%%%%%%%%%%%%%%%%%%%%%%%%%%%%%%%%%%%%%%%%%%%%%%%%%%%%%%%%%%%%%%%%%%%%
158 % CALCULATING THE TIME DERIVATIVES FOR LIQUID CONCENTRATION
159 %%%%%%%%%%%%%%%%%%%%%%%%%%%%%%%%%%%%%%%%%%%%%%%%%%%%%%%%%%%%%%%%%%%%%%%%%
160 dC_dt(1)=KG(1)*a*P*(y(1)-(C(1)*H(1)/P)) + R(1);
161
162 for i=2:N
163     dC_dt(i)=KG(i)*a*P*(y(i)-(C(i)*H(i)/P)) + R(i);
164 end
165 %%%%%%%%%%%%%%%%%%%%%%%%%%%%%%%%%%%%%%%%%%%%%%%%%%%%%%%%%%%%%%%%%%%%%%%%%
166 % CALCULATING THE TIME DERIVATIVES FOR GAS MOLE FRACTION
167 %%%%%%%%%%%%%%%%%%%%%%%%%%%%%%%%%%%%%%%%%%%%%%%%%%%%%%%%%%%%%%%%%%%%%%%%%
168 dy_dt(1)=- (KG(1)*a*GASCONST*T*(VL/VG)*(y(1) - (C(1)*H(1)/P)))+O2LEAK;
169 for i=2:N
170     dy_dt(i)=- (KG(i)*a*GASCONST*T*(VL/VG)*(y(i) - (C(i)*H(i)/P)));
171 end
172
173 %Gathering the time derivatives in one vector
174 t_der=[dC_dt'; dy_dt'];

```

D.2.7 batchpicture.m

```

1 function h=batchpicture(t,C,y)
2 h=4;
3 l=4;
4
5 BATCHexperimental
6
7 figure(2)
8
9 subplot(h,l,1)
10 plot(t,y(:,1),tcexp,ycO2exp,'ro')
11 title('O2(g)')
12 xlabel('Time [Days]')
13 axis tight
14
15 subplot(h,l,2)
16 plot(t,C(:,1))
17 title('O2(aq)')
18 xlabel('Time [Days]')

```

D MATLAB FILES

```
19 ylabel(' [kmol/m3] ')
20 axis tight
21
22 subplot(h,1,3)
23 plot(t,y(:,4))
24 title('NH3(g)')
25 xlabel('Time [Days]')
26 axis tight
27
28 subplot(h,1,4)
29 plot(t,C(:,4),21,6495e-3/MWNH3,'ro')
30 title('NH3(aq)')
31 xlabel('Time [Days]')
32 ylabel(' [kmol/m3] ')
33 axis tight
34
35 subplot(h,1,5)
36 plot(t,C(:,2),tcexp,CcMEAexp,'ro')
37 title('MEA(aq)')
38 xlabel('Time [Days]')
39 ylabel(' [kmol/m3] ')
40 axis tight
41
42 subplot(h,1,6)
43 plot(t,C(:,3))
44 title('Formaldehyde(aq)')
45 xlabel('Time [Days]')
46 ylabel(' [kmol/m3] ')
47 axis tight
48
49 subplot(h,1,7)
50 plot(t,C(:,5),tcexp,CcFORMexp2,'ro')
51 title('Formic acid(aq)')
52 xlabel('Time [Days]')
53 ylabel(' [kmol/m3] ')
54 axis tight
55
56 subplot(h,1,8)
57 plot(t,C(:,7),tcexp,CcHEFexp2,'ro')
58 title('HEF(aq)')
59 xlabel('Time [Days]')
60 ylabel(' [kmol/m3] ')
61 axis tight
62
63 subplot(h,1,9)
64 plot(t,C(:,9))
65 title(' Glyoxal(aq) ')
66 xlabel('Time [Days]')
67 ylabel(' [kmol/m3] ')
68 axis tight
69
70 subplot(h,1,10)
71 plot(t,C(:,10),tcexp,CcHEIexp2,'ro')
72 title('HEI(aq)')
73 xlabel('Time [Days]')
74 ylabel(' [kmol/m3] ')
75 axis tight
76
```

```

77 subplot(h,1,11)
78 plot(t,C(:,12),21,9.088946705e-4,'ro')
79 title('Oxalic acid(aq)')
80 xlabel('Time [Days]')
81 ylabel('[kmol/m3]')
82 axis tight
83
84 subplot(h,1,12)
85 plot(t,C(:,13),tcexp,CcBHEOXexp2,'ro')
86 title('BHEOX(aq)')
87 xlabel('Time [Days]')
88 ylabel('[kmol/m3]')
89 axis tight
90
91 subplot(h,1,13)
92 plot(t,C(:,14),tcexp,CcHEGlyexp2,'ro')
93 title('HEGly(aq)')
94 xlabel('Time [Days]')
95 ylabel('[kmol/m3]')
96 axis tight
97
98 subplot(h,1,14)
99 plot(t,C(:,11),tcexp,CcFeexp2,'ro')
100 title('Fe3+(aq)')
101 xlabel('Time [Days]')
102 ylabel('[kmol/m3]')
103 axis tight

```

D.2.8 MetalSFBRrun.m

```

1 %%%%%%%%%%%%%%%%%%%%%%%%%%%%%%%%%%%%%%%%%%%%%%%%%%%%%%%%%%%%%%%%%%%%%%%%%
2 %
3 %           SEMI-FLOW BATCH REACTOR /W METAL CATALYST
4 %           Well-mixed  gas-well-mixed batch liquid
5 %
6 %           |
7 %           // \
8 %           |   GAS EXIT (G2)
9 %
10 %           |
11 %           %-----%
12 %           % O O O %
13 %           % O O O O% LIQUID BATCH (VL)
14 %           % o o o %
15 %           %   o   o %
16 %           %~~~~~%
17 %           |
18 %           // \
19 %           |   GAS FEED (G1)
20 %%%%%%%%%%%%%%%%%%%%%%%%%%%%%%%%%%%%%%%%%%%%%%%%%%%%%%%%%%%%%%%%%%%%%%%%%
21 function [t,C,y]=MetalSFBRrun(RX_in,tm)
22
23 global KG a P VG VL H y0 N T GASCONST G1 G2
24
25 N=14;           %Total number of components
26 constant;
27 reaction;

```

D MATLAB FILES

```

28
29 %%%%%%%%%%%%%%%%%%%%%%%%%%%%%%%%%%%%%%%%%%%%%%%%%%%%%%%%%%%%%%%%%%%%%%%%%
30 %NON-REACTION SPECIFIC CONSTANTS
31 %%%%%%%%%%%%%%%%%%%%%%%%%%%%%%%%%%%%%%%%%%%%%%%%%%%%%%%%%%%%%%%%%%%%%%%%%
32 %%%%%%%%%%%%%%%%%%%%%%%%%%%%%%%%%%%%%%%%%%%%%%%%%%%%%%%%%%%%%%%%%%%%%%%%%
33 kL=1e1*ones(N,1);%Liquid mass transfer coefficient ...
34                    %[kmol/m2-Days-bar]
35 kL(4)=3e-3;        %Liquid mass transfer coefficient NH3...
36                    % (found to fit experimental data)
37
38 a=200;             %Mass transfer area per unit volume of continous...
39                    % phase [m2/m3]
40 P=1.02;           %Total pressure [bar]
41 VL=1.082e-3;     %Volume of liquid phase [m3]
42 T=273.15+55;
43
44 Vf=350;           % Liquid flow rate [ml/min]
45 nf=(P*1e5*Vf*1e-6)/(GASCONST2*T); % Molar flow rate [mol/min]
46 Gf=nf*1440/1000; %Gas flow rate [kmol/Days]
47 G1=Gf;           %Molar gas flow rate [kmol/Days] @ reactor inlet
48 G2=Gf;           %Molar gas flow rate [kmol/Days] @ reactor outlet
49
50 [H]=henrys(MW02,rhoL ,N,T,GASCONST2);
51
52 KG=kL./H'; %Over-all gas-phase mass transfer coefficient , vector
53
54 % NO MASS TRANSFER OF THE FOLLOWING COMPONENTS:
55 %(Either due to low concentrations or low volatility)
56 %(Values set zero , to avoid infinite values)
57 KG(5)=0; %Formic acid
58 KG(6)=0; %H3O+
59 KG(7)=0; %HEF
60 KG(9)=0; %Glyoxal
61 KG(10)=0;%HEI
62 KG(11)=0;%Fe2+/3+
63 KG(12)=0;%Oxalic acid
64 KG(13)=0;%BHEOX
65 KG(14)=0;%HEGly
66
67 %%%%%%%%%%%%%%%%%%%%%%%%%%%%%%%%%%%%%%%%%%%%%%%%%%%%%%%%%%%%%%%%%%%%%%%%%
68 % INITIAL CONCENTRATIONS
69 %%%%%%%%%%%%%%%%%%%%%%%%%%%%%%%%%%%%%%%%%%%%%%%%%%%%%%%%%%%%%%%%%%%%%%%%%
70 Psat=watvappres(T); %Calculating the saturation pressure of
71                    %water vapor to determine the initial
72                    %concentraion of gas phase water
73
74 %GAS MOLE FRACTIONS [-]
75 y0(1)=0.2055944;   %Mol-fraction of component in gas phase...
76                    % @ reactor inlet
77
78 y0(2)=0;
79 y0(3)=0;
80 y0(4)=0;
81 y0(5)=0;
82 y0(6)=0;
83 y0(7)=0;
84 y0(8)=(Psat/100000)/P; %Gas is saturated with water
85 y0(9)=0;
86 y0(10)=0;

```

```

86     y0(11)=0;
87     y0(12)=0;
88     y0(13)=0;
89     y0(14)=0;
90
91     %LIQUID CONCENTRATIONS [kmol/m3]
92     C0(1)=0;
93     C0(2)=5.25;
94     C0(3)=0;
95     C0(4)=0;
96     C0(5)=0;
97     C0(6)=0;
98     C0(7)=0;
99     C0(8)=51;
100    C0(9)=0;
101    C0(10)=0;
102    C0(11)=1.2e-5;
103    C0(12)=0;
104    C0(13)=0;
105    C0(14)=0;
106
107    C0=C0';
108
109    %%%%%%%%%%%%%%%%%%%%%%%%%%%%%%%%%%%%%%%%%%%%%%%%%%%%%%%%%%%%%%%%%%%%%%%%%%%
110    % ODE SOLVER
111    %%%%%%%%%%%%%%%%%%%%%%%%%%%%%%%%%%%%%%%%%%%%%%%%%%%%%%%%%%%%%%%%%%%%%%%%%%%
112    RTOL=1E-2;
113    ATOL=1E-2;
114
115    [t ,C]=ode15s (@MetalSFBRmodel ,tm ,C0 ,odeset ('RelTol' ,RTOL , 'AbsTol' ...
116    ,ATOL) ,RX_in);
117
118    %GAS PHASE EQUATION (Not time dependent)
119    for i=1:N
120        y(:,i)=((G1*y0(i) + KG(i)*a*VL.*C(:,i)*H(i))./(G2 + KG(i)*a*VL*P));
121    end

```

D.2.9 MetalSFBRmodel.m

```

1  function t_der=MetalSFBRmodel(t,C,RX_in)
2  global KG a P VG VL H y0 N T GASCONST G1 G2 tini
3
4  %Routine to prevent negative concentrations when
5  %searching for rate coefficients
6  for i=1:N
7      if C(i)<0
8          C(i)=0;
9      end
10 end
11
12 %%%%%%%%%%%%%%%%%%%%%%%%%%%%%%%%%%%%%%%%%%%%%%%%%%%%%%%%%%%%%%%%%%%%%%%%%%%
13 % ASSIGNING RATE COEFFICIENTS
14 %%%%%%%%%%%%%%%%%%%%%%%%%%%%%%%%%%%%%%%%%%%%%%%%%%%%%%%%%%%%%%%%%%%%%%%%%%%
15 O2LEAK=RX_in(1);
16 k1A=RX_in(2);
17 k2A=RX_in(3);
18 k3A=RX_in(4);

```

D MATLAB FILES

```

19 k_3A=RX_in(5);
20 k4A=RX_in(6);
21 k5A=RX_in(7);
22 k_5A=RX_in(8);
23 k6A=RX_in(9);
24 k_6A=RX_in(10);
25 k7A=RX_in(11);
26 k_7A=RX_in(12);
27 k8A=RX_in(13);
28 k_8A=RX_in(14);
29
30 q=14; %Number scalar values before the vectors
31      %(Not always equal to number of components)
32
33 ro1=RX_in(q+1:q+N);
34 ro2=RX_in(q+N+1:q+(2*N));
35 ro3=RX_in(q+(2*N)+1:q+(3*N));
36 ro4=RX_in(q+(3*N)+1:q+(4*N));
37 ro5=RX_in(q+(4*N)+1:q+(5*N));
38 ro6=RX_in(q+(5*N)+1:q+(6*N));
39 ro7=RX_in(q+(6*N)+1:q+(7*N));
40 ro8=RX_in(q+(7*N)+1:q+(8*N));
41
42 rs1=RX_in(q+(8*N)+1:q+(9*N));
43 rs2=RX_in(q+(9*N)+1:q+(10*N));
44 rs3=RX_in(q+(10*N)+1:q+(11*N));
45 rs4=RX_in(q+(11*N)+1:q+(12*N));
46 rs5=RX_in(q+(12*N)+1:q+(13*N));
47 rs6=RX_in(q+(13*N)+1:q+(14*N));
48 rs7=RX_in(q+(14*N)+1:q+(15*N));
49 rs8=RX_in(q+(15*N)+1:q+(16*N));
50
51 ro_3=RX_in(q+(16*N)+1);
52 ro_5=RX_in(q+(16*N)+2);
53 ro_6=RX_in(q+(16*N)+3);
54 ro_7=RX_in(q+(16*N)+4);
55 ro_8=RX_in(q+(16*N)+5);
56
57 k1B=RX_in(q+(16*N)+6);
58 k2B=RX_in(q+(16*N)+7);
59 k3B=RX_in(q+(16*N)+8);
60 k_3B=RX_in(q+(16*N)+9);
61 k4B=RX_in(q+(16*N)+10);
62 k5B=RX_in(q+(16*N)+11);
63 k_5B=RX_in(q+(16*N)+12);
64 k6B=RX_in(q+(16*N)+13);
65 k_6B=RX_in(q+(16*N)+14);
66 k7B=RX_in(q+(16*N)+15);
67 k_7B=RX_in(q+(16*N)+16);
68 k8B=RX_in(q+(16*N)+17);
69 k_8B=RX_in(q+(16*N)+18);
70
71 %%%%%%%%%%%%%%%%%%%%%%%%%%%%%%%%%%%%%%%%%%%%%%%%%%%%%%%%%%%%%%%%%%%%%%%%%
72 % DETERMINING HENRYS LAW COEFFICIENT FOR WATER
73 %%%%%%%%%%%%%%%%%%%%%%%%%%%%%%%%%%%%%%%%%%%%%%%%%%%%%%%%%%%%%%%%%%%%%%%%%
74 Psat=watvappres(T);
75 H(8)=(Psat/100000)/C(8); %Henrys constant water vapor
76

```



```

77 %%%%%%%%%%%%%%%%%%%%%%%%%%%%%%%%%%%%%%%%%%%%%%%%%%%%%%%%%%%%%%%%%%%%%%%%%
78 % CALCULATING THE RATE COEFFICIENTS
79 % Dependant on Fe-concentration
80 %%%%%%%%%%%%%%%%%%%%%%%%%%%%%%%%%%%%%%%%%%%%%%%%%%%%%%%%%%%%%%%%%%%%%%%%%
81 k1      = k1A      + k1B*(abs(C(11))^ro1(11));
82 k2      = k2A      + k2B*(abs(C(11))^ro2(11));
83 k3      = k3A      + k3B*(abs(C(11))^ro3(11));
84 k_3     = k_3A     + k_3B*(abs(C(11))^ro_3);
85 k4      = k4A      + k4B*(abs(C(11))^ro4(11));
86 k5      = k5A      + k5B*(abs(C(11))^ro5(11));
87 k_5     = k_5A     + k_5B*(abs(C(11))^ro_5);
88 k6      = k6A      + k6B*(abs(C(11))^ro6(11));
89 k_6     = k_6A     + k_6B*(abs(C(11))^ro_6);
90 k7      = k7A      + k7B*(abs(C(11))^ro7(11));
91 k_7     = k_7A     + k_7B*(abs(C(11))^ro_7);
92 k8      = k8A      + k8B*(abs(C(11))^ro8(11));
93 k_8     = k_8A     + k_8B*(abs(C(11))^ro_8);
94
95 %%%%%%%%%%%%%%%%%%%%%%%%%%%%%%%%%%%%%%%%%%%%%%%%%%%%%%%%%%%%%%%%%%%%%%%%%
96 % CALCULATING THE REACTION RATES
97 %%%%%%%%%%%%%%%%%%%%%%%%%%%%%%%%%%%%%%%%%%%%%%%%%%%%%%%%%%%%%%%%%%%%%%%%%
98 Rx1=k1*(C(1)^ro1(1))*(C(2)^ro1(2));
99 Rx2=k2*(C(1)^ro2(1))*(C(3)^ro2(3));
100 Rx3=k3*(C(2)^ro3(2))*(C(5)^ro3(5)) - k_3*(C(7)^ro3(7));
101 Rx4=k4*(C(1)^ro4(1))*(C(2)^ro4(2));
102 Rx5=k5*(C(2)^ro5(2))*(C(3)^ro5(3))*(C(4)^ro5(4))*(C(9)^ro5(9))...
103 - k_5*(C(10)^ro5(10));
104 Rx6=k6*(C(1)^ro6(1))*(C(9)^ro6(9)) - k_6*(C(12)^ro6(12));
105 Rx7=k7*(C(2)^ro7(2))*(C(12)^ro7(12)) - k_7*(C(13)^ro7(13));
106 Rx8=k8*(C(1)^ro8(1))*(C(2)^ro8(2)) - k_8*(C(14)^ro8(14));
107
108 %%%%%%%%%%%%%%%%%%%%%%%%%%%%%%%%%%%%%%%%%%%%%%%%%%%%%%%%%%%%%%%%%%%%%%%%%
109 % ASSIGNING THE REACTION STOICHIOMETRY FOR EACH COMPONENT
110 %%%%%%%%%%%%%%%%%%%%%%%%%%%%%%%%%%%%%%%%%%%%%%%%%%%%%%%%%%%%%%%%%%%%%%%%%
111 %A O2
112 R(1)=-rs2(1)*Rx2 - rs4(1)*Rx4 - rs6(1)*Rx6 - rs8(1)*Rx8;
113 %B MEA
114 R(2)=-rs1(2)*Rx1 - rs3(2)*Rx3 - rs4(2)*Rx4 - rs5(2)*Rx5...
115 - rs7(2)*Rx7 - rs8(2)*Rx8;
116 %C Formaldehyde
117 R(3)=rs1(3)*Rx1 - rs2(3)*Rx2 - rs5(3)*Rx5;
118 %D NH3
119 R(4)=rs1(4)*Rx1 + rs4(4)*Rx4 - rs5(4)*Rx5 + rs8(4)*Rx8;
120 %E Formic acid
121 R(5)=rs2(5)*Rx2 - rs3(5)*Rx3;
122 %F H+
123 R(6)=rs1(6)*Rx1 + rs3(6)*Rx3 + rs4(6)*Rx4 + rs5(6)*Rx5 + rs8(6)*Rx8;
124 %G HEF
125 R(7)=rs3(7)*Rx3;
126 %H H2O
127 R(8)=-rs1(8)*Rx1 - rs3(8)*Rx3 + rs7(8)*Rx7 - rs8(8)*Rx8;
128 %I Glyoxal
129 R(9)=rs4(9)*Rx4 - rs5(9)*Rx5 - rs6(9)*Rx6;
130 %J HEI
131 R(10)=rs5(10)*Rx5;
132 %K Fe2+/3+
133 R(11)=0;
134 %L Oxalic acid

```

D MATLAB FILES

```
135 R(12)=rs6(12)*Rx6 - rs7(12)*Rx7;
136 %M BHEOX
137 R(13)=rs7(13)*Rx7;
138 %N HEGly
139 R(14)=rs8(14)*Rx8;
140
141
142 %%%%%%%%%%%%%%%%%%%%%%%%%%%%%%%%%%%%%%%%%%%%%%%%%%%%%%%%%%%%%%%%%%%%%%%%%%%
143 % CALCULATING THE TIME DERIVATIVES FOR LIQUID CONCENTRATION
144 %%%%%%%%%%%%%%%%%%%%%%%%%%%%%%%%%%%%%%%%%%%%%%%%%%%%%%%%%%%%%%%%%%%%%%%%%%%
145 for i=1:N
146     t_der(i,1)=KG(i)*a*P*(((G1*y0(i) + KG(i)*a*VL*C(i)*H(i))/...
147 (G2 + KG(i)*a*VL*P)) - (C(i)*H(i)/P)) + R(i);
148 end
149
150 %IRON LEVEL IS CONSTANT
151 t_der(11,1)=0;
```

D.2.10 MetalSFBRpicture.m

```
1 function h=MetalSFBRpicture(t,C,y);
2 h=4;
3 l=4;
4 Metalexperimental
5
6 figure(3)
7 subplot(h,l,1)
8 plot(t,y(:,1))
9 title('O2(g)')
10 xlabel('Time [Days]')
11 axis tight
12
13 subplot(h,l,2)
14 plot(t,C(:,1))
15 title('O2(aq)')
16 xlabel('Time [Days]')
17 ylabel('[kmol/m3]')
18 axis tight
19
20 subplot(h,l,3)
21 plot(t,y(:,4))
22 title('NH3(g)')
23 xlabel('Time [Days]')
24 axis tight
25
26 subplot(h,l,4)
27 plot(t,C(:,4))
28 title('NH3(aq)')
29 xlabel('Time [Days]')
30 ylabel('[kmol/m3]')
31 axis tight
32
33 subplot(h,l,5)
34 plot(t,C(:,2),tmexp,CmMEAexp,'ro')
35 title('MEA(aq)')
36 xlabel('Time [Days]')
37 ylabel('[kmol/m3]')
```

```
38 axis tight
39
40 subplot(h,1,6)
41 plot(t,C(:,3))
42 title('Formaldehyde(aq)')
43 xlabel('Time [Days]')
44 ylabel('[kmol/m3]')
45 axis tight
46
47 subplot(h,1,7)
48 plot(t,C(:,5))
49 title('Formic acid(aq)')
50 xlabel('Time [Days]')
51 ylabel('[kmol/m3]')
52 axis tight
53
54 subplot(h,1,8)
55 plot(t,C(:,7),tmexp,CmHEFexp2,'ro')
56 title('HEF(aq)')
57 xlabel('Time [Days]')
58 ylabel('[kmol/m3]')
59 axis tight
60
61 subplot(h,1,9)
62 plot(t,C(:,9))
63 title('Glyoxal(aq)')
64 xlabel('Time [Days]')
65 ylabel('[kmol/m3]')
66 axis tight
67
68 subplot(h,1,10)
69 plot(t,C(:,10),tmexp,CmHEIexp2,'ro')
70 title('HEI(aq)')
71 xlabel('Time [Days]')
72 ylabel('[kmol/m3]')
73 axis tight
74
75 subplot(h,1,11)
76 plot(t,C(:,12))
77 title('Oxalic acid.(aq)')
78 xlabel('Time [Days]')
79 ylabel('[kmol/m3]')
80 axis tight
81
82 subplot(h,1,12)
83 plot(t,C(:,13))
84 title('BHEOX(aq)')
85 xlabel('Time [Days]')
86 ylabel('[kmol/m3]')
87 axis tight
88
89 subplot(h,1,13)
90 plot(t,C(:,14))
91 title('HEGly(aq)')
92 xlabel('Time [Days]')
93 ylabel('[kmol/m3]')
94 axis tight
95
```

D MATLAB FILES

```
96 subplot(h,1,14)
97 plot(t,C(:,11),0,1e-3,'ro')
98 title('Fe3+(aq)')
99 xlabel('Time [Days]')
100 ylabel('[kmol/m3]')
101 axis([0 25 1e-6 1.1e-3])
```

D.2.11 reaction.m

```
1 %%%%%%%%%%%%%%%%%%%%%%%%%%%%%%%%%%%%%%%%%%%%%%%%%%%%%%%%%%%%%%%%%%%%%%%%%%
2 %
3 %           REACTION STOICHIOMETRY
4 %
5 %%%%%%%%%%%%%%%%%%%%%%%%%%%%%%%%%%%%%%%%%%%%%%%%%%%%%%%%%%%%%%%%%%%%%%%%%%
6 ro1=zeros(1,N);
7 ro2=zeros(1,N);
8 ro3=zeros(1,N);
9 ro4=zeros(1,N);
10 ro5=zeros(1,N);
11 ro6=zeros(1,N);
12 ro7=zeros(1,N);
13 ro8=zeros(1,N);
14
15 rs1=zeros(1,N);
16 rs2=zeros(1,N);
17 rs3=zeros(1,N);
18 rs4=zeros(1,N);
19 rs5=zeros(1,N);
20 rs6=zeros(1,N);
21 rs7=zeros(1,N);
22 rs8=zeros(1,N);
23
24 %REACTION 1
25 %%%%%%%%%%%%%%%%%%%%%%%%%%%%%%%%%%%%%%%%%%%%%%%%%%%%%%%%%%%%%%%%%%%%%%%%%%
26 %
27 %   MEA(aq) + 3 H2O(1) = 2 CH2O(aq) + NH3(aq) + 2 H+ (aq)
28 %
29 %%%%%%%%%%%%%%%%%%%%%%%%%%%%%%%%%%%%%%%%%%%%%%%%%%%%%%%%%%%%%%%%%%%%%%%%%%
30
31 %Stoichiometrics
32 rs1(1) = 0;
33 rs1(2) = 1;
34 rs1(3) = 2;
35 rs1(4) = 1;
36 rs1(6) = 2;
37 rs1(8) = 3;
38
39 %REACTION 2
40 %%%%%%%%%%%%%%%%%%%%%%%%%%%%%%%%%%%%%%%%%%%%%%%%%%%%%%%%%%%%%%%%%%%%%%%%%%
41 %
42 %   CH2O(aq) + 0.5 O2(aq) = CHOOH (aq)
43 %
44 %%%%%%%%%%%%%%%%%%%%%%%%%%%%%%%%%%%%%%%%%%%%%%%%%%%%%%%%%%%%%%%%%%%%%%%%%%
45
46 %Stoichiometrics
47 rs2(1) = 0.5;
48 rs2(3) = 1;
```

```

49 rs2 (5)      =    1;
50
51 %REACTION 3
52 %%%%%%%%%%%%%%%%%%%%%%%%%%%%%%%%%%%%%%%%%%%%%%%%%%%%%%%%%%%%%%%%%%%%%%%%%%
53 %
54 %   CHOOH(aq) + MEA(aq) + 2 H2O(1) = HEF(aq) + 2 H3O+(aq)
55 %
56 %%%%%%%%%%%%%%%%%%%%%%%%%%%%%%%%%%%%%%%%%%%%%%%%%%%%%%%%%%%%%%%%%%%%%%%%%%
57
58 %Stoichiometrics
59 rs3 (5)      =    1;
60 rs3 (2)      =    1;
61 rs3 (7)      =    1;
62 rs3 (6)      =    2;
63 rs3 (8)      =    2;
64
65 %REACTION 4
66 %%%%%%%%%%%%%%%%%%%%%%%%%%%%%%%%%%%%%%%%%%%%%%%%%%%%%%%%%%%%%%%%%%%%%%%%%%
67 %
68 %   O2(aq) + MEA(aq)   = Glyoxal(aq) + H2O(1) + NH3(aq)
69 %
70 %%%%%%%%%%%%%%%%%%%%%%%%%%%%%%%%%%%%%%%%%%%%%%%%%%%%%%%%%%%%%%%%%%%%%%%%%%
71
72 %Stoichiometrics
73 rs4 (1)      =    1;
74 rs4 (2)      =    1;
75 rs4 (4)      =    1;
76 rs4 (8)      =    1;
77 rs4 (9)      =    1;
78
79 %REACTION 5
80 %%%%%%%%%%%%%%%%%%%%%%%%%%%%%%%%%%%%%%%%%%%%%%%%%%%%%%%%%%%%%%%%%%%%%%%%%%
81 %
82 % MEA(aq) + CH2O(aq) + NH3(aq) + Glyoxal(aq)  -> HEI(aq) + 3 H2O (1)
83 %
84 %%%%%%%%%%%%%%%%%%%%%%%%%%%%%%%%%%%%%%%%%%%%%%%%%%%%%%%%%%%%%%%%%%%%%%%%%%
85
86 %Stoichiometrics
87 rs5 (2)      =    1;
88 rs5 (3)      =    1;
89 rs5 (4)      =    1;
90 rs5 (8)      =    3; %H2O
91 rs5 (9)      =    1;
92 rs5 (10)     =    1;
93
94 %REACTION 6
95 %%%%%%%%%%%%%%%%%%%%%%%%%%%%%%%%%%%%%%%%%%%%%%%%%%%%%%%%%%%%%%%%%%%%%%%%%%
96 %
97 %   Glyoxal(aq) + O2(aq)   ->   Oxalic acid (aq)
98 %
99 %%%%%%%%%%%%%%%%%%%%%%%%%%%%%%%%%%%%%%%%%%%%%%%%%%%%%%%%%%%%%%%%%%%%%%%%%%
100
101 rs6 (1)      =    1;
102 rs6 (9)      =    1;
103 rs6 (12)     =    1;
104
105 %REACTION 7
106 %%%%%%%%%%%%%%%%%%%%%%%%%%%%%%%%%%%%%%%%%%%%%%%%%%%%%%%%%%%%%%%%%%%%%%%%%%

```

D MATLAB FILES

```

107 %
108 % 2 MEA(aq) + Oxalic acid (aq) -> BHEOX(aq) + 2 H2O(1)
109 %
110 %%%%%%%%%%%%%%%%%%%%%%%%%%%%%%%%%%%%%%%%%%%%%%%%%%%%%%%%%%%%%%%%%%%%%%%%%%
111
112 rs7(2)      = 2;
113 rs7(8)      = 2;
114 rs7(12)     = 1;
115 rs7(13)     = 1;
116
117 %REACTION 8
118 %%%%%%%%%%%%%%%%%%%%%%%%%%%%%%%%%%%%%%%%%%%%%%%%%%%%%%%%%%%%%%%%%%%%%%%%%%
119 %
120 % 2 MEA(aq) + 0.5 O2 (aq) + 2 H2O(1)
121 % -> HEGly(aq) + NH3(aq) + 2 H+(aq)
122 %
123 %%%%%%%%%%%%%%%%%%%%%%%%%%%%%%%%%%%%%%%%%%%%%%%%%%%%%%%%%%%%%%%%%%%%%%%%%%
124
125 rs8(1)      = 0.5;
126 rs8(2)      = 2;
127 rs8(6)      = 2;
128 rs8(8)      = 2;
129 rs8(4)      = 1;
130 rs8(14)     = 1;
131
132 % A 1 O2
133 % B 2 MEA
134 % C 3 CH2O Aldehyde
135 % D 4 NH3
136 % E 5 CHOOH Acid
137 % F 6 H3O+
138 % G 7 HEF
139 % H 8 H2O
140 % I 9 Glyoxal
141 % J 10 HEI
142 % K 11 Fe2+/3+
143 % L 12 Oxalic acid
144 % M 13 BHEOX
145 % N 14 HEGly

```

D.2.12 watvappres.m

```

1 %%%%%%%%%%%%%%%%%%%%%%%%%%%%%%%%%%%%%%%%%%%%%%%%%%%%%%%%%%%%%%%%%%%%%%%%%%
2 % WATER VAPOUR PRESSURE
3 %
4 % Input:
5 % T      Temperature [K]      (vector)
6 % Pz     Points in z-direction [-] (vector)
7 %
8 % Output:
9 % Psat   Vapour pressure of H2O [Pa] (vector)
10 %
11 %%%%%%%%%%%%%%%%%%%%%%%%%%%%%%%%%%%%%%%%%%%%%%%%%%%%%%%%%%%%%%%%%%%%%%%%%%
12
13 function Psat=watvappres(T) %Goff-Gratch
14 Tst=373.15; %[K]
15 Pst=1013.25; %[hPa]

```

```

16
17
18 logPsat=(-7.90298*((Tst/T)-1)+(5.02808*log10(Tst/T))...
19 -(1.3816e-7*((10^(11.344*(1-(T/Tst))))-1))...
20 +(8.1328e-3*((10^-(3.49149*((Tst/T)-1)))-1)))+(log10(Pst));
21
22 Psat=(10^logPsat)*100; %[Pa]
23 end

```

D.2.13 henrys.m

```

1 %%%%%%%%%%%%%%%%%%%%%%%%%%%%%%%%%%%%%%%%%%%%%%%%%%%%%%%%%%%%%%%%%%%%%%%%%%
2 %
3 %                HENRY'S LAW COEFFICIENTS
4 %
5 %%%%%%%%%%%%%%%%%%%%%%%%%%%%%%%%%%%%%%%%%%%%%%%%%%%%%%%%%%%%%%%%%%%%%%%%%%
6 function [H]=henrys(MWO2,rhoL ,N,T,GASCONST)
7     constant;
8 % A 1 O2
9 H_dimless(1)=0; %Calculated later
10 % B 2 MEA
11 H_dimless(2)= 2.46776688109146E-07;
12 % C 3 CH2O Aldehyde
13 H_dimless(3)=0.000557239020795048;
14 % D 4 NH3
15 H_dimless(4)=0.000708486592459356;
16 % E 5 Formic acid
17 H_dimless(5)=0; %Not volatile
18 % F 6 H+
19 H_dimless(6)=0; %Not volatile
20 % G 7 HEF
21 H_dimless(7)=3.043786691768E-09;
22 % H 8 H2O
23 H_dimless(8)=0; %Calculated later
24 % I 9 Glyoxal
25 H_dimless(9)=0; %Not volatile
26 % J 10 HEI
27 H_dimless(10)=1.90918900382257E-11;
28 % K 11 Fe3+
29 H_dimless(11)=0;
30 % L 12 Oxalic acid
31 H_dimless(12)=0;
32 % M 13 BHEOX
33 H_dimless(13)=1.73429e-12;
34 % N 14 HEGly
35 H_dimless(14)=2.6717e-49;
36
37 H=(H_dimless.*GASCONST.*T); % [bar m3/kmol]
38
39 H(1)=exp(3.71814 + (5.59617e3/T) - ...
40 (1.049668e6/(T^2)))*1.02300*MWO2/rhoL;
41 %Henrys law coefficient [bar-m3/kmol] Rooney(1998)
42
43 %%%%%%%%%%%%%%%%%%%%%%%%%%%%%%%%%%%%%%%%%%%%%%%%%%%%%%%%%%%%%%%%%%%%%%%%%%
44 % DETERMINING HENRY'S LAW COEFFICIENT FOR WATER
45 %%%%%%%%%%%%%%%%%%%%%%%%%%%%%%%%%%%%%%%%%%%%%%%%%%%%%%%%%%%%%%%%%%%%%%%%%%
46 Psat=watvappres(T);

```

D MATLAB FILES

```
47 H(8)=(Psat/100000)/(rhoL/MWH2O); %Henry's constant water vapor
48
49 if length(H)<N
50     'ENTER MORE COMPONENTS IN henry.m FILE!'
51 else
52     return
53 end
```

D.2.14 constant.m

```
1 %%%%%%%%%%%%%%%%%%%%%%%%%%%%%%%%%%%%%%%%%%%%%%%%%%%%%%%%%%%%%%%%%%%%%%%%%%
2 %
3 %                GLOBAL CONSTANTS
4 %
5 %%%%%%%%%%%%%%%%%%%%%%%%%%%%%%%%%%%%%%%%%%%%%%%%%%%%%%%%%%%%%%%%%%%%%%%%%%
6
7 MWamine=61.08;      %Molweight [kg/kmol]
8 MWO2=32;           %Molweight [kg/kmol]
9 MWform=45.01864;   %Molweight [kg/kmol]
10 MWNH3=17.031;      %Molweight [kg/kmol]
11 MWHEF=89.093;     %Molweight [kg/kmol]
12 MWHEI=112.13132;  %Molweight [kg/kmol]
13 MWFe=55.845;      %Molweight [kg/kmol]
14 MWBHEOX=176.17;   %Molweight [kg/kmol]
15 MWHEGly=119.11916;%Molweight [kg/kmol]
16 MWH2O=18.01528;   %Molweight [kg/kmol]
17
18 rhoL=1000;         %Liquid density [kg/m3]
19
20 GASCONST=8.314e-2; %Gas constant [m3 bar/K kmol]
21 GASCONST2=8.314;
```